Bimetallic Metal-Organic Chains, Networks and Frameworks (MOC's, MON's & MOF's) Based on Cyanides: Structure and Physical Properties.

Thèse présentée à la Faculté des Sciences
Institut de Microtechnique
Université de Neuchâtel

par

Olha Sereda

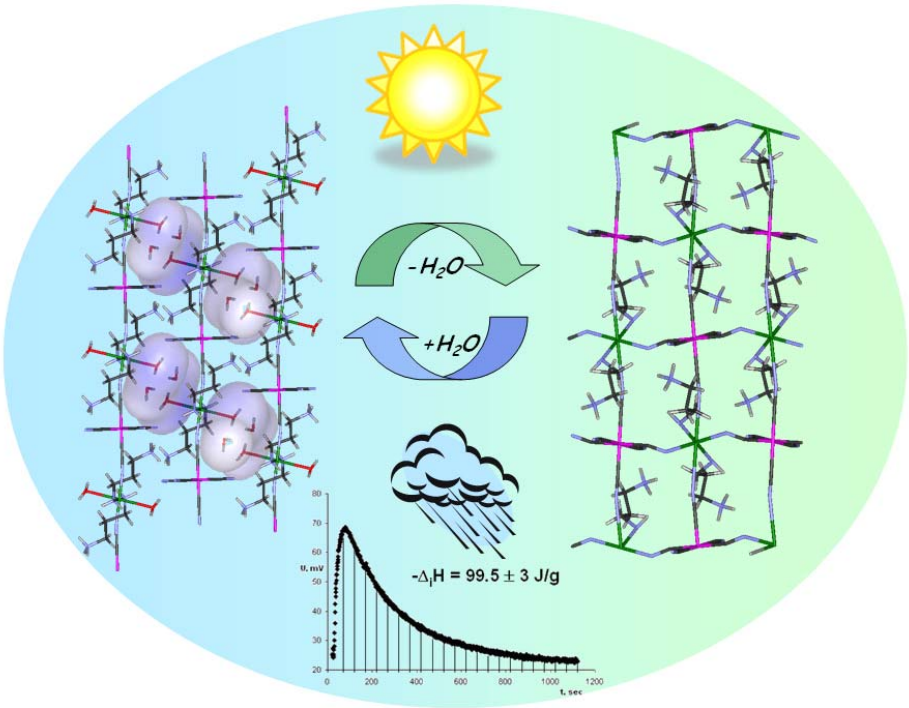

Soutenue le 22 Mai 2008
Université de Neuchâtel

Université de Neuchâtel

FACULTE DES SCIENCES
Secrétariat-Décanat de la faculté
- Rue Emile-Argand 11
- CP 158
- CH-2009 Neuchâtel

IMPRIMATUR POUR LA THESE

Bimetallic Metal-Organic Chains, Networks and Frameworks (MOC's, MON's & MOF's) Based on Cyanides: Structure and Physical Properties

Olha SEREDA

UNIVERSITE DE NEUCHATEL

FACULTE DES SCIENCES

La Faculté des sciences de l'Université de Neuchâtel,
sur le rapport des membres du jury

Mmes H. Stoeckli-Evans (directrice de thèse),
T. Centeno (Oviedo E),
MM. F. Stoeckli, T. Bürgi et S. Decurtins (Berne)

autorise l'impression de la présente thèse.

Neuchâtel, le 2 juin 2008

Le doyen :
F. Kessler

UNIVERSITE DE NEUCHATEL
FACULTE DES SCIENCES
Secrétariat - décanat de la faculté
Rue Emile-Argand 11 - CP 158
CH-2009 Neuchâtel

Acknowledgement

A journey is easier when you travel together. Interdependence is certainly more valuable than independence. This thesis is the result of three years work during which I have been accompanied and supported by many people. I have now the pleasant opportunity to express my gratitude to all of them.

The first person I would like to thank is my direct supervisor Professor Helen Stoeckli-Evans. I can not imagine it is possible to have a better advisor and mentor for my PhD. Without her knowledge, great support, hard work, her enthusiasm and integral view of research I would never have finished. She could not even realize how much I have learned from her. Besides being an excellent supervisor, Madame Stoeckli was as close as a relative and very good to me. I am really glad that Professor Helen Stoeckli-Evans has become part of my life.

I am forever indebted to Prof. Fritz Stoeckli, who has introduced me to the exciting world of adsorption and immersion calorimetry. I wish to express my warm and sincere thanks to Prof. Dariya Semenyshyn, who has opened up the field of cyanide compounds for me and who has given me lots of useful advise over these past three years!

My gratitude also goes to Prof. K. Bernauer, for all of his scientific advise and to Prof. P.-A. Farin, who has given me the great opportunity to participate in a “Smart Bottle” project. I would also like to deeply thank Dr. Antonia Neels. Thank you, Antonia, for being there for me and for giving me such excellent advice throughout the years.

It is difficult to overstate my appreciation to Dr. Olga Borova, who first brought me into the world of research and with whom I began to learn chemistry. Not only a great mentor and colleague, she has also been a cornerstone in my professional development.

I thank all my friends who have always stood by me and given me their moral support, no matter what. I would like to thank particularly Julieta, Inga, Natalia, Seva and Vladimir.

The chain of my gratitude would be definitely incomplete, if I would forget to thank my family who has always supported me. Last but not least, my husband Andrij, who has made me a happy person and gave me that extra force, motivation and love necessary to get things done.

Table of Contents

Abbreviations ***i***

Keywords ***ii***

Abstract ***iii***

1. Introduction 1

1.1. Chemistry of Porous Coordination Polymers 3

1.2. Prussian Blue Analogues Still a Hot Topic: "inorganic evergreen" 6

1.3. Multidimensional Compounds Based on Cyanide-Bridged Assemblies 7

1.4. Adsorption: Overview of Nanoporous Properties 11

1.5. General Objectives of the Present Research 15

1.6. References 16

2. Structural Transformations and Ferromagnetism 19

Preface 21

2.1 "Sponge-Like" Reversible Transformations 23

2.2 New 3D and Chiral 1D $Cu^{II}Cr^{III}$ Coordination Polymers 47

2.3 Chiral Polymers Based on Tetracyanonickelate 71

3. Adsorption and Immersion Studies 91

Preface 93

3.1 Bimetallic Metal Organic Cyano Bridged Frameworks 95

3.2 Transformation of a Chiral Nanoporous Cyano-Bridged Framework 119

4. Construction of Metal-Organic Cyano-Bridge (MOCB) Polymers 153

Preface 155

4.1 Bimetallic Chiral Cyano-Bridged Assemblies 157

4.2 A 2D Network based on Hexacyanocobaltate (III) 173

4.3 Poly [(*trans*-bis-(μ-4,4'-bipyridine-*N*,*N*'))-diaquacopper(II)-tetracyanonickelate(II)] 185

5. Another example of Adsorption and Immersion Calorimetry Studies on a Nanoporous Solid 195

5.1. Adsorption of Morphine from Aqueous Solutions by Carbons 197

6. Conclusions 211

7. Appendix 217

CV 225

Abbreviations

MOC	Metal-Organic Chain
MON	Metal-Organic Network
MOF	Metal-Organic Framework
MOCB	Metal-Organic Cyano-Bridged
1D, 2D, 3D	One-, two-, three-dimensional
PXRD	Powder X Ray Diffraction
a, b, c	Unit-cell lengths in Å
α, β, γ	Unit-cell angles in °
V	Unit-cell volume in $Å^3$
Z	Number of molecules per unit cell
D_c	Calculated density in g/cm^3
R1, wR2	Final structure agreement factors
en	ethylendiamine
Lpn	(R)-1,2-diaminopropane
tn	1,3-diaminopropane
***trans*-(1S,2S-chxn)**	*trans*-cyclohexane-(1S, 2S)-diamine
***trans*-(1R,2R-chxn)**	*trans*-cyclohexane-(1R, 2R)-diamine
4,4'bpy	4,4'-Bipyridine
2,2'bpy	2,2'-Bipyridine
4,5pbpy	4,5,4',5'-bis(pinene)-2,2'-bipyridine
MeOH	Methanol
EtOH	Ethanol
MeCN	acetonitrile
DMSO	Dimethyl sulfoxid
IR	Infrared
$\tilde{\nu}$	Vibration frequency in cm^{-1} (IR)
T	Temperature
t	Time

TG	Thermogravimetric analysis
EA	Elemental analysis
$\mathbf{N_a}$	Amount of gas adsorbed in moles per gram of solid when the relative pressure is p/p_0
$\mathbf{N_{a0}}$	Total amount of gas adsorbed in moles per gram of solid
p	Pressure
$\mathbf{p_0}$	Saturation vapour pressure of the adsorptive
A	Polanyi adsorption potential
B	Structural constant of the adsorbent
β	Affinity coefficient
$\mathbf{E_0}$	Characteristic energy of the solid in kJ/mol
α	Expansion coefficient of the adsorbate
Γ	Gamma function
$\mathbf{-\Delta h_i}$	Enthalpy of immersion in J/g
$\mathbf{W_0}$	Micropore volume in cm^3/g
$\mathbf{S_e}$	External surface area in m^2/g
$\mathbf{-h_i}$	Enthalpy of immersion of the external surface in J/m^2
$\mathbf{V_m}$	Liquid molar volume in cm^3/mol
MW	Molecular weight in g/mol
L	Molecule width in nm
μ	Dipole moment in D
Q	Electric quadrupole moment in multiples of barns [$\cdot 10^{-24}$ cm^2]
k	Kinetic rate constant

Keywords: Metal-organic frameworks, Nanoporous, Adsorption, Desorption, Cyanometallate.

Mot clés: Structures organométalliques nanoporeuses, Adsorption, Désorption, Cyanométallique.

Abstract

Dynamic structural transformations, based on flexible porous frameworks are one of the major challenges for chemists from a fundamental and a practical point of view. The present work deals in particular with the construction of the metal-organic frameworks based on metallocyanides. The metal-organic cyano-bridged frameworks (MOCBF's) synthesized and developed in this thesis have been used for immersion calorimetry and gravimetrical adsorption studies.

This thesis is divided into five Chapters. Chapter 1 gives an introduction to the subject of porous coordination polymers and cyano-bridged bimetallic assemblies and on the experimental methods used in this work. Chapter 2 is dedicated to the structural transformations and ferromagnetism (Section 2.2). The "sponge-like" behaviour of the molecular transformations, described in Sections 2.1 and 2.3, are accompanied by a colour change and it has been shown by *in-situ* X-ray powder diffraction and immersion calorimetry to be completely reversible. In Section 2.2 the two systems studied exhibit ferromagnetism. The first system shows three-dimensional ferromagnetic ordering at ca. 4K, and second shows a weak intra-chain ferromagnetic exchange, as a result of Jahn-Teller elongation in copper (II) ions.

Chapter 3 describes the studies in the field of immersion calorimetry and adsorption. In Section 3.1 new MOCBF's are described, two of which show dynamic behaviour triggered by guest removal and inclusion. The dehydration processes, which involve changes in the structures, are reversible, and this was shown using powder X-ray diffraction (PXRD) methods. By a combination of the DSC, PXRD and immersion calorimetry it was possible to find the net heat of the transformation. A remarkable structural transformation, driven by solvent molecules, is presented in Section 3.2. It was found that the two types of reported networks show different behaviour upon drying, falling within the category of "recoverable collapsing" and "guest-induced reformation" frameworks. The methanol adsorption isotherm for the fully out-gassed compound indicates that it is a two step process. Immersion calorimetric studies with different

solvents were carried out. By the gravimetric adsorptions studies it was shown that the synthetic strategy based on cyanide-bridged bimetallic assemblies is advantageous for the formation of flexible nanoporous materials.

Chapter 4 illustrates the different methods used for the construction of MOCBF's and describes their structural properties.

Chapter 5 describes the adsorption of morphine from aqueous solutions by various nanoporous carbons. It was shown than 99% of morphine can be adsorbed in 5 minutes from an aqueous solution by activated carbon PC94-11, with particles of less than 400 μm and an amount in excess by a factor three with respect to the actual saturation capacity. It was found that the main parameters for a speedy elimination are: an excess of carbon, small particles and good initial mixing of the solid with the solution. This specific study has also provided subsidiary information on the affinity coefficient for the adsorption of morphine from aqueous solutions, β_s(morphine) = 1.37 ± 0.02. This new parameter, of relevance to pharmacology, will allow the prediction of the adsorption equilibrium of this molecule by activated carbons, by using the modified Dubinin-Radushkevich-Kaganer equation.

In conclusion, this work describes the synthesis and physical properties of new MOCBF's which exhibit striking structural transformations. Powder X-Ray diffraction combined with adsorption and immersion studies provides insights into these transformations.

Chapter 1. Introduction

1. Introduction

1.1 Chemistry of the Porous Coordination Polymers

Recently, remarkable progress has been made in the area of molecular inorganic–organic hybrid compounds. The synthesis and characterization of infinite one-, two-, and three dimensional (1D, 2D, and 3D) networks has been an area of rapid growth. Coordination compounds with infinite structures have been intensively studied, in particular, compounds with backbones constructed from metal ions as connectors and ligands as linkers, the so-called coordination polymers[1-14] The phrase, "coordination polymers" appeared in the early 1960s, and the area was first reviewed in 1964.[15] Versatile synthetic approaches for the assembly of target structures from molecular building blocks have been developed. The key to success is the design of the molecular building blocks which direct the formation of the desired architectural, chemical, and physical properties of the resulting solid-state materials. In a surprisingly short time, the structural chemistry has attained a very mature level. Figure 1 shows the extraordinary increase over the years of the number of articles published in this area.

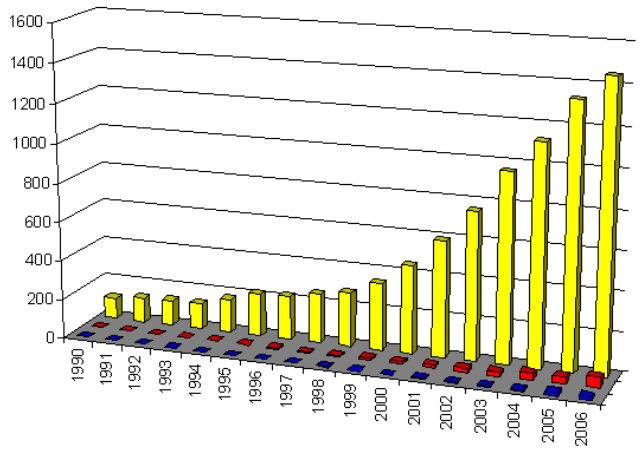

Figure 1. The number of published articles containing the keywords "coordination polymers" (yellow), "porous coordination polymers" (blue), and "adsorption of porous coordination polymers" (pink), survey by SciFinder.

Coordination polymers have now taken an important position in the porous-materials area and added a new category to the conventional classification (Figure 2).

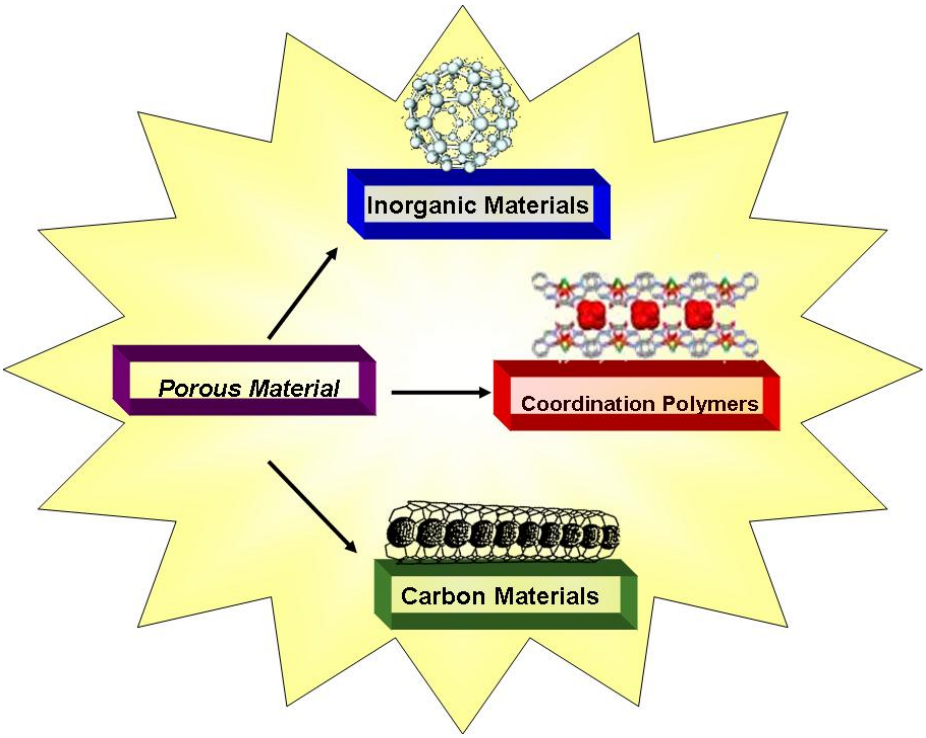

Figure 2. Classes of porous materials.

Porous compounds have attracted the attention of chemists, physicists, and materials scientists because of interest in the creation of nanometer-sized spaces and the novel phenomena in them. There is also commercial interest in their application in separation, storage, and heterogeneous catalysis. Until the mid 1990s, there were basically two types of porous materials, namely, inorganic and carbon-based materials. In the case of microporous inorganic solids, the largest two subclasses are the aluminosilicates and aluminophosphates. Zeolites are 3D crystalline, hydrated alkaline or alkaline-earth aluminosilicates with the general formula $M^{n+}{}_{x/n}[(AlO_2)_x(SiO_2)_y]^{x-} \cdot wH_2O$[16-18] (M=metal). Their framework, built from corner-sharing TO_4 tetrahedra (T=Al, Si), defines interconnected tunnels or cages in which water molecules and M ions are inserted. The porosity is then provided through the elimination of the water molecules, the framework usually remains unaffected by this. The cavities, whose structure is usually determined by the number of polyhedra surrounding the pore, were initially exploited for molecular-sieve requirements in gas separation and catalytic

processes. Synthetic zeolites were first observed in 1862.[19] Aluminophosphates (AlPO4s) consist of tetrahedra of Al^{3+} and P^{5+} ions linked by corner-sharing oxygen atoms, and which build up a 3D neutral framework with channels and/or pores of molecular dimensions.[20] Many aluminophosphates have crystal structures, which are not observed in zeolites. The first publication on microporous crystalline aluminophosphates appeared in 1982[21]. Since then, not only several related crystalline oxides, such as silicoaluminophosphates, metallosilicates, metalloaluminophosphate, and metallophosphates, but also porous chalcogenides, halides, and nitrides, have been discovered.[22, 23] Mesoporous materials have also been extensively studied; they afford intriguing and useful porous properties, characteristic of meso-sized structures.[24-26]

The activated carbons have a high open porosity and a high specific surface area, but have a disordered structure. The essential structural feature is a twisted network of defective hexagonal carbon layers, cross-linked by aliphatic bridging groups. The width of the layers varies, but typically is about 5 nm. Simple functional groups and heteroelements are incorporated into the network and are bound to the periphery of the carbon layers.

Recently, porous coordination polymers have been developed, which are beyond the scope of the former two classes of porous materials. They are completely regular, have high porosity, and highly designable frameworks. Their syntheses occur under mild conditions and the choice of a certain combination of discrete molecular units leads to the desired extended network, this is the so-called bottom-up method. There is an early report on the use of organic bridging ligands to form the porous coordination polymer $[Cu(NO_3)(adiponitrile)_2]_n$ which has a diamond net, however, the adsorption behavior was not reported.[27] Since the early 1990s, research on the structures of porous coordination polymers has increased greatly, and examples with functional micropores soon started to appear. In 1990, Robson et al. reported a porous coordination polymer capable of anion exchange.[28] The catalytic properties of the 2D $[Cd^{II}(4,4'\text{-bpy})_2]$ coordination polymer were studied by Fujita et al. in 1994.[29] In 1995, the adsorption of guest molecules was studied by the groups of Yaghi[30] and Moore[31], and in 1997 Kondo et al. reported gas adsorption at ambient temperature.[32] Our aim in this work was to focus on the construction of regular microporous structures.

1.2 Prussian Blue Analogues Still a Hot Topic: "inorganic evergreen"

Three hundred years ago, adventurous scientists working in the fledgling discipline of chemistry often weren't sure what they would get when cooking up a recipe. That was how Prussian blue (PB) was discovered. This quintessential inorganic pigment, later identified as ferric ferrocyanide, $Fe_4[Fe(CN)_6]_3$, was first synthesized by a German artist in 1704 as he attempted to make a red pigment. Despite of not very red, Prussian blue quickly became a highly desired substance and remained in strong demand until the 1970s. Beyond its use as a pigment, Prussian blue is perhaps the most studied compound in chemistry. Later Prussian Blue was re-investigated, opening a new area of interest, concerning the substitution of Fe(II) and Fe(III) by other paramagnetic metal ions M, and M', giving rise a new series of Prussian Blue analogues. Even after three centuries, Prussian blue analogues are still a hot material, as judged by the SciFinder search (Figure 3).

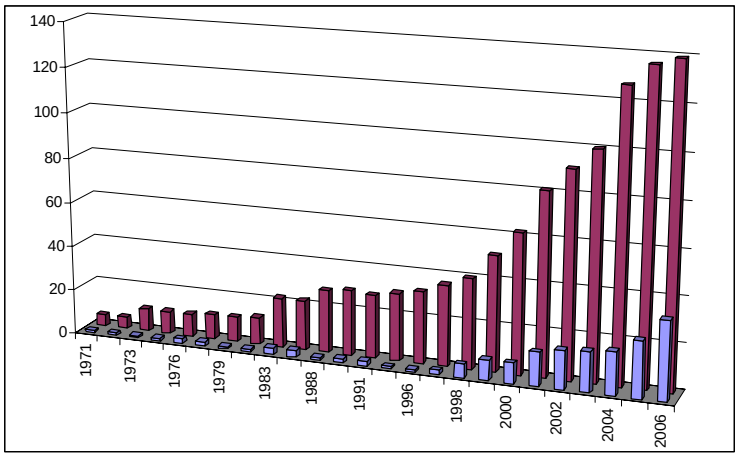

Figure 3. The number of published articles containing the keywords "Prussian blue analog" (blue) and "cyano-bridged" (red), survey by SciFinder.

Prussian blue started as a very simple material, a pigment, but gradually grew into a compound that provided scientific challenges, especially nowadays become of the interest in nanomaterials and molecular-magnet applications. The metaphorical label "inorganic evergreen" is used for Prussian blue and the analogues of PB, because of its perpetual attraction for chemists.

1.3 Multidimensional Compounds based on Cyanide-Bridged Assemblies

The design and synthetic strategy of multidimensional compounds are of current interest in the field of coordination polymers. A promising approach for this purpose consists in the assembling two building blocks that are frequently transition metal complexes: one with terminal ligands able to act as bridges, and the other with available co-ordination sites.

1.3.1. One-dimensional cyano-bridged complexes.

Self-assembly of the anionic building-block $[M(CN)_6]^{3-}$ and transition metal ions in the presence of various blocking ligands has frequently resulted in the formation of one-dimensional chains: (i) $\{trans\text{-}[Cr(CN)_4(\mu\text{-}CN)_2Ln(H_2O)_4(bpy)]_n \cdot 3.5nH_2O \cdot 1.5nbpy\}_n$ (Ln = Nd, Sm, Eu, Tb, Dy, Ho, Er, Tm, Yb, and Lu; bpy= 2,2'-bipyridine)[33]; (ii) $PPh_4[Ni(pn)_2][M(CN)_6] \cdot H_2O$ (M^{III}=Fe, Cr, Co; pn= *rac*-1,2-propanediamine)[34]; (iii) $[NEt_4]_2[Mn(acacen)][Fe(CN)_6]$ (acacen= N,N'-ethylenedi(acetylacetonilideneaminato) [35]; (iv) $[\{Cu(dien)\}_2\{Cr(CN)_6\}]\{Cu(dien)\}\{Cr(CN)_6\}] \cdot 4H_2O$[36]. The synthesis of these complexes employs the reaction of the transition metal salts and $[M(CN)_6]^{3-}$ building-blocks (M = Mn(III), Fe(III), Co(III)) in a 1:1 stoichiometry and in the presence of the corresponding organic ligand.

The first complete characterization of a cyano-bridged one-dimensional polymer chain, $[Ni(en)_2]_3[M(CN)_6]_2 \cdot 2H_2O$ (M^{III}= Fe(**1**), Mn(**2**), Cr(**3**), Co(**4**)), has been reported by Ohba et al. in 1994.[37] These assemblies arise from the reaction of $[Ni(en)_3]Cl_2$ and $K_3[M(CN)_6]$ in the molar ratio 3:2 in aqueous solution which resulted in the immediate precipitation of compounds **1-4.** However, they were found to be polycrystalline and their magnetic properties were studied. X-ray structure analysis of compounds **1** and **4** has revealed that they are isomorphous. The asymmetric unit consists of one $[M(CN)_6]^{3-}$ anion, one *cis*-$[Ni(en)_2]^{2+}$ cation, one-half of a *trans*-$[Ni(en)_2]^{2+}$ cation, and one water molecule, with the inversion centre at the Ni of *trans*-$[Ni(en)_2]^{2+}$. Three cyano nitrogens in the meridional mode coordinate to adjacent Ni ions. The magnetic susceptibility data

for the complexes **1-3** revealed a ferromagnetic intermolecular interaction between M^{III} and Ni^{II}.

The reaction of $Ln(NO_3)_3{\cdot}xH_2O$ with $K_3[M(CN)_6]$ and bpy in aqueous solutions leads to the formation of one-dimensional cyano-bridged complexes of formula $\{[Ln(bpy)(H_2O)_4M(CN)_6]{\cdot}4H_2O{\cdot}1.5bpy\}_n$[33]. In all cases, the one-dimensional chain comprises alternating $Ln(bpy)(H_2O)_4$–$M(CN)_6$ fragments linked by cyano-bridges (Fig. 4).

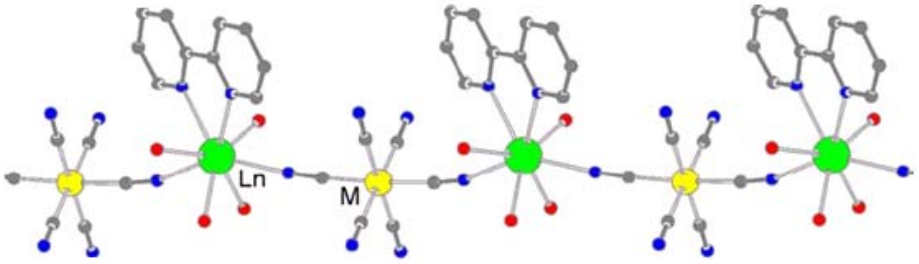

Figure 4. View of the zig-zag chain structure of $\{[Ln(bpy)(H_2O)_4M(CN)_6]{\cdot}\ 4H_2O{\cdot}1.5bpy\}_n$ [33]

The lanthanide(III) ion has a coordination number of eight, being surrounded by four oxygen atoms of four water molecules, two nitrogen atoms of the bpy ligand and two nitrogen atoms of two cyano bridges. Each $[M(CN)_6]^{3-}$ moiety coordinates to two lanthanide(III) ions using two *trans*-cyano ligands, while each $Ln(bpy)(H_2O)_4$ group connects two $[M(CN)_6]^{3-}$ moiety in a *cis*-fashion. The Ln─M─Ln angles fall in the range 159.1–159.7º, in agreement with the *trans*-geometry of the $[M(CN)_6]^{3-}$ moiety. The intramolecular Ln· · ·M distances are in the range of 5.421–5.612 Å. The molecular structure is further stabilized by the interplay of hydrogen-bonding and π– π interactions.
In this family of complexes, the magnetic exchange coupling between Ln^{III} and $Fe^{II}I$ is found to be antiferromagnetic for Ln = Gd^{III}, Dy^{III}, Tb^{III}, and no significant magnetic interaction has been observed for Eu^{III}, Ho^{III}, Er^{III}, Tm^{III}.

1.3.2. Two-dimensional cyano-bridged complexes.

One of the first two dimensional cyano-bridged networks $[Cu(dien)]_3[Fe(CN)_6]_2{\cdot}6H_2O$ (dien = diethylenetriamine), has been reported by Kou and co-workers[38]. The structure consists of a one-dimensional chain of $\{[Cu(dien)]_2[Fe(CN)_6]\}^+$ cations and binuclear $\{[Cu(dien)(H_2O)][Fe(CN)_6]\}^-$ moieties bridged by one CN^- ligand of the $[Fe(CN)_6]^{3-}$

anion. The chains are linked by hydrogen bonds giving rise to a unique step-shaped two-dimensional network. In the crystal all the copper(II) ions have a distorted square-based-pyramidal geometry. From magnetic susceptibility measurements the complex was found to exhibit a weak ferromagnetic interaction between the copper(II) and iron(III) atoms.

Bimetallic assemblies, $[Ni(N\text{-men})_2]_3[M(CN)_6]_2 \cdot nH_2O$ (M^{III}= Fe or Co; N-men= N-methylethylenediamine), have been prepared by the reaction of $[Ni(N\text{-men})_3]Cl_2$ and $K_3[M(CN)_6]$ in the 3:2 molar ratio in water[39]. The X-ray crystallographic study revealed that the network is two-dimensional based on a honeycomb sheet structure. In spite of the different space groups (*P-3* for the Fe complex and *C2/c* for the Co complex), their network structures are essentially the same. Three cyano nitrogens of $[M(CN)_6]^{3-}$ in the facial mode coordinate to the adjacent *trans*-$[Ni(N\text{-men})_2]^{2+}$ forming a hexagonal unit having M^{III} at each corner and Ni^{II} at the center of each edge. The introduction of one methyl substituent on an ethylenediamine nitrogen gives rise to a dramatic change in the network structure of $[Ni(L)_2]_3[M(CN)_6]_2 \cdot nH_2O$, from a 1D zigzag chain with L=en[37] to the 2D honeycomb sheet with L=N-men. At least 15 water molecules per unit cell are present in the porous sheet structure of the crystalline sample. Elemental, TGA and DSC analyses indicate a partially dehydrated formula, $[Ni(N\text{-men})_2]_3[M(CN)_6]_2 \cdot 12H_2O$, after allowing the sample to stand in air.

The reaction of $Gd(NO_3)_3 \cdot nH_2O$, dmf and $K_3[Cr(CN)_6]$ in the molar ratio 1:2:1 in an aqueous solution affords the complex $[Gd(dmf)_2(H_2O)_3Cr(CN)_6] \cdot H_2O$ with a brick-wall-like structure (dmf = *N*,*N*-dimethylformamide) (Fig. 5).[40]

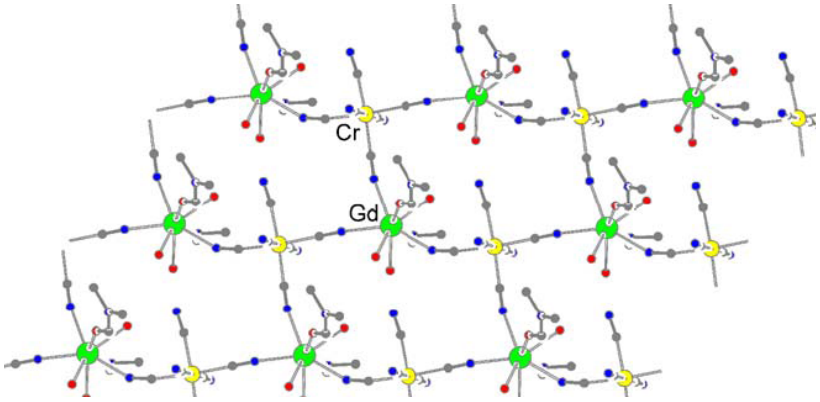

Figure 5. View of the brick-wall structure of the complex $[Gd(dmf)_2(H2O)_3Cr(CN)_6] \cdot H_2O$[40]

In the crystal lattice, each $[Cr(CN)_6]^{3-}$ unit uses three cyano groups in a meridional arrangement to connect three $[Gd(dmf)_2(H_2O)_3]^{3+}$ anions, thus forming neutral layers with slightly distorted Gd_3Cr_3 rectangles. The bridging cyano ligands coordinate to the gadolinium(III) ions in two different fashions: two nearly linear (Gd─N≡C= 174.9º and 167.5º, respectively) and one bent (Gd─N≡C= 154.1º). The adjacent Gd···Cr distances are in the range 5.469–5.692 Å and the shortest interlayer metal–metal distance is 7.738 Å. The uncoordinated water molecules are positioned between the parallel flat layers and link to one terminal cyano ligand of $[Cr(CN)_6]^{3-}$, and to the coordinated water molecules via hydrogen-bonding. The non-bridging cyano ligands are hydrogen bonded to coordinated water molecules, thus connecting the layers to form a three-dimensional structure.

1.3.3. Three-dimensional cyano-bridged complexes.

Several new bimetallic assemblies $[Ni^{II}(L)_2]_3[Fe^{II}(CN)_6]X_2$ (L= ethylene-diamine, trimethylenediamine; X = PF^{6-}, ClO^{4-}) with a three-dimensional (3-D) network of the cubic Fe_8Ni_{12} unit using the ferrocyanic anion, $[Fe^{II}(CN)_6]^{4-}$, as a building block have been reported by Okawa and co-workers.[41] All the assemblies have an isotropic three-dimensional network structure extended through Fe-CN-Ni linkages. The network is based on a cube formed by 8 $[Fe(CN)_6]^{4-}$ anions at the corners and 12 $[Ni(L)_2]^{2+}$ cations at the edges. Two hexafluorophosphate or perchlorate anions are located in the cavity of the Fe_8Ni_{12} cube and align along a diagonal axis that coincides with the *c* axis. Magnetic measurements show a ferromagnetic interaction between the nearest Ni^{II} ions through the diamagnetic Fe^{II} ion.

A novel molecular-based magnet of three-dimensional cyanide-bridged bimetallic assembly, $[\{Ni(tn)_2\}_5\{Fe^{III}(CN)_6\}_3]_n(ClO_4)_n{\cdot}2.5nH_2O$ where tn = trimethylenediamine, has also been synthesized and structurally characterized.[42] The assembly has a 3-D network structure extended by three different types of Fe^{III}-CN-Ni^{II}-NC-Fe^{III} linkages. The iron (Fe^{III}) atoms are located in two different chemical environments; this was confirmed by Mössbauer spectroscopy. The Ni^{II} atoms have three different coordination environments. Cryomagnetic properties revealed that 3-D magnetic ordering occurs over the lattice below the Curie temperature around 10 K.

Recently, a three-dimensional Cu^{II}-containing Prussian Blue analogue with two types of $[Cr(CN)_6]^{3-}$ units, $[Cu(2,2'\text{-dpa})]_3[Cr(CN)_6]_2 \cdot 3H_2O$ (2,2'-dpa=2,2'-dipicolyl-amine), was synthesized and characterized by Liu and co-workers.[43] One type of $[Cr(CN)_6]^{3-}$ unit in this complex coordinates to six copper(II) atoms to form the heptanuclear $[CrCu_6]$ unit, which connects with the other $[CrCu_6]$ units through a second type of $[Cr(CN)_6]^{3-}$ unit acting as a bidentate spacer link only.

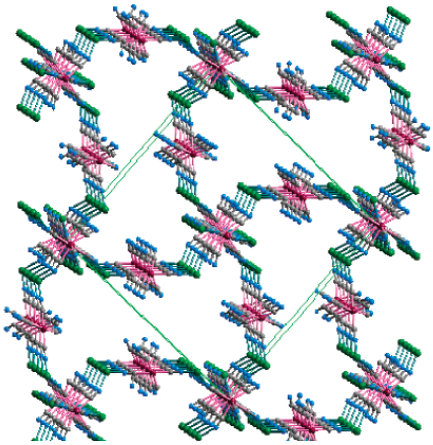

Figure 6. A view of the 3D network structure along the *a*-axis for complex $[Cu(2,2'\text{-dpa})]_3[Cr(CN)_6]_2 \cdot 3H_2O$.[43] 2,2'-Dipicolyl-amine ligands and solvent H_2O molecules are omitted for clarity.

Magnetic investigations of this complex revealed that long range ferromagnetic ordering occurs below the Curie temperature of 3 K. It is the first example of a 3D complex-based Prussian blue analogue containing aromatic amine capping ligands.

1.4 Adsorption: Overview of Nanoporous Properties of MOF's

Porous materials have attracted the attention of chemists, physicists, and material scientists not only because of industrial applications, such as separation processes, heterogeneous catalysis and gas storage, but also because of their scientific interest in the formation of molecular assemblies, such as clusters and 1D arrays, and in the anomalous physical properties of confined molecules. The adsorption of guest molecules on the solid surface plays an essential role in determining the properties of these porous compounds.

Adsorption is governed not only by the interaction between guest molecules and the surface but also by the pore size and shape. Pores are classified according to their size as shown in Table 1.[44]

There is no fundamental difference between adsorption in a macropore and on an open surface, and in the submonolayer region they can often be described by the Dubinin─Radushkevich─Kaganer (DRK) equation.[45]. The adsorption by a mesoporous solid is dominated by capillary condensation, which is responsible for a sharp adsorption rise around the mid relative-pressure region. This effect is not attributable to molecule–solid interactions but to a purely geometrical requirement, which is illustrated well by the Kelvin equation.

Table 1. Classification of pores.

Pore type	Pore size [Å]
Ultramicropore	<5
Micropore	5–20
Mesopore	20–500
Macropore	>500

Adsorption in micropores should not be compared with that of molecules onto an open solid surface, as it corresponds to a volume filling process. It results from the relatively strong overlap of the adsorption potential of the walls. In this case, the adsorption isotherm shows a steep rise at very low relative pressure and a plateau after saturation of the micropore volume. There are six representative adsorption isotherms that reflect the relationship between porous structure and sorption type.[46, 47] This IUPAC classification of adsorption isotherms is shown in Figure 7. Type I corresponds to microporous solids, although it may also reflect chemically-induced saturation processes such as the adsorption on specific sites (e.g. hydrogen bonding of water on oxygen-containing surface groups in carbons). Nonporous and macroporous solids lead to types II, III, and VI, and mesoporous are characterized by types IV and V (hysteresis on desorption, due to capillary condensation). The differences between types II and III and

between types IV and V arise from the relative strength of the gas–solid and adsorbate–adsorbate attractive interactions. When the fluid–solid interaction is stronger than that of fluid–fluid, the adsorption isotherm is of types II and IV, and the opposite situation leads to types III and V. The type VI isotherm represents adsorption on nonporous or macroporous solid surfaces where stepwise multiplayer adsorption occurs. A large number of articles have been published on the adsorption processes in zeolites and activated carbons.[48-50]

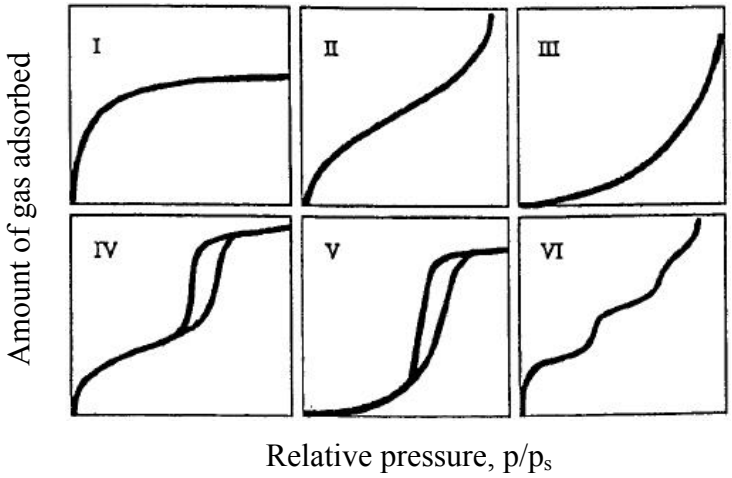

Figure 7. The IUPAC classification for adsorption isotherms.

Dubinin's theory for the volume filling of micropores (TVFM) is used to describe the gas-solid adsorption by our nanoporous solids. The fundamental expression of Dubinin's theory is the Dubinin-Astakhov (DA) equation,

$$N_a = N_{a0} \exp\left[-\left(\frac{A}{E}\right)^n\right] \qquad (1)$$

where A = RTln(p_s/p), N_a is the amount adsorbed (usually given in mol/g) at relative pressure p/p_s and temperature T, and N_{ao} is the limiting amount filling the micropores. From the limiting amount adsorbed, N_{ao}, it is possible to estimate the micropore volume W_0, which is equal to $N_{a0}V_m$, where V_m is the molar volume of the condensed adsorbate at the given temperature. In principle, W_o is invariant, whereas N_{ao} may vary slightly with temperature.

The so-called characteristic energy E depends on the system under investigation. For adsorption of different adsorbates, $E = \beta \cdot E_0$, where β is a specific scaling factor relative to benzene, taken as the reference, and $\beta(C_6H_6) = 1$. Both parameters E and β depend on the gas-solid system and may vary considerably from one solid to another.

For activated carbons, exponent n varies between 1.5 – 3.0, against 3 – 6 for zeolites. The most frequent case, where n is equal to 2, corresponds to the classical Dubinin-Radushkevich (DR) equation [51]. It applies to a variety of nanoporous solids, including those reported in the present study.

Dubinin's theory can be extended to the adsorption of vapors on certain nonporous surfaces, microporous solids and the DR equation takes the form of the so-called Dubinin─ Radushkevich─Kaganer (DRK) equation:

$$N_a = N_{am}(DRK)\exp\left[-\left(\frac{A}{E}\right)^2\right] \qquad (2)$$

where the limiting amount $N_{am}(DRK)$ represents the monolayer capacity of the surface. It is often close to N_{am}(BET) (BET=Brunauer-Emmett-Teller), the monolayer capacity obtained from the same isotherm at higher relative pressures ($0.05 < p/p_s < 0.30$-0.35). In this region, the adsorption process corresponds to the formation of multilayers on the surface.

Dubinin's fundamental equation (1) relates the amount adsorbed N_a to a thermodynamic potential, $A = RT\ln(p_s/p)$, which implies straightforward consequences. For example, analytical expressions can be derived for the isosteric and the net heat of adsorption. The same is true for $\Delta_i H$, the enthalpy of immersion of the solid into a liquid whose vapour is adsorbed according to Eq. (1). In the case of a microporous solid, $\Delta_i H$ is the integral of the net enthalpy of adsorption, since the term $S_{Lv}h_{Lv}$, corresponding to the liquid─vapour interface vanishes. The thermodynamic treatment of Eq. (1) leads to

$$\Delta H_i\left(Jg^{-1}\right) = -\beta E_0(W_0/V_m)\left(1+\alpha T\right)\Gamma\left(1+1/n\right) + h_i S_e \qquad (3)$$

where α is the expansion coefficient of the liquid, $\Gamma(1+1/n)$ is the tabulated gamma function and $-h_i(J/m^2)$, a negative quantity like $\Delta_i H$, represents the wetting of the external (non-microporous) surface area of the solid, S_e. The combination of adsorption and immersion techniques for a given adsorbate provides an interesting test for self-consistency of the adsorption data.

Immersion calorimetry has the advantage of being sensitive and accurate, but it requires the preparation of sealed thin-walled or brittle-ended glass bulbs enclosing the out-gassed sample. It is a somewhat delicate operation.

The combination of adsorption isotherm and immersion calorimetry provides useful information for the characterisation of microporous solids. As shown recently by Stoeckli and co-workers,[52] gate effects can be revealed unambiguously by the combination of adsorption and immersion techniques[53]. For example, the adsorption of a small molecule like CH_2Cl_2 (0.38 nm) may indicate an average pore-size of 1 nm or more, but immersion into a liquid such as CCl_4 (0.63 nm) may be unusually low. This suggests the presence of constrictions preventing the access of larger molecules to micropores wide enough to accommodate them.

To the best of our knowledge, although several coordination cyanide-bridged polymers providing an open framework have been published, their characterization has mainly focused on their physical properties, especially their magnetic properties. Their immersion and adsorption properties have received little attention so far [54]. There are quite a few examples of gas adsorption by Prussian blue analogues[55-57]. For this reason we focused our research on the inherent structural flexibility of 3-D porous magnets, which are expected to show remarkable structural conversions in response to adsorption/desorption of small molecules.

1.5 General Objectives of the Present Research

Our work is focused on the design and synthesis of new coordination polymers, metal-organic chains (1D), networks (2D) and frameworks (3D), based mainly on metallo-hexacyanides. The cyano bridged frameworks must be sufficiently robust to display permanent porosity allowing the reversible adsorption of small molecules.

The present study combines various techniques based on physical adsorption (gas-solid) and immersion calorimetry (liquid-solid), together with single crystal and powder X-ray diffraction. We hope by combining these techniques to build up a coherent picture for the adsorption of small molecules by nanoporous metal-organic framework materials.

1.6 References

[1] C. Janiak, *Angew. Chem.* **1997**, *109*, 1499.
[2] S. R. Batten, R. Robson, *Angew. Chem.* **1998**, *110*, 1558.
[3] A. J. Blake, N. R. Champness, P. Hubberstey, W.-S. Li, M. A. Withersby, M. SchrTder, *Coord. Chem. Rev.* **1999**, *183*, 117.
[4] O. R. Evans, W. Lin, *Acc. Chem. Res.* **2002**, *35*, 511.
[5] I. Goldberg, *Chem. Eur. J.* **2000**, *6*, 3863.
[6] P. J. Hagrman, D. Hagrman, J. Zubieta, *Angew. Chem.* **1999**, *111*, 2798.
[7] A. N. Khlobystov, A. J. Blake, N. R. Champness, D. A. Lemenovskii, A. G. Majouga, N. V. Zyk, M. SchrTder, *Coord. Chem. Rev.* **2001**, *222*, 155.
[8] K. Kim, *Chem. Soc. Rev.* **2002**, *31*, 96.
[9] S. Kitagawa, S. Kawata, *Coord. Chem. Rev.* **2002**, *224*, 11.
[10] B. Moulton, M. J. Zaworotko, *Chem. Rev.* **2001**, *101*, 1629.
[11] O. M. Yaghi, H. Li, C. Davis, D. Richardson, T. L. Groy, *Acc.Chem. Res.* **1998**, *31*, 474.
[12] C. Janiak, *J. Chem. Soc. Dalton Trans.* **2003**, 2781.
[13] O. M. Yaghi, M. O'Keeffe, N. W. Ockwig, H. K. Chae, M. Eddaoudi, J. Kim, *Nature* **2003**, *423*, 705.
[14] S. L. James, *Chem. Soc. Rev.* **2003**, *32*, 276.
[15] J. C. Bailar, *Coordination Polymers, Vol. 1*., Prep. Inorg. React., Jr., **1964**.
[16] D. W. Breck, *Zeolite Molecular Sieves: Structure, Chemistry,and Use*, Wiley, New York, **1974**.
[17] W. M. Meier, D. H. Olsen, C. Baerlocher, *Atlas of Zeolite Structure Types*, Elsevier, London, **1996**.
[18] P. B. Venuto, *Microporous Mater.* **1994**, *2*, 297.
[19] H. de Sainte Claire Deville, C. R. Hebd, *Seances Acad. Sci.* **1862**, *54*, 324.
[20] J. V. Smith, *Chem. Rev.* **1988**, *88*, 149.
[21] S. T. Wilson, B. M. Lok, C. A. Messina, T. R. Cannan, E. M. Flanigen, *J. Am. Chem. Soc.* **1982**, *104*, 1146.
[22] B. M. Weckhuysen, R. R. Rao, J. A. Martens, R. A. Schoonheydt, *Eur. J. Inorg. Chem.* **1999**, 565.
[23] A. K. Cheetham, G. Ferey, T. Loiseau, *Angew. Chem.* **1999**, *111*, 3466.
[24] A. Corma, *Chem. Rev.* **1997**, *97*, 2373.
[25] J. Y. Ying, C. P. Mehnert, M. S. Wong, *Angew. Chem.* **1999**, *111*, 58.
[26] S. Inagaki, S. Guan, T. Ohsuna, O. S. Terasaki, **2002**, *416*, 304.
[27] Y. Kinoshita, I. Matsubara, T. Higuchi, Y. Saito, *Bull. Chem.Soc. Jpn.* **1959**, *32*, 1221.

[28] B. F. Hoskins, R. Robson, *J. Am. Chem. Soc.* **1990**, *112*, 1546.
[29] M. Fujita, Y. J. Kwon, S. Washizu, K. Ogura, *J. Am. Chem. Soc.* **1994**, *116*, 1151.
[30] O. M. Yaghi, G. Li, H. Li, *Nature* **1995**, *378*, 703.
[31] D. Venkataraman, G. B. Gardner, S. Lee, J. S. Moore, *J. Am.Chem. Soc.* **1995**, *117*, 11 600.
[32] M. Kondo, T. Yoshitomi, K. Seki, H. Matsuzaka, S. Kitagawa, *Angew. Chem.* **1997**, *109*, 1844.
[33] A. Figuerola, J. Ribas, D. Casanova, M. Maestro, S. Alvarez, C. Diaz, *Inorg. Chem.* **2005**, *44*, 6949.
[34] M. Ohba, N. Usuki, N. Fukita, H. Okawa, *Inorg. Chem.* **1998**, *37*, 3349.
[35] N. Re, E. Gallo, C. Floriani, H. Miyasaka, N. Matsumoto, *Inorg. Chem.* **1996**, *35*, 6004.
[36] H.-Z. Kou, D.-Z. Liao, P. Cheng, Z.-H. Jiang, S.-P. Yan, G.-L. Wang, X. K. Yao, H. G. Wang, *J. Am. Chem. Soc.* **1997**, 1503.
[37] M. Ohba, N. Maruono, H. Okawa, T. Enoki, J. M. Latour, *J. Am. Chem. Soc.* **1994**, *116*, 11566.
[38] H.-Z. Kou, D.-Z. Liao, P. Cheng, Z.-H. Jiang, S.-P. Yan, G.-L. Wang, X. K. Yao, H.-G. Wang, *J. Chem. Soc., Dalton Trans.* **1997**, 1503–1506.
[39] M. Ohba, H. Okawa, *Coord. Chem. Rev.* **2000**, *198*, 331.
[40] H. Z. Kou, S. Gao, B. W. Sun, J. Zhang, *Chem. Mater.* **2001**, *13*, 1431.
[41] N. Fukita, M. Ohba, H. Okawa, K. Matsuda, H. Iwamura, *Inorg. Chem.* **1998**, *37*, 842.
[42] S. W. Zhang, D.-G. Fu, W.-Y. Sun, Z. Hu, K.-B. Yu, W.-X. Tang, *Inorg. Chem.* **2000**, *39*, 1142.
[43] C.-M. Liu, S. Gao, H.-Z. Kou, D.-Q. Zhang, H.-L. Sun, D.-B. Zhu, *Cryst. Growth. Des.* **2006**, *6*, 94.
[44] *IUPAC Manual of Symbols and Terminology, Appendix 2, Pt.1, Colloid and Surface Chemistry, Vol. 31*, Pure Appl. Chem., **1972**.
[45] F. Stoeckli, *Russ. Chem. Bull. Int. Ed.* **2001**, *50*, 2265.
[46] S. Brunauer, L. S. Deming, W. E. Deming, E. Teller, *J. Am.Chem. Soc.* **1940**, *62*, 1723.
[47] S. J. Gregg, K. S. W. Sing, *Adsorption, Surface Area, and Porosity*, Academic Press, London, **1984**.
[48] A. K. Cheetham, G. Ferey, T. Loiseau, *Angew. Chem. Int. Ed.* **1999**, *38*, 3268 – 3292.
[49] F. Stoeckli, A. Lavanchy, D. Hugi-Cleary, *Fundamentals of adsorption* **1998**, *6*, 24.
[50] F. Stoeckli, *Adsorpt. Sci. Technol.* **1993**, *10*.
[51] F. Stoeckli, D. Hugi-Cleary, T. A. Centeno, *J. Eur. Ceram. Soc.* **1998**, *18*, 1177.
[52] F. Stoeckli, T. A. Centeno, *Carbon* **1997**, *35*, 1097.
[53] F. Stoeckli, *Russ. Chem. Bull. Int. Ed.* **2001**, *50*, 2265.
[54] N. Yanai, W. Kaneko, K. Yoneda, M. Ohba, S. Kitagawa, *J. Am. Chem. Soc.* **2007**, *129*, 3496.
[55] K. W. Chapman, P. D. Southon, C. L. Weeks, C. J. Kepert, *Chem. Commun.* **2005**, 3322.
[56] S. S. Kaye, J. R. Long, *J. Am. Chem. Soc.* **2005**, *127*, 6506.

[57] S. Natesakhawat, J. T. Culp, Matranga, C., B. Bockrath, *J. Phys. Chem. C* **2007**, *111*, 1055.

Chapter 2. Structural Transformations and Ferromagnetism

Preface

This part is focused on the studies of the bimetallic cyano-bridged polymers, showing interesting structural transformations as well as magnetic properties. As prime technique X-ray diffraction was used to analyze the structures. The *in-situ* measurements using Powder X-ray diffraction method provided information on structural transformations.

Sections 2.1 and 2.3 are dedicated to reversible structural transformations of the bimetallic cyano-bridged polymers. The novelty of the work reported concerns the demonstration of the existence of a reversible structural phase transition induced by dehydration and subsequent rehydration of a well-characterized crystalline material. The transition, and its reversibility, has been demonstrated by *in-situ* synchrotron Powder diffraction measurements (Section 2.1) and Powder diffraction measurements (Section 2.3). Section 2.2 focuses on the magnetic properties of two new $Cu^{II}Cr^{III}$ cyano-bridged polymers. From the magnetic point of view, the 3D polymer shows three-dimensional ferromagnetic ordering at ca. 4K. The new chiral 1D polymer shows a weak intra-chain ferromagnetic exchange, as a result of magnetic orbital orthogonality between Cr^{III} and Cu^{II} in the chain, with very long Cu-N(cyano) distances (2.665(5) and 2.671(5) Å) due to the long Jahn-Teller axis of the copper(II) ions.

2. 1

"Sponge-Like" Reversible Transformation of a Bimetallic Cyanometallate Polymer

Olha Sereda, Antonia Neels, Fritz Stoeckli, Helen Stoeckli-Evans,* and Yaroslav Filinchuk

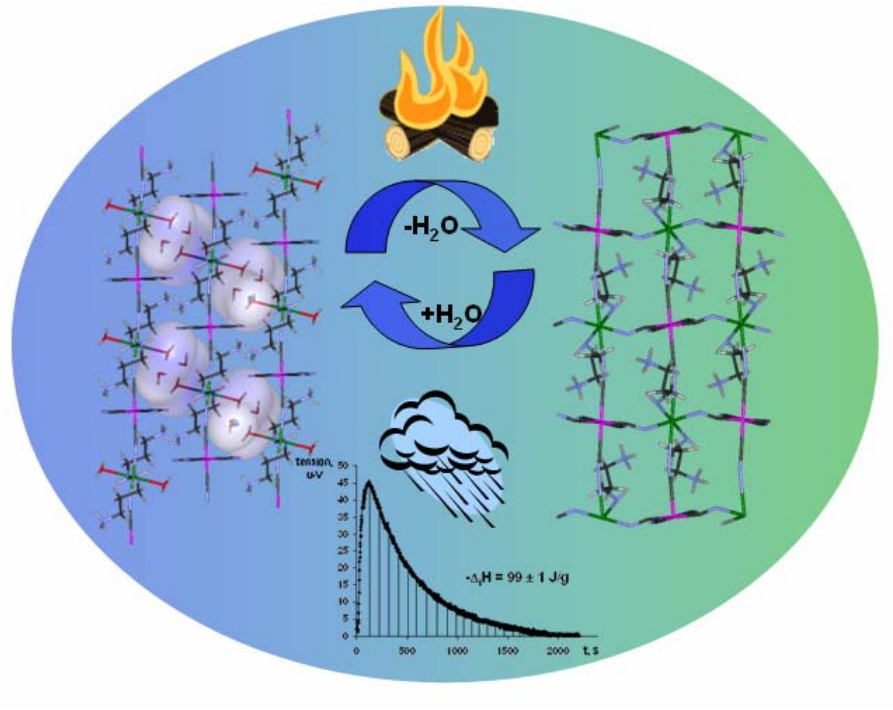

ABSTRACT: Two new cyano-bridged Ru-Cu polymers, the one-dimensional chain $\{[Cu(tnH^+)_2(H_2O)_2][Ru(CN)_6]\cdot 2H_2O\}_\infty$ (**1**) (where tn = 1,3-diaminopropane), and the pseudo-two-dimensional network, $\{[Cu(tnH^+)_2][Ru(CN)_6]\}_\infty$ (**2**), have been prepared and fully characterized. Compounds **1** and **2,** both crystallizes in the same monoclinic space group, $P2_1/n$. Complex **1** was characterized by single crystal X-ray analysis and compound **2** by X-ray powder diffraction (XRPD) techniques. Compound **2** was prepared by dehydration of **1;** structure **1** can be regenerated by rehydration of **2**. The "sponge-like" behavior of this molecular transformation is accompanied by a color change and has been shown by *in-situ* X-ray powder diffraction and immersion calorimetry to be completely reversible.

Introduction

The design and synthesis of nanoporous materials mimicking zeolities has drawn a great deal of attention due to their potential applications as gas adsorbents,[1-4] ion-exchanger,[5-8] chemical adsorbents,[4, 9-11] and heterogeneous catalysts.[11, 12] Some examples of these materials include cyano-bridged coordination polymers prepared by assembling cyanometallate anions [for example, $M(CN)_2^{2-}$ (M=Au, Ag), $Ni(CN)_4^{2-}$, $M1(CN)_6^{3-}$ (M1=Fe(III), Cr), $M2(CN)_6^{4-}$ (M2=Fe(II), Ru)] and transition metal complexes as building blocks. Since copper (II) ion exhibits great stereochemical plasticity, a variety of compounds with hexacyanometalates can be prepared, using ligands such as 1,2-ethylendiamine (en) $Cu(en)_2[Au(CN)_4]_2$,[13] cyclohexane-1,2-diamine (chxn) $[Ni(\textit{cis}\text{-}chxn)_2]_3[Fe(CN)_6]_2$ [14] or 1,3-diaminopropane (tn) $[Cu(tn)]_3[Cr(CN)_6]_2 \cdot 3H_2O$.[15] Cyano groups are useful owing to their ability to link metal atoms for the construction of multidimensional systems. Currently, hexacyanometallates have been used to develop a wide range of architectures, some of which exhibit interesting magnetic properties.[16-19] The Prussian blue family are amongst the earliest known coordination compounds and their diverse magnetic and electronic properties have been extensively studied.[20] Up till now the gas sorption properties of such systems have remained largely unexplored.[21] Only few examples of cyano-bridged inorganic coordination polymers based on hexacyanometallates, have been reported as being porous materials.[22-24] We have focused our efforts on the study of crystalline materials since the attainment of well-defined structures is intimately linked to an understanding of the design, synthesis and properties of these materials.

Experimental Section

Elemental analyses of carbon, hydrogen, and nitrogen were performed by the Microanalysis Service of the Laboratory of Pharmaceutical and Organical Propedeutical Chemistry at the University of Geneva (Geneva, Switzerland). Infrared spectra were measured using KBr pellets in the interval of 4000-400 cm^{-1} and were recorded on a Perkin-Elmer 1720X FT-IR spectrometer. Thermogravimetric (TG) analyses were carried out using a Mettler 4000 module. DSC measurements were done with a modified differential scanning calorimeter (Mettler Toledo DSC 822e. Samples were introduced in a closed aluminum oxide crucible and heated at a rate of 0.1°C min^{-1} under nitrogen at atmospheric pressure. Immersion calorimetry experiments were carried out at 293 K on samples of 0.150-0.200 g using a TIAN-CALVET type calorimeter[25, 26]. The out-gassed samples were placed in the calorimetric cells, which were immersed in a water bath controlled by a thermo-regulator system LUDA MS. The thermal flow was provided by 180 thermocouples of Cu/constantan connected to a nanovoltmeter PREMA 8017. The integral of the curve, $V=f(t)$, is proportional to the energy generated during the immersion process, $\Delta_i H$. The normal calibration of the calorimetry system was carried out with an electric resistance. The accuracy varies between 4 and 5 % depending on the absolute energy liberated in the process and on the amount of solid used.

General Synthetic Procedures

$\{[Cu(tnH^+)_2(H_2O)_2][Ru(CN)_6]\cdot 2H_2O\}_\infty$ (1). 1,3-Diaminopropane (tn) (1.0mL, 12.0 mmol) was added under aerobic conditions to a concentrated aqueous solution (10 mL) of

$CuSO_4 \cdot 5H_2O$ (2.9g, 12.0 mmol) with continuous stirring, leading to the immediate precipitation of a green powder. After addition of an aqueous solution of potassium hydroxide (12 mmol) the resulting dark-blue solution was warmed (60°C for about 10min) and then filtered in order to remove the small amount of precipitate that remained. An aqueous warm solution (10 mL) of $K_4[Ru(CN)_6]$ (2.47 g, 6 mmol) was then added with continuous stirring. Further evaporation afforded hexagonal dark blue crystals of **1** after several weeks under aerobic conditions; these were filtered and air-dried. All the operations for the synthesis were carried out in the dark to avoid the decomposition of $[Ru(CN)_6]^{4-}$. Yield: 80%. The results of elemental analyses (found C, 26.36; H, 5.51; N, 25.67. $C_{12}H_{30}N_{10}Cu_1Ru_1O_4$ requires C, 26.54; H, 5.57 N, 25.79 %) were consistent with the formula of the sample used for X-ray analysis.

$\{[Cu(tnH^+)_2][Ru(CN)_6]\}_\infty$ (2). Compound **2** was obtained as a green powder by heating crystals of complex **1** to 120°C. The results of elemental analyses for compound **2** (found C, 30.36; H, 4.52; N, 29.61. $C_{12}H_{22}N_{10}Cu_1Ru_1$ requires C, 30.60; H, 4.71 N, 29.74%) were consistent with the formula of the sample used for powder diffraction analysis.

X-ray Structural Determination.

A blue hexagonal shaped crystal of **1** (0.45 x 0.42 x 0.05 mm^3) was mounted on a Stoe Mark II-Imaging Plate Diffractometer System equipped with a graphite-monochromator. Data collection was performed using Mo-Kα radiation (λ = 0.71073 Å) at 173 K. The structure was solved by direct methods using the program SHELXS-97[27] and refined by full matrix least squares on F^2 with SHELXL-97.[28] All non-hydrogen atoms were refined anisotropically. The water hydrogen atoms in **1** were derived from difference

Fourier Maps and were refined isotropically, while the remaining hydrogen atoms were included in calculated positions and treated as riding atoms using SHELXL-97 default parameters.

X-Ray powder diffraction.

X-ray powder diffraction data were collected at room temperature on a computer controlled STOE-STADIP focusing powder diffractometer equipped with a curved Ge(111) monochromator ($CuK\alpha_1$; λ = 1.54051Å). A STOE linear position sensitive detector was used. The green powder sample **2** was inserted in a glass capillary of 0.5 mm diameter. The compounds were measured in the range of $4° \leq 2\theta \leq 80°$ using a step width of 0.1°. The indexing procedure was performed using ITO[29] in WinXPow.[30] The structure solution was carried out using the program DASH[31] introducing a structural model.[32] The obtained position of the molecule in the given symmetry and unit cell was used for Rietveld refinement in GSAS/EXPGUI.[33, 34] After the initial refinement of the scale and unit cell constants, the atomic positions were refined using soft constraints defining the geometry of the molecule within some allowable errors. Subsequent Rietveld refinement was carried out using gradually relaxing bond restraints. The non-hydrogen atoms were refined isotropically applying an overall temperature factor for the all C and all N atoms. The H-atoms were treated as riding atoms, their temperature factors were fixed. In the final cycles of refinement, the shifts in all parameters were less than their estimated standard deviations. Further details of the data collection and refinement are given in Table 1.

Table 1. Crystal and Structure Refinement Data for **1** (single crystal) and **2** (powder).

	1	**2**
formula	$C_{12}H_{30}N_{10}O_4CuRu$	$C_{12}H_{22}N_{10}Cu_2Ru$
Mw	543.07	470.99
λ(Å)	0.71073	1.54051
T(K)	173	293
crystal system	monoclinic	monoclinic
space group	$P2_1/n$	$P2_1/n$
a(Å)	10.3003(9)	9.7292(5)
b(Å)	9.0112(8)	12.0350(5)
c(Å)	12.0042(11)	8.2574(4)
β(°)	105.136(7)	111.701(3)
V(Å^3)	1075.55(17)	898.34(4)
Z	2	2
ρ_{calcd}(Mg/m^3)	1.677	1.741
μ(mm^{-1})	1.730	8.41
refl. collected	12515	-
indep. refl.	2897	-
indep. refl. >2σ(I)	2318	1078
no. of param.	141	84
R1[a] [$I > 2\sigma(I)$]	0.027	-
wR2[b] [$I > 2\sigma(I)$]	0.0574	-
No.contributing reflns	-	1078
No. of struct. param.	-	84
No. of restraints	-	70
R_{wp}[c]	-	0.0716
R_p[d]	-	0.055
R_F[e]	-	0.125
$\Delta\rho_{max}/\Delta\rho_{min}$ (eÅ^{-3})	0.576/-0.741	1.041/-0.728

[a] $R1 = \Sigma||F_O| - |F_C||/\Sigma|F_O|$. [b] $wR2 = [\Sigma w(F_O^2 - F_C^2)^2/\Sigma wF_O^4]^{1/2}$. [c] $R_{wp} = [\Sigma w(I_O - I_C)^2/\Sigma wI_O^2]^{1/2}$, [d] $Rp = \Sigma|I_O - I_C|/\Sigma I_C$, [e] $R_F = \Sigma|F_O| - |F_C|/\Sigma|F_O|$.

Results and Discussion

Synthesis, IR analysis and structure description.

Complex $\{[Cu(tnH^+)_2(H_2O)_2][Ru(CN)_6]\cdot 2H_2O\}_\infty$ (**1**) was formed as dark-blue hexagonal plate-like crystals by treating $K_4[Ru(CN)_6]$ with a mononuclear copper(II) complex, generated in situ from 1,3-diaminopropane (tn) and copper sulfate. In the IR spectrum the bands expected for both the ligand and the counter ions are present (Figure S1 in the Supporting Information). Coordination of the CN ligand to a second metal ion through its nitrogen atom results in a shift of these values to around 2065 -2110 cm^{-1} for $[Ru(CN)_6]^{4-}$.[35] Three strong cyanide absorption bands were found at 2106, 2068 and 2044 cm^{-1}; this is in good agreement with the presence of $[Ru(CN)_6]^{4-}$ units having at least one terminal CN ligand, as indicated by the lower wave number band.[35, 36] For compound **1,** the supplementary weak bands observed in the 2700-2500 cm^{-1} region could be tentatively assigned to ν(NH) stretching vibrations of the uncoordinated NH_3^+ group. The X-ray structural analysis of complex **1** revealed the formation of a one-dimensional polymer (Figure 1), which is isostructural with the $[Fe(CN)_6]^{4-}$ analogue $[Cu(tnH)_2(H_2O)_2][Fe(CN)_6]\cdot 2H_2O$.[37] The structure can be described as a linear chain with alternating $[Cu(tnH^+)_2(H_2O)_2]^{4+}$ and $[Ru(CN)_6]^{4-}$ units, bridged by the CN groups. The asymmetric unit in **1** consists of half a $[Ru(CN)_6]^{4-}$ anion, half a $[Cu(tnH^+)]^{2+}$ cation, and two water molecules, one of which is coordinated to the copper(II) atom (Figure S2 in the Supporting Information). The Cu atom is hexacoordinate with a strong pseudo Jahn-Teller effect. In the equatorial plane it is bonded to two nitrogen atoms of the linear tn ligands, Cu1─N(tn) = 2.049(1) Å, and to two nitrogen atoms from the CN groups, Cu1─N(CN) = 1.973(2) Å. The apical positions are occupied by two water molecules,

Cu1-O(H_2O) = 2.606(1) Å. The coordination polyhedron of the Cu atoms can be described as Cu(tnH^+)$_2$(H_2O)$_2$(NC)$_2$ or CuN4O2. It is worth noting that the tn unit is protonated and coordinates in a monodentate manner (Figure 1 and see Table 1).

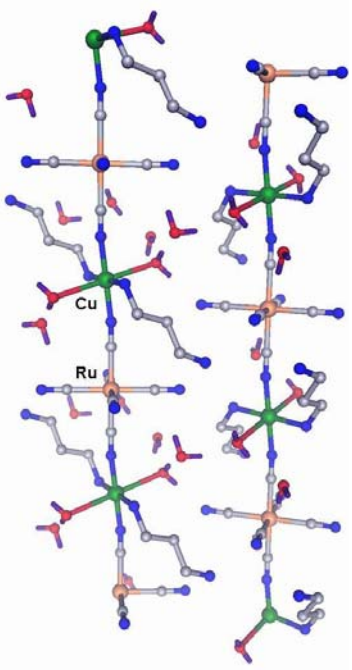

Figure 1. A partial view of the 1D polymer structure of **1** (H-atoms on the ligand tn have been omitted for clarity).

Four of the six CN^- groups are non-bridging, while the other two bond to the Cu atoms giving rise to Ru─C≡N─Cu bridges. The Ru^{II} ion has an almost perfect octahedral RuC6 coordination geometry [Ru─C bond lengths 2.0307(15) - 2.0361(15) Å; Ru─C≡N bond angles 178.82(13) - 179.55(13)°]. The Ru─C and C─N bond distances and C─Ru─C angles are in good agreement with those in similar compounds.[36, 38, 39]

TG and DSC analysis. The thermal stability of **1** has been studied by thermogravimetric analysis (TGA) and differential scanning calorimetry (DSC). Compound **1** contains two coordinated water molecules and two water molecules of crystallization. It was expected

that dehydration of **1** would dramatically change the structure. Thermal analysis indicates that the weight loss is 13.52% in the temperature range 45-105°C, which corresponds to the loss of four water molecules (theoretical value 13.65%) (Figure S3 in the Supporting Information). The DSC studies, after sample incubation at 0ºC followed by heating at a rate of 1º min^{-1} to 150ºC, showed only one endothermic effect at 95ºC (ΔH = 390 J/g). The dehydrated compound, **2**, is green, insoluble in most common solvents, but highly micro-crystalline. Powder X-ray diffraction methods were used to determine its three-dimensional structure (Figure 2),

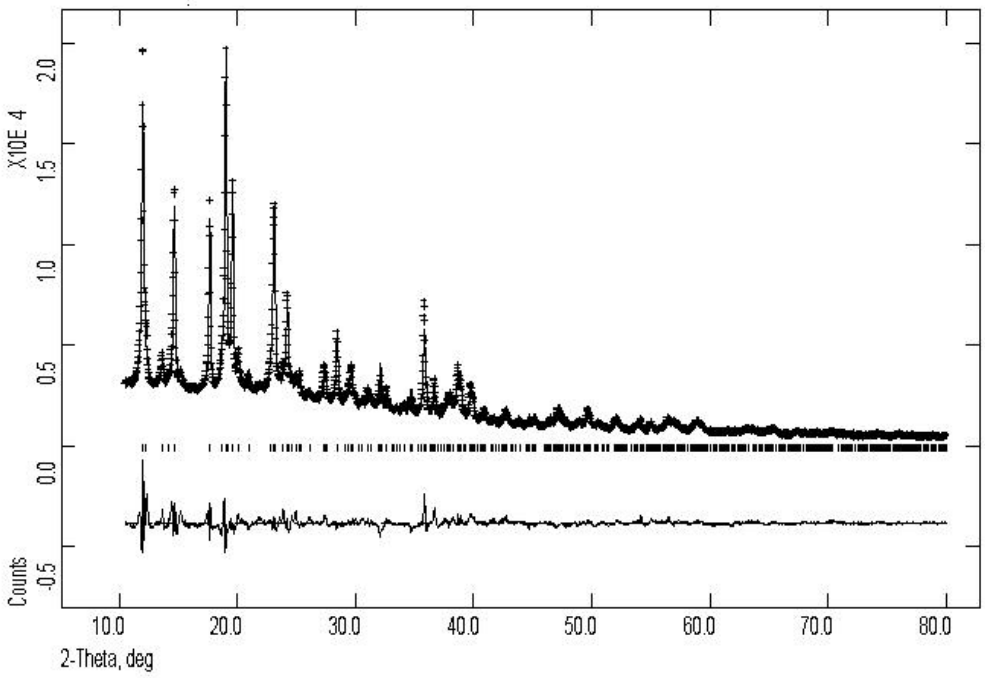

Figure 2. The Rietveld refinement for compound **2**; including the difference curve between the calculated (-) and measured (+) X-ray powder diffractograms.

which indicates that **1** has been transformed from a 1D polymer into a grid-like polymer structure (Figure 3), with a reduction in the unit cell volume of ca. 10%.

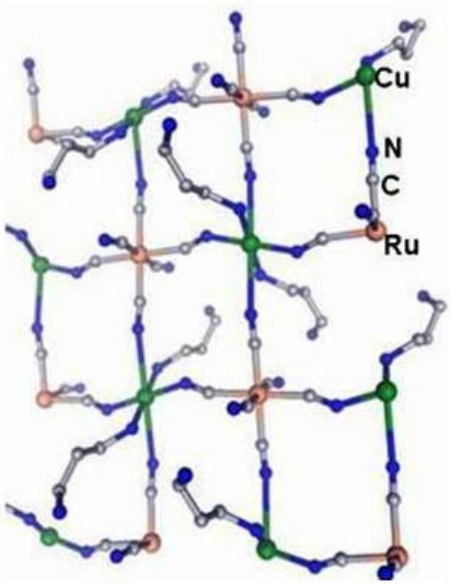

Figure 3. A partial view of the grid-like polymer structure of **2** (H-atoms have been omitted for clarity).

The IR spectra of **2** (Figure S1 in the Supporting Information) confirmed the absence of water bands in the region 3400-3360 cm^{-1} for $\nu_{as,s}$ (OH) and 1650-1600 cm^{-1} for δ (HOH). The Cu atom is again hexacoordinated with a strong pseudo Jahn-Teller effect. This time in the equatorial plane it is bonded to two nitrogen atoms of the linear tn ligands (2.057(7) Å) and to two nitrogen atoms from the CN groups (2.025(5) Å) (Figure S4 in the Supporting Information). The apical positions are occupied by two nitrogen atoms of CN groups but with unusually long bonds, 2.902(2) Å. Such long bonds are not uncommon, for example, in $[Cu(cis\text{-chxn})_2]_3[Fe(CN)_6]_2 \cdot 7H_2O$[40] the Cu–N(cyano) distance is 2.818Å, in $[Cu(N\text{-en})_2]_3[Co(CN)_6]_2$[41] (where N-en= N-ethylethylene-1,2-diamine) the same distance is 2.828 Å, while in $[Cu^{II}(tetrenH_2)][Cu^{II}(tetrenH)][W^{V}(CN)_8][W^{IV}(CN)_8] \cdot 2.5H_2O$ (where tetren = tetraethylenepentamine)[42] and $[Cu(chxn)_2][Ni(CN)_4] \cdot 2H_2O$[43] extremely long Cu–N(cyano) distances are observed, 3.114 and 3.12 Å, respectively. The coordination polyhedron of the Cu atoms can be

described as $Cu(tnH^{+})_2(NC)_4$ or CuN6. Hence, in **2** four of the six CN^- are bridging. The Ru^{II} ion has an octahedral RuC6 coordination geometry [Ru─C bonds 2.0307(15) - 2.0361(15) Å]. In contrast to **1** the Ru-C≡N bond angles vary from 155.5(14) to 173.8(26)º.

When the green powder (that is, **2**) was exposed to water the color changed to blue, suggesting a change in the coordination geometry of the metal center. Solid state UV spectra of both **1** and **2** indicate a clear bathochromic shift of the maximum from 380 nm in **1** to 470 nm in **2**, Figure 4. In the IR spectrum the bands associated with the presence of the water molecules reappeared, showing that the water loss is reversible in nature.

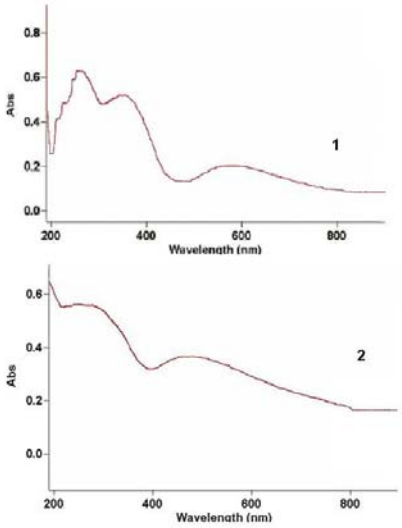

Figure 4. Solid state UV/vis absorption spectra of compounds **1** and **2**.

The reversibility of this process was also confirmed by *in-situ* synchrotron powder X-ray diffraction (PXRD) measurements (Figure 5 and Table 1). A capillary containing a powdered sample of **1** (Figure 5, **A**) was slowly heated and its transformation to **2** was observed (Figure 5, **B**). By passing a stream of nitrogen gas saturated with water vapour through the capillary, it was possible to regenerate the blue solid (Figure 5, **C**), which has

peak positions and intensities fully coincident to those observed for the single crystal of **1** (Figure 5, **A**). Complex **2**, therefore, exhibits "sponge-like" molecular properties: it can easily take up water molecules and return to the original structure, **1**.

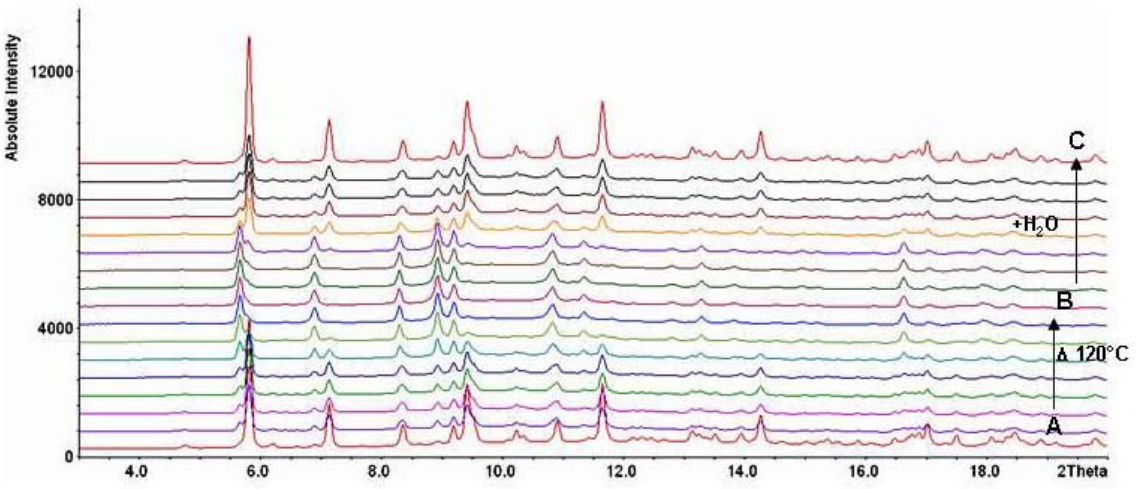

Figure 5. *In-situ* synchrotron powder X-ray diffraction (PXRD) patterns: **A** - powdered single-crystals of **1**; **B** - after thermal treatment of **1**; i.e. transforms to compound **2; C** - after flowing H_2O vapour through the capillary containing **2**; i.e. structure **1** is regenerated.

It was possible to repeat this process a number of times without any loss of crystallinity of either compounds, **1** or **2.** Complex **1** originally forms parallel polymer chains slightly displaced with respect to one another and separated by two water molecules of crystallization (Figure 6). They are linked by O-H…O hydrogen bonds which give rise to the formation of helical chains of water molecules running parallel to the 2-fold crystallographic screw axis (Figure 6, **1** on l-h-s). After heating, a grid-like structure, (**2**), is obtained (Figure 6, **2** on r-h-s). The TG analysis indicates that all four water molecules are lost between 45-105°C.

We assume that the water molecules of crystallization are lost first, allowing the chains to approach one another. After loss of the coordinated water molecules the chains

slip parallel to one another enabling a $C\equiv N^-$ group to fill the free coordination site on the copper atoms. This in turn weakens the original Cu…N≡C bond in **1**. The direction of the pseudo Jahn-Teller effect in **2** is now perpendicular to that in **1**. These changes involve a reduction from 12.004 Å in the length of the c axis of **1** to 8.257 Å in the length of the c axis of **2** (ratio ca. 4:3), and a corresponding increase from 9.011 to 12.035 Å (ratio ca. 3:4) in the length of the b axes (Figure S5 in the Supporting Information).

Evidently, the key to the observed phenomena is the ability to break and reform the network, which is turn results in the change in the copper atom coordination sphere, from CuN4O2 to CuN6 (Figure 6).

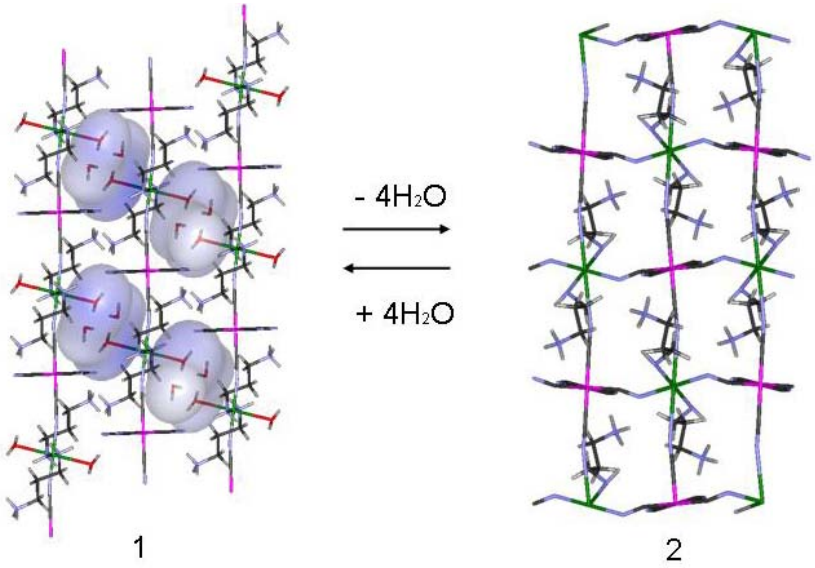

Figure 6. View of the reversible transformation of compound **1** to **2**, as the result of a simple dehydration-rehydration process. The helical chains of hydrogen bonded water molecules are represented by the large white surfaces in **1** (l-h-s).

Surprisingly the system **1/2** is selective for water only. Attempts to adsorb other small molecules, like CH_3OH or CH_3CN, were unsuccessful, as shown by PXRD (Figure S6 in the Supporting Information), immersion calorimetry (Table S1 in the Supporting

Information), and the color of the solid which, remained green. The unique property of this assembly is the complete reversibility of the molecular structure, as well as the color change, under a simple dehydration-rehydration process.

Immersion calorimetry. Immersion calorimetric studies were carried out with compound **2**. This technique, applied mainly to carbons, provides an insight into the filling of nanopores.[44-46] The enthalpies of immersion of **2**, $\Delta_i H$, into acetonitrile and methanol are very low, which suggests exclusion from the structure. On the other hand, for water (Table S1 in the Supporting Information) an average value of – 99.5 ± 3 J per gram of solid was obtained, which corresponds to - 46.6 kJ per mole of **2.** It is likely, that this value reflects essentially the heat of transformation of the grid-like structure into the original 1D polymer.

Kinetics measurements for complex **2** at different temperatures have also been carried out by exposing it to H_2O vapor close to the corresponding saturation pressures (Figure 7). During these isobaric processes, which lasted between 50 and 130 minutes, the sample color changed from green to blue. The activation energy for the reaction **2 →1** obtained from the classical Arrhenius plot (Figure S7 in the Supporting Information) is *ca*. 60 kJ mol^{-1}. It is also found that complex **2** adsorbs 7.3 mmol of H_2O per gram, which corresponds to ca. 3.5 water molecules per mole of **2**. This is close to the expected number of 4 water molecules in the resulting complex $\{[Cu(tnH^+)_2][Ru(CN)_6]\cdot 4H_2O\}_\infty$ (**1**).

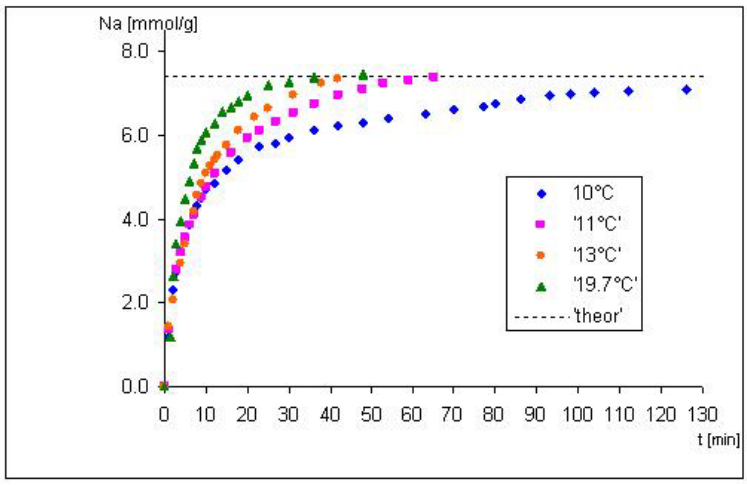

Figure 7. Kinetics of water vapour adsorption by compound **2** between 10 and 19.7°C.

Conclusions

Compound **1** is, to the best of our knowledge, the first example of a reversible structural transformation in a bimetallic hexacyanoruthenate coordination complex. X-ray powder diffraction analysis confirmed the transformation of the 1D polymer structure, (**1**), into a grid-like structure, (**2**), giving rise to coexistence of pseudo Jahn-Teller elongation. The unique aspect of this system is the "sponge-like" behavior of the molecular transformation and the color change, which are completely reversible under a simple dehydration-rehydration process. These results also present further evidence that solid materials do not need to be porous to reversibly adsorb small molecules.[47, 48] Future investigations of the vapor adsorption properties of **2** using a combination of *in-situ* Raman spectroscopy and powder X-ray diffraction will, we hope, help to explain the mechanism of this reversible process and why it is apparently selective for water only.

Acknowledgements. We thank the Swiss National Science Foundation for financial support (Grant № 20-111738).

References

[1] O. M. Yaghi, G. Li, H. Li, *Nature* **1995**, *378*, 703.
[2] H. Li, M. Eddaoudi, M. O'Keeffe, O. M. Yaghi, *Nature* **1999**, *402*, 276.
[3] H. Li, M. Eddaoudi, T. L. Groy, O. M. Yaghi, *J. Am. Chem. Soc.* **1998**, *120*, 8571.
[4] M. Eddaoudi, O. M. Yaghi, *J. Am. Chem. Soc.* **2000**, *122*, 1391.
[5] X. Zhao, B. Xiao, A. J. Fletcher, K. M. Thomas, D. Bradshaw, M. J. Rosseinsky, *Science* **2004**, *306*, 1012.
[6] O. M. Yaghi, H. Li, *J. Am. Chem. Soc.* **1995**, *117*, 10401.
[7] O. M. Yaghi, H. Li, *J. Am. Chem. Soc.* **1996**, *118*, 295.
[8] B. F. Hoskins, R. Robson, *J. Am. Chem. Soc.* **1990**, *112*, 1546.
[9] S. S.-Y. Chui, S. M.-F. Lo, J. P. H. Charmant, A. G. Orpen, I. D. Williams, *Science* **1999**, *283*, 1148.
[10] O. M. Yaghi, C. E. Davis, G. Li, H. Li, *J. Am. Chem. Soc.* **1997**, *119*, 2861.
[11] T. Sawaki, T. Dewa, Y. Aoyama, *J. Am. Chem. Soc.* **1998**, *120*, 8539.
[12] M. Fujita, Y. J. Know, S. Washizu, K. Ogura, *J. Am. Chem. Soc.* **1994**, *116*, 1151.
[13] C. J. Shorrock, H. Jong, R. J. Batchelor, D. B. Leznoff, *Inorg. Chem.* **2003**, *42*, 3917.
[14] E. Coronado, C. J. Gomez-Garcia, A. Nuez, F. M. Romero, J. C. Waerenborgh, *Chem. Mater.* **2006**, *18*, 2670.
[15] F. Thétiot, S. Triki, J.-S. Pala, C. J. Gómez-García, S. Golnen, *Chem. Commun.* **2002**, 1078.
[16] M. Ohba, N. Fukita, H. Okawa, *J. Am. Chem. Soc.* **1997**, *119*, 1011.
[17] H. Miyasaka, N. Matsumoto, H. Okawa, N. Re, E. Gallo, C. Floriani, *J. Am. Chem. Soc.* **1996**, *118*, 981.
[18] E. Coronado, C. Gimenez-Saiz, J. M. Martinez-Agudo, A. Nuez, F. M. Romero, H. Stoeckli-Evans, *Polyhedron* **2003**, *22*, 2435.
[19] I. P.-Y. Shek, W.-F. Yeung, T.-C. Lau, J. Zhang, S. Gao, L. Szeto, W.-T. Wong, *Eur. J. Inorg. Chem* **2005**, 364.
[20] M. Verdaguer, A. Bleuzen, V. Marvaud, J. Vaissermann, M. Seuleiman, C. Desplanchas, A. Scuiller, C. Train, R. Garde, G. Gelly, C. Lomenech, I. Rosenman, P. Veillet, C. Cartier, F. Villain, *Coord. Chem. Rev.* **1999**, *190-192*, 1023.
[21] L. G. Beauvais, J. R. Long, *J. Am. Chem. Soc.* **2002**, *124*, 12096.
[22] T. Pretsch, K. W. Chapman, G. J. Halder, C. J. Kepert, *Chem. Commun.* **2006**, 1857.
[23] K. W. Chapman, P. J. Chupas, C. J. Kepert, *J. Am. Chem. Soc.* **2006**, *128*, 7009.
[24] R. C. Bansal, J. B. Donnet, F. Stoeckli, *Active Carbon*, Marcel Dekker, New York, **1988**.
[25] F. Stoeckli, D. Hugi-Cleary, T. A. Centeno, *J. Eur. Ceram. Soc.* **1998**, *18*, 1177.
[26] G. M. Sheldrick, SHELXS-97 & *SHELXL-97*, University of Göttingen, Germany, **1997**.
[27] J. W. Visser, *J. Appl. Cryst.* **1969**, *2*, 89.
[28] WinXPow, *STOE Powder Diffraction Software*, Stoe & Cie GmbH, Darmstadt, Germany.
[29] DASH, *CCDC Software*, 12 Union Road, Cambridge CB2 1EZ, UK.

[30] PCMODEL V8.5, *Serena Software*, Box 3076, Bloomington, IN 47402-3076.
[31] A. Larson, R. Von Dreele, *General Structure Analysis System*, Los Alamos National Laboratory Report LAUR 86-748., **2000**.
[32] B. H. Toby, *J. Appl. Cryst.* **2001**, *34*, 210.
[33] K. Nakamoto, *Infrared and Raman Spectra of Inorganic and coordination Compounds*, 3rd ed., Wiley, New York, **1978**.
[34] D. F. Mullica, P. K. Hayward, E. L. Sappenfield, *Inorg. Chim. Acta* **1996**, *253*, 97.
[35] S. Triki, J. Sala-Pala, F. Thétiot, C. J. Gomes-Garcia, J.-C. Daran, *Eur. J. Inorg. Chem* **2006**, 185.
[36] D. F. Mullica, P. K. Hayward, E. L. Sappenfield, *Inorg. Chim. Acta* **1995**, *237*, 111.
[37] M. Rüegg, A. Ludi, K. Rieder, *Inorg. Chem.* **1971**, *10*, 1773.
[38] E. Coronado, C. Gimenez-Saiz, A. Nuez, V. Sanchez, F. M. Romero, *Eur. J. Inorg. Chem* **2003**, 4289.
[39] T. Akitsu, Y. Einaga, *Acta Crystallogr.,Sect.E:Struct.Rep.Online* **2006**, *62*, m750.
[40] R. Podgajny, T. Korzeniak, K. Stadnicka, Y. Dromzée, N. W. Alcock, W. Errington, K. Kruczała, M. Bałanda, T. J. Kemp, M. Verdaguer, B. Sieklucka, *Dalton Trans.* **2003**, 3458.
[41] T. Akitsu, Y. Einaga, *Inorg. Chem.* **2006**, *45*, 9826.
[42] F. Stoeckli, *Adsorption Science and Technology* **1993**, *10*, 3.
[43] F. Stoeckli, A. Lavanchy, D. Hugi-Cleary, *Fundamentals of adsorption* **1998**, *6*, 24.
[44] F. Stoeckli, D. Hugi-Cleary, T. A. Centeno, *J. Eur. Ceram. Soc.* **1998**, *18*, 1177.
[45] E. Colacio, F. Lloret, R. Kivekas, J. Riuz, J. Suarez-Varela, M. R. Sundberg, *Chem. Commun.* **2002**, 592.
[46] L. J. Barbour, *Chem. Commun.* **2006**, *11*, 1163.
[47] E. Colacio, F. Lloret, R. Kivekas, J. Riuz, J. Suarez-Varela, M. R. Sundberg, *Chem. Commun.* **2002**, 592.
[48] L. J. Barbour, *Chem. Commun.* **2006**, *11*, 1163.

Supporting Information

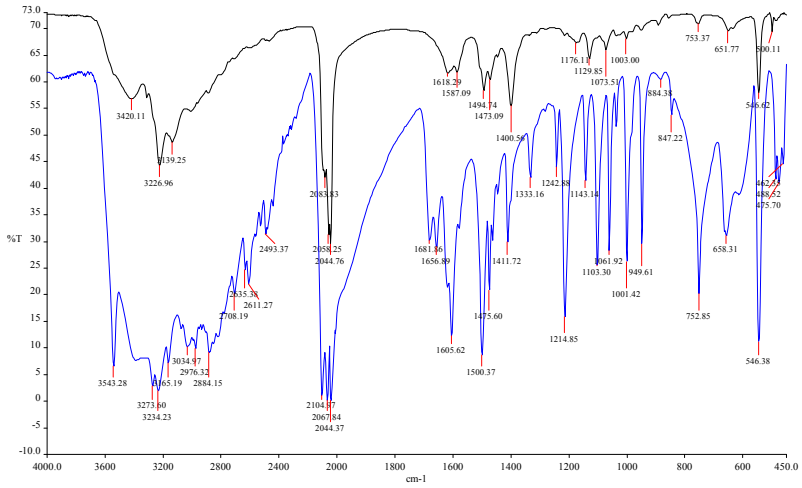

Figure S1. IR spectra of compounds **1** (blue) and **2** (black).

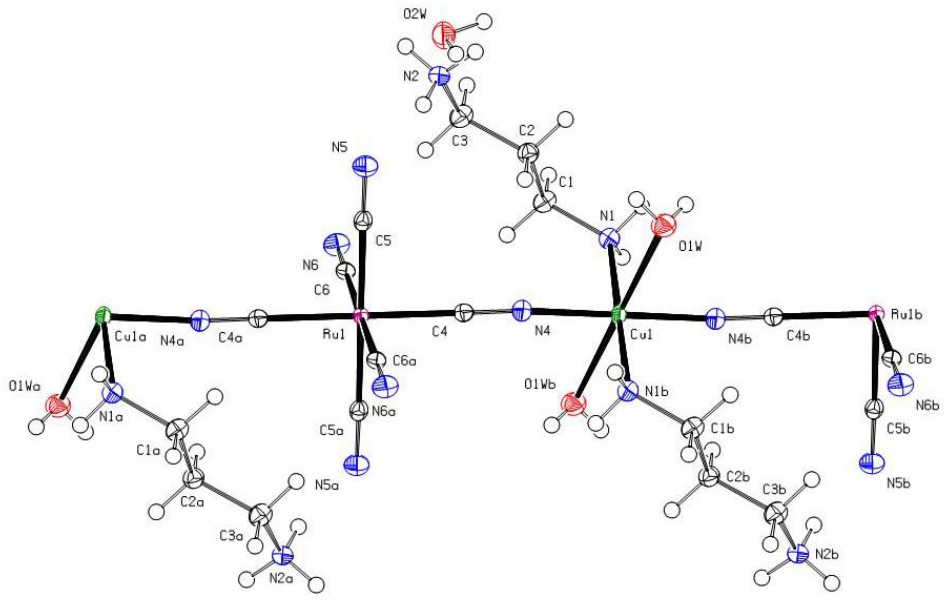

Figure S2. View of the molecular structure of compound **1**, showing the labelling scheme and thermal ellipsoids drawn at the 50% probability level.

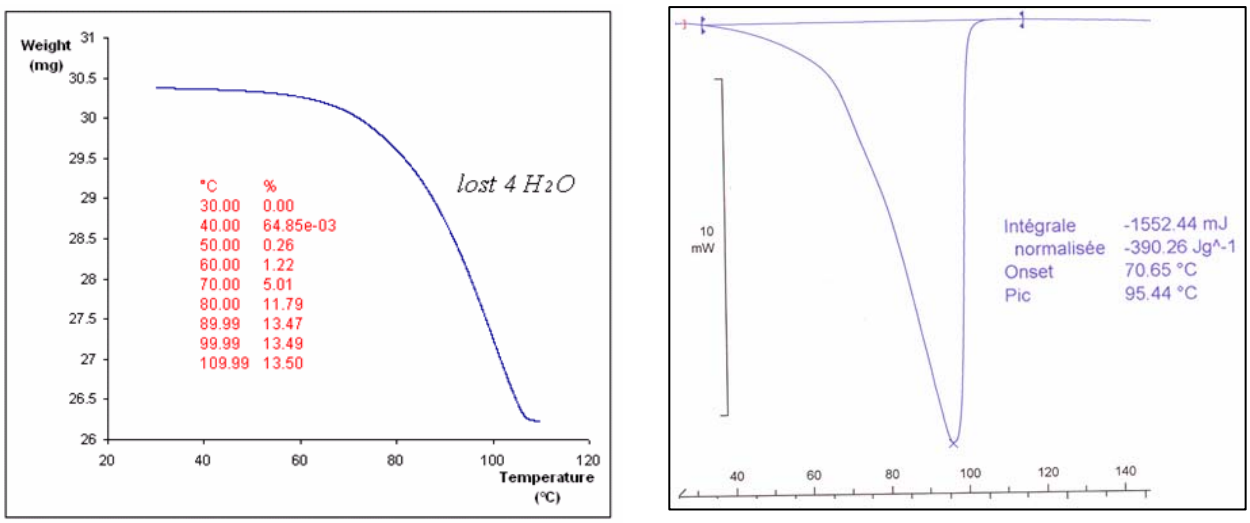

(a) **(b)**

Figure S3. TGA (a) and DSC (b) curves for $\{[Cu(tnH^{+})_2][Ru(CN)_6]\cdot 4H_2O\}_\infty$ (**1**); heating rate 1°C/min.

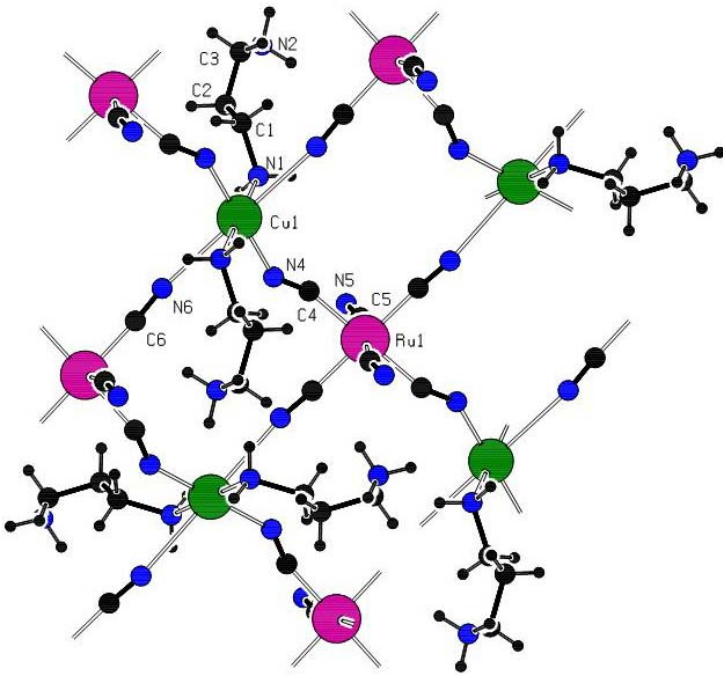

Figure S4. View of the molecular structure of compound **2**, showing the labeling scheme.

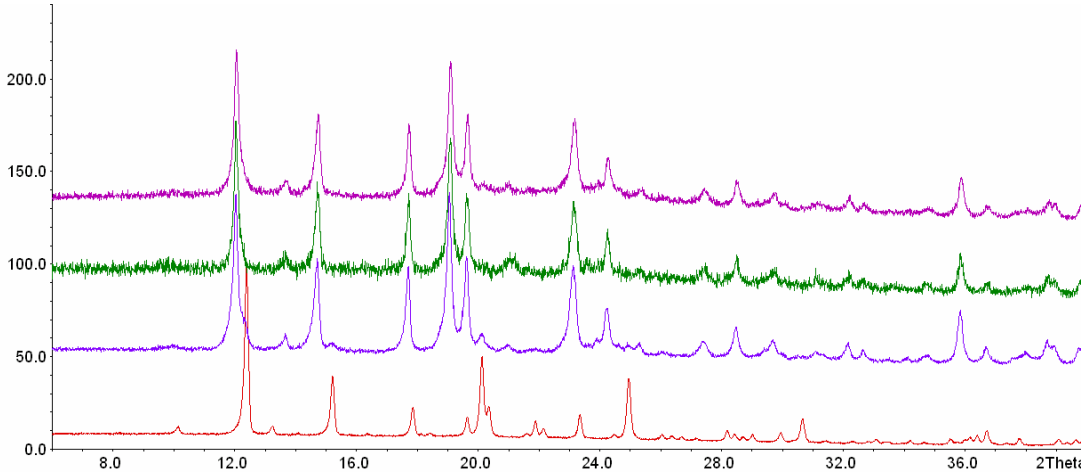

Figure S5. The PXRD patterns of (A, red) **1;** (B, violet) **2**; (C, green) dehydrated solid **2**, which was kept in methanol for one week; (D, pink) dehydrated solid **2**, which was kept in acetonitrile for one week.

Kinetics measurements

Kinetic measurements have been carried out by exposing **2** to H_2O vapour close to saturation pressure. The data fitted a first order kinetic and the corresponding rate constants, k, were analyzed by using the logarithmic form of the Arrhenius equation (Figure S7). It led to an activation energy of approximately 60 kJ mol^{-1}.

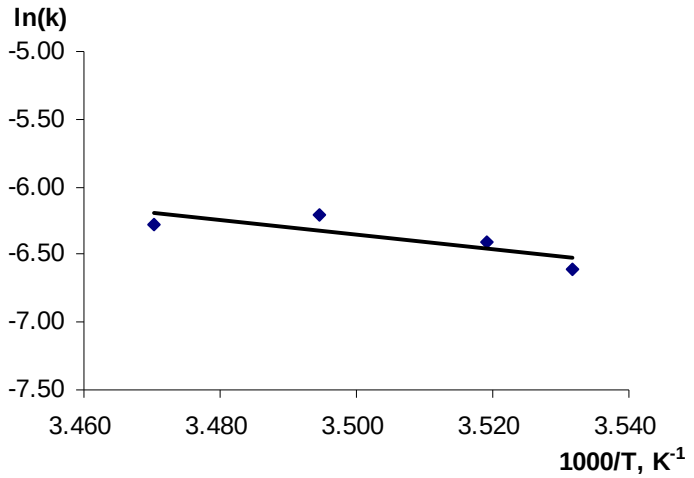

Figure S5. Arrhenius plot for the adsorption kinetics of the process **2→1** at 283, 284, 286, and 293 K.

Immersion calorimetry.

Immersion calorimetry experiments were carried out at 293 K on samples of 0.014-0.020 g using a TIAN-CALVET type calorimeter.[1-3] The outgassed samples of **2** were placed in the calorimetric cells which in turn are placed in a water bath controlled by a thermo-regulator system LUDA MS. The thermal flow was monitored by the current through 180 Cu/constantan thermocouples connected to a nanovoltmeter PREMA 8017. The integral of the voltage versus time curve, is proportional to the energy generated during the immersion process, typically between 1 and 10 J. The accuracy varies between 4 and 5 % depending on the absolute energy liberated in the process and on the amount of solid used. For water, the average value of $\Delta_i H$ was found to be -99 ± 1 J/g.

Table S1. Enthalpies of immersion, $\Delta_i H$, of compound **2** into water, methanol and acteonitrile.

Solvent	Weight, g	$-\Delta_i H$, J/g
Water	0.0156	97.6
	0.0143	96.3
	0.0145	98.5
	0.0145	99.4
	0.0156	98.5
	0.0150	98.9
	0.0174	104.5
	0.0173	102.3
Methanol	0.0175	5.7
	0.0124	4.2
Acetonitrile	0.0167	1.2
	0.0153	0.8

[1]. R. C. Bansal, J. B. Donnet, F. Stoeckli, *Active Carbon*, Marcel Dekker, New York, **1988**.
[2]. F. Stoeckli, D. Hugi-Cleary, T. A. Centeno, *J. Eur. Ceram. Soc.* **1998**, *18*, 1177.
[3]. F. Stoeckli, *Russ. Chem. Bull. Int. Ed.* **2001**, *50*, 2265.

2. 2

New 3D and Chiral 1D $Cu^{II}Cr^{III}$ Coordination Polymers Exhibiting Ferromagnetism

Olha Sereda, Joan Ribas and Helen Stoeckli-Evans*

Inorganic Chemistry (2008), 47(12), 5107-5113.

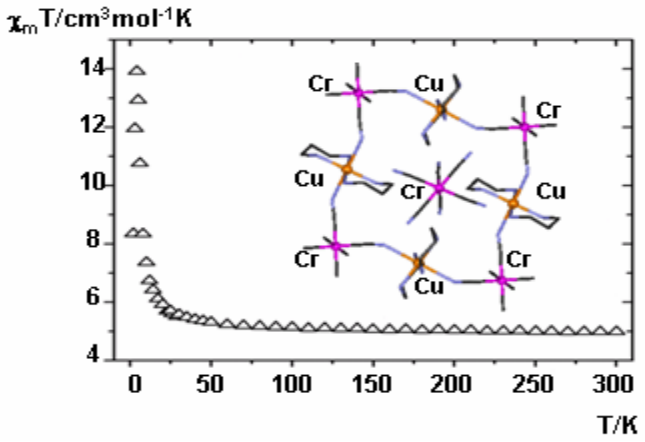

Abstract

The reaction of $K_3[Cr(CN)_6]$ and the copper (II) bis-diamino complex of the ligand 1,3-diaminopropane (tn) lead to the new cyanide-bridged three-dimensional polymer $\{[(Cu(tn)_2)_3(Cr(CN)_6)][Cr(CN)_6]\}_\infty$ (**1**). Crystallographic data for **1**: trigonal space group R-3, a = b = 15.4908(11) Å, c = 16.7699(13) Å, Z = 3, V = 3485.0(4) $Å^3$. By the same reaction using *trans*-cyclohexane-(1R,2R)-diamine [1R,2Rchxn] or *trans*-cyclohexane-(1S,2S)-diamine [1S,2Schxn] as ligand, the chiral one-dimensional polymers $\{[Cu(1R,2Rchxn)_2]_3[Cr(CN)_6]_2 \cdot 4.75H_2O\}_\infty$ (**2**) and $\{[Cu(1S,2Schxn)_2]_3[Cr(CN)_6]_2 \cdot 4.25H_2O\}_\infty$ (**3**), respectively, were obtained. Complexes **2** and **3** are isostructural and crystallize in the triclinic space group *P1,* with a = 8.5421(6), b = 12.6379(9), c = 16.1571(11) Å, α = 104.594(5)°, β = 98.425(6)°, γ = 97.440(5)°, Z = 1, V = 1644.3(2) $Å^3$ for **2**, and a = 8.5435(8), b = 12.6309(12), c = 16.1711(17) Å, α = 104.632º, β = 98.429(8)º, γ = 97.375(8)º, Z = 1, V = 1645.1(3) $Å^3$ for **3**. The complexes have been characterized by X-ray crystallography, IR and magnetic susceptibility measurements. The chirality of complexes **2** and **3** has been confirmed by circular dichroism measurements in the solid state. From the magnetic point of view, complex **1** shows three-dimensional ferromagnetic ordering at ca. 4K, and complex **2** shows a weak intra-chain ferromagnetic exchange, as a result of magnetic orbital orthogonality between Cr(III) and Cu(II) in the chain, with very long Cu-N(cyano) distances (2.665(5) and 2.671(5) Å) due to the long Jahn-Teller axis of the copper(II) ions.

Keywords: ferromagnetism, chiral, hexacyanochromate (III), metal-organic framework.

Introduction

The design and synthesis of well-characterized molecular-based magnets remains a challenge. They have been developed in an interdisciplinary research area in the past two decades. On the basis of past achievements, current interest is targeted on multifunctional magnets with other physical and/or chemical properties such as optical properties, electric conductivity, chirality, porosity, etc.[1-8] Here, we targeted the preparation of a "complete ferromagnet", that is a magnet exhibiting a 3-D ferromagnetic interaction through a 3-D isotropic network structure, similar to the CrNi structure described by Kitagawa et al.[9] Such magnets having a three dimensional structure and a ferromagnetic network are rare among general metal-oxides and molecule-based magnets; antiferromagnetic interactions usually operate between such magnetic centers. Innovative molecular design and synthetic strategies are necessary for the creation of a "complete ferromagnet". A promising strategy for producing molecular-based magnets is to create a bimetallic network by assembling two kinds of paramagnetic metal ions. Cyano-complexes were among the first coordination compounds ever prepared and they are still popular in coordination and organometallic chemistry. Metal cyanide extended networks, analogs of Prussian blue, are of great interest to the molecule-based magnetism community,[10-12] because of the nature of the magnetic exchange, which can be anticipated in advance from basic orbital interaction arguments. The predictable structure directing quality of the cyanide bridge can facilitate supramolecular and network design.[5] Prussian blue analogs, derived from hexacyanometallate anions and hexa-solvated metal complexes, exhibit novel magnetic and electronic properties, and some of them present magnetic ordering at a critical temperature (Tc) as high as 376 K.[7, 13, 14] A wide range of magnetic phenomena have been observed in metal cyanides, including high-spin clusters,[15-17]

metamagnetism,[5, 18, 19] room temperature magnetic ordering,[6, 13] spin-glass behavior,[20, 21] and photomagnetism.[22, 23] However, the difficulty of obtaining single crystals suitable for X-ray structure determination precludes a thorough magneto-structural correlation of these 3D systems of high symmetry.[24]

Using the $[Cr(CN)_6]^{3-}$ anion three new bimetallic complexes have been prepared: The three dimensional framework $\{[(Cu(tn)_2)_3(Cr(CN)_6)][Cr(CN)_6]\}_\infty$ (**1**) (tn = 1,3-diaminopropane) and the chiral one dimensional polymeric complexes $\{[Cu(1R,2Rchxn)_2]_3[Cr(CN)_6]_2 \cdot 4.75H_2O\}_\infty$ (**2**) (1R,2Rchxn = *trans*-cyclohexane-(1R,2R)-diamine) and $\{[Cu(1S,2Schxn)_2]_3[Cr(CN)_6]_2 \cdot 4.25H_2O\}_\infty$ (**3**) (1S,2Schxn = *trans*-cyclohexane-(1S,2S)-diamine). Here we report on the crystal structures and magnetic susceptibility studies of these compounds. The chiral nature of complexes **2** and **3** has been confirmed by solid state circular dichroism (CD) measurements.

Experimental Section

Physical Measurements. Elemental analyses of carbon, hydrogen, and nitrogen were performed by the Microanalysis Service of the Laboratory of Pharmaceutical and Organical Propedeutical Chemistry at the University of Geneva (Geneva, Switzerland). Infrared spectra were measured using KBr pellets in the interval of 4000-400 cm^{-1} were recorded on a Perkin-Elmer 1720X FT-IR spectrometer. Circular dichroism (CD) spectra were measured as KBr pellets on a J-500C spectropolarimeter in the range of 800-300 nm at 298K. Magnetic measurements were carried out in the "Servei de Magnetoquímica (Universitat de Barcelona)" on polycrystalline samples (20 - 30 mg) with a Quantum Design SQUID MPMS-XL susceptometer working in the 2-300 K range. The magnetic field was 0.05 T. The diamagnetic corrections were evaluated from Pascal's constants.

Synthesis. All reagents were purchased from chemical sources and used without further purification. All the operations for the synthesis were carried out in the dark to avoid the decomposition of $[Cr(CN)_6]^{3-}$.

$\{[(Cu(tn)_2)_3(Cr(CN)_6)][Cr(CN)_6]\}_\infty$ (**1**). Under aerobic conditions, 1,3-diaminopropane (0.084 mL, 1.0 mmol) was slowly added with stirring to a concentrated aqueous solution of $CuCl_2 \cdot 2H_2O$(0.171g, 1.0mmol) leading to the immediate appearance of a pale green precipitate. A concentrated aqueous solution of NaOH (2.0 mmol) was added dropwise in order to obtain a clear solution. This was then heated at ca. 70°C for 10 min and subsequently filtered. An aqueous solution of $K_3[Cr(CN)_6]$ (0.195g, 0.6 mmol) was then added dropwise to the hot filtrate. The reaction mixture was stirred for 30 min and then $NaClO_4$ (0.12g, 1 mmol) was added in order to aid crystallization. After stirring for a few minutes, the mixture was filtered and after 4-5 days dark blue-green plate-like crystals appeared. Elemental anal. Found C, 34.02; H, 5.98; N, 31.62 %; $C_{30}H_{60}N_{24}Cr_2Cu_3$: requires C, 34.27; H, 5.75 N, 31.97 %. IR (KBr): ν(NH) 3324 and 3295 (vs), ν(CH) 2947 (s) and 2881 (s), ν(CN) 2152, 2135 and 2124 (vs), δ(NH_2) 1619(m) and 1593 (m), δ(CH_2) 1471 (s), 1440 (s), ν(Cr─C) 581 (m), δ(Cr─CN) 464(s).

$\{[Cu(1R,2Rchxn)_2]_3[Cr(CN)_6]_2 \cdot 4.75H_2O\}_\infty$ (**2**). To a stirred aqueous solution (3 ml) of $Cu(NO_3)_2 \cdot H_2O$ (145 mg, 0.6 mmol) was added dropwise a methanol solution (3 ml) of *trans*-cyclohexane-(1R,2R)-diamine (136 mg, 1.2 mmol). The mixture was stirred for 10 min and the violet precipitate obtained was filtered-off, washed with methanol and dried in air. This solid was dissolved in 10 ml of a methanol-water (1:1) mixture and was then added slowly to an aqueous solution of $K_3[Cr(CN)_6]$ (66 mg, 0.15 mmol). By slow diffusion of the two solutions purple block-shaped crystals of **2** were obtained after

several days. Elemental anal. Found C, 41.32; H, 6.56; N, 24.22 %; calcd. for $C_{48}H_{84}N_{24}Cr_2Cu_3 \cdot 4.75H_2O$: C, 41.85; H, 6.84; N, 24.40 %. IR (KBr) ν(OH) 3447(s), ν(NH) 3326 (s), 3264 (vs), ν(CH) 2932 (s), 2854 (m), ν(CN) 2126 (vs), δ(NH_2) 1591 (s), δ(CH_2) 1452 (s), ν(Cr─C) 678 (s), δ(Cr─CN) 562 (s).

$\{[Cu(1S,2Schxn)_2]_3[Cr(CN)_6]_2 \cdot 4.25H_2O\}_\infty$ (**3**). Prepared starting from *trans*-cyclohexane-(1S,2S)-diamine as described above for **2**. Elemental anal. Found C, 41.55; H, 6.77; N, 24.33 %; calcd. for $C_{48}H_{84}N_{24}Cr_2Cu_3 \cdot 4.25H_2O$: C, 42.11; H, 6.81; N, 24.55 %. IR (KBr) ν(OH) 3418(vs), ν(NH) 3272 (vs), 3138 (s), ν(CH) 2939 (s), 2855 (s), ν(CN) 2127 (vs), δ(NH_2) 1589 (vs), δ(CH_2) 1384 (s), ν(Cr─C) 708 (m), δ(Cr─CN) 564 (s), 495 (s).

X-ray Structural Determination. A dark blue-green crystal of **1** (0.5 x 0.5 x 0.5 mm^3) and dark violet crystals of **2** (0.4 x 0.25 x 0.38 mm^3) and **3** (0.4 x 0.3 x 0.3 mm^3) were mounted on a Stoe Mark-I Image Plate for **1** and a Mark-II Image Plate diffractometer system for **2** and **3**, both equipped with a graphite-monochromator. Data collection were performed using Mo-Kα radiation (λ = 0.71073 Å) at 173 K. The structures ware solved by direct methods using the program SHELXS-97[25] and refined by full matrix least squares on F^2 with SHELXL-97.[25] All non-hydrogen atoms were refined anisotropically. Semi empirical absorption corrections were applied for **1** - **3** using MULscanABS in PLATON.[26] Four fully occupied and one partially occupied [occupancy 0.75 for **2** and 0.25 for **3**] water molecules of crystallization were located in both crystal structures; giving a total of $4.75H_2O$ for **2** and $4.25H_2O$ for **3**. Some of the NH_2 and water hydrogen atoms in the complexes could be located from difference Fourier syntheses and were freely refined (N-H) or with distance restraints (O─H). The remainder of the H-atoms were included in calculated positions and treated as riding atoms using SHELXL-97

default parameters. The absolute configurations of **2** and **3** were determined by Flack's method.[27]. Further details of the data collection and refinement are given in Table 1.

Table 1. Crystal and Structure Refinement Data for **1**, **2** and **3**.

	1	**2**	**3**
formula	$C_{30}H_{60}N_{24}Cr_2Cu_3$	$C_{48}H_{93.5}N_{24}Cr_2Cu_3O_{4.75}$	$C_{48}H_{92.5}N_{24}Cr_2Cu_3O_{4.25}$
fw	1051.64	1377.59	1369.08
λ(Å)	0.71073	0.71073	0.71073
T(K)	173(2)	173(2)	173(2)
crystal system	trigonal	triclinic	triclinic
space group	R-3	P 1	P 1
a(Å)	15.4908(11)	8.5421(6)	8.5435(8)
b(Å)	15.4908(11)	12.6379(9)	12.6309(12)
c(Å)	16.7699(13)	16.1571(11)	16.1711(17)
α(°)	90.00	104.594(5)	104.632(8)
β(°)	120.00	98.425(6)	98.429(8)
γ(°)	90.00	97.440(5)	97.375(8)
V(Å^3)	3485.0(4)	1644.3(2)	1645.1(3)
Z	3	1	1
ρ_{calcd}(Mg/m^3)	1.503	1.391	1.382
μ(mm^{-1})	1.855	1.334	1.332
refl. measured	8944	22711	8017
indep. refl./R_{int}	1511/0.0244	11837/0.0437	7760/0.0362

obsd.refl: I>2σ(*I*)	1344	10507	6466
no. of params.	92	751	756
R1[a] [$I > 2\sigma(I)$]	0.0252	0.0395	0.0343
wR2[b] [$I > 2\sigma(I)$]	0.0699	0.0981	0.0648
S	1.094	1.008	0.946
$\Delta\rho_{max}/\Delta\rho_{min}$ (eÅ^{-3})	1.546/-0.206	0.552/-0.681	0.370/-0.237
Flack x factor	-	0.006(11)	0.027(16)

[a] $R1 = \Sigma||F_O| - |F_C||/\Sigma|F_O|$. [b] $wR2 = [\Sigma w(F_O^2 - F_C^2)^2/\Sigma wF_O^4]^{1/2}$.

Results and Discussion

Crystal Structures. The crystal structure analysis of **1** $\{[(Cu(tn)_2)_3(Cr(CN)_6)][Cr(CN)_6]\}_\infty$ shows that it is a three dimensional metal-organic framework. The asymmetric unit consists of a centrosymmetric $[Cu(tn)]^{2+}$ cation and two independent $[Cr(CN)_6]^{3-}$ anions, both situated on 3-fold rotation axes (Figure 1a). All the cyanide groups of the $[Cr(CN)_6]^{3-}$ anion involving atom Cr1, are coordinated to adjacent copper atoms. The second $[Cr(CN)_6]^{3-}$ anion, involving atom Cr2, is situated on a 3-fold rotation axis and is not involved in coordination to the copper(II) cation. Each chromium anion has a perfect octahedral geometry (Cr1─C4 = 2.067(2) Å and Cr2─C5 = 2.085(2) Å). The Cu1 ion is coordinate to four amino nitrogen atoms (N1, N2 and the symmetry related atoms) of the ligand tn and to two cyanide nitrogen atoms (N3 and the symmetry related atom N3').

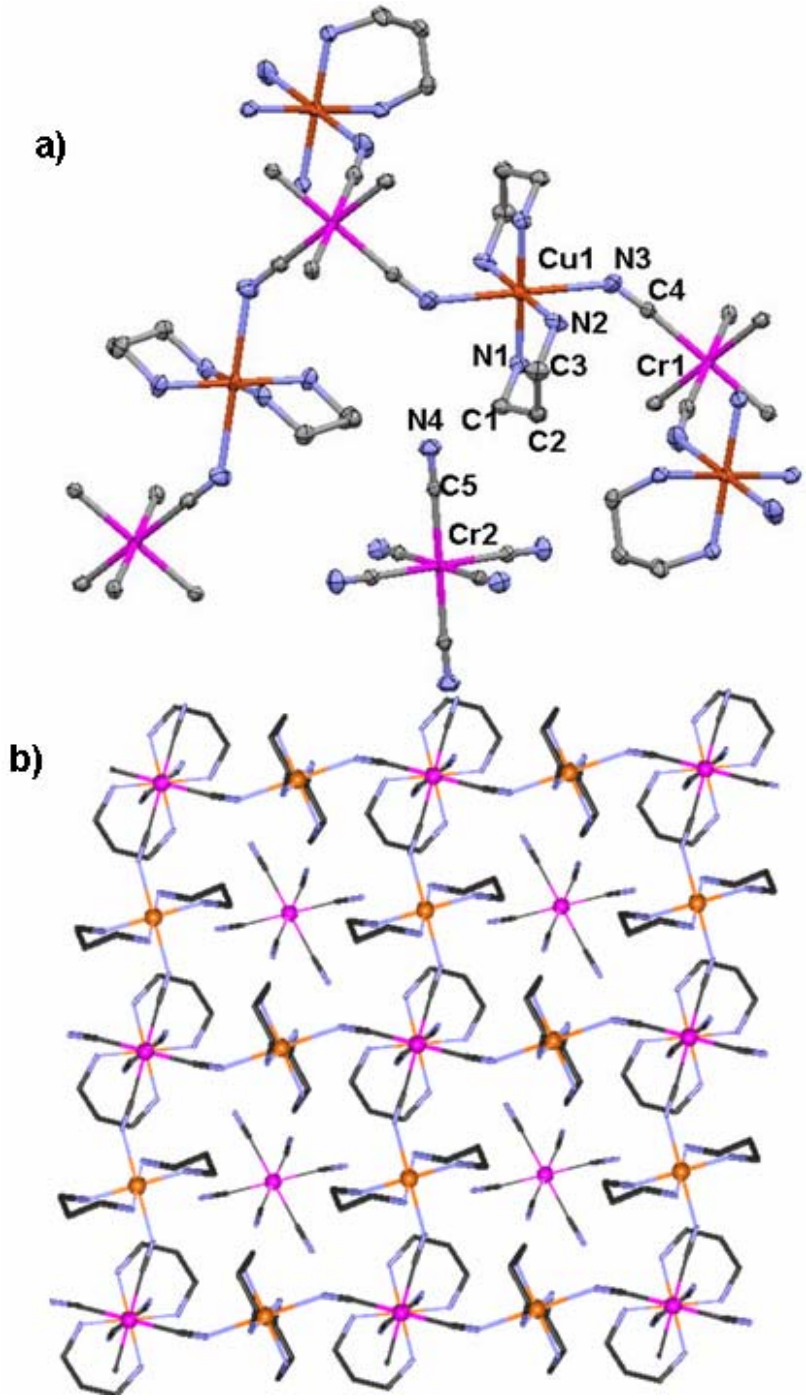

Figure 1. (a) A partial view of the molecular structure of $\{[(Cu(tn)_2)_3(Cr(CN)_6)][Cr(CN)_6]\}_\infty$ (**1**), showing the numbering scheme and displacement ellipsoids at the 50% probability level; (b) A view of the octanuclear Cu_4Cr_4 cyclic units of the 3D network of **1**, with the isolated $[Cr(CN)_6]^{3-}$ ion in the center.

In the lattice, a 3D framework is constructed on the basis of a Cr_4Cu_4 octanuclear cyclic unit (Figure 1b). This is formed by the μ_6-$[Cr(CN)_6]^{3-}$ array and the $[Cu(tn)]^{2+}$ cations through Cr1─CN─Cu1─NC─Cr1 linkages.

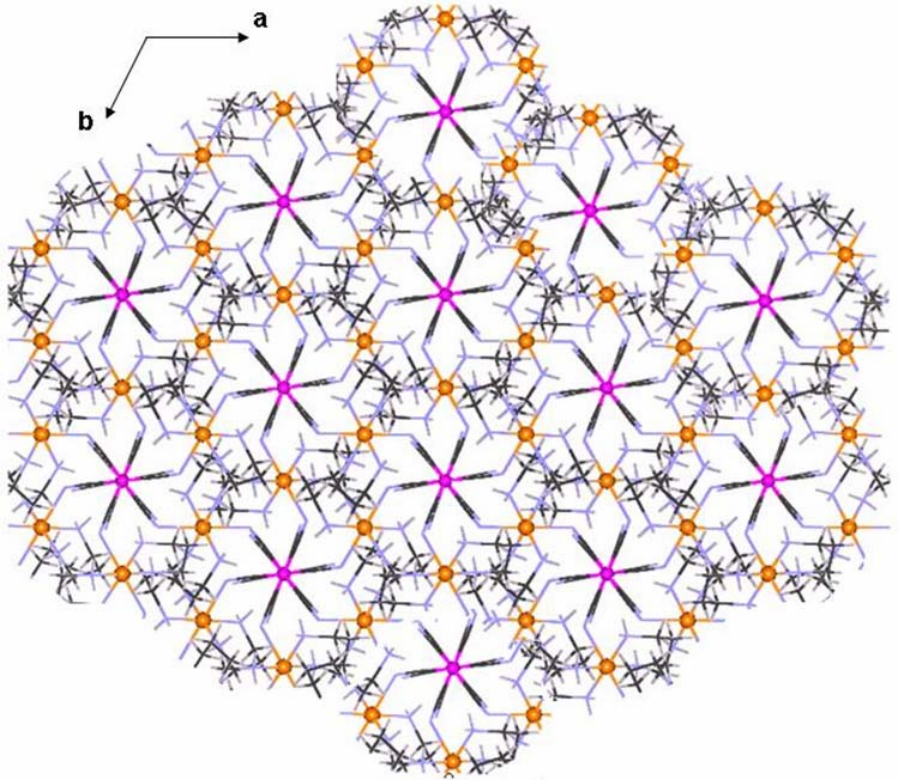

Figure 2. A view of the 3-D network structure of $\{[(Cu(tn)_2)_3(Cr(CN)_6)][Cr(CN)_6]\}_\infty$ (**1**) along the 3-fold c-axis.

The non coordinated $[Cr(CN)_6]^{3-}$ anion, involving atom Cr2, is situated in the center of the cyclic unit and equilibrates the charges (Figure 2). Atom Cu1 is situated on an inversion center and has an elongated octahedral geometry. The Cu1-N1(eq) and Cu1-N2(eq) bond distances are 2.038(2) and 2.045(2) Å, respectively, while the Cu-N3(ax) distance is 2.503(3) Å. The Cu1─N1─C1 and Cu1─N2─C3 bond angles are 116.4(1) and 119.6(2) °, respectively, and bond angle Cu1─N3─C4 is 135.3(2)°.

Compounds $\{[Cu(1R,2Rchxn)_2]_3[Cr(CN)_6]_2 \cdot 4.75H_2O\}_\infty$ (**2**) and $\{[Cu(1S,2Schxn)_2]_3[Cr(CN)_6]_2 \cdot 4.25H_2O\}_\infty$ (**3**), crystallize in the non-centrosymmetric triclinic space group *P1*. They are isostructural to the $[Fe(CN)_6]^{3-}$ analogues.[28] The asymmetric unit of **2** is shown in Figure 3. The one-dimensional zig-zag chains consists of two independent negatively charged units consisting of a $[Cu(1R,2R\ chxn)_2]^{2+}$ cation linked to a $[Cr(CN)_6]^{3-}$ anion. The overall negative charge of -2 is compensated for by an isolated $[Cu(1R,2Rchxn)_2]^{2+}$ cation. The axial positions on the copper atoms, Cu1 and Cu2, are occupied by cyano groups. These Cu─N distances are very long compared to those in the equatorial plane: Cu1─N(ax) 2.665(5) and 2.671(5) Å, compared to Cu1─N(eq) 1.997(4)-2.021(5) Å, and Cu2─N(ax) 2.595(4) and 2.603(4) Å, compared to Cu2─N(eq) 2.003(3)-2.025(4) Å. Thus the Cu─N(ax) bond distances can be considered as a Jahn-Teller distortion.[29] The Cu─N─C bond angles are non-linear, with values ranging between 126.3(4)° and 131.3(3)°. This phenomenon has been observed previously in similar compounds.[28, 30-37]

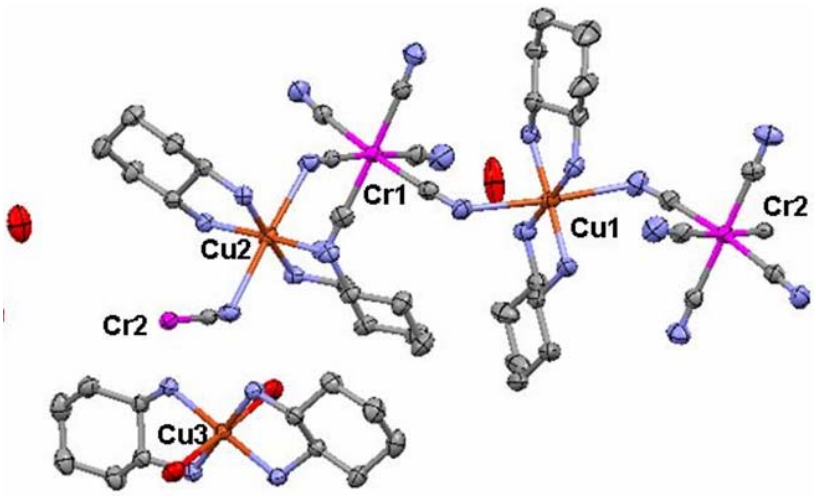

Figure 3. A view of the asymmetric unit of $\{[Cu(1R,2Rchxn)_2]_3[Cr(CN)_6]_2 \cdot 4.75H_2O\}_\infty$ (**2**), showing the numbering scheme and displacement ellipsoids at the 50% probability level.

Each chromium anion, with four terminal and two bridging CN ligands, has a slightly deformed octahedral coordination geometry (Cr ─ C bond lengths vary from 2.061(5) to 2.093(4) Å). Copper atom Cu3 of the isolated *trans*-$[Cu(1R,2R\text{-}chxn)_2(2H_2O)_2]^{2+}$ cation, has a distorted octahedral geometry (Cu3 ─ N(eq): 2.016(4) ─ 2.038(4) Å; Cu3 ─ O1(ax): 2.433(4) Å; Cu ─ O2(ax): 2.462(4) Å). Two water molecules of crystallization (O3 and O4) hydrogen-bond to both the terminal and the bridging CN-groups of the Cr1 unit and to the NH_2-groups of the Cu1 moiety.

Circular dichroism measurements. Solid-state diffuse reflectance CD spectra of compounds, **2** and **3** are shown in Figure 4. For the compound **2**, the R,R-isomer exhibits a maximum positive Cotton effect at 510nm, as was observed for the aqueous solution of the precursor. The S,S-isomer has, as expected, a negative Cotton effect at the same wavelength. The chirality and enantiomeric nature of compounds **2** and **3** were controlled in view of a future study of magneto-chiral dichroism.

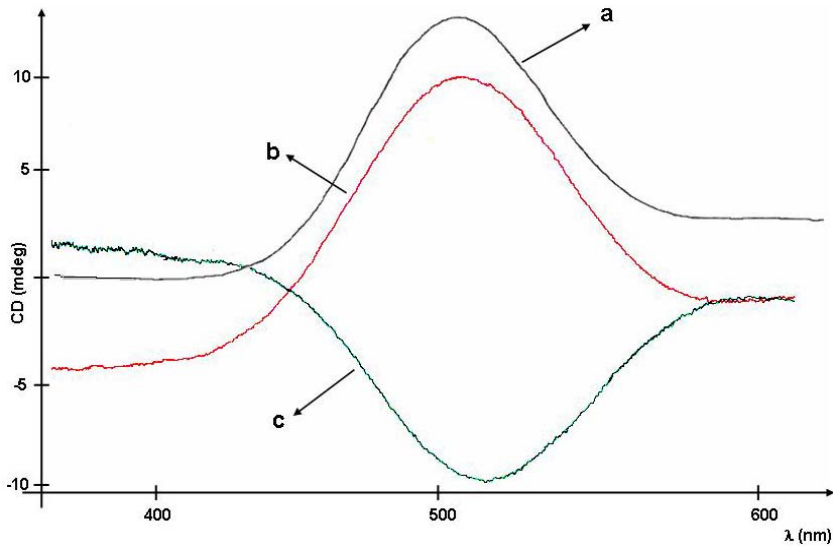

Figure 4. CD spectra of: a) - an aqueous solution of the bis-chelated precursor $[Cu(trans\text{-}(1R,2R)\text{-}chxn)_2(H_2O)_2](NO_3)_2$, b) - $\{[Cu(1R,2Rchxn)_2]_3[Cr(CN)_6]_2 \cdot 4.75H_2O\}_\infty$ (**2**) in KBr pellet; c) - $[Cu(1S,2Schxn)_2]_3[Cr(CN)_6]_2 \cdot 4.25H_2O\}_\infty$ (**3**) in KBr pellet.

Magnetic properties. Magnetic data for **1** were measured at 0.05 T. At room temperature $\chi_m T$ (for each Cu_3Cr_2 unit) is near 5 cm^3 mol^{-1} K, which corresponds to two chromium(III) and three copper(II) not coupled ions (spin-only value, i.e. with g = 2.00, would give $\chi_m T$ = 4.875 cm^3 mol^{-1} K). From r.t. to 75 K $\chi_m T$ is practically constant. It then increases rapidly to a value of 14 cm^3 mol^{-1} K at 3.5 K and decreases to 8 cm^3 mol^{-1} K at 2 K (limit of the measurement) (Figure 5).

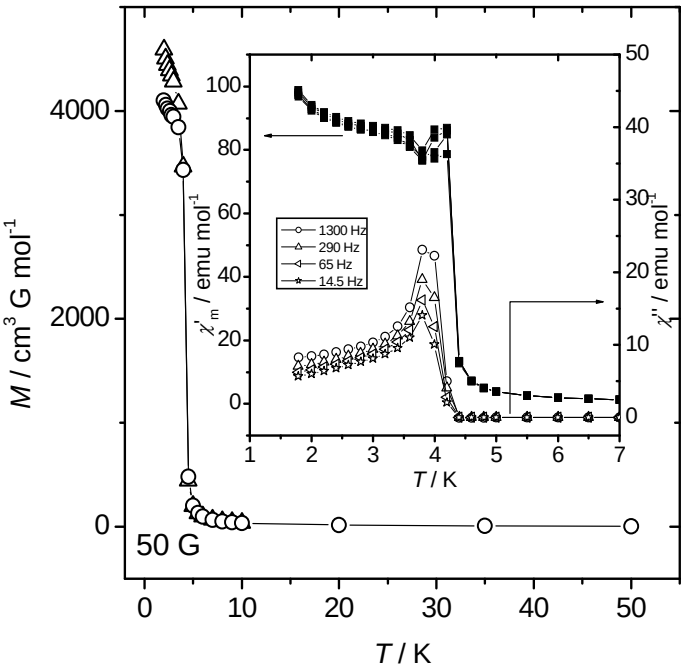

Figure 5. Thermal variation $\chi_m T$ for **1**. Inset: plot of $\chi_m T$ vs T varying the applied field (20, 100, 500 and 1000 G).

It is important to note that there is a clear variation of the $\chi_m T$ curves at low temperature on varying the magnetic field: 20 G, 100 G, 500 G and 1000 Gauss. The lower the magnetic field, the higher the magnetization (Figure 5 inset). At 20 Gauss there is a maximum at 4 K of ca. 400 cm^3 mol^{-1} K. This feature can indicate ferromagnetic ordering at low temperature.

The ferromagnetic ordering in **1** is corroborated by the following data: (i) the shape of the $M/N\mu_B$ curve (Figure 6). There is a rapid increase from 0 to 200 G and then it increases more slowly to a maximum value of 8 $N\mu_B$ at 5 T without reaching saturation.

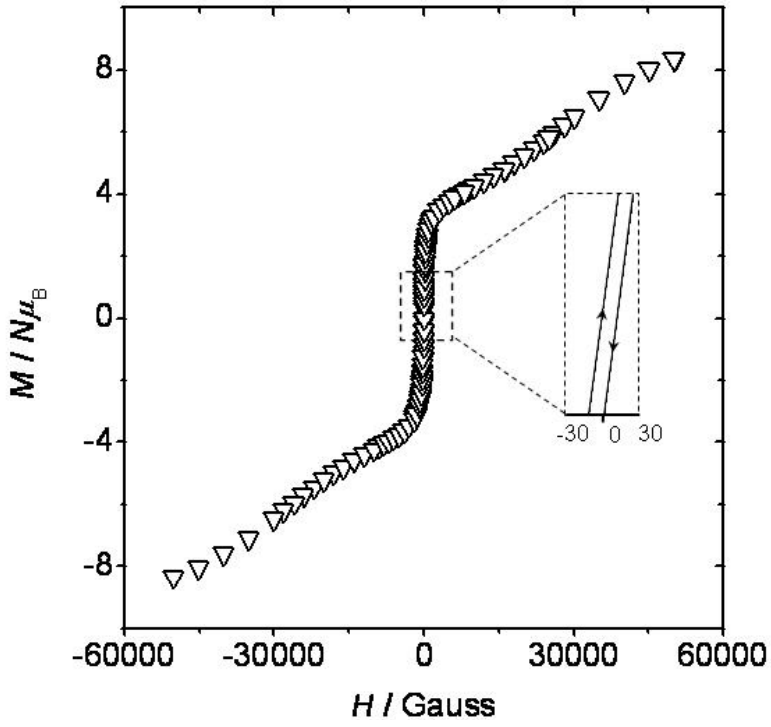

Figure 6. Plot of the $M/N\mu_B$ vs H for complex **1**. Inset: view of the very small hysteresis loop.

However, the hysteresis is extremely small at the minimum temperature (2 K) of the SQUID [Figure 6: inset]; (ii) the zero-field cooled/field cooled magnetization (at 50 G) exhibits an abrupt change at ca. 4 K and both curves diverge in the ferromagnetic phase (Figure 7); (iii) the most important and clear proof is the presence of the out-of-phase ac measurement (χ'') frequency independent (Figure 7 inset). According to the ZFC/FC and the maximum in the ac measurements, the T_c (critical temperature of the phase change) is very close to 4 K.

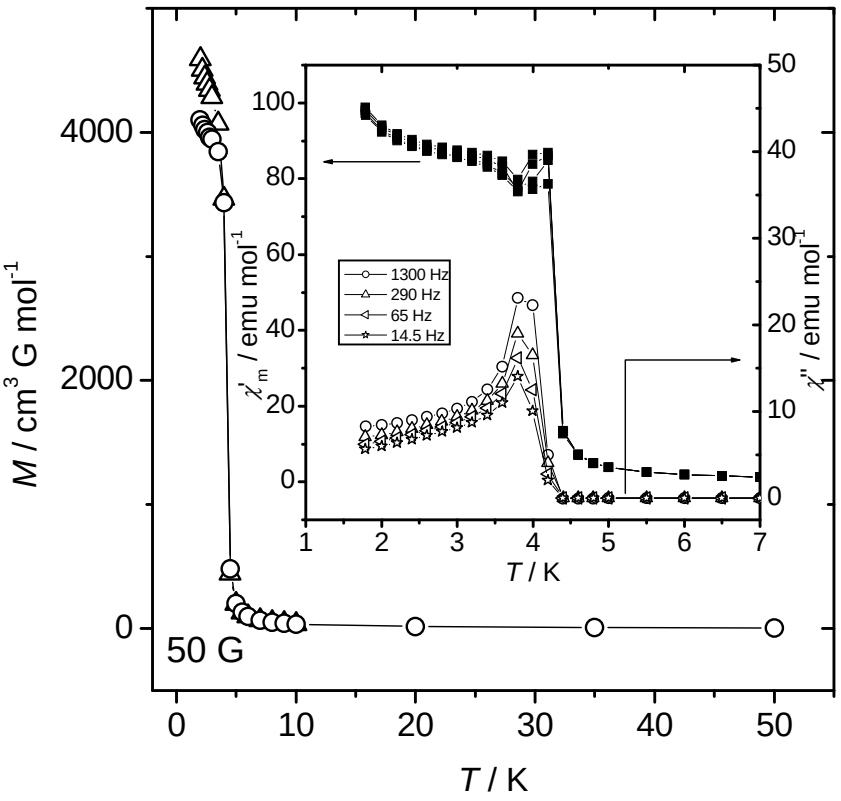

Figure 7. ZFC/FC at 50 G for complex **1**. Inset **:** Thermal variation χ' and χ'' for **1**. The frequencies used were 1300, 290, 65 and 14.5 Hz (solid lines are only present as a visual guide).

As a consequence, this material is a molecule-based magnet. Although the *J* value between Cr^{III} and Cu^{II} ions is not possible to calculate in this 3D system, the topology of the magnetic orbitals allow us to propose that the magnetic exchange is ferromagnetic in character. Indeed, the Cu^{II} and Cr^{III} magnetic orbitals are, per se, orthogonal. As a consequence the magnetic ordering, even if at very low temperature, is not due to a canting of a not-compensated antiferromagnetic system but to a ferromagnetic ordering. This feature is evidenced from the study of the magnetic coupling of the similar complex **2** and, furthermore, with previous literature data. Similar behavior has been reported for a 2-D $Cu^{II}Cr^{III}$ cyanide-bridged magnet Tc = 9.5 K.[38]

The magnetic behavior of complex **2** in the form of $\chi_M T$ versus T plot is shown in Figure 8a. The global feature is characteristic of a weak ferromagnetic interaction. The $\chi_M T$ value per $[Cu_3Cr_2]$ unit at 300 K is 5.20 cm^3 mol^{-1} K, which practically corresponds to three isolated Cu^{II} ions (S_1 = 1/2) and two Cr^{III} ions (S_2 = 3/2) ($\chi_M T$ = 4.875 cm^3 mol^{-1} K in the spin-only approach). $\chi_M T$ increases smoothly from room temperature to *ca*. 50 K, and then increases rapidly at lower temperatures reaching a maximum value of 11.1 cm^3 mol^{-1} K at 2 K. This is consistent with the behavior expected for ferromagnetic intramolecular interactions between the Cu^{II} and Cr^{III} ions. The field dependence of the magnetization (0-5 T) measured at 2 K is shown in Figure 8a (inset) in the form of $M/N\mu_B$ (per Cu_3Cr_2 fragment) vs H. The magnetization tends to 9.18 $N\mu_B$ which is close to the expected value for three Cu^{II} ions and two Cr^{III} system (S_T = 9/2). The shape of the curve matches rather well with the Brillouin function for an S = 9/2 ground state, assuming $g_{average}$ = 2.1. This feature indicates that complex **2** does not present magnetic ordering, such as occurs in complex **1**.

In order to calculate the J parameter, it is necessary to consider the overall structure and the possible pathways in the one-dimensional Cu^{II} — Cr^{III} chain. The overall structure consists of a mixture of one-dimensional Cu^{II} — Cr^{III} chains separated by isolated $[Cu(1R,2Rchxn)_2]^{2+}$ cations. The interpretation of the magnetic data can be made assuming that: i) the isolated $[Cu(diamine)_2]^{2+}$entity follows the Curie law (except at very low temperatures); (ii) a standard value of g_{Cu} of 2.1 for the Cu^{2+} ion in this isolated $[Cu(diamine)_2]^{2+}$ entity. With this g value, $\chi_m T$ = constant = 0.41 cm^3 mol^{-1} K. Thus, for the treatment of the magnetic data, we can subtract 0.41 from the values obtained for the magnetic measurements given in Figure 8b. After subtraction, the final magnetic entity

will depend only of the Cu^{II}-Cr^{III} chain, corresponding to the one-dimensional system. The 'modified' plot of $\chi_m T$ vs T is indicated in Figure 8b. It is very important to underline here, that this plot is given for only one Cu^{II}-Cr^{III} entity, given that now we assume that we are dealing with an heteronuclear [Cu-Cr] 1D system. Based on these considerations, the experimental magnetic data can be fitted using the following isotropic Heisenberg Hamiltonian:

$$H = - \Sigma J \, (S_{Cu(i)} S_{Cr(i+1)})$$

There is no exact mathematical formula for fitting such an alternating chain (S = 3/2 – ½). However, assuming that all the J values for Cr-CN-Cu are the same, which is in agreement with the structural data, calculations were carried out with the CLUMAG program[39], using the irreducible tensor operator formalism (ITO), employing a closed rings of eight atoms: Cu4Cr4. The experimental data for **2** were then fitted in the range 300-2 K, with allowance for variation in all the parameters. The best least-square fit, shown in Figure 8b (per one CuCr unit, see above), gives $J = 1.64 \pm 0.3$ cm^{-1}, $g_{av} = 2.03$ and $R = 2.80 \times 10^{-4}$, where $R = \Sigma[(\chi_M T)_{exp} - (\chi_M T)_{calc}]^2 / \Sigma[(\chi_M T)_{exp}]$. The assumption of equal g values for Cu^{II} and Cr^{III} is an approximation, since g_{Cu} must be > 2.00 and g_{Cr} must be < 2.00.

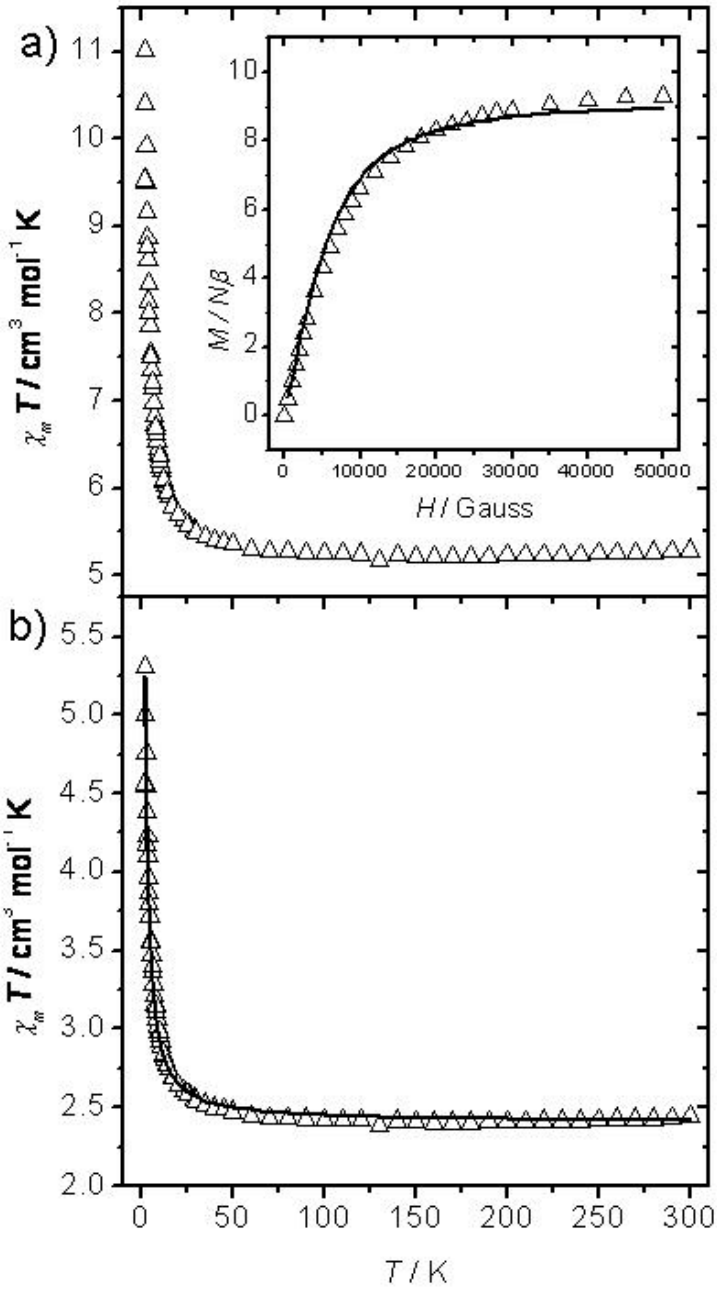

Figure 8. **a**) Thermal variation of $\chi_M T$ for **2** per $[Cr_2Cu_3]$ unit. Inset: plot of the reduced magnetization ($M/N\mu_B$) vs H at 2 K; **b**) Fit of the thermal variation of $\chi_M T$ for **2** after subtraction of $\chi_m T = 0.41$ cm^3 mol^{-1} K (see text). **Note**: The fit was made with a $[Cr_4Cu_4]$ ring, but the plot is given for only one Cu^{II}-Cr^{III} entity.

The value of the exchange parameter J = +1.64 cm^{-1} for compound **2**, is placed in the lowest limit of the magnetic data found in the literature for analogous complexes: The coupling is always ferromagnetic, ranging from +1.31 cm^{-1} [40] to +45 cm^{-1},[41] depending on the Cu-N distance and on the position of the NC group with respect to the magnetic orbital of the copper(II) ion. The Cu-N distance in the complex with J = +45 cm^{-1} is 1.971 Å,[41] whereas in complex **2** the same distance varies between 2.595(4) to 2.671(5) Å: For the complex with J = +1.31 cm^{-1},[40] no structural data are available. However, for two other analogous compounds, reported by Kou et al.,[37] values of J = +2.4 and +12 cm^{-1} with Cu-N distances of 2.505 and 2.378 Å, respectively, have been reported. The magnetic behavior of Prussian Blue analogues is well-known and the general trends of their magnetic properties are well established. In particular the ferromagnetic interaction between Fe^{III} or Cr^{III}, and Cu^{II} ions can be rationalized in terms of the strict orthogonality of the magnetic orbitals of these ions. According to the crystal structure and ligand-field theory, a copper (II) ion in an elongated octahedral surroundings has one unpaired electron in a $d_{x^2-y^2}$ orbital (x and y axes are taken along the donor atoms), which interacts with the molecular orbitals of the cyano bridge having the same symmetry, producing a magnetic orbital with σ character. A chromium (III) ion in an octahedral environment has three unpaired electrons in the t_{2g} orbitals, which interacts with other molecular orbitals of the cyano-bridge having appropriate symmetry, which produces a magnetic orbital with π character. Consequently strict orthogonality is obeyed and the interaction between Cu^{II} and Cr^{III} should be ferromagnetic. The strict orthogonality is through the long Cu-N distances (2.595(4) - 2.671(5) Å), resulting from the Jahn-Teller distortion on each

copper ion. Hence, this long distance explains the weak magnitude of the ferromagnetic coupling

Conclusions

Three new bimetallic complexes, $\{[(Cu(tn)_2)_3(Cr(CN)_6)][Cr(CN)_6]\}_\infty$ (**1**), with a three-dimensional structure based on a Cr_4Cu_4 octanuclear cyclic unit, and $\{[Cu(1R,2Rchxn)_2]_3[Cr(CN)_6]_2 \cdot 4.75H_2O\}_\infty$ (**2**) and $\{[Cu(1S,2schxn)_2]_3[Cr(CN)_6]_2 \cdot 4.25H_2O\}_\infty$ (**3**), with chiral one-dimensional zig-zag chains, were successfully synthesized and fully characterized. Complex **1** exhibits three dimensional magnetic ordering over the crystal lattice, with T_C close to ca. 4K. Compound **2** shows weak ferromagnetic coupling which is due to the orthogonality of the corresponding magnetic orbitals. Its weak character is due to the long Jahn-Teller axis of the copper (II) ions [2.595(4) – 2.671(5) Å].

Acknowledgments

This work was supported by the Swiss National Science Foundation for financial support (Grant № FN 20-111738). JR acknowledges the financial support from the Spanish Government (Grant CTQ2006/03949/BQU).

References.

[1] O. Kahn, *Molecular Magnetism*, VCH: Weinheim, Germany, **1993**.

[2] M. Ohba, N. Fukita, H. Okawa, *J. Am. Chem. Soc.* **1997**, *119*, 1011.

[3] O. Kahn, *Advances in Inorganic Chemistry, Vol. 43*, Academic Press, San Diego, **1995**.

[4] J. S. Miller, A. J. Epstein, *Angew. Chem., Int. Ed.* **1994**, *33*, 385.

[5] M. Verdaguer, A. Bleuzen, V. Marvaud, J. Vaissermann, M. Seuleiman, C. Desplanches, A. Scuiller, C. Train, R. Garde, G. Gelly, C. Lomenech, I. Rosenman, P. Veillet, C. Cartier, F. Villain, *Coord. Chem. Rev.* **1999**, *190-192*, 1023.

[6] S. Ferlay, T. Mallah, R. Ouahes, P. Veillet, M. Verdaguer, *Nature* **1995**, *378*, 701.

[7] M. Verdaguer, *Science* **1996**, *272*, 698.

[8] E. Coronado, J. R. Galan-Mascaros, C. J. Gomez-Garcıa, V. Laukhin, *Nature* **2000**, *408*, 447.

[9] W. Kaneko, M. Ohba, H. Okawa, S. Kitagawa, *Inorg. Chem.* **2006**, *45*, 7191.

[10] V. Gadet, T. Mallah, I. Castro, M. Verdaguer, *J. Am. Chem. Soc.* **1992**, *114*, 9213.

[11] T. Mallah, S. Thiebaut, M. Verdaguer, P. Veillet, *Science* **1993**, *262*, 1554.

[12] W. R. Entley, G. S. Girolami, *Science* **1995**, 397.

[13] S. M. Holmes, G. S. Girolami, *J. Am. Chem. Soc.* **1999**, *121*, 5593.

[14] E. Dujardin, S. Ferlay, X. Phan, C. Desplanches, C. Cartier dit Moulin, P. Sainctavit, F. Baudelet, F. Dartyge, P. Veillet, M. Verdaguer, *J. Am. Chem. Soc.* **1998**, *120*, 11347.

[15] R. J. Parker, L. Spiccia, K. J. Berry, G. D. Fallon, B. Moubaraki, K. S. Murray, *Chem. Commun.* **2001**, 333.

[16] M. P. Shores, J. J. Sokol, J. R. Long, *J. Am. Chem. Soc.* **2002**, *124*, 2279.

[17] P. A. Berseth, J. J. Sokol, M. P. Shores, J. L. Heinrich, J. R. Long, *J. Am. Chem. Soc.* **2000**, *122*, 9655.

[18] M. Ohba, H. Okawa, *Coord. Chem. Rev.* **2000**, *198*, 331.

[19] A. Marvilliers, S. Parsons, E. Riviere, Audiere, M. Kurmoo, T. Mallah, *Eur. J. Inorg. Chem.* **2001**, 1287.

[20] W. E. Buschmann, J. S. Miller, *Inorg. Chem.* **2000**, *39*, 2411.

[21] W. E. Buschmann, J. Ensling, P. Gutlich, J. S. Miller, *Chem. Eur. J.* **1999**, *5*, 3019.

[22] N. Shimamoto, S. Ohkoshi, O. Sato, K. Hashimoto, *Inorg. Chem.* **2002**, *41*, 678.

[23] V. Escax, A. Bleuzen, C. C. D. Moulin, F. Villain, A. Goujon, F. Varret, M. Verdaguer, *J. Am. Chem. Soc.* **2001**, *123*, 12536.

[24] W. Dong, L.-N. Zhu, H.-B. Song, D.-Z. Liao, Z.-H. Jiang, S.-P. Yan, P. Cheng, S. Gao, *Inorg. Chem.* **2004**, *43*, 2465.

[25] G. M. Sheldrick, *SHELXS-97 & SHELXL-97*, University of Göttingen, Germany, **1997**.

[26] A. L. Spek, *J.Appl.Cryst.* **2003**, *36*, 7.

[27] H. D. Flack, *Acta Crystallogr., Sect. A* **1983**, *39*, 876.

[28] E. Coronado, C. Gimenez-Saiz, J. M. Martinez-Agudo, A. Nuez, F. M. Romero, H. Stoeckli-Evans, *Polyhedron* **2003**, *22*, 2435.

[29] I. B. Bersuker, *Chem. Rev.* **2001**, *101*, 1067.

[30] D.-F. Li, T. Okamura, W.-Y. Sun, N. Ueyama, W.-X. Tang, *Acta Crystallogr., Sect.C: Cryst.Struct.Commun.* **2002**, *58*, m280.

[31] E. Coronado, C. J. Gomes-Garcia, A. Nuez, F. M. Romero, E. Rusanov, H. Stoeckli-Evans, *Inorg. Chem.* **2002**, *41*, 4615.

[32] Z. Smékal, I. Cisarova, J. Mrozinski, *Polyhedron* **2001**, *20*, 3301.

[33] C. W. Liu, J. M. Shi, W. Xu, Y. Q. Chen, *Pol. J. Chem.* **2003**, *77*, 929.

[34] J. Cernak, J. Lipkowski, I. Potocnak, A. Hudak, *Monastsh. Chem*. **2001**, *132*, 193.

[35] M. S. El Fallah, J. Ribas, X. Solans, M. Font-Bardia. *New J. Chem.* **2003**, *27*, 895.

[36] M. K. Saha, F. Lloret, I. Bernal. *Inorg. Chem.* **2004**, *43*, 1069.

[37] H.-Z. Kou, B. C. Zhou, S.-F. Si, R.-J. Wang. *Eur. J. Inorg. Chem.* **2004**, 401.

[38] F. Thétiot, S. Triki, J.-S. Pala, C. J. Gómez-García, S. Golnen, *Chem. Commun.* **2002**, 1078.

[39] D. Gatteschi, L. Pardi, *Gazz. Chim. Ital.* **1993**, *123(4)*, 231.

[40] R.J. Parker, K.D. Lu, S.R. Batten, B. Moubaraki, K.S. Murray, L. Spiccia, J.D. Cashion, A. D. Rae, A.C. Willis, *J. Chem. Soc. Dalton Trans*. **2002**, 3723.

[41] V. Marvaux, C. Decroix, A. Scuiller, C. Guyard-Duhayon, J. Vaissermann, F. Gonnet, M. Verdaguer, *Chem. Eur. J*. **2003**, *9*, 1677.

2. 3

Chiral bimetallic assemblies and coordination polymers based on tetracyanonickelate: a striking reversible structural transformation

Olha Sereda,Antonia Neels, Fritz Stoeckli and Helen Stoeckli-Evans

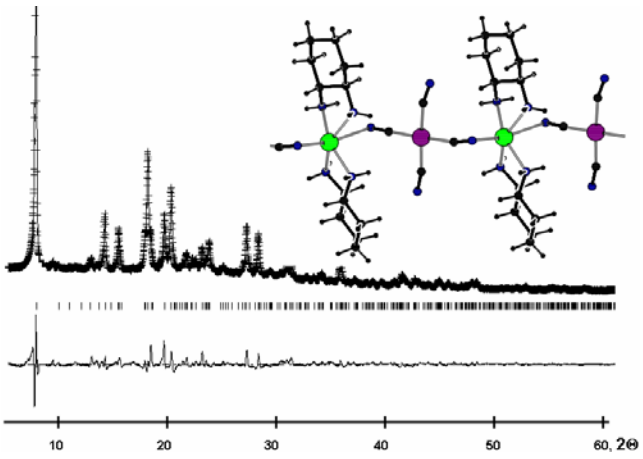

Accepted to Crystal Growth and Design

ABSTRACT: Four bimetallic assemblies involving chiral metal complexes and tetracyanonickelate, $\{[M(L)_m][Ni(CN)_4]\cdot nH_2O\}_\infty$ (M = Ni^{II}, m = 3, n = 4 (**1**), M = Cu^{II}, m = 2, n = 2 (**2** and **4**), M = Cu^{II}, m = 2, n = 0 (**3**), and where L= R,R-chxn = *trans*-cyclohexane-(1R,2R)-diamine for **1**, **2** and **3**; and S,S-chxn = *trans*-cyclohexane-(1S,2S)-diamine for **4**), have been synthesized and structurally characterized. The crystal structure analysis of compound **1** reveals that it consists of discrete $[Ni(CN)_4]^{2-}$ and $[Ni(R,R\text{-}chxn)_3]^{2+}$. Compound **2** is a bimetallic assembly of the a $[Cu(R,R\text{-}chxn)_3]^{2+}$ anion and a $[Ni(CN)_4]^{2-}$ anion. For compound **2** an interesting reversible phase transformation was observed. This bimetallic complex can be transformed into a one-dimensional polymer structure, **3**, accompanied by a colour change from violet to purple, simply by the removal of the water molecules of crystallization on heating. Rehydration of **3** gives **2**, confirmed by powder X-ray diffraction. Compound **4** is also a one-dimensional zig-zag polymer composed of alternating *trans*-$[Cu(S,S\text{-}chxn)_2]^{2+}$ cations and $[Ni(CN)_4]^{2-}$ anions. Circular Dichroism (CD) measurements for **2** and **4**, and Immersion calorimetric studies on compound **3** have been carried out.

KEYWORDS: structural transformation, immersion calorimetry, powder diffraction, chirality, cyanide-bridged.

Introduction

Chirality is of fundamental importance for life and plays a key role in biological systems and pharmacy.[1-3] At the same time, chirality is a key factor for exhibiting specific physical properties, such as second harmonic generation (SHG), magneto-chiral dichroism (MChD), ferroelectricity, etc.[4-7] On the other hand, the study of cyanide-

bridged metal complexes is an old but ever green branch in the field of coordination chemistry. Cyanide-bridged bimetallic complexes deserve special attention as they exhibit interesting electrochemical, zeolitic, magnetic and photomagnetic properties.[8-12] However, most of the cyanide-bridged bimetallic complexes obtained so far involve achiral components, and consequently, only a limited number of chiral structures have been studied. Here we report on the characterization, including the structural and physical properties, of four new chiral cyano-bridged bimetallic compounds based on tetracyanonickelate(II): $[Ni(R,R\text{-chxn})_3][Ni(CN)_4]\cdot 4H_2O$ (**1**) and $[Cu(R,R\text{-chxn})_2][Ni(CN)_4]\cdot 2H_2O$ (**2**), $\{[Cu(R,R\text{-chxn})_2][Ni(CN)_4]\}_\infty$ (**3**) and $\{[Cu(S,S\text{-chxn})_2][Ni(CN)_4]\cdot 2H_2O\}_\infty$ (**4**) (where R,R-chxn = *trans*-cyclohexane-(1R, 2R)-diamine and S,S-chxn = *trans*-cyclohexane-(1S, 2S)-diamine).

Syntheses

$[Ni(R,R\text{-chxn})_2][Ni(CN)_4]\cdot 4H_2O$ (1)

Compound **1** was obtained as pink rod-like crystals by slow diffusion of an aqueous solution of $[Ni(R,R\text{-chxn})_3]SO_4$ layered onto a H_2O-EtOH (1:1) solution of $K_2[Ni(CN)_4]$ after several weeks. Elemental analysis for $C_{22}H_{46}N_{10}Ni_2O_4$: calc. C, 41.81; H, 7.34; N, 22.16, found C, 41.54; H, 7.92; N, 22.02%.

$[Cu(R,R\text{-chxn})_2][Ni(CN)_4]\cdot 2H_2O$ (2)

Compound **2** was obtained as violet plate-like crystals by layering an aqueous solution of $[Cu(R,R\text{-chxn})_3]SO_4$ layered onto a H_2O-EtOH(1:1) solution of $K_2[Ni(CN)_4]$ after several weeks. The crystals have a slightly smaller unit cell than the same structure published by Akitsu et al[13], due to the fact the crystal was measured at -100°C. Elemental analysis for $C_{16}H_{32}N_8CuNiO_2$: calc. C, 39.16; H, 6.57; N, 22.83, found C, 39.26; H, 6.48; N, 22.99%.

{[Cu(R,R-chxn)$_2$][Ni(CN)$_4$]}$_\infty$ (3)

Complex **3** was obtained as a purple powder by heating compound **2** to 110°C, using thermogravimetric analysis. Elemental analysis (%) calculated for $C_{16}H_{28}N_8CuNi$: C, 42.27; H, 6.21; N, 24.64, found C, 42.26; H, 6.36; N, 24.26%.

{[Cu(S,S-chxn)$_2$][Ni(CN)$_4$]·2H$_2$O}$_\infty$ (4)

Compound **4** was obtained as violet block-like crystals by slow diffusion of an acetonitrile solution of [Cu(*trans*-(S,S-chxn)$_2$(H$_2$O)](NO$_3$)$_2$ (1mmol, 10mL) layered onto an aqueous solution of K$_2$[Ni(CN)$_4$]·H$_2$O (1mmol, 10mL). Elemental analysis for $C_{16}H_{32}N_8CuNiO_2$: calc. C, 39.16; H, 6.57; N, 22.83, found C, 39.32; H, 6.71; N, 22.93%.

Crystal Structure Analyses

The intensity data for crystals of compounds **1**, **2**, and **4** were collected at 173K (-100°C) on Stoe Image Plate Diffraction Systems, equipped either with a one-circle or a two-circle goniometer, using MoKα graphite monochromated radiation (λ = 0.71083 Å). The structures were solved by Direct methods using the program SHELXS-97.[14] The refinement and all further calculations were carried out using SHELXL-97.[14] The water and NH$_2$ H-atoms were located from Fourier difference maps and freely refined. The remainder of the H-atoms were included in calculated positions and treated as riding atoms using SHELXL default parameters. The non-H atoms were refined anisotropically, using weighted full-matrix least-squares on F^2. The structure of complex **3** was solved and refined by X-ray powder methods (Supporting Information: Figure S1). The micro-crystalline powder was inserted in a glass capillary of a 0.5 mm diameter. X-ray powder data were collected at room temperature on a computer controlled STOE-STADIP

focusing powder diffractometer[15, 16] equipped with a curved Ge(111) monochromator ($CuK\alpha_1$, λ=1.54051Å). A STOE linear position sensitive detector (PSD) was used. The data were collected in the range of $4° \leq 2\theta \leq 90°$ using a step width of 0.1°. The indexing procedure was performed using ITO[17] in WinXPow.[18] The structure solution was carried out using the program DASH[19] introducing a structural model.[20] The obtained position of the molecule in the given symmetry and unit cell was used for Rietveld refinement in GSAS/EXPGUI.[21, 22] One small impurity peak at $2\theta = 8.2°$ has been excluded from the refinement. After the initial refinement of the scale and unit cell constants, the atomic positions were refined using soft constraints defining the geometry of the molecule within some allowable errors.[23] Subsequent Rietveld refinement was carried out gradually relaxing the bond restraints. The non-hydrogen atoms were refined isotropically applying an overall temperature factor for the all C and N atoms. The H-atoms were treated as riding atoms, with fixed temperature factors. In the final cycles of refinement, the shifts for all of the parameters were less than their standard uncertainties. Further crystallographic and refinement details for compounds **1** – **4** are given in Table 1.

Table 1. Crystal and Structure Refinement Data for **1, 2** and **4** (single crystals), and **3** (powder).

	1	**2**	**3**	**4**
formula	$C_{22}H_{46}N_{10}Ni_2O_4$	$C_{16}H_{32}N_8CuNiO_2$	$C_{16}H_{28}N_8CuNi$	$C_{16}H_{32}N_8CuNiO_2$
Mw	632.11	490.75	454.70	490.75
Colour/habit	Pink/rods	Violet/blocks	Purple/powder	Violet/blocks

crystal system	orthorhombic	monoclinic	orthorhombic	monoclinic
space group	$P2_12_12_1$	$P2_1$	$P2_12_12_1$	$P2_1$
a(Å)	11.7485(4)	7.9483(8)	9.9528(5)	11.5836(10)
b(Å)	16.1467(5)	15.2611(11)	23.3963(13)	9.1343(5)
c(Å)	16.3226(5)	9.7985(10)	8.8936(6)	11.6110(11)
α°	90	90	90	90
β°	90	109.792(11)	90	111.699(7)
γ°	90	90	90	90
V(Å^3)	3096.39(17)	1118.35(18)	2070.96(19)	1141.48(16)
Z	4	2	4	2
ρ_{calcd}(Mg/m^3)	1.356	1.457	1.458	1.428
λ(Å)	0.71073	0.71073	1.54051	0.71073
T(K)	173	173	293	173
μ(mm^{-1})	1.259	1.820	2.53	1.783
refl. collected	60093	8848	1526	10958
indep. refl.	8400	4221	-	4277
obsd. refl. >2σ(I)	7370	3229	-	3819
no. of params.	342	265	172	325
R1[a] [$I > 2\sigma(I)$]	0.0368	0.0332	0.0821[c]	0.0211
wR2[b] [$I > 2\sigma(I)$]	0.0882	0.0633	0.0603[d]	0.0505
R_F[e]	-	-	0.036	-
$\Delta\rho_{max}/\Delta\rho_{min}$ (eÅ^{-3})	0.631/-0.582	0.335/-0.486	0.303/-0.268	0.362/-0.430
Flack factor	0.014(13)	0.009(18)	NA	-0.013(13)

[a] $R1 = \Sigma||F_O| - |F_C||/\Sigma|F_O|$. [b] $wR2 = [\Sigma w(F_O^2 - F_C^2)^2/\Sigma wF_O^4]^{1/2}$. [c] $R_{wp} = [\Sigma w(I_O - I_C)^2/\Sigma wI_O^2]^{1/2}$, [d] $Rp = \Sigma|I_O - I_C|/\Sigma I_C$, [e] $R_F = \Sigma|F_O| - |F_C|/\Sigma|F_O|$.

Crystal structure of $[Ni(R,R\text{-chxn})_2][Ni(CN)_4]\cdot 4H_2O$ (1)

The crystal structure analysis of **1** revealed that it consists of discrete $[Ni(R,R\text{-chxn})_3]^{2+}$ cations and $[Ni(CN)_4]^{2-}$ anions and four molecules of water of crystallization (Figure 1). The coordination geometry around the nickel atom of the cation, Ni1, has a slightly distorted octahedral geometry (average distance Ni1 – N = 2.119(3) Å).

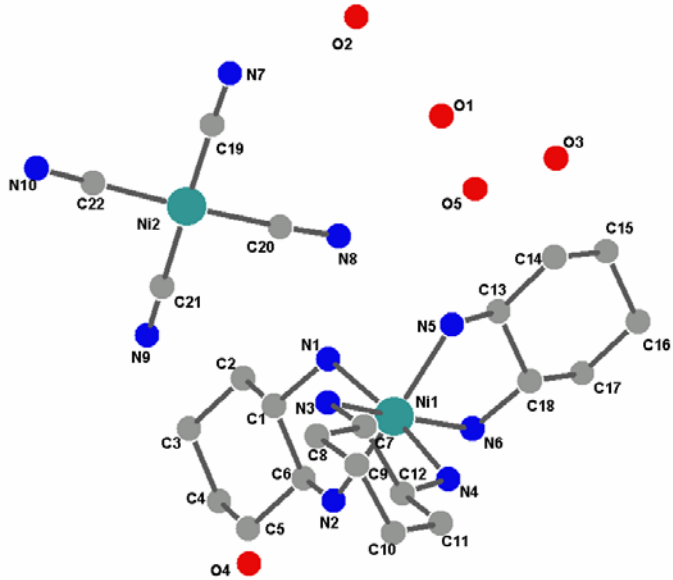

Figure 1. View of the asymmetric unit of **1** (H-atoms omitted for clarity).

As is usual, the $[Ni(CN)_4]^{2-}$ anion exhibits a nearly planar structure (average bond lengths Ni2 ─ C = 1.856(3) Å and C─N = 1.141(5) Å). The crystal packing of complex **1** viewed along the a-axis is shown on Figure 2. All four cyanide groups of the anion are engaged in hydrogen bonds with the three water molecules and the NH_2 group of the ligand (d_{N7-O2} = 2.914(5) Å, d_{N7-N4} = 3.010(3) Å, d_{N8-O5} = 2.914(7) Å, d_{N8-N5} = 3.086(3) Å, d_{N9-O3} = 2.969(5) Å, d_{N9-O5} = 2.902(8) Å, d_{N10-O2} = 2.779(4) Å).

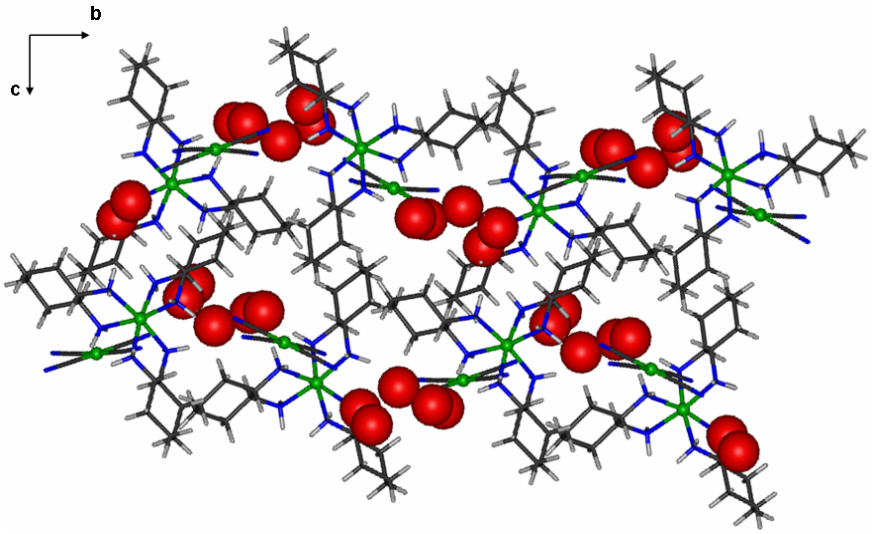

Figure 2. Crystal packing of complex **1** viewed along the a-axis. The water molecules are shown as red balls.

Crystal structures of $[Cu(R,R\text{-chxn})_2][Ni(CN)_4]\cdot 2H_2O$ (2) and $\{[Cu(R,R\text{-chxn})_2][Ni(CN)_4]\}_\infty$ (3)

Compound **2** was obtained as violet block-like crystals. The structure consists of a chiral $[Cu(R,R\text{-chxn})_2]^{2+}$ cation linked to a $[Ni(CN)_4]^{2-}$ anion, so forming a binuclear complex arranged in the crystal in a *zig-zag* manner (Figure 3). The average bond lengths and angles, for example, the Cu1 – N bond lengths involving the cyanide groups, are slightly shorter (by 0.03 Å) than those reported for the room temperature structure.[13] In the crystal structure of **2** the bimetallic complexes are arranged head-to-tail in a zig-zag fashion, separated by the water molecules of crystallization, and with the shortest non-bonded electrostatic Cu…N≡C interaction being Cu1…N1 of 3.153(3) Å (Figures 3 & 5).

On heating crystals of **2**, the water molecules of crystallization are lost and a purple microcrystalline powder was obtained. Structure analysis of the high-resolution powder X-ray diffractogram (Supporting Information: Figure S1) revealed that compound **2** had

been transformed into a one-dimensional polymer $\{[Cu(R,Rchxn)_2][Ni(CN)_4]\}_\infty$ (**3**) (Figure 3). The binuclear molecules of **2** have aligned themselves and the copper atoms in **3** are now bridged by cyano groups, with Cu…N≡C bond distances of 2.146(12) and 2.722(11) Å (Table 2).

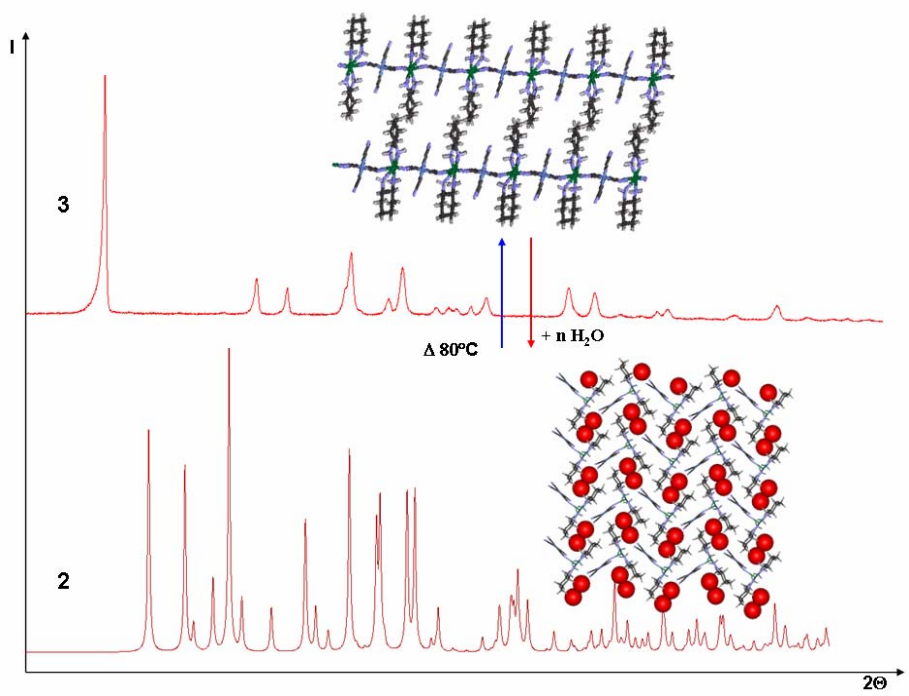

Figure 3. PXRD diffractograms illustrating the transformation of compound **2** to compound **3**.

Immersion of powder **3** into water revealed that the system is reversible; the original structure **2** was recovered, as shown by powder X-ray diffraction (Figure 4a-c). The color of the sample also changed reverting from purple to violet. Immersion of powder **3** into methanol, acetonitrile or ethyleneglycol gave violet-like microcrystalline solids with different powder X-ray diffractograms (Figure 4d-f). In all cases the reactions were found to be reversible. Simple heating of these new species released the solvent molecules and

the final diffractograms were found to be identical to that of compound **3**. Work is currently in progress to resolve the structures of these new species from their powder X-ray diffractograms.

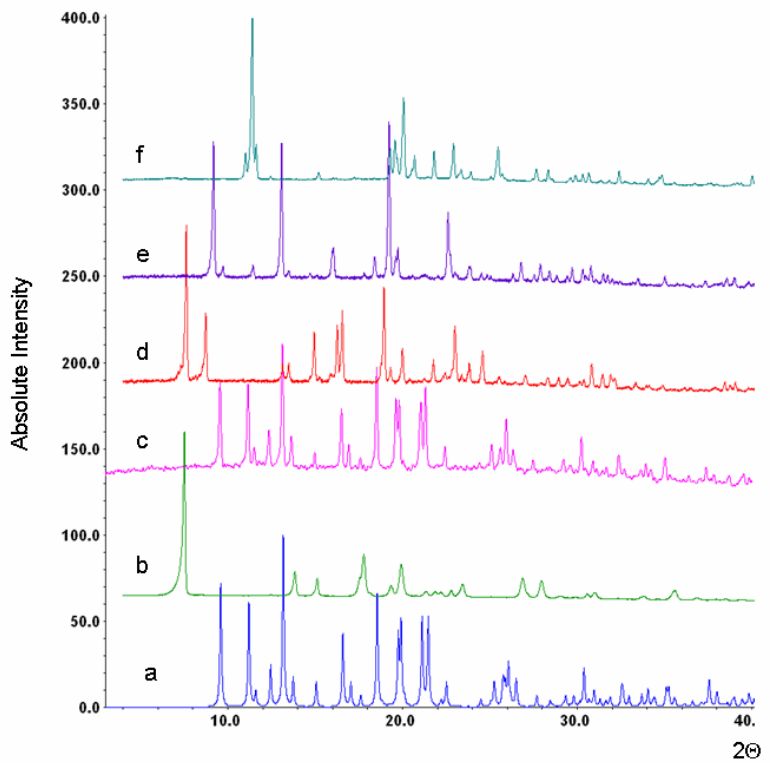

Figure 4. PXRDs of $\{[Cu(R,Rchxn)_2][Ni(CN)_4]\}_\infty$ **(3)** immersed in different solvents: a– theoretical pattern of the single crystal of **2**; b– measured pattern of the sample after thermogravimetric analysis (= **3**); c– sample **3** immersed into water, giving again compound **2**; d– sample **3** immersed into methanol; e– sample **3** immersed into acteonitrile; f– sample **3** immersed into ethyleneglycol.

Crystal structure of $\{[Cu(S,S\text{-}chxn)_2][Ni(CN)_4]\cdot 2H_2O\}_\infty$ (4)

Using *trans*-cyclohexane-(1S,2S)-diamine instead of *trans*-cyclohexane-(1R,2R)-diamine we expected to obtain the enantiomer of the ionic complex **2**. However, the

crystal structure analysis of compound **4** revealed that it is a new one-dimensional chiral polymer $\{[Cu(S,S\text{-}chxn)_2][Ni(CN)_4]\cdot 2H_2O\}_\infty$ [see Figure 5c]. Complex **4** crystallized in the monoclinic space group $P2_1$, compared to the orthorhombic space group $P2_12_12_1$ for compound **3**, hence it is a pseudo polymorph of **3**. In **4** the Cu1 atoms of the cationic units have elongated octahedral geometry due to Jahn-Teller effects. Bond distances and angles involving the C ≡ N groups for compounds **2**, **3** and **4** as compared in Table 2.

Table 2. Bridging bond lengths (Å) and angles (deg) in compounds **2, 3** and **4**.

2		**3**		**4**	
Cu1 – N1	3.153(3)	Cu1 – N1	2.722(11)	Cu1 – N3	2.465(4)
Cu1 – N3	2.299(4)	Cu1 – N3	2.146(12)	Cu1 – N4	2.538(4)
Cu1-N1-C1	94.68(7)	Cu1-N1-C13	103.11(8)	Cu1-N3-C3	131.2(3)
Cu1-N3-C3	138.1(4)	Cu1-N3-C15	104.09(7)	Cu1-N4-C4	129.7(3)

The geometrical parameters for the $[Ni(CN)_4]^{2-}$ anion are comparable to those in known related complexes.[24, 25] Like complex **3**, **c**omplex **4** is a one-dimensional zig-zag chain composed of alternating *trans*-$[Cu(chxn)_2]^{2+}$ cations and $[Ni(CN)_4]^{2-}$ anions running along the crystallographic b-axis (Figure 5a).

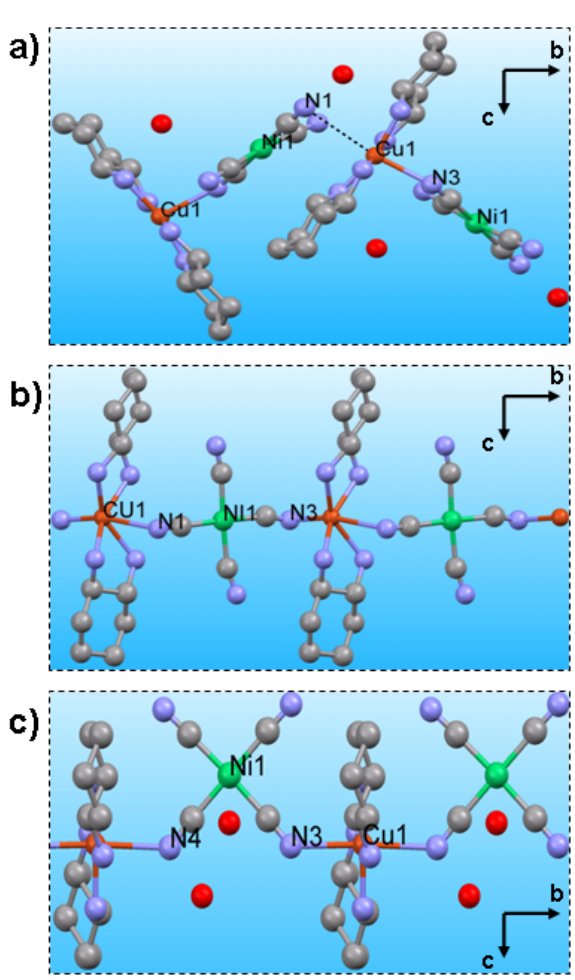

Figure 5. View of the crystal packing down the a-axis for: a) compound **2**; b) compound **3**; and c) compound **4** (H-atoms have been omitted for clarity. Red balls in **2** and **4** represent water molecules).

In the crystal structure of **4**, hydrogen bonding leads to the formation of a three-dimensional network (Figure 6). The non-bridging C≡N groups of the Ni1 tetracyanonickelate moiety form hydrogen bonds with both water molecules: [D…A] 2.930(5) Å for O1w…N1, and 2.937(5) Å for O1w…N2. One of the bridging C≡N groups hydrogen bonds to water O2w: O2w…N4 is 3.0084Å. The same water molecule

hydrogen bonds to a NH_2-group: N8….O2w is 2.8623Å, and to water molecule O1w: O2w….O1w is 2.716(3) Å.

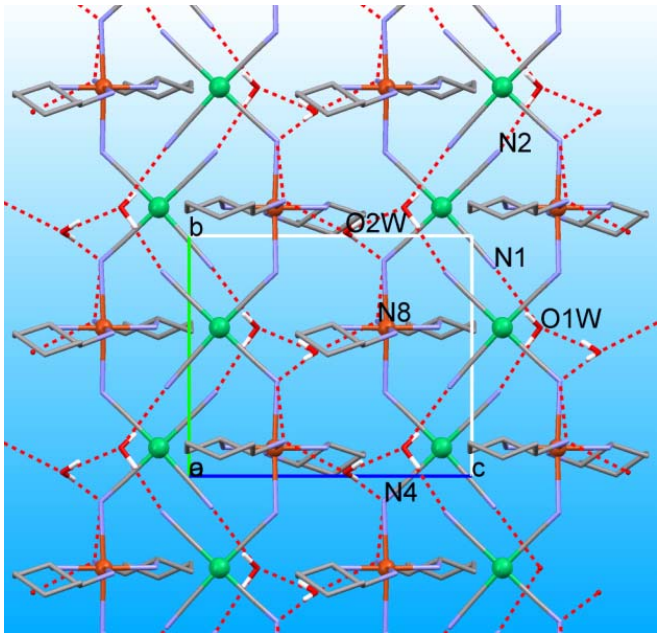

Figure 6. Crystal packing of compound **4** viewed along the a-axis, showing the hydrogen bonding network as red dashed lines (Ligand H-atoms removed for clarity).

Spectroscopic analysis

In the IR spectra, characteristic vibrations for ν(C≡N) were assigned. For complex **1** one strong band at 2133 cm^{-1}, can be attributed to the C≡N stretching vibration. In the spectra of the **2**, **3** and **4** there are two CN strong bands in the region 2116 - 2132 cm^{-1}. The splitting of the ν_{as}(C≡N) compared with that of $K_2[Ni(CN)_4]$ (2127 cm^{-1})[26] indicates the presence of two different coordination modes (monodentate and bridging) of the cyanide ligands.

Circular dichroism measurements (Figure 7) were used to establish the enantiomeric character of the coordination polymers (solid state, using KBr discs) and [Cu(*trans*-

(1*R*,2*R*)-chxn)$_2$(H_2O)$_2$](NO_3)$_2$ (in solution). The enantiopure bis-chelated precursor shows a positive Cotton effect at λ=515 nm. Compound **2** exhibits a positive Cotton effects at the same wavelength, while compound **4** (S,S isomer) shows, as expected, a Cotton effect of the opposite sign at the same wavelength.

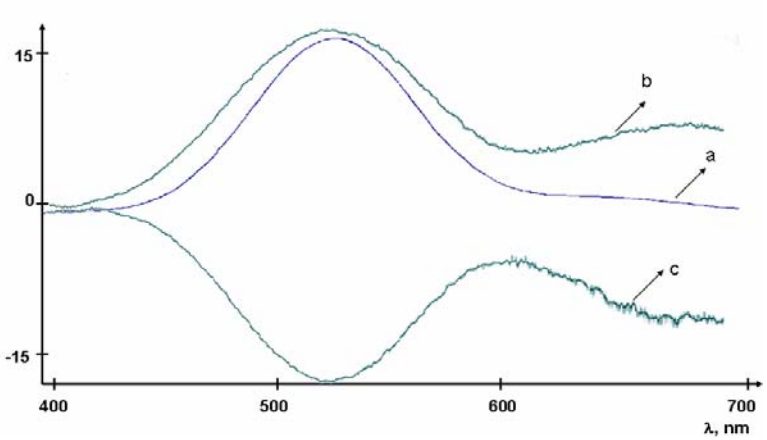

Figure 7. CD spectra of : a) - an acetonitrile - water solution of the bis-chelated precursor [Cu(trans-(1R,2R)-chxn)$_2$(H_2O)$_2$](NO_3)$_2$; b) - a powder sample of [Cu(1R,2Rchxn)$_2$][Ni(CN)$_4$]·2H_2O (2) in a KBr matrix; c) - a powder sample of {[Cu(1S,2Schxn)$_2$][Ni(CN)$_4$]·2H_2O}$_\infty$ (4) in a KBr matrix.

Immersion calorimetry

Immersion calorimetric studies were carried out for compound **3** (Supporting Information: Table S1). This technique, applied mainly to carbons and zeolites, provides an insight into the filling of nanopores.[27-30] It is based on the determination of the enthalpy change occurring on immersing an out-gassed nanoporous sample into a liquid. The enthalpy change is related to the chemical and structural nature of the surface, and the enthalpy of immersion, -Δ_iH, is equal to the integral of the net heat of adsorption.[29, 31] The enthalpy of immersion of **3**, Δ_iH, for water gave an average value of – 55.7 ± 3 J per gram of solid**.** This value is much higher than obtained on immersion into MeOH

(average value of– 40.2 ± 3 J/g) or CH_3CN (average value of – 19.19 ± 3 J/g). It is interesting to note that for water the heat measured is not the heat of filling of nanopores but the heat of transformation of the one-dimensional chiral polymer into the original binuclear structure, **2**. In the case of immersion of **3** into methanol and acetonitrile the X-ray diffractograms indicate the formation of new compounds, whose structures are unknown at present (Figure 4): Hence the values obtained must also reflect structural transformations.

Conclusions

Four new bimetallic chiral tetracyanonickelate (II) complexes, two of which are one-dimensional polymers, have been synthesized and full characterized. The crystal structure of **1** consists of discrete $[Ni(R,R\text{-chxn})_3]^{2+}$ cations and $[Ni(CN)_4]^{2-}$ anions, while that of **2** consists of a bimetallic assembly of the $[Cu(R,R\text{-chxn})_3]^{2+}$ cation and $[Ni(CN)_4]^{2-}$ anion. Compound **2** shows an interesting reversible phase transformation, triggered by heating to remove the water molecules of crystallization, to form a one-dimensional chiral polymer, **3**. Changing *trans*-cyclohexane-(1R,2R)-diamine for *trans*-cyclohexane-(1S,2S)-diamine gave not the enantiomer of compound **2**, but a new one-dimensional polymer with alternating *trans*-$[Cu(S,S\text{-chxn})_2]^{2+}$ cations and $[Ni(CN)_4]^{2-}$ anions. The chiral nature of complexes **2** and **4** has been confirmed by solid state CD measurements. By immersion calorimetric studies it was possible to determine the heat of transformation of the one-dimensional chiral polymer **3** into the binuclear structure **2**. Immersion of **3** into methanol, acetonitrile or ethyleneglycol gave violet-like microcrystalline solids with

different powder X-ray diffractograms. In all cases the reactions were found to be reversible. Work is currently in progress to resolve the structures of these new species.

Acknowledgments: This work was supported by the Swiss National Science Foundation for financial support (Grant № FN 20-111738).

References

[1] W. S. Knowles, *Angew. Chem., Int. Ed.* **2002**, *41*, 1999.
[2] R. Noyori, *Angew. Chem., Int. Ed.* **2002**, *41*, 2008.
[3] K. B. Sharpless, *Angew. Chem., Int. Ed.* **2002**, *41*, 2024.
[4] P. G. Lacroix, R. Clément, K. Nakatani, J. Zyss, I. Ledoux, *Science* **1994**, *263*, 658.
[5] J.-F. Nicoud, *Science* **1994**, *263*, 636.
[6] G. L. J. A. Rikken, E. Raupach, *Nature* **1997**, *390*, 493.
[7] T. Kimura, T. Goto, H. Shintani, K. Ishizaka, T. Arima, Y. Tokura, *Nature* **2003**, *426*, 55.
[8] K. R. Dunbar, R. A. Heintz, *Prog. Inorg. Chem.,* **1997**, *45*, 283.
[9] J. Cernák, M. Orendác, I. Potocnák, J. Chomic, A. Orendácová, J. Skorsepa, A. Feher, *Coord. Chem. Rev.* **2002**, *224*, 51.
[10] M. Vergaguer, *Science* **1996**, *272*, 698.
[11] M. Verdaguer, A. Bleuzen, V. Marvaud, J. Vaissermann, M. Seuleiman, C. Desplanches, A. Scuiller, C. Train, R. Garde, G. Gelly, C. Lomenech, I. Rosenman, P. Veillet, C. Cartier, F. Villain, *Coord. Chem. Rev.* **1999**, *190-192*, 1023.
[12] M. Ohba, H. Okawa, *Coord. Chem. Rev.* **2000**, *198*, 331.
[13] T. Akitsu, Y. Einaga, *Inorg. Chem.* **2006**, *45*, 9826.
[14] G. M. Sheldrick, *Acta Cryst.* **2008**, *A64*, 112.
[15] E. R. Wolfel, *J. Appl. Cryst.* **1981**, *14*, 291.
[16] E. R. Wolfel, *J. Appl. Crystallogr* **1983**, *16*, 341.
[17] J. W. Visser, *J. Appl. Cryst.* **1969**, *2*, 89.
[18] WinXPow, *STOE Powder Diffraction Software*, Stoe & Cie GmbH, Darmstadt, Germany.
[19] DASH, *CCDC Software*, 12 Union Road, Cambridge CB2 1EZ, UK.
[20] PCMODEL V8.5, *Serena Software*, Box 3076, Bloomington, IN 47402-3076.
[21] A. Larson, R. Von Dreele, *General Structure Analysis System*, Los Alamos National Laboratory Report LAUR 86-748, **2000**.
[22] B. H. Toby, *J. Appl. Cryst.* **2001**, *34*, 210.
[23] J. C. Wilson, E. Prince, *International Tables for X-ray Crystallography, Vol. C*, Kluwer Academic Publishers, Dordrecht, The Netherlands, **1999**.

[24] M. Broring, S. Prikhodovski, C. D. Brandt, E. C. Tejero, *Chem. Eur. J.* **2007**, *13*, 396.
[25] H. Yuge, Y. Noda, T. Iwamoto, *Inorg. Chem.* **1996**, *35*, 1842.
[26] H. Freund, C. R. Schneider, *J. Am. Chem. Soc.* **1959**, *81*, 4780.
[27] F. Stoeckli, *Adsorption Science and Technology* **1993**, *10*, 3.
[28] F. Stoeckli, A. Lavanchy, D. Hugi-Cleary, *Fundamentals of adsorption* **1998**, *6*, 24.
[29] F. Stoeckli, D. Hugi-Cleary, T. A. Centeno, *J. Eur. Ceram. Soc.* **1998**, *18*, 1177.
[30] J. Silvestre-Albero, C. Gomez de Salazar, A. Sepulveda-Escribano, F. Rodriguez-Reinoso, *Colloid Surface Physicochem Eng Aspect* **2001**, *187-188*, 151.
[31] F. Stoeckli, *Adsorpt. Sci. Technol.* **1993**, *10*.

Supporting Information

Figure S1. The Reitveld refinement of PXRD for $\{[Cu(R,Rchxn)_2][Ni(CN)_4]\}_\infty$ (**3**), (— calculated pattern, + observed pattern). The bottom curve is the difference curve on the same intensity scale.

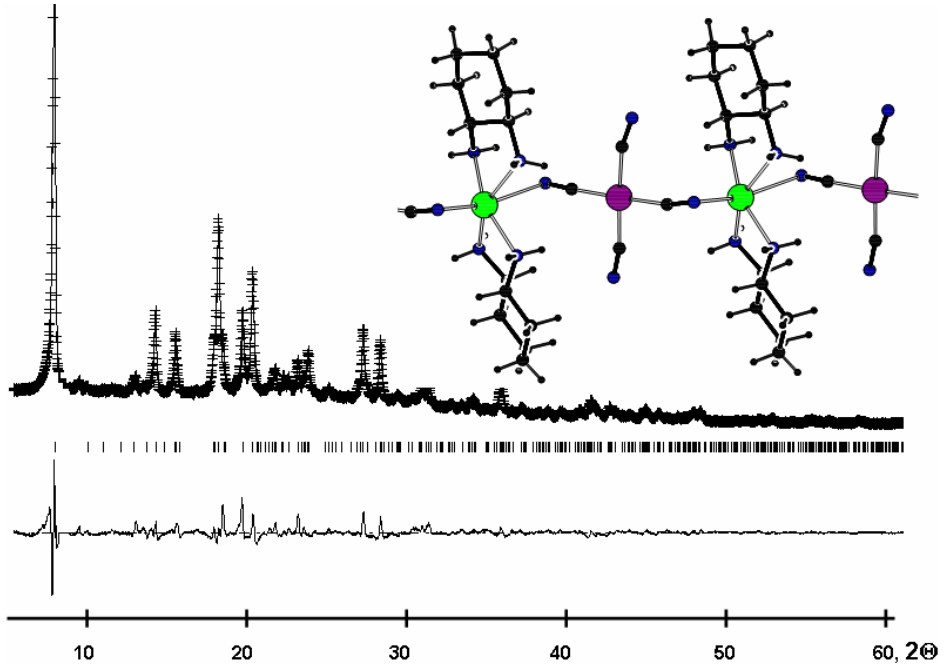

Immersion calorimetry

Immersion calorimetry experiments were carried out at 293 K on samples of 0.014-0.020 g using a TIAN-CALVET type calorimeter.[1-3] The outgassed samples of **2** were placed in the calorimetric cells which in turn are placed in a water bath controlled by a thermo-regulator system LUDA MS. The thermal flow was monitored by the current through 180 Cu/constantan thermocouples connected to a nanovoltmeter PREMA 8017. The integral of the voltage versus time curve, is proportional to the energy generated during the immersion process, typically between 1 and 10 J. The accuracy varies between 4 and 5 % depending on the absolute energy liberated in the process and on the amount of solid used.

Table S1. Enthalpies of immersion, $\Delta_i H$, of compound **3** into water, methanol and acteonitrile.

Solvent	Weight, g	$-\Delta_i H$, J/g
Water	0.0095	54.95
	0.0116	56.42
	0.0145	54.01
	0.0121	57.41
Methanol	0.0140	40.83
	0.0175	38.65
	0.0161	41.09
	0.0140	40.24
Acetonitrile	0.0084	18.64
	0.0110	16.90
	0.0094	22.03

[1]. R. C. Bansal, J. B. Donnet, F. Stoeckli, *Active Carbon*, Marcel Dekker, New York, **1988**.
[2]. F. Stoeckli, D. Hugi-Cleary, T. A. Centeno, *J. Eur. Ceram. Soc.* **1998**, *18*, 1177.
[3]. F. Stoeckli, *Russ. Chem. Bull. Int. Ed.* **2001**, *50,* 2265.

Chapter 3. Adsorption and Immersion Studies

Preface

This part is focused on the construction of metal-organic cyano-bridge frameworks (MOCBF) with the large cavities and the evaluation of their adsorption behavior. The two studies presented here have in common the fact that the systems show reversible structural transformations. In order to understand and interpret the structural transformations the main techniques used were PXRD, immersion calorimetry and gravimetric adsorption. In Section 3.1 three new MOCBF are described, two of which have channels occupied by water molecules of crystallization. They show "sponge-like" dynamic behaviour triggered by guest removal and inclusion. The dehydration processes, which involve changes in the structures, are reversible, and this was shown using powder X-ray diffraction methods. By a combination of the DSC, PXRD and immersion calorimetry studies it was possible to find the net heat of the transformation. A remarkable structural transformation, driven by solvent molecules, is presented in Section 3.2. It was found that the two types of reported networks show different behavior upon drying, falling within the category of "recoverable collapsing" and "guest-induced reformation" frameworks. These changes are fully reversible and dependant on the nature of the guests. The methanol adsorption isotherm for the fully out-gassed compound indicates that it is a two step process, and the desorption isotherm shows that it is also reversible. Immersion calorimetric studies with different solvents were carried out for both compounds. By the gravimetric adsorptions studies it was shown that the synthetic strategy based on cyanide-bridged bimetallic assemblies is advantageous for the formation of flexible nanoporous materials.

3. 1

Bimetallic Metal-Organic Cyano-Bridged Frameworks

Olha Sereda, Fritz Stoeckli and Helen Stoeckli-Evans

Submitted to Crystal Growth and Design

Abstract

Three new Metal-Organic Cyano-Bridged Framework compounds (MOCBF's), namely $\{\{[Cd_3(tn)_4][Co(CN)_6]_2\}\cdot 5H_2O\}_\infty$ (**1**), $\{[Cd(tn)]_3[Cr(CN)_6]_2\}_\infty$ (**2**), and $\{[Cu_2(tn)_2][Ru(CN)_6]\cdot 4H_2O\}_\infty$ (**3**), incorporating the organic ligand 1,3-diaminopropane, have been synthesized and characterized by IR, X-ray diffraction, elemental analysis and immersion calorimetry. All three compounds have three-dimensional network structures, with both the organic ligand and the cyano groups acting as bridges. Compounds **1** and **3** have channels occupied by water molecules of crystallization. All three complexes are stable indefinitely when exposed to the air at room temperature. However, when compounds **1** and **3** are heated they loose the water molecules of crystallization. The X-ray powder diffractograms of these dried, and as yet unknown species, are different to those of the original compounds. However, in a humid atmosphere both dried compounds readsorb water molecules and revert to the original structures, as shown by X-ray Powder diffraction measurements. The adsorptive properties of compounds **1** and **3**, with regards to water, have been studied using both in situ powder X-ray diffraction and immersion calorimetry.

Keywords: metal-organic frameworks / hexacyanometallate / structural transformations / immersion calorimetry

Introduction

Porous metal–organic frameworks (MOFs) have received a great deal of attention recently owing to their potential applications in several areas, for example, gas storage, gas separation, and heterogeneous catalysis.[1-4] Cyano-bridged inorganic coordination polymers prepared by assembling cyanometallate anions and transition metal complexes as building blocks have also been found to have framework structures. Hexacyanometallates, $M^{II}(CN)_6^{3-}$ and $M^{III}(CN)_6^{4-}$, are good building blocks and they have been used to develop a wide range of architectures that exhibit various structures, some with interesting magnetic properties.[5-8] The Prussian blue family are amongst the earliest known coordination compounds and their diverse magnet and electronic properties have been studied extensively.[9] Until recently gas sorption properties of these compounds have remained largely unexplored.[10] A few examples of cyano-bridged inorganic coordination polymers based on hexacyanometallates, have been reported as being porous materials,[11, 12] despite the fact that the building blocks show various geometrical structures.

We have focused our efforts on the study of crystalline materials since the attainment of well-defined structures is intimately linked to an understanding of the design, synthesis and properties of such materials. In particular, we have been interested in the construction of porous materials in which phase transformations can be effected. In this work, we report on three new three-dimensional metal-organic cyano-bridged frameworks prepared from the hexacyanometallates $[Co(CN)_6]^{3-}$, $[Cr(CN)_6]^{3-}$ and $[Ru(CN)_6]^{2-}$, the ligand 1,3-diaminopropane (tn), and a metal(II) sulfate ($M^{II}SO4$: M = Cd^{2+}, Cu^{2+}).

Results and Discussion

Crystal Structure of $\{\{[Cd_3(tn)_4][Co(CN)_6]_2\}\cdot 5H_2O\}_\infty$ (1)

The crystal structure analysis of **1** revealed that it is a three-dimensional network with both tn and cyano bridges. The asymmetric unit consists of half a $[Co(CN)_6]^{3-}$ anion, one and a half $[Cdtn]^{2+}$ cations, and 2.5 water molecules (Figure 1). Atom Cd2 is located on a 2-fold axis, while all the other atoms are at general positions.

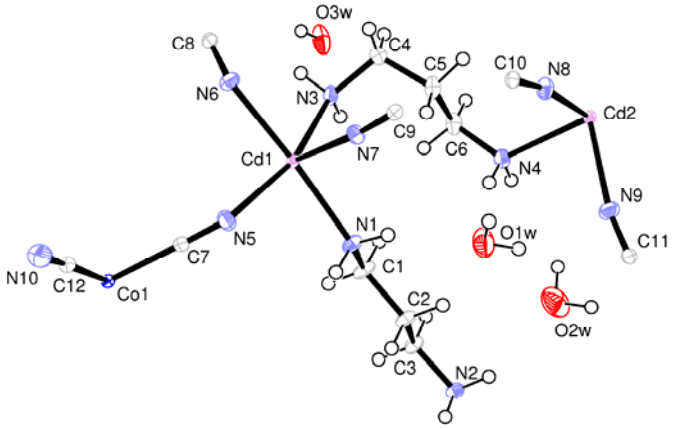

Figure 1. View of the asymmetric unit of **1**, showing the atom numbering scheme and displacement ellipsoids drawn at the 50% probability level.

Atom Cd1 is coordinated to three N-atoms from tn ligands (one is bridging to Cd2 and the two others to Cd1) and three N-atoms from the CN groups. Atom Cd2 also has an octahedral coordination, but is coordinated to only two N-atoms from tn ligands (bridged to Cd1) and four from CN groups. The bond distances and angles in the diamine skeletons are in the expected range (average values: 1.483 (2) Å for N–C, 1.518(2) Å for C–C, with bond angles of 123.02(11)° for Cd–N–C, and 114.05(14) for C–C–C); in good agreement with published work.[13] The metal coordination environment of the hexacyanocobaltate (III) moiety is in good agreement with reported structures.[14, 15] The Cd–N bond lengths vary from 2.318(2) to 2.416(2) Å.

Five of the six CN groups are bridging, while the sixth hydrogen bonds with water O3w located in the cavity (Fig. 2). Finally, it is worth noting the unusual bridging coordination mode of the tn ligand, which leads to a Cd···Cd separation of 6.986(1) Å. The structure can be described as being formed of hexa-metallocycles of the type (─Cd1─tn─Cd1─tn─Cd2─tn─Cd1─tn─Cd1─tn─Cd2─) consisting of only Cd atoms and tn ligands, which are connected via cyano bridges to form a three dimensional network (Figure 2).

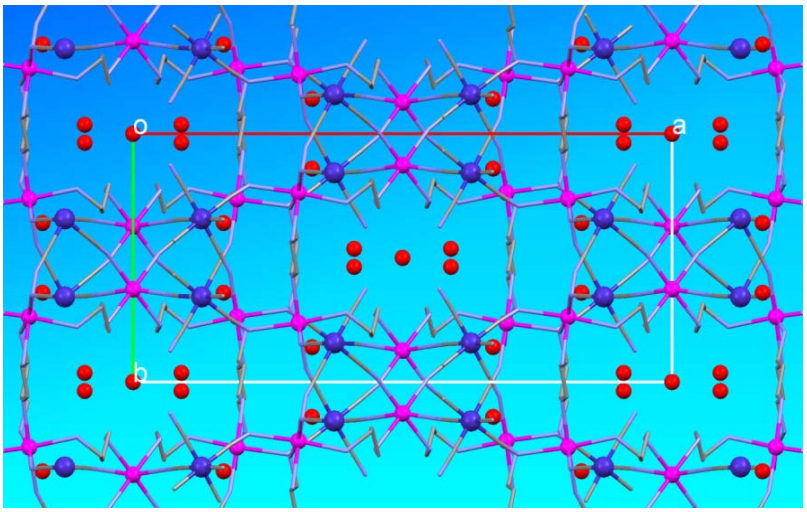

Figure 2. View down the c-axis of the crystal packing in **1**. In the center can be seen the hexa-metallocycle, which is formed of Cd atoms (pink) bridged by tn ligands only. The water molecules in the cavities are shown as red balls. The H atoms omitted for clarity.

The cyano bridges involve tetra- (─Cd2─NC─Co1─CN─Cd2─NC─Co1─CN-) and tris- (─Cd1─NC─Co1─CN─Cd2─tn─) metallocycles. The water molecules in the cavities are hydrogen bonded to the terminal CN groups [N….O3w 2.871(2) Å], and water O2w is hydrogen bonded to the NH_2-group of the tn ligand [N…O2w 3.042(2) Å]. In the crystal structure of **1** the potential solvent volume of 484.4 $Å^3$, occupied by the water molecules of crystallization, accounts for 11.8% of the volume of the unit cell (4092.2 $Å^3$).[16]

Crystal Structure of $\{[Cd(tn)]_3[Cr(CN)_6]_2\}_\infty$ (2)

The crystal structure analysis of **2** revealed that it is a three-dimensional network with both tn and cyano bridges. The asymmetric unit consists of two half $[Cr(CN)_6]^{3-}$ anions and 1.5 $[Cd(tn)]^{2+}$ cations (Figure 3).

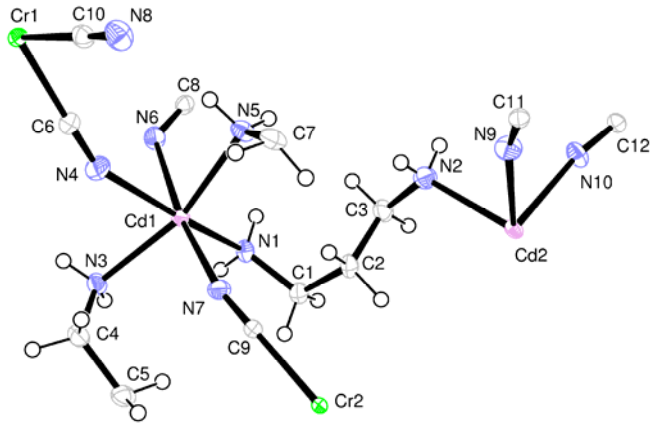

Figure 3. View of the asymmetric unit of **2**, showing the atom numbering scheme and displacement ellipsoids drawn at the 50% probability level.

The Cr atoms of the hexacyanochromate (III) anions, Cr1 and Cr2, are located on inversion centers. Atom Cr1 coordinates to three adjacent $[Cd1(tn)]^{2+}$ cations through four cyano nitrogens, while atom Cr2 coordinates to four adjacent $[Cd2(tn)]^{2+}$ cations. Each Cr^{III} ion has almost regular octahedral coordination geometry. The Cr–C bond lengths are 0.16–0.18 Å longer than the Co–C bond lengths, as is usually observed.[17, 18] The Cd atoms have octahedral coordination geometries. Atom Cd1 sits at a general position, while atom Cd2 is located on an inversion center. The Cd – N(cyano) distances lie in the range 2.2878(16) - 2.4511(16) Å, while the Cd-N(tn) distances average 2.385(15) Å, which is normal in six coordinated CdN_6.[13]

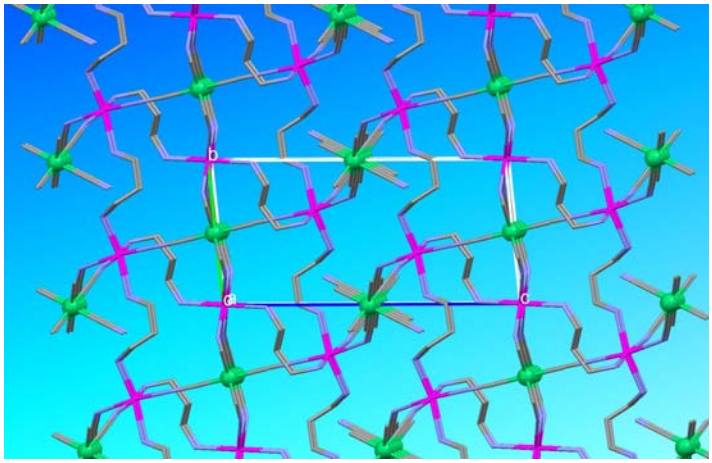

Figure 4. View down the a-axis of the crystal packing in **2**, (Cd–pink, Cr–green). The H atoms omitted for clarity.

Again the structure can be described as being formed of hexa-metallocycles of the type (─Cd1─tn─Cd1─tn─Cd1─tn─Cd1─tn─Cd1─tn─Cd1─) consisting of only Cd1 atoms and tn ligands. They are connected via cyano bridges to form a three dimensional network (Figure 4). This time the cyano bridges involve penta- (─Cd1─NC─Cr2─CN─Cd2─tn─Cd1─NC─Cr1─CN─), tetra- (─Cd1─NC─Cr1─CN─Cd1─NC─Cr1─CN-) and tris- (─Cd1─tn─Cd2─NC─Cr2─CN─) metallocycles.

Crystal Structure of $\{[Cu_2(tn)_2][Ru(CN)_6]\cdot 4H_2O\}_\infty$ (3)

Complex **3** is isostructural with the iron(II) analog.[19] Its structural features are similar to those of compounds **1** and **2**. The asymmetric unit of **3** consists of half a $[Ru(CN)_6]^{4-}$ anion, half a $[Cu(tn)_2]^{2+}$ cation, and two water molecules of crystallization (Figure 5). Atoms Ru1 and Cu1 both lie on inversion centers. The Ru─C and C─N bond distances and C─Ru─C angles are in good agreement with published values found in the Cambridge Crystallographic Data Base.[20-23] The Cu^{II} ion is penta-coordinated, bonding to two nitrogen atoms of two equivalent tn ligands (N4, N5), and to three nitrogen atoms of the cyano groups (N1, N2 and N3).

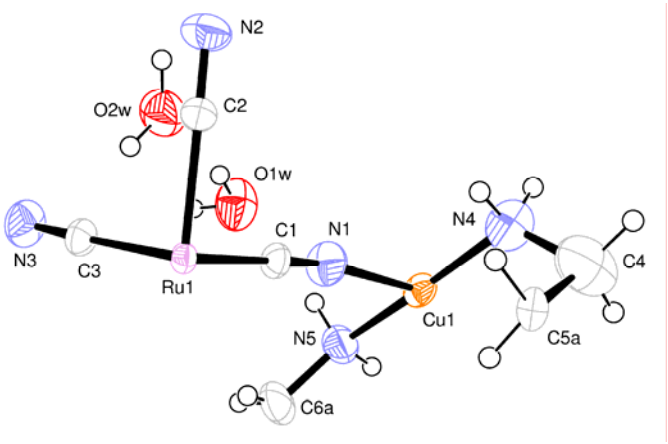

Figure 5. View of the asymmetric unit of the compound **3**, showing the atom numbering scheme and displacement ellipsoids drawn at the 50% probability level. The disorder atoms of the tn ligand have been omitted for clarity.

The N─Cu─N angles in the pseudo base deviate strongly from ideal trigonal-bipyramidal geometry (Figure 6). Such a distortion can be quantified using the τ parameter, as defined by Addison et al. (τ = 1 for trigonal bipyramidal and 0 for square pyramidal).[24] The calculated value τ = 0.57 indicates the extremely high degree of distortion of the coordination polyhedron.

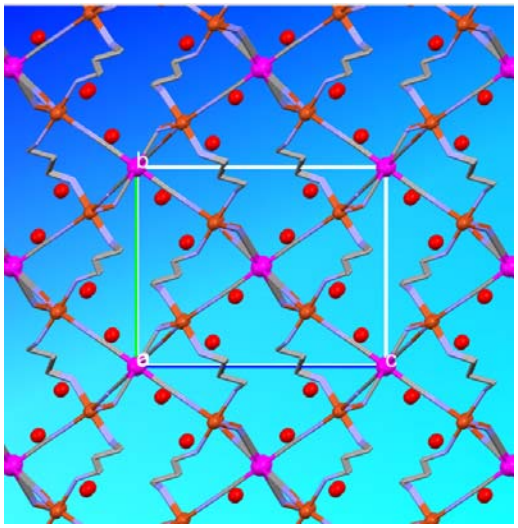

Figure 6. View of the structure of compound **3** (Cu-orange, Ru-pink) along the a-axis, showing the hexa-metallocycles (The red balls represent water molecules. The H atoms omitted for clarity).

In this structure the tn ligand is again acting as a bridging ligand. The ruthenium ion, which has an almost regular octahedral geometry, is linked to six copper (II) ions by six cyanide bridges, while the copper ion is linked to three equivalent $[Ru(CN)_6]^{3-}$ anions. This leads to the formation of a three dimensional arrangement in which the Ru─C─N units are essentially linear, while the Cu─N─C bond angles vary between 149.7(7) – 176.1(8)º. This structure can be described as being formed of hexa-metallocycles of the type (─Cu1─tn─Cu1─NC─Ru1─CN─Cu1─tn─Cu1─NC─Ru1─CN-), consisting this time of both tn and cyano bridges. They are further connected via cyano bridges to form a three dimensional network (Figure 6). This time the supplementary cyano bridges involve tetra- (─Cu1─NC─Ru1─CN─Cu1─NC─Ru1─CN-) and tris- (─Cu1─tn─Cu1─NC─Ru1─CN─) metallocycles only.

In the crystal structure of **3** the potential solvent volume of 174.3 $Å^3$, occupied by the water molecules of crystallization, accounts for 15.8% of the volume of the unit cell (1102.4 $Å^3$).

Infrared Spectra.

The infrared spectra of compounds **1**, **2** and **3** exhibit the absorption bands expected for the tn ligand and the hexacyanometallate counter ions. The presence of the latter is clearly indicated by the strong absorption bands assignable to the ν(C≡N) stretching vibrations in the range 2000-2200cm^{-1}. Coordination of the CN ligand to a second metal ion through its nitrogen atom results in a displacement to higher wavenumber.[25] For **1** the shifts in the ν(CN) stretching frequencies are from 2135 cm^{-1} in $K_3[Co(CN)_6]$[26] to 2172cm^{-1}**,** and for **2** the shifts are from 2130cm^{-1} in $K_3[Cr(CN)_6]$[26] to 2158cm^{-1}. This clearly indicates the assembly of a Co^{III}─CN─Cu^{II} bridge for **1** and a Cr^{III}─CN─Cu^{II} bridge for **2**. The ν(C≡N) stretching frequencies for **3** are found at 2095 cm^{-1}, which is in good agreement with the presence of

$[Ru(CN)_6]^{4-}$ units having at least one terminal CN ligand.[8, 22] The 1,3-diaminopropane ligand is also characterized by the presence in the IR spectrum of bands due to the ν(NH) stretching vibrations of the NH_2 groups, in the 3150-3350 cm^{-1} region, and to the ν(CH) stretching vibrations of the CH_2 groups, in the 2800-2980 cm^{-1} region.[27]

Thermal Analyses, DSC and X-ray Powder Diffraction.

The thermal stability of the water solvated compounds **1** and **3** have been studied by the thermogravimetric analysis (TGA) (Figure S1 in the Supporting information) and differential scanning calorimetry (DSC) (Figure S2 in the Supporting information). TGA for **1** indicates that the water molecules are completely removed at 130°C in one step. There is a weight loss of 7.79% in the temperature range 25-125°C, corresponding to the loss of five water molecules (theoretical value 7.78%). The TG curve for compound **3** clearly shows two steps in the weight loss. The first step is at ca. 60°C with a weight loss of 6.10%, which correspond to two molecules of water (theoretical 5.9%). A final plateau is reached at ca. 85°C with a weight loss of 6.04%. The total weight loss of 12.14% corresponds to the loss of four water molecules (theoretical value is 11.75%). The lability of the water molecules was shown by DSC measurements. The samples were incubated at 20°C followed by heating at a rate of 10° min^{-1} to 100°C. For compound **1** one endothermic effect of 113 J/g was observed at 95.4°C, and for complex **3** one endothermic effect of 131 J/g was observed at 73.5°C.

Some unique and intriguing phenomena were observed upon heating compound **3,** confirmed by in-situ synchrotron powder X-ray diffraction (PXRD) measurements (Figure 7). A capillary containing a powdered sample of **3** was slowly heated to 120°C. Two phase transformations were observed, at ca. 65°C and 105°C, giving

finally a sample whose diffractogram is identical to that of the sample recuperated after TGA, see Figure 8b. The structures of these two new phases are unknown at present.

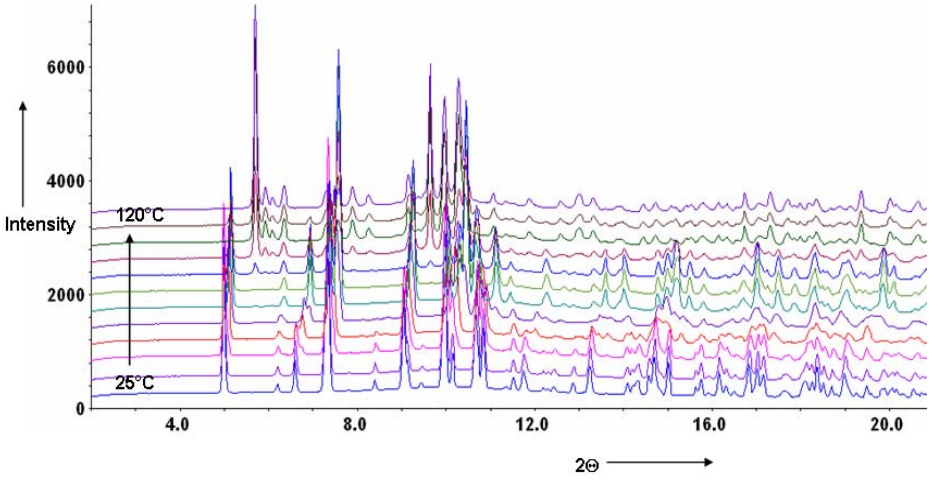

Figure 7. In-situ synchrotron powder X-ray diffraction (PXRD) patterns, showing the phase transformations of compound **3** at *ca.* 65°C and 105°C.

An interesting reversible structural transformation involving a crystalline, and not so highly crystalline state (after TG), was observed for compound **1** (Figure 8). The reversibility of this process was confirmed by PXRD measurements (Figure 8c & d). A capillary containing a powdered sample of **1** after TG (Figure 8b) was immersed into water for 90 minutes. The PXRD was then re measured (Figure 8c), and it was found that the peak positions and intensities were fully coincident with those observed for the single crystal of **1** (Figure 8a). Therefore, complex **1** exhibits "sponge-like" molecular properties: it can easily take up water molecules and return to the original structure. It was possible to repeat this process a number of times without any loss of the crystallinity of **1** (Figure 8d).

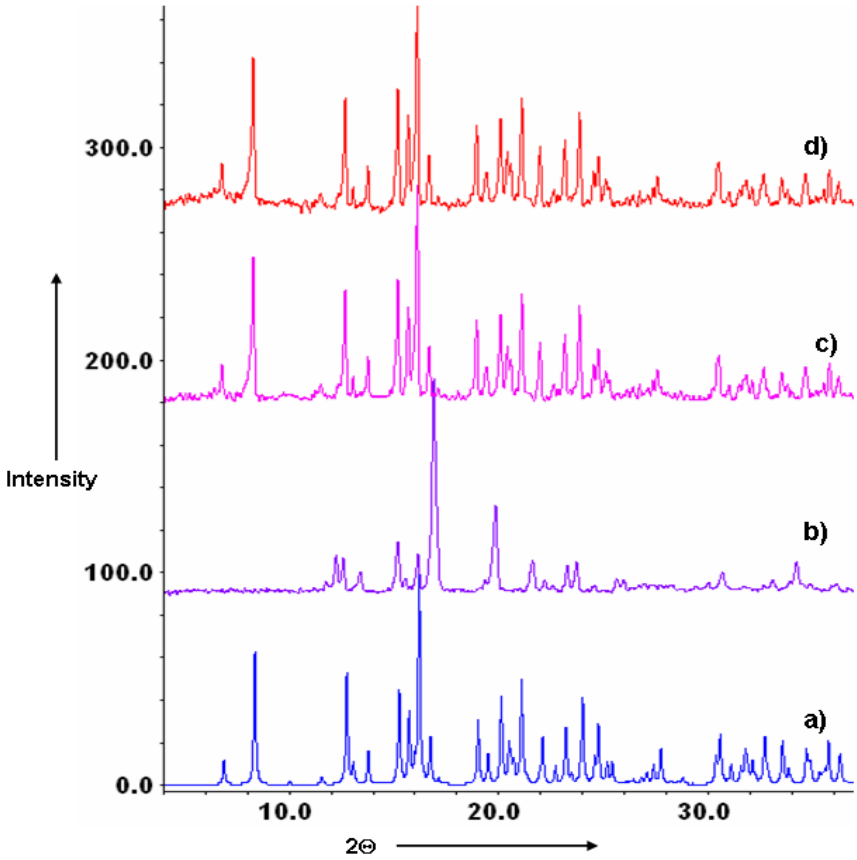

Figure 8. PXRD patterns for **a**) a single-phase polycrystalline sample of **1**; **b**) sample after being heated to 140°C, at which point all five water molecules are lost; **c**) sample from b) after being placed in water for 90 minutes; and **d**) sample after repeating the above procedure [**a** –> **b** –> **c**/**a**] at least three times.

The same "sponge-like" behavior was also found for complex **3**. Figure 9a shows the PXRD pattern of **3** before heating. After heating to 120°C under an inert atmosphere, all four water molecules were removed and the colour of the sample changed from the original light-green to dark-green. The PXRD pattern taken at this point is shown in Figure 9b, and clearly indicates that a change in the crystal structure had taken place.

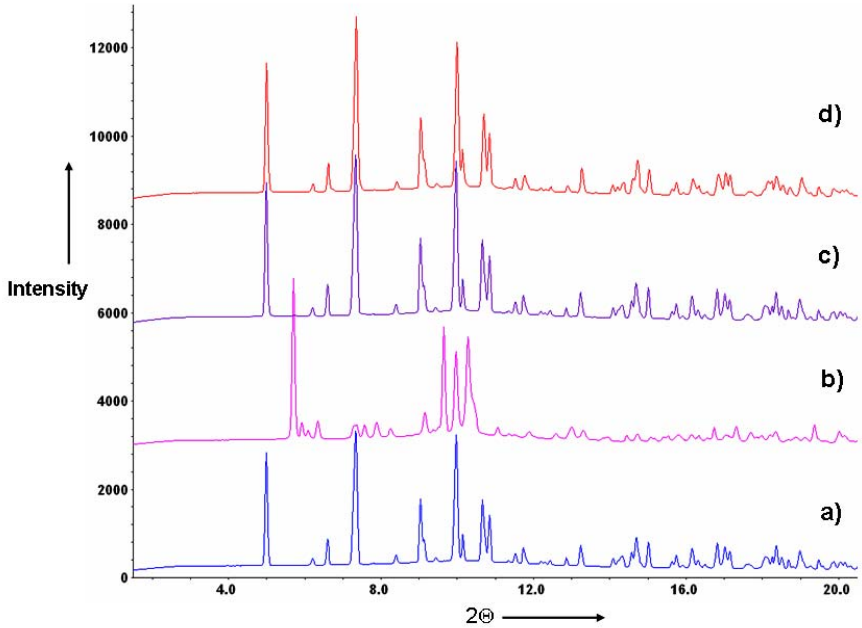

Figure 9. PXRD patterns for **a**) a single-phase polycrystalline sample of **3**; **b**) sample after being heated to 100°C, at which point all four water molecules are lost and the sample colour changed (from light to dark-green); **c**) sample from b) after being placed in water for 30 minutes (the colour turned back to light-green); and **d**) sample after repeating the above procedure [**a** –> **b** –> **c**/**a**] at least four times.

In the IR spectrum of the dried sample there is no absorption band at ~3537 cm^{-1}, which corresponds to the vibration of the water O–H bonds. This is in full agreement with the observation of the loss of the water molecules after TGA. The results of the elemental analysis for this dried sample (found C, 27.39; H, 3.93; N, 26.86. $C_{12}H_{20}N_{10}Cu_2Ru_1$ requires C, 27.07; H, 3.79; N, 26.30 %) confirmed the lost of all four water molecules. This dried sample was then placed in water for 30 minutes. The colour turned from dark-green to the original light-green, and the powder pattern taken at this stage (Figure 9c) is in excellent agreement with the original one, Figure 9a. The IR spectrum of this "wet" sample showed the reappearance of a strong band at 3537 cm^{-1}, indicative of the presence of water molecules in the structure. This reversible structural transformation process associated with a colour change was repeated a number of times. Figure 9d is the PXRD pattern taken after the same

procedure had been repeated four times on the original sample, indicating a very high reversibility.

Immersion calorimetry.

Immersion calorimetry is based on the determination of the enthalpy change occurring on immersing an out-gassed nanoporous sample into a liquid.[28] The enthalpy change is related to the chemical and structural nature of the surface, and the enthalpy of immersion, $-\Delta_t H$, is equal to the integral of the net heat of adsorption.[29, 30] Immersion calorimetry has the advantage of being sensitive and accurate. The studies carried out with compounds **1** and **3** showed that they have similar behaviour for the adsorption of water (Table 1). In both cases, for the samples out gassed at 70ºC (**1**) and 75ºC (**3**), the heat of immersion is equivalent to the heat of filling of the nanopores plus the heat of the structural transformation.

In order to determine the heat of the structural transformation alone compound **3** was out-gassed at 20°C for 7 hours under vacuum (10^{-3} Torr), giving a final weight loss of 12%. The objective of this method was to avoid any change in the structure of the compound on loss of the water molecules of crystallization. The powder X-ray diffractogram of this sample is indeed identical to that of the original compound **3** (Figures 9a & Figure S3 in the Supporting information). It is seen in Table 1 that the heat of immersion of the sample out-gassed at 20°C, which gives the heat of filling of the nanopores alone, is higher than that for the sample out gassed at 75°C, which corresponds to the heat of filling of the nanopores plus the heat of the structural transformation. The difference in $-\Delta_t H$, i.e. ca. 19 ±3 J/g, corresponds to the heat of transformation of the structure. To verify this, a sample of compound **3** out-gassed at 20°C was incubated at 25°C for DSC measurement (heating from 25°C to 120°C at a rate of 10° min^{-1}). One endothermic effect of 21 J/g was observed. This value agrees

well with the value expected from immersion calorimetry, that is, ca. 19 ± 3 J/g. The PXRD pattern of the sample after DSC corresponds to the PXRD pattern of **3** after TGA analysis (Figure S3 in the Supporting information), indicating that on heating the change in the crystal structure had taken place. To the best of our knowledge this is the first time that the heat of a structural transformation has been demonstrated by two different methods.

Table 1. Summary of the immersion calorimetric experiments performed on compounds **1** and **3**.

Sample	Out-gassing conditions	Liquid	- Δ_iH(average) ± 3, J/g
1	70°C for 6 hs	water	32.4
3	75°C for 7 hs	water	28.8
	20°C for 7 hs	water	47.8

Conclusions

Three new cyano-bridged metal-organic frameworks, $\{\{[Cd_3(tn)_4][Co(CN)_6]_2\}\cdot 5H_2O\}_\infty$ (**1**), $\{[Cd(tn)]_3[Cr(CN)_6]_2\}_\infty$ (**2**), and $\{[Cu_2(tn)_2][Ru(CN)_6]\cdot 4H_2O\}_\infty$ (**3**), have been synthesized and fully characterized. Compounds **1** and **3** have channels occupied by water molecules of crystallization. They show "sponge-like" dynamic behaviour triggered by guest removal and inclusion. The dehydration processes, which involve changes in the structures of **1** and **3**, are reversible. Work is in progress to understand how these structural transformations take place. Further gas/solid and liquid/solid

adsorption studies, and in-situ X-ray diffraction studies, involving both water and other solvents are also currently in progress.

Experimental Section

Synthesis of $\{\{[Cd_3(tn)_4][Co(CN)_6]_2\}\cdot 5H_2O\}_\infty$ (1).

To a solution of tn (0.220 ml, 2 mmol) and $CdSO_4$ (0.312 g, 1 mmol) in 30 ml of water, was added drop wise an aqueous solution of the $K_3[Co(CN)_6]$ (0.332 g, 1 mmol). The reaction mixture was stirred for 30 min and then $NaClO_4$ (0.12 g, 1 mmol) was added to aid crystallization. After stirring and heating at 75°C for a few minutes, the mixture was filtered. Light yellow square-shaped crystals of compound **1** appeared from the filtrate after some days. Elemental analysis: found C, 25.05; H, 4.26; N, 24.50; $C_{24}H_{52}N_{20}Cd_3Co_2O_5$ requires C, 24.94; H, 4.53 N, 24.24 %.

Synthesis of $\{[Cd(tn)]_3[Cr(CN)_6]_2\}_\infty$ (2).

To a solution of tn (0.220 ml, 2 mmol) and $CdSO_4$ (0.312 g, 1 mmol) in 30 ml of water, was added dropwise an aqueous solution of the $K_3[CrCN)_6]$ (0.332 g, 1 mmol). The reaction mixture was stirred for 30 min and then $NaClO_4$ (0.12 g, 1 mmol) was added to aid crystallization. After stirring and heating at 75°C for a few minutes the mixture was filtered. Light yellow square-shaped crystals of compound **2** appeared from the filtrate after some days. Elemental analysis: found: C, 27.10; H, 2.78; N, 26.31; $C_{24}H_{30}Cd_3Cr_2N_{20}$ requires C, 27.72; H, 2.91 N, 26.94 %.

Synthesis of $\{[Cu_2(tn)_2][Ru(CN)_6]\cdot 4H_2O\}_\infty$ (3).

1,3-Diaminopropane (1.0 mL, 12.0 mmol) was added under aerobic conditions to a concentrated aqueous solution (5 mL) of CuCl2·2H2O (2.05 g, 12.0 mmol) with continuous stirring, leading to the immediate precipitation of a green powder. An aqueous solution of Et_4NOH (0.52 g, 3.5 mmol) was then added with stirring and the

resulting dark-blue solution was warmed (at ca. 60°C for about 5 min) and then filtered in order to remove the small amount of precipitate that remained. An aqueous solution (20 mL) of $K_4[Ru(CN)_6]$ (2.47 g, 6.0 mmol) was then added with continuous stirring. Slow concentration of the resulting solution at room temp afforded prismatic green crystals of **3**, which were filtered off and air-dried. Elemental analysis: found C, 23.39; H, 4.43; N, 22.86; $C_{12}H_{28}N_{10}Cu_2Ru_1O_4$ requires C, 23.84; H, 4.67; N, 23.17 %.

X-ray Structural Determination: A yellow crystal of **1** (0.5 x 0.5 x 0.5), a yellow crystal of **2** (0.50 x 0.50 x 0.50) and a green crystal of **3** (0.40 x 0.30 x 0.30) were mounted on a Stoe Mark II-Imaging Plate Diffractometer System[31] equipped with a graphite-monochromator; Mo-Kα radiation (λ = 0.71073 Å). Data collections were performed at 173 K. The structures were solved by direct methods using the program SHELXS-97[32] and refined by full matrix least squares on F^2 with SHELXL-97.[32] The tn ligand is disordered in **3**. The hydrogen atoms were included in calculated positions and treated as riding atoms. In general the water H-atoms were refined with distance restraints. Further crystallographic and refinement details for complexes **1, 2** and **3** are given in Table 3. The crystallographic CIF files (excluding structure factors) for the structures **1**, **2** and **3** have been deposited with the Cambridge Crystallographic Data Centre as supplementary publication nos. CCDC 682763 (**1**), CCDC 682764 (**2**), CCDC 682765 (**3**). Copies of the data can be obtained free of charge on application to CCDC, 12 Union Road, Cambridge CB2 1EZ, UK [Fax: (internat.) +44-1223/336-033; E-mail: deposit@ccds.cam.ac.uk].

X-Ray powder diffraction: The powder samples were inserted in a glass capillary of a 0.5 mm diameter. X-ray powder data were collected at room temperature on a computer controlled STOE-STADIP focusing powder diffractometer[33,34] equipped with a curved Ge(111) monochromator ($CuK\alpha_1$; λ=1.54051Å). A STOE linear

position sensitive detector was used. The compounds were measured in the range of $4° \leq 2\theta \leq 90°$ using a step width of 0.1°.

Table 3. Crystallographic and Structure Refinement Data for **1, 2** and **3.**

	1	**2**	**3**
Empirical formula	$C_{24}H_{50}N_{20}O_5Cd_3Co_2$	$C_{24}H_{40}N_{20}Cd_3Cr_2$	$C_{12}H_{28}N_{10}O_4Cu_2Ru$
Formula mass	1153.90	1049.96	604.59
Wavelength [Å]	0.71073	0.71073	0.71073
Temperature [K]	173	173	173
Crystal system	monoclinic	triclinic	monoclinic
Space group	*C*2/c	*P-1*	$P2_1/n$
a(Å)	27.4141(15)	7.7143(7)	7.7882(10)
b(Å)	11.6135(6)	7.8308(7)	10.6489(17)
c(Å)	13.7184(9)	16.1529(14)	13.2933(16)
α(°)	90	95.474(7)	90
β(°)	105.136(7)	95.669(7)	90.70(1)
γ(°)	90	91.569(7)	90
Volume [$Å^3$]	4092.2(4)	965.91(15)	1102.4(3)
Z	4	1	2
Calculated density [Mg/m^3]	1.873	1.805	1.821
Absorption coefficient [mm^{-1}]	2.387	2.215	2.627
Measured refl.	21665	13543	8591
indep. refl.	5508	5137	2862
observd. refl. [$I > 2\sigma(I)$]	5229	4981	2681
no. of param. refnd.	261	251	182
R1[a] [$I > 2\sigma(I)$]	0.0153	0.0200	0.0365
wR2[b] [$I > 2\sigma(I)$]	0.0344	0.0531	0.0990

[a] $R1 = \Sigma||F_O| - |F_C||/\Sigma|F_O|$. [b] $wR2 = [\Sigma w(F_O^2 - F_C^2)^2/\Sigma wF_O^4]^{1/2}$

Physical Measurements: Elemental analyses of carbon, hydrogen, and nitrogen were performed by the Microanalysis Service of the Laboratory of Pharmaceutical and Organical Propedeutical Chemistry at the University of Geneva (Geneva, Switzerland). Infrared spectra were measured using KBr pellets in the interval of

4000-400 cm^{-1} were recorded on a Perkin-Elmer 1720X FT-IR spectrometer. Thermogravimetric (TG) analyses were carried out using a Mettler 4000 module. Samples were introduced in a closed aluminium oxide crucible and heated a rate 0.1°C min^{-1} under nitrogen at atmospheric pressure. DSC measurements were done with a modified differential scanning calorimeter (Mettler Toledo DSC 822e), under N_2/He at a rate of 1°C/min. Immersion calorimetry experiments were carried out at 293 K on samples of 0.150-0.200 g using a TIAN-CALVET type calorimeter[35, 36]. The out-gassed sample was placed in the calorimetric cell which was then immersed into a water bath controlled by a thermo-regulator system LUDA MS. The thermal flow was provided by 180 thermocouples of Cu/constantan connected to a nanovoltmeter PREMA 8017. The integral of the curve, $V=f(t)$, is proportional to the energy generated during the immersion process, $\Delta_i H$. The normal calibration of the calorimetry system was carried out with an electrical resistance. The accuracy varies between 4 and 5% depending on the absolute energy liberated in the process and on the amount of solid used.

Acknowledgments. We thank Drs Y. Filinchuk and P. Pattison for considerable help and useful discussions during our stay at the Swiss Norwegian Beam Lines, ESRF, Grenoble, while collecting in situ synchrotron powder diffraction data for compound 3. This work was financed by the Swiss National Science Foundation (Grant № 20-111738).

REFERENCES

[1] S. Kitagawa, R. Kitaura, S.-i. Noro, *Angew. Chem.* **2004**, *116*, 2388.
[2] B. Moulton, M. Zaworotko, *Chem. Rev.* **2001**, *101*, 1629.
[3] M. Eddaoudi, D. B. Moler, H. Li, B. Chen, T. M. Reineke, M. O'Keeffe, O. M. Yaghi, *Acc. Chem. Res.* **2001**, *34*, 319.
[4] M. Fujita, Y. J. Know, S. Washizu, K. Ogura, *J. Am. Chem. Soc.* **1994**, *116*, 1151.
[5] M. Ohba, N. Fukita, H. Okawa, *J. Am. Chem. Soc.* **1997**, *119*, 1011.
[6] H. Miyasaka, N. Matsumoto, H. Okawa, N. Re, E. Gallo, C. Floriani, *J. Am. Chem. Soc.* **1996**, *118*, 981.

[7] E. Coronado, C. Gimenez-Saiz, J. M. Martinez-Agudo, A. Nuez, F. M. Romero, H. Stoeckli-Evans, *Polyhedron* **2003**, *22*, 2435.
[8] I. P.-Y. Shek, W.-F. Yeung, T.-C. Lau, J. Zhang, S. Gao, L. Szeto, W.-T. Wong, *Eur. J. Inorg. Chem* **2005**, 364.
[9] M. Verdaguer, A. Bleuzen, V. Marvaud, J. Vaissermann, M. Seuleiman, C. Desplanches, A. Scuiller, C. Train, R. Garde, G. Gelly, C. Lomenech, I. Rosenman, P. Veillet, C. Cartier, F. Villain, *Coord. Chem. Rev.* **1999**, *190-192*, 1023.
[10] L. G. Beauvais, J. R. Long, *J. Am. Chem. Soc.* **2002**, *124*, 12096.
[11] T. Pretsch, K. W. Chapman, g. J. Halder, C. J. Kepert, *Chem. Commun.* **2006**, 1857.
[12] K. W. Chapman, P. J. Chupas, C. J. Kepert, *J. Am. Chem. Soc.* **2006**, *128*, 7009.
[13] H. Yuge, A. Mamada, M. Asai, S. Nishikiori, T. Iwamoto, *Dalton Trans.* **1995**, 3195.
[14] V. Marvaud, C. Decroix, A. Scuiller, C. Guyard-Duhayon, J. Vaissermann, F. Gonnet, M. Verdaguer, *Chem.-Eur. J.* **2003**, *9*, 1677.
[15] R. Eckhardt, H. Hanika-Heidl, R. D. Fischer, *Chem. Eur. J.* **2003**, *9*, 1795.
[16] A. L. Spek, *J. Appl. Crystallogr.* **2003**, *36*, 7.
[17] J. A. Kohn, W. D. Townes, *Acta Cryst.* **1961**, *14*, 617.
[18] S. Jagner, E. Ljungstrom, N.-G. Vannerberg, *Acta Chem.Scand.,Ser.A,* **1974**, *28*, 623.
[19] S. Triki, J. Sala-Pala, F. Thétiot, C. J. Gomes-Garcia, J.-C. Daran, *Eur. J. Inorg. Chem* **2006**, 185.
[20] D. F. Mullica, P. K. Hayward, E. L. Sappenfield, *Inorg. Chim. Acta* **1995**, *237*, 111.
[21] D. F. Mullica, P. K. Hayward, E. L. Sappenfield, *Inorg. Chim. Acta* **1996**, *253*, 97.
[22] M. Rüegg, A. Ludi, K. Rieder, *Inorg. Chem.* **1971**, *10*, 1773.
[23] D. F. Mullica, E. L. Sappenfield, *Inorg. Chim. Acta* **1997**, *258*, 101.
[24] A. W. Addison, T. N. Rao, J. Reedijk, J. van Rijn, G. Verschoor, *C. J. Chem. Soc., Dalton Trans.* **1984**, *7*, 1349.
[25] K. Nakamoto, *Infrared and Raman Spectra of Inorganic and coordination Compounds*, 3rd ed., Wiley, New York, **1978**.
[26] A. Uehara, S. Terabe, R. Tsuchiya, *Inorg. Chem.* **1983**, *22*, 2864.
[27] N. Mondal, M. K. Saha, B. Bag, S. Mitra, V. Gramlich, J. Ribas, M. S. E. Fallah, *J. Chem. Soc., Dalton Trans.* **2000**, 1601.
[28] *IUPAC Recommendations, Vol. 66*, Pure Appl. Chem., **1994**.
[29] F. Stoeckli, *Adsorpt. Sci. Technol.* **1993**, *10*.
[30] F. Stoeckli, D. Hugi-Cleary, T. A. Centeno, *J. Eur. Ceram. Soc.* **1998**, *18*, 1177.
[31] Stoe, &, Cie., *IPDS Software, Stoe & Cie GmbH*, Darmstadt, Germany, **2005.**
[32] G. M. Sheldrick, *Vol. A64*, Acta Crystallogr., **2008**.
[33] E. R. Wolfel, *J. Appl. Cryst.* **1981**, *14*, 291.
[34] E. R. Wolfel, *J. Appl. Crystallogr* **1983**, *16*, 341.
[35] R. C. Bansal, J. B. Donnet, F. Stoeckli, *Active Carbon*, Marcel Dekker, New York, **1988**.
[36] F. Stoeckli, D. Hugi-Cleary, T. A. Centeno, *J. Eur. Ceram. Soc.* **1998**, *18*, 1177.

Supporting Information

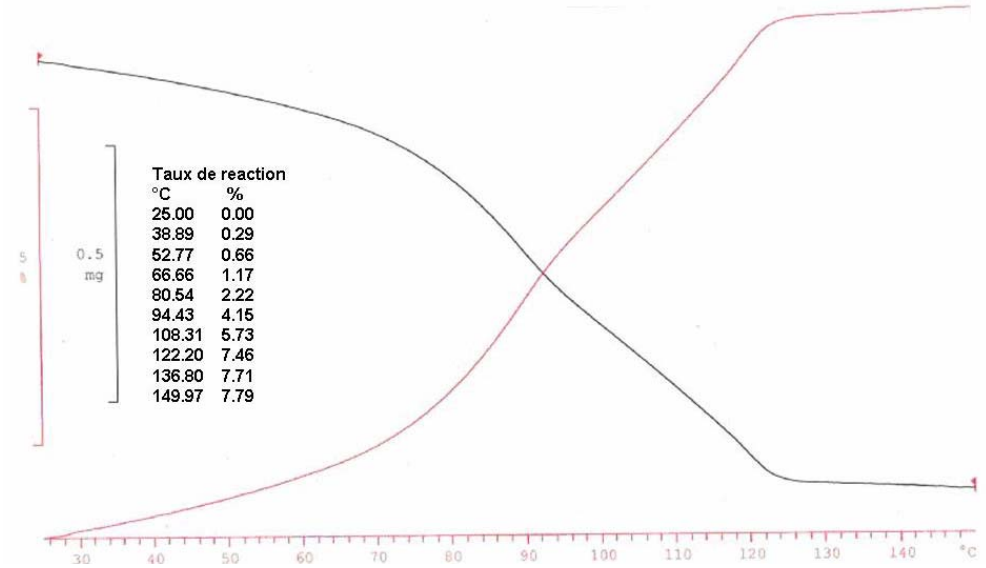

a)

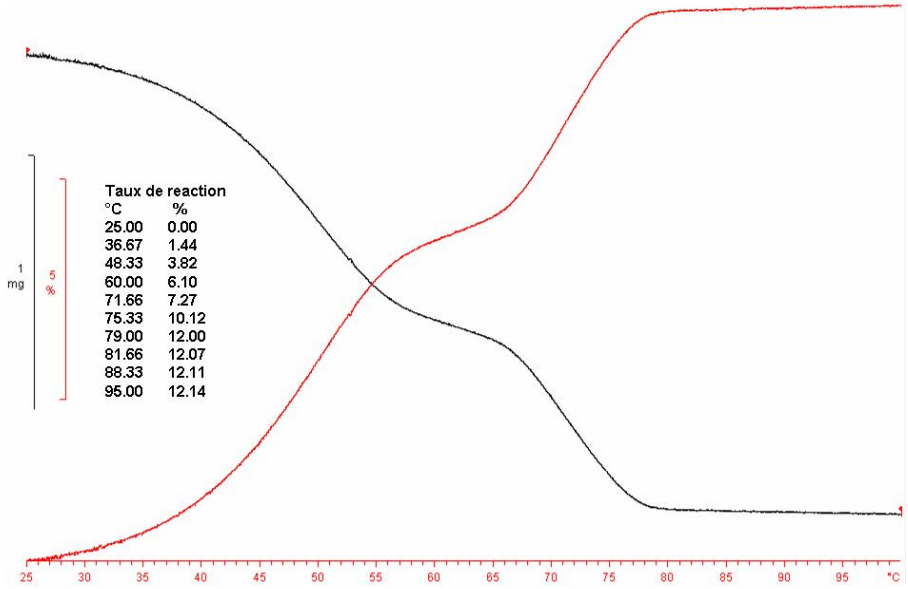

b)

Figure S1. TG curve of:
a) compound **1,** $\{\{[Cd_3(tn)_4][Co(CN)_6]_2\}\cdot 5H_2O\}_\infty$; final weight loss corresponds to $5H_2O$
b) compound **3,** $\{[Cu_2(tn)_2][Ru(CN)_6]\cdot 4H_2O\}_\infty$, final weight loss corresponds to $4H_2O$

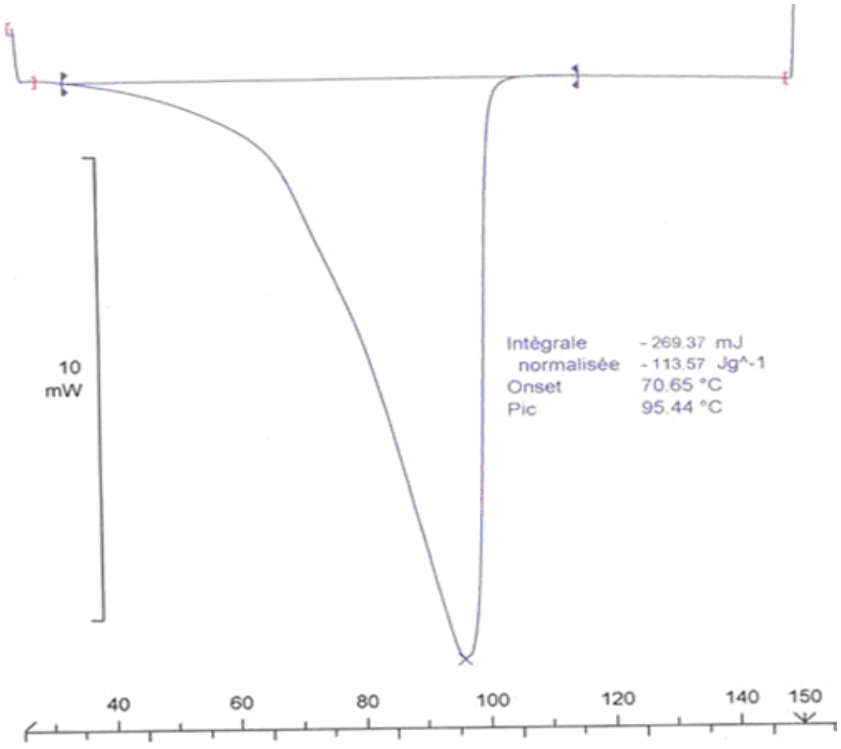

a)

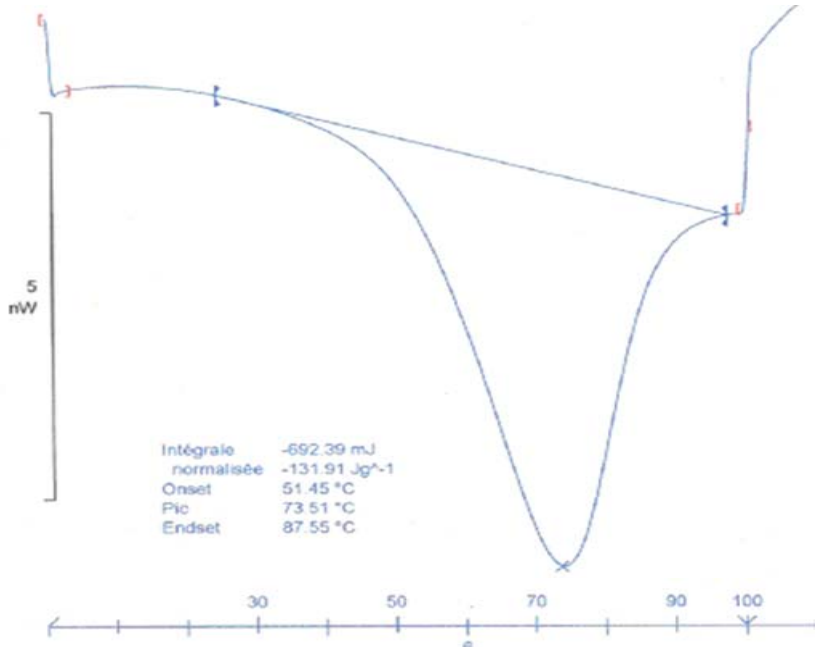

b)

Figure S2. DSC curve for: a) compound **1,** $\{\{[Cd_3(tn)_4][Co(CN)_6]_2\}\cdot 5H_2O\}_\infty$; b) compound **3,** $\{[Cu_2(tn)_2][Ru(CN)_6]\cdot 4H_2O\}_\infty$.

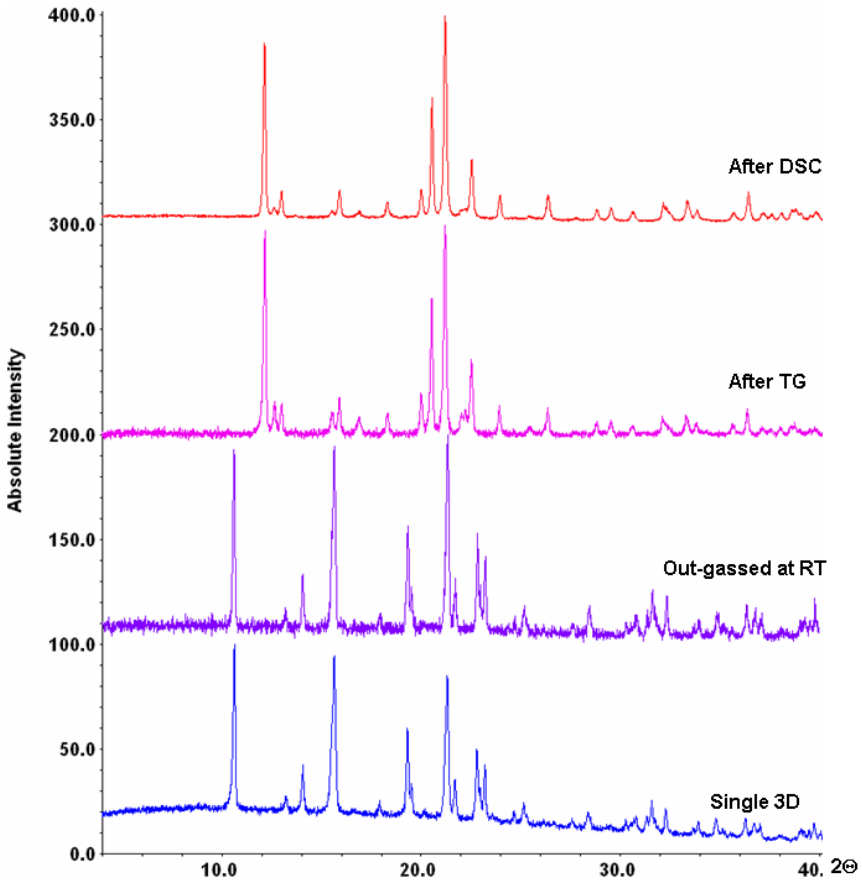

Figure S3. Powder X-ray diffractograms (PXRD) for compound **3:**
blue- measured PXRD of complex **3**; violet - measured PXRD of complex **3** ***after*** out-gassing under vacuum at room temperature; pink – measured PXRD of complex **3** ***after*** thermal gravimetric analysis; red - measured PXRD of complex **3** ***after*** DSC analysis.

3. 2

Transformation of a Chiral Nanoporous Cyano-Bridged Framework Triggered by Dehydration/Rehydration

Olha Sereda, Fritz Stoeckli, Yaroslav Filinchuk, Phil Pattison and Helen Stoeckli-Evans

Abstract

The syntheses, crystal structures, and adsorption/desorption properties of two novel chiral three dimensional cyano-bridged bimetallic assemblies, $\{[Cu(1R,2Rchxn)_2]_2[Ru(CN)_6]\cdot 6H_2O\}_\infty$ (**1**) and $\{[Cu(1R,2Rchxn)_2]_{12}[Ru(CN)_6]_6\cdot 26H_2O\}_\infty$ (**2**) (where 1R,2Rchxn = *trans*-cyclohexane-(1R, 2R)-diamine), are reported. Complex **1** crystallizes in the monoclinic space group *C2,* with a = 18.9979(11) Å, b = 17.8507(11) Å, c = 15.5853(8) Å, β = 119.062(4)°, V = 4619.9(4) Å^3, and Z = 4, while **2** crystallizes in the triclinic space group *P1,* with a = 13.7183(8) Å, b = 21.3378(12) Å, c = 24.4177(13) Å, α = 68.715(4)°, β = 78.284(4)°, γ = 73.004(5)°, V = 6331.3(6) Å^3, and Z = 1. Structures **1** and **2** can be described as nanoporous cyano-bridged frameworks (CBF's), in which alternating *trans*-[Cu-(*trans*-(1R,2R-chxn)$_2$]$^{2+}$ cations and $[Ru(CN)_6]^{4-}$ anions are linked by CN^- bridges. In both structures there are large cavities filled with H_2O molecules, which show guest-dependent dynamic behavior. The chemical rearrangement of the framework is driven by the loss or addition of water molecules, as proved unequivocally by single-crystal and powder X-ray diffraction analyses. These changes are fully reversible and dependant on the nature of the guests. The methanol adsorption isotherm for the fully out-gassed form of compound **2** indicates that it is a two step process, and the desorption isotherm shows that it is reversible. Immersion calorimetric studies with different solvents were carried out for both compounds. The two types of networks reported show different behavior upon drying, falling within the category of "recoverable collapsing" and "guest-induced reformation" frameworks.

Keywords: metal-organic framework, reversible, adsorption/desorption, cyanometallate

Introduction

The synthesis and characterization of metal-organic frameworks (MOFs) have attracted much attention due to the variety of interesting structural topologies and the numerous potential applications as functional materials, such as porosity, chirality, catalysis, luminescence, magnetism, conductivity, spin-transition, nonlinear optics (NLO) and gas storage[1-4]. Unfortunately, the inability of many such open frameworks to support permanent porosity and to avoid collapsing in the absence of guest molecules, such as solvents, has hindered further progress in these various fields.[5, 6] Up to now, examples of stable frameworks structurally characterized by single-crystal X-ray diffraction in both solvated and desolvated forms are rare,[7-11] and only a very few porous metal–organic polymers have been reported to have cell volume changes upon guest exchange.[10, 12-14] Dynamic structural transformation, based on flexible porous frameworks, is one of the most interesting phenomena in coordination polymers. So far there are very limited studies on such dynamic porous coordination networks[15-17]. Three types of these so called new generation compounds have been described by Kitagawa[8]: Type I - the "recoverable collapsing" framework, which collapses due to the close-packing forces on removal of the guest molecules; however, it can be regenerated under the initial conditions;[15, 18-20] Type II - the "guest-induced transformation" framework, where the structural shifts in the network are induced by the simultaneous exchange of guest molecules;[21-23] Type III - the "guest-induced reformation", where the removal of guest molecules induces a structural change in the network, however, again it reverts to the original structure under the initial conditions.[24, 25] Several examples of discrete

molecular assemblies have been obtained,[26, 27] however, reports on three dimensional coordination polymers are still sparse. This is probably due to the fact that the flexibility of the coordination polymers is incompatible with the robustness necessary for a porous framework to be maintained without the guest molecules. In this respect, cyanometallate complexes have been widely studied in many fields, mainly because of their rich and interesting structures, magnetic, catalytic, and adsorption properties.[28-30] They also have the potential to form dynamic porous materials as they can adapt to changes caused by external stimuli, either within the layer or in between the layers. Such unique and novel dynamic processes in single crystals of cyano-bridged frameworks have been described.[31] At the same time only a few examples of coordination polymers containing $[Ru(CN)_6]^{4-}$ have been reported.[32-35] On the other hand, chiral structures are a new target for such lattice architectures. Chirality is an essential factor for inducing specific physical properties, for example, second harmonic generation (SHG), magneto-chiral dichroism (MChD), ferroelectricity, etc.[36-39] A chiral network would allow selective binding of chiral guests, and the presence of different types of metal ions could enable specific tuning of the electronic properties. A number of reports have appeared recently on new cyano-bridged bimetallic complexes, but only a small number of chiral structures have been described.[36, 40-42] Their characterization has mainly focused on, their physical properties, their adsorptive and calorimetric properties have scarcely been evaluated. Herein, we report on two new novel chiral CBF's with permanent porosity, based on hexacyanoruthenate (II), that show unusual guest-induced dynamic behavior. The chemical rearrangement of the framework is driven by the loss or addition of water molecules, as proved unequivocally by single-crystal and powder X-ray diffraction analyses. These changes are fully reversible and dependant on the nature of the guest.

The two types of frameworks reported here show different behavior upon drying, falling within the category of "recoverable collapsing" (Type I) and "guest-induced reformation" (Type III) frameworks.

Experimental Section

Materials. The precursor complex, [Cu(*trans*-(1R,2R-chxn)$_2$(H_2O)](NO_3)$_2$ was prepared according to the literature method.[43] High-purity (98%) *trans*-cyclohexane-(1R, 2R)-diamine (Aldrich) and others reagents and solvents were purchased from chemical sources and used without further purification. All products were kept away from the light.

Preparation of {[Cu(1R,2Rchxn)$_2$]$_2$[Ru(CN)$_6$]·6H_2O}$_\infty$ (1). To a solution of [Cu(*trans*-(1R,2R-chxn)$_2$(H_2O)](NO_3)$_2$ (125 mg, 0.3mmol) in a water/acetonitrile mixture (1/1 40mL) 0.1 equiv. of $Cu(ClO_4)_2$·6H_2O was added with continuous stirring. This was followed by the dropwise addition of an aqueous (10mL) solution of $K_4[Ru(CN)_6]$·H_2O (71.91 mg, 0.17mmol). The resulting blue-violet solution was kept away from the light. Dark violet crystals formed after a few days. Elemental analysis for $C_{30}H_{68}N_{14}Ru_1Cu_2O_6$: found C, 37.81; H, 6.94; N, 19.99; calc. C, 37.96; H, 7.22; N, 20.66%. IR (KBr, cm^{-1}): ν(N─H) 3193, 3109cm^{-1}, ν(C─H) 2936, 2856cm^{-1}, ν(C≡N) 2053, 2083cm^{-1}.

Preparation of {[Cu(1R,2Rchxn)$_2$]$_{12}$[Ru(CN)$_6$]$_6$·26H_2O}$_\infty$ (2). The violet crystals of compound **2** were obtained within one week by slow diffusion of an aqueous solution of [Cu(*trans*-(1R,2R-chxn)$_2$(H_2O)](NO_3)$_2$ (0.1mmol, 10mL) layered onto an aqueous solution of $K_4[Ru(CN)_6]$·H_2O (0.06mmol, 24mL). Elemental analysis for

$C_{180}H_{388}N_{84}Ru_6Cu_{12}O_{26:}$ found C, 39.38; H, 7.01; N, 21.29; calc. C, 39.20; H, 7.09 N, 21.34%. IR (KBr, cm^{-1}): ν(N─H) 3221, 3111cm^{-1}, ν(C─H) 2930, 2857cm^{-1}, ν(C≡N) 2037, 2104cm^{-1}.

Physical Measurements. Elemental analyses of carbon, hydrogen, and nitrogen were performed by the Microanalysis Service of the Laboratory of Pharmaceutical and Organical Propedeutical Chemistry at the University of Geneva (Geneva, Switzerland). Infrared spectra were measured using KBr pellets in the interval of 4000-400 cm^{-1} and were recorded on a Perkin-Elmer 1720X FT-IR spectrometer. Thermogravimetric (TG) analyses were carried out using a Mettler 4000 module. Samples were introduced in a closed aluminum oxide crucible and heated at a rate of 0.1°C min^{-1} under nitrogen at atmospheric pressure. Immersion calorimetry experiments were carried out at 293 K on samples of 0.150-0.200 g using a TIAN-CALVET type calorimeter[44, 45]. The out-gassed samples were placed in the calorimetric cells, which were immersed in a water bath controlled by a thermo-regulator system LUDA MS. The thermal flow was provided by 180 thermocouples of Cu/constantan connected to a nanovoltmeter PREMA 8017. The integral of the curve, $V=f(t)$, is proportional to the energy generated during the immersion process, $\Delta_i H$. The normal calibration of the calorimetry system was carried out with an electrical resistance. Different low polar organic solvents were used with the aim of testing the size of the nanopores. The accuracy varies between 4 and 5 % depending on the absolute energy liberated in the process and on the amount of solid used. The enthalpy of immersion was calculated within the framework of Dubinin's theory.[44, 46, 47]

X-ray Crystallography. Intensity data on violet plate-like single crystals of **1** (0.40 x 0.40 x 0.10 mm^3) and **2** (0.50 x 0.20 x 0.20 mm^3) were measured using a Stoe Mark II-

Imaging Plate Diffractometer System[48] equipped with a graphite-monochromator, using Mo-K_α radiation (λ = 0.71073 Å) at -100°C. The structures were solved by Direct methods using the program SHELXS-97.[49] The refinement and all further calculations were carried out using SHELXL-97.[49] The H-atoms were included in calculated positions and treated as riding atoms using SHELXL default parameters. The non-H atoms were refined anisotropically using weighted full-matrix least-squares on F^2. The hydrogen atoms of the water molecules could not be located in difference Fourier maps. An empirical absorption correction was applied using the multi-scan routine in PLATON;[56] transmission factors: T_{min}/T_{max} = 0.604/0.9055 for **1** and T_{min}/T_{max} = 0.9368/1.0678 for **2.** Crystallographic data for compounds **1** and **2** are summarized in Table 1.

X-Ray powder diffraction (XPRD). X-ray powder diffraction data were collected at room temperature on a computer controlled STOE-STADIP focusing powder diffractometer equipped with a curved Ge(111) monochromator (λ=1.54051Å). A STOE linear position sensitive detector was used. The powders of samples **1** or **2** were inserted in glass capillaries of 0.5 mm diameter. The compounds were measured in the range of 4° ≤ 2θ ≤ 80° using a step width of 0.1°.

Variable temperature synchrotron powder X-Ray diffraction (VTPXRD). Variable temperature synchrotron powder diffraction measurements were carried at the Swiss Norwegian Beam Lines (BM01-A) using a MAR345 Image Plate detector, wavelength =0.724312 Å, capillary to image plate distance 400mm, exposure times 60secs, 20º oscillations about ϕ, 2θ limits 0 - 24º.

Results and Discussion

Description of the Structures. Structures **1** and **2** can be described as three dimensional frameworks, in which alternating *trans*-[Cu-(*trans*-(1R,2R-chxn)$_2$]$^{2+}$ cations and [Ru(CN)$_6$]$^{4-}$ anions are linked by CN$^-$ bridges. In both structures large cavities, filled with H_2O molecules, are present.

Crystal Structure of {[Cu(1R,2Rchxn)$_2$]$_2$[Ru(CN)$_6$]·6H$_2$O}$_\infty$ (1). The molecular structure of the asymmetric unit of **1** is shown in Figure 1.

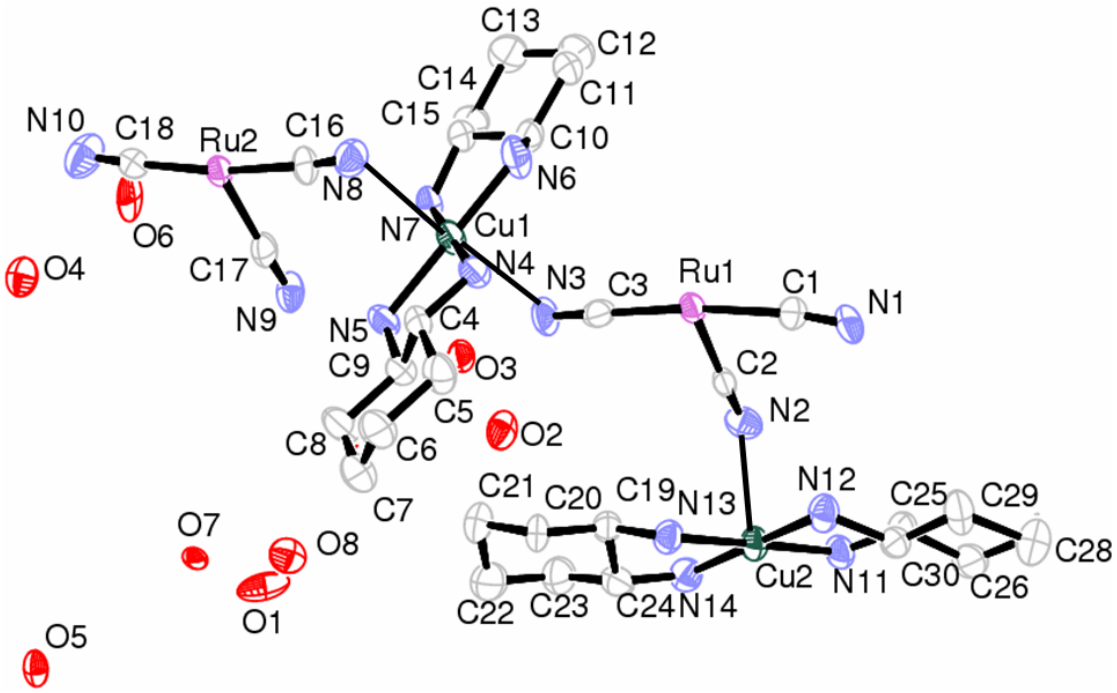

Figure 1. View of the asymmetric unit of **1**, showing the numbering scheme and displacement ellipsoids at the 50% probability level. Hydrogen atoms are omitted for clarity.

Complex **1** crystallizes in the non-centrosymmetric monoclinic space group *C*2. The asymmetric unit consists of two half [Ru(CN)$_6$]$^{4-}$ anions, two *trans*-[Cu(*trans*-(1R,2R-chxn)$_2$]$^{2+}$ cations and six water molecules. The Ru atoms are located on two-fold rotation axes. The bond length and angles in **1** are similar to those in [Cu(chxn)$_2$(H$_2$O)$_2$]Cl$_2$[50],

$\{[Cu(dipn)]_3[Ru(CN)_6]\}(ClO_4)_2 \cdot 4H_2O$[35] and $GdKRu(CN)_6 \cdot 4H_2O$[51]. The six-membered cyclohexane rings of the chxn ligands have *trans* chair-chair conformations. The $[Ru(CN)_6]^{4-}$ anions have almost regular octahedral geometry with average Ru─C bond distances of 2.035(11) Å and average C≡N bond distance of 1.159(15) Å. The ruthenium ions are linked to four copper (II) ions by four cyanide bridges, while each copper ion is linked to two equivalent ruthenium (II) ions. The solvent-accessible voids in the framework, in the absence of the water molecules, is estimated to be ca. 27.0% of the volume of the unit cell.[52] The water molecules in the voids form hydrogen bonded chains as shown in Figure 2a.

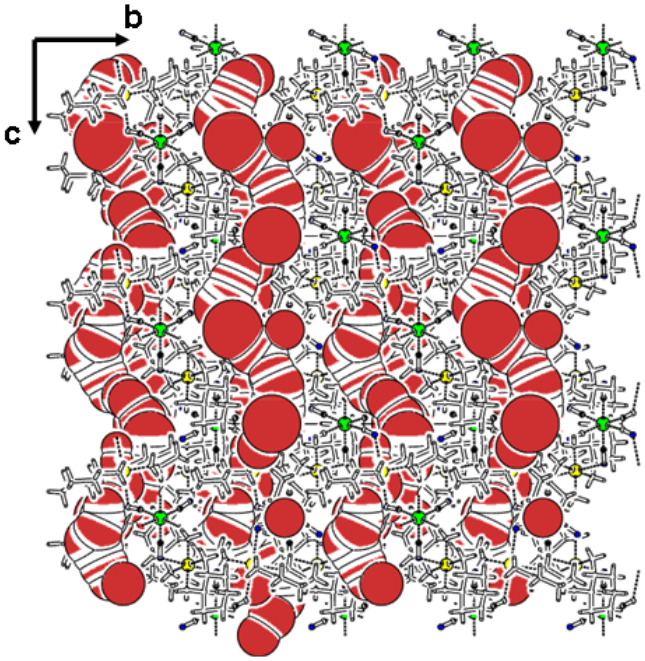

a)

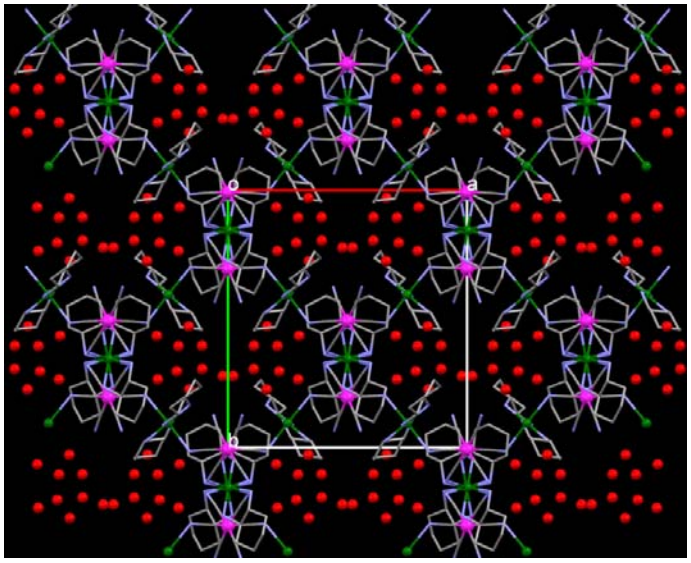

b)

Figure 2. Crystal packing diagrams of complex **1** viewed along: a) the a axis and b) the *c* axis (hydrogen atoms are omitted for clarity). The water molecules are represented by: a) red CPK balls; b) small red spheres.

The two non-equivalent copper(II) ions (Cu1 and Cu2) exhibit octahedral CuN6 coordination geometry, involving four nitrogen atoms of the *trans*-(1R,2R-chxn) ligands (N4, N5, N6, N7 for Cu1 and N11,N12, N3, N14 for Cu2) and two nitrogen atoms of the cyano groups (N3, N8 for Cu1 and N2, N9 for Cu2). The average value of the Cu─N≡C angles is 110.01(7)º. The axial Cu─N bonds are long, varying between 2.482(9) to 2.614(8) Å, while the average equatorial Cu─N bond distance is 2.014(10) Å. This shows that both copper(II) atoms have a pseudo Jahn-Teller distortion,[53] as shown in Figure 3.

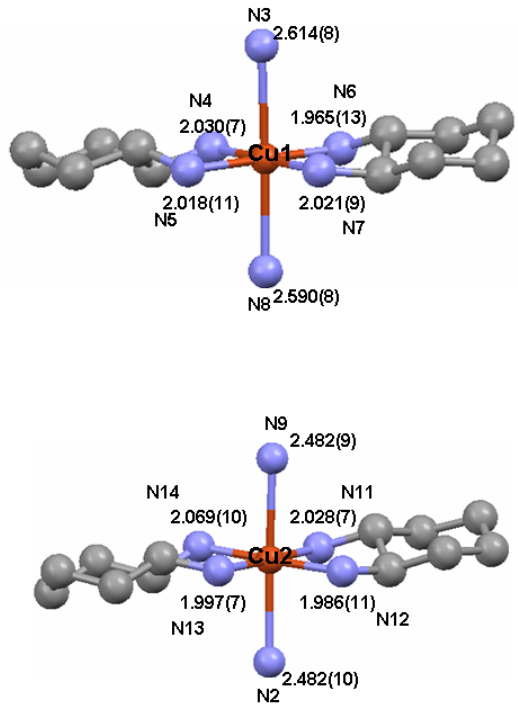

Figure 3. Cu─N bond lengths (Å) for complex **1,** showing the Jahn-Teller effect.

Using the conventional index of Jahn-Teller distortion, *T* [= the ratio of average value of the equatorial Cu─N bond distances to the value of the axial Cu─N bond distance],[54] the degree of distortion of the axial bonds Cu1─N3 and Cu2─N2 was found to be 0.764 and 0.825, respectively. For bonds Cu1─N8 and Cu2─N9 the *T* values are 0.779 and 1.010, respectively. To date the longest Cu─N distances reported are: 2.902Å in [Cu(*L*)Fe(CN)$_5$(NO)], (where *L*=1,8-bis(2-hydroxyethyl)-1,3,6,8,10,13-hexaazacyclo-tetradecane)[55] with a Cu─N≡C bond angle of 133.89°, and 2.827Å in [Cu(tn)$_2$][Ni(CN)$_4$]·H$_2$O (where tn=1,3-diaminopropane)[56] with a Cu─N≡C bond angle of 115.35°.

Table 1. Crystallographic data and Structure Refinement Parameters for $\{[Cu(1R,2Rchxn)_2]_2[Ru(CN)_6]\cdot 6H_2O\}_\infty$ (**1**) and $\{[Cu(1R,2Rchxn)_2]_{12}[Ru(CN)_6]_6\cdot 26H_2O\}_\infty$ (**2**).

	1	**2**
formula	$C_{30}H_{68}N_{14}Ru_1Cu_2O_6$	$C_{180}H_{388}N_{84}Ru_6Cu_{12}O_{26}$
fw,[a] g/mol	949.12	5514.64
Crystal colour/habit	violet/plates	violet/plates
Crystal system	monoclinic	triclinic
Space group	C2 (No. 5)	P1 (No. 1)
a, Å	18.9979(11)	13.7183(8)
b, Å	17.8507(11)	21.3378(12)
c, Å	15.5853(8)	24.4177(13)
α, deg	90	68.715(4)
β, deg	119.062(4)	78.284(4)
γ, deg	90	73.004(5)
V, Å^3	4619.9(5)	6331.3(6)
Z	4	1
Cryst dimens,mm^3	0.40 x 0.40 x 0.10	0.48 x 0.26 x 0.18
T(K)	173(2)	173(2)
λ, Å	0.71073	0.71073
ρ_{calc}, g/cm^3	1.359	1.446
μ, mm^{-1}	1.286	1.403
R[b][I>2σ(I)]	0.0707	0.0446
wR2[c][I>2σ(I)]	0.2075	0.0785
GOF[d]	1.062	0.935
Flack factor	0.09(3)	0.017(12)

[a]Including solvent molecules. [b]$R = \sum(||F_o| - |F_c||)/\sum |F_o|$. [c]$wR2 = [(w(\sum(|F_o|^2 - |F_c|^2)^2)/\sum(w|F_o|^4)]^{1/2}$. [d]$GOF = [(w(\sum(|F_o|^2 - |F_c|^2)^2]/(n - p)^{1/2}$, where *n* is the number of reflections, and *p* is the number of the refined parameters.

Crystal Structure of $\{[Cu(1R,2Rchxn)_2]_{12}[Ru(CN)_6]_6 \cdot 26H_2O\}_\infty$ (2).

Compound **2**, which was prepared by a different method to **1** (see Experimental section), crystallizes in the non-centrosymmetric triclinic space group *P1*. This structure can be described as layers of large cyclic units, in which alternating $[Cu(trans\text{-}(1R, 2R\text{-}chxn)_2]^{2+}$ cations and $[Ru(CN)_6]^{4-}$ anions are linked by CN^- bridges (Figure 4).

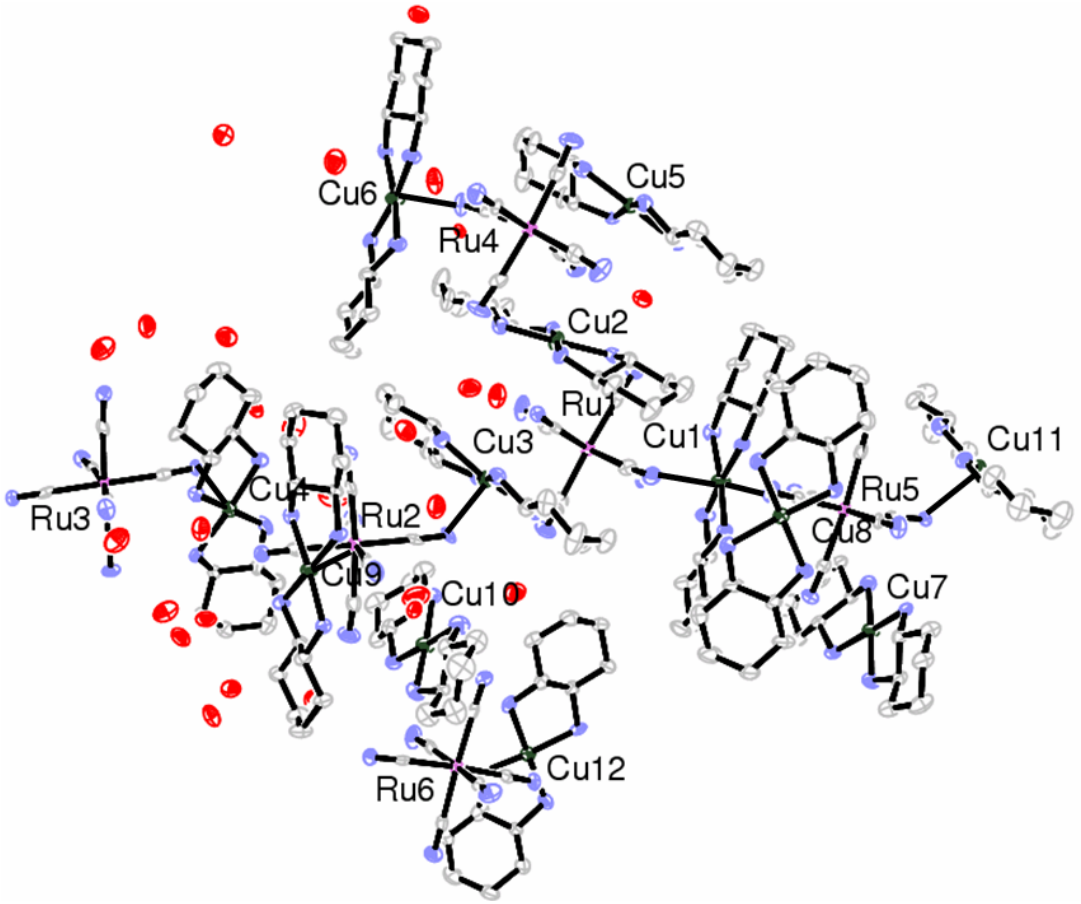

Figure 4. View of the asymmetric unit of **2**, showing the metal atom numbering scheme and displacement ellipsoids at the 50% probability level. Hydrogen atoms are omitted for clarity.

The structure is composed of six independent ruthenium atoms, twelve independent copper (II) atoms and 26 water molecules. Five of the copper (II) atoms (Cu3, Cu5, Cu6, Cu8, Cu12) can be considered to be pentacoordinate, while the other seven (Cu1, Cu2, Cu4, Cu7, Cu9, Cu10, Cu11) are hexacoordinated. The Cu-N bond distances in the basal or equatorial planes vary from 1.99(1) – 2.053(9) Å. The pentacoordinated copper atoms have apical Cu-N(cyano) bond lengths varying between 2.259(10) – 2.513(12) Å. On the opposite side of the basal plane the nearest N(cyano) atoms are at distances varying between 2.87(1) – 3.57(1) Å. For the hexacoordinated copper atoms the axial Cu-N(cyano) bond lengths vary between 2.512(9) – 2.797(10) Å. The longest axial Cu─N(cyano) bond distance reported to date is 2.539(1) Å in complex $\{[Cu(en)_2]_3[Ru_2N(CN)_{10}]\cdot ClO_4\}_n$ (where en = 1,2-ethylendiamine).[57] The existence of extremely long Cu─N bonds has been attributed to the coexistence of pseudo-Jahn-Teller elongation and electrostatic interactions.[58] The average Ru─C and C≡N bond length of 2.041(12) Å and 1.1159(14) Å, respectively, are similar to those observed in compound **1**. Four of the $[Ru(CN)_6]^{4-}$ anions are involved in four Ru-CN-Cu bridges, while two $[Ru(CN)_6]^{4-}$ anions are involved in only three Ru-CN-Cu bridges. It can also be seen that the Ru1-C2≡N2 and the Ru4-C19≡N11 cyano groups are involved in unusual bifurcated bonds with copper atoms Cu2/Cu3 for the former, and Cu5/Cu2 for the latter. To our knowledge this a rare occurrence of bifurcated cyano bonds in cyano-bridged complexes, although recently Rodrıguez-Hernandez *et al*. have analyzed there presence in Prussian Blue type compounds.[59]

Table 2. Selected Cu─N bond distances (Å) and Jahn-Teller distortion indices, *T*, of the copper(II) atoms in complex **2**.

Bond, Å	**Cu1**	**Cu2**	**Cu3**	**Cu4**	**Cu5**	**Cu6**
$Cu\text{-}N_{cyano}$	N27 = 2.690(10)	N2 = 2.295(11)	N7 = 2.303(10)	N8 = 2.568(9)	N10 = 2.259(10)	N12 = 2.513(12)
	N1 = 2.743(11)	N11 = 2.545(11)	N2 = 2.87(1)]	N9 = 2.685(11)	[N11= 2.91(1)]	[N66=3.08(1)]
$Cu\text{-}N_{chxn}$	2.010(8)	2.015(9)	2.019(9)	2.016(9)	2.036(9)	2.022(8)
*T**	0.747	0.878	----	0.785	----	----
	0.733	0.792		0.751		
Bond, Å	**Cu7**	**Cu8**	**Cu9**	**Cu10**	**Cu11**	**Cu12**
$Cu\text{-}N_{cyano}$	N25 = 2.516(11)	N29 = 2.382(11)	N47 = 2.512(9)	N53 = 2.570(11)	N28=2.540(10)	N59=2.413(10)
	N26 = 2.797(10)	[N80 = 3.38(1)]	N40 = 2.694(9)	N52 = 2.796(12)	N54=2.610(10)	[N20= 3.57(1)]
$Cu\text{-}N_{chxn}$	2.008(9)	2.022(9)	2.024(7)	2.025(9)	2.021(9)	2.016(9)
*T**	0.798	----	0.806	0.788	0.796	----
	0.718		0.752	0.724	0.774	

*T** - conventional index of Jahn-Teller distortion = average equatorial Cu─N bond distance / axial Cu─N bond distance.

In compounds **1** and **2** there are a number of non-linear Cu─N≡C bond angles. In compound **2** there are only two Cu─N≡C angles which can be described as normal [Cu5─N10≡C18 is 133.5(9)° and Cu3─N7≡C15 is 131.0(9)°] when compared to the values commonly observed in copper-containing compounds (Supporting information: Figure S1). The other Cu─N≡C angles vary from 94.2(9) to 120.2(9)º (Supporting information: Table S1). Both the valence bond and molecular orbital descriptions of the M'─N≡C system indicate that the M'─N bond should be collinear with the triple N≡C bond.[60] This situation holds for most of the CN bridges observed to date, although a few compounds with angles of ca. 140° have been reported. For example, in $[\{Cu(dien)_2Fe(CN)_6\}_n][Cu(H_2O)(dien)Fe(CN)_6]_n{\cdot}4nH_2O$ the Cu─N≡C angles are 139 and 140°, with corresponding Cu─N distances of 2.32(1) and 2.31(1) Å, respectively[61] and

in $[\{Cu(tn)\}_3\{Co(CN)_6\}_2]\cdot 3H_2O$, where one of the Cu─N≡C angles is 140.7(4)° with a Cu─N distance of 2.617(5) Å.[30] The non-linearity in the M'─O≡C- fragment has been explained on the basis of two valence bond structures,[60] and since Cu─N≡C- is an isoelectronic system, a similar explanation can be applied here, as a first approximation (Supporting information: Figure S2).

IR and CD Spectroscopies.

The IR spectra shows two sharp ν_{CN} bands at 2053 and 2083 cm^{-1} for **1** and 2037 and 2104 cm^{-1} for **2**, indicating the existence of two types of cyanide groups in the crystal lattice. The lower frequency band corresponds to that of $K_4[Ru(CN)_6]\cdot 1H_2O$ and can be ascribed to a non-bridging cyanide group. The higher frequency band is attributed to the bridging cyanide group.[34, 62]

Circular dichroism measurements (Figure 5) were used to establish the enantiomeric character of the coordination polymers (solid state, using KBr discs) and [Cu(*trans*-(1*R*,2*R*)-chxn)$_2$(H$_2$O)$_2$](NO$_3$)$_2$ (in solution). The enantiopure bis-chelated precursor shows a positive Cotton effects at λ=513 nm and compound **1** exhibits a positive Cotton effects at λ=560 nm. In addition, the similar signs of the Cotton effect for **1** and **2** in the same wavenumber region are attributed to the two chiral coordination polymers having as expected the same absolute configuration.[63]

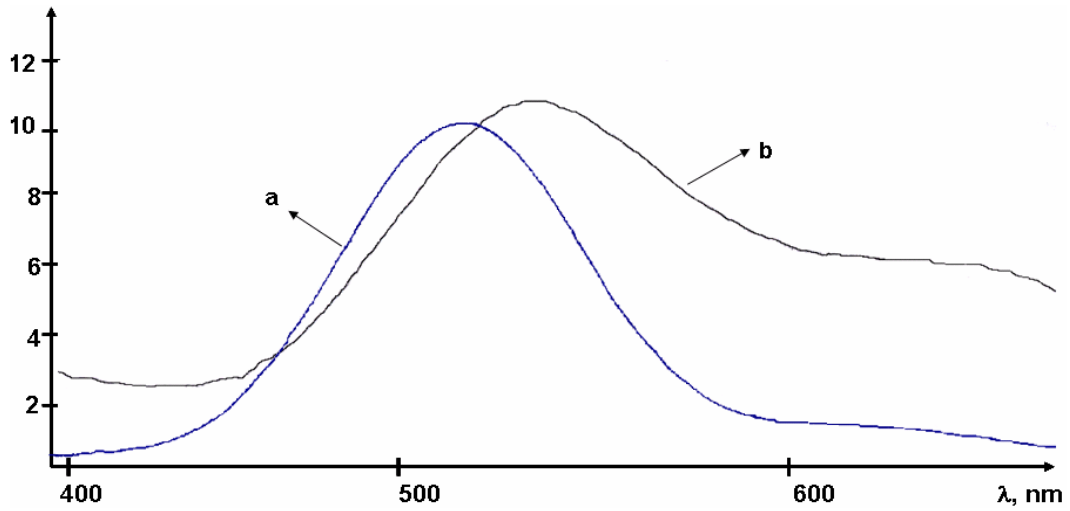

Figure 5. CD spectra of: **a)** an acetonitrile - water solution of the bis-chelated precursor [Cu(*trans*-(1*R*,2*R*)-chxn)$_2$(H_2O)$_2$](NO_3)$_2$, and **b)** a powder sample of {[Cu(1R,2Rchxn)$_2$]$_2$[Ru(CN)$_6$]· 6H_2O}$_\infty$ (**1**) in a KBr matrix.

Powder and Synchrotron X-ray Diffraction.

The water molecules in complexes **1** and **2** can be removed by heating at 100°C, or simply under vacuum, and exchanged for other organic solvents (for example, methanol or acetonitrile). Compounds **1** and **2** show very similar thermal behavior, as shown by TG analysis (Supporting Information: Figure S3). Between 20-140°C weight losses of 11.43% for **1** and 8.03% for **2** are observed. This corresponds to the loss of 6 water molecules (expected 11.38%) for **1** and 24 water molecules for **2** (expected 7.89%). On loss of solvent molecules the violet crystalline samples of **1** and **2** transform into deep bluish-purple micro-crystalline powders, **1a** and **2a**, respectively. We believe that dehydration of compounds **1** and **2** does not induce a loss of framework structure, as the powder X-ray diffractograms (PXRD) are almost identical to those of **1** and **2** (Supporting Information: Figure S4). Compounds **1a** and **2a** are stable in a dry environment, however, once in contact with moisture, their colour rapidly reverts to violet. Soaking **1a** (the guest-free phase of **1**) in water for one day regenerated the guest-

filled phase, i.e. compound **1**. The PXRD pattern of this product is identical to that of the as-synthesized complex **1** (Supporting Information: Figure S4). This reversible cycle can be repeated many times without loss of crystallinity. Although some dynamic nanoporous framework materials are known, those exhibiting reversible open–dense framework transformations in the crystalline state are still rare.[10]

In the case of **2a** when soaked in water the resulting PXRD shows dramatic changes as compared to the original pattern, that is, it reverts not to **2** but transforms into **1**. The conversion from the triclinic *P1* structure to the monoclinic *C2* structure, having taken place (Supporting Information: Figure S4). Further studies using in-situ synchrotron radiation PXRD enabled us to follow the behavior of these transformations on heating or on addition of moisture via a stream of N_2 saturated with water vapour. While heating the capillary filled with complex **1** to 80°C the transformation of **1** to **2a** was observed (Figure 6). On continued heating to 120°C complex **1a** was obtained. Hence, it was observed that the formation of **2a** is an intermediate step to obtain **1a** (Figure 6). On addition of moisture, via a stream of N_2 saturated with water vapour, it was observed that **1a** does not revert to **1** immediately but first complex **2** is formed, which then transforms to **1** on continued wetting of the sample.

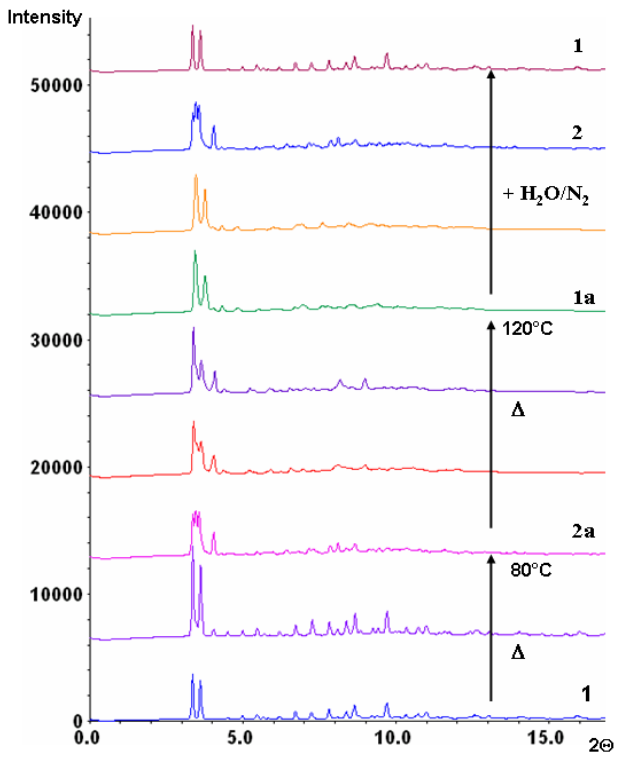

Figure 6. Variable temperature XRPD of complexes **1**, showing the transformations during the loss/addition of water molecules.

The heating of complex **2** to 80°C shows almost the same powder pattern, which indicates that the framework is not destroyed and complex **2a** is formed. With continued heating to 120°C the final pattern corresponds to that of complex **1a**. When passing a stream of N_2 saturated with water vapour through an original sample of **2a** (obtained from **2** by thermogravimetrical analysis) an almost instantaneous transformation into **1** was observed (Supporting Information: Figure S5). Because the solvent-exchange processes are carried out in the presence of water vapour (not a condensed liquid), we believe that no dissolution of the framework materials occur.

The transformations are driven by loss/addition of the water molecules and the process can be repeated a number of times without loss of crystallinity. The two types of networks reported here show different behavior upon drying, falling within the category

of "guest-induced reformation" frameworks. These reversible transformation processes involving complexes **1** and **2** are summarized in Figure 7.

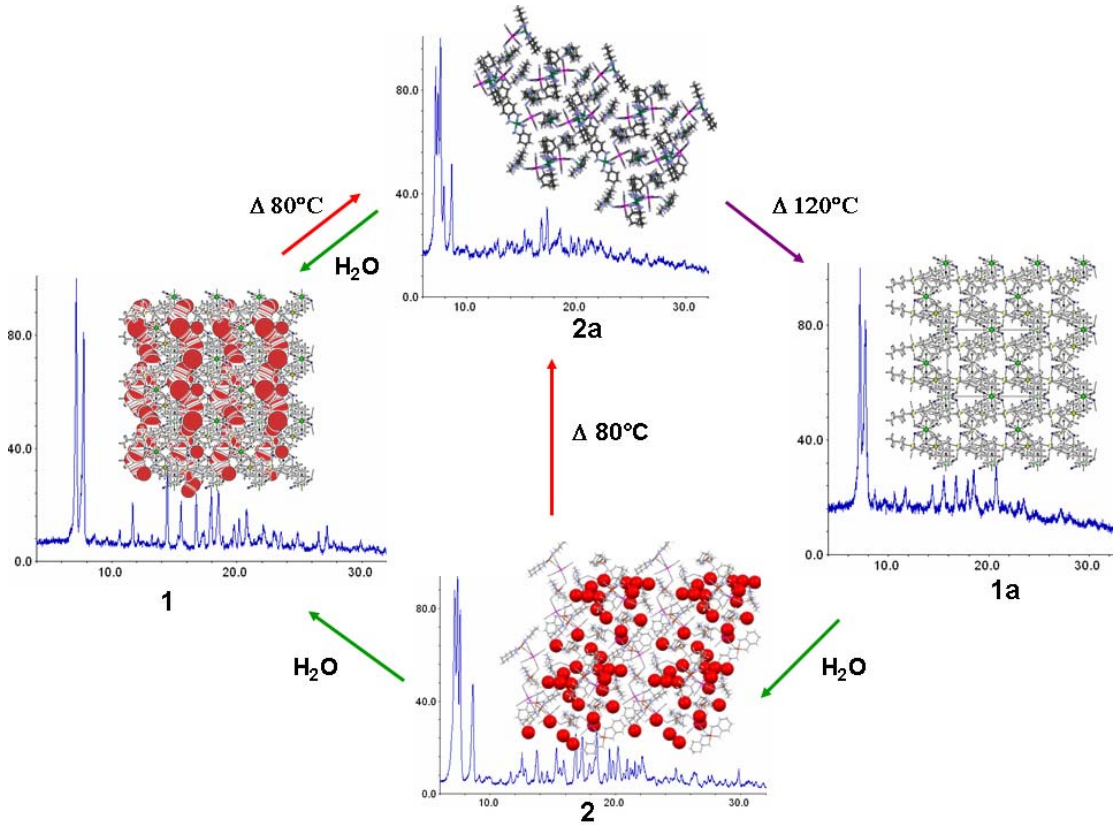

Figure 7. Schematic representation of the reversible transformation processes involving complexes **1** and **2.**

It is interesting to note that by grinding a sample of **2a** obtained after TG analysis, it became amorphous (Figure 8b). However, when passing a stream of N_2 saturated with water vapour through a capillary filled with this material, the crystalline structure of complex **1** was regenerated (Figure 8c). This transformation associated with water is characterized by a process of "crystal-to-crystal through an amorphous phase".

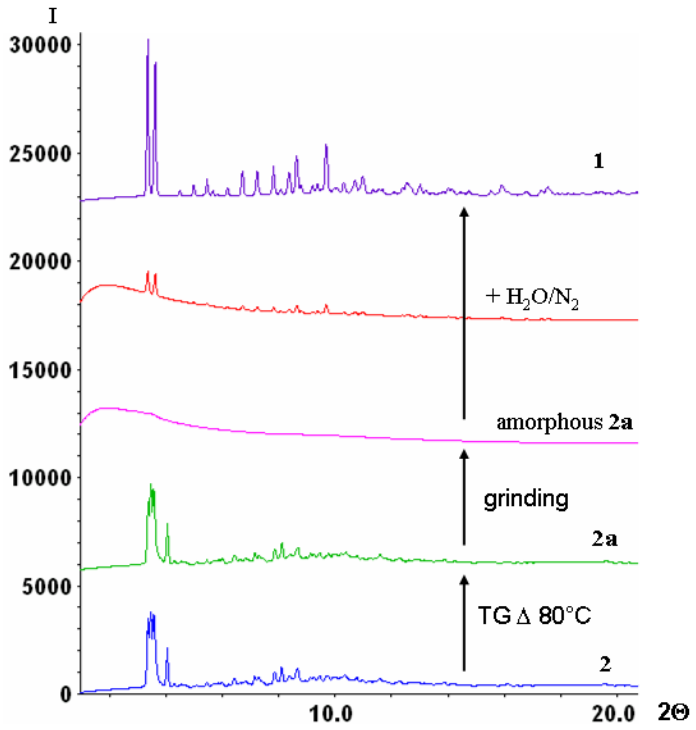

Figure 8. PXRD patterns of: blue - a fresh sample of complex **2** at room temperature; green – **2a**, was obtained after the heating **2** at 80 °C; pink - amorphous **2a** was obtained by grinding a sample of **2a**; red – initial diffractogram obtained after passing a stream of nitrogen gas saturated with water vapour through amorphous **2a**; violet – the crystallinity of this last sample improved with time to finally resemble the diffractogram for complex **1**.

Immersion calorimetry studies.

Immersion calorimetric studies[64] were carried out for systems **1** and **2** in different solvents (Table. 3). This method has the advantage of being experimentally simple and accurate. It is a very useful complement to the physical adsorption of vapours by solids and provides direct information on the surface energy. For complexes **1** and **2** the largest volume of the heat of immersion was observed for water, and the smallest for benzene. The heat of immersion for both compounds decreases with increasing size of the solvent used. After the immersion studies all the samples were examined by Powder X-ray diffraction. The diffractograms of the samples immersed into MeOH (for both system **1** and **2**) are identical to the original diffractograms for **1** and **2** with water inside the

cavities. Even if the guest molecule of MeOH is larger than a water molecule, the unit cell volume of **1** with MeOH has not increased (Supplementary information: Figure S6a).

Table 3. Heat of immersion* in different solvents for complex **1** and **2**.

	$-\Delta H_i \pm 3$ J/g					
Compound	H_2O	CH_3OH	C_2H_5OH	CH_2Cl_2	$CHCl_3$	C_6H_6
1	136.7	106.1	79.2	60.4	31.8	27.6
2	142.5	107.9	83.8	73.1	39.4	31.6

* On average three independent measurements were made for each solvent.

Adsorption measurement.

The MeOH and EtOH vapour-sorption isotherms of **2a** at 293 K (Figure 10) were measured to evaluate its permanent porosity (equilibrium time = 24hours). A sample of **2** was evacuated at room temperature for 14 h to remove the included solvent molecules before adsorption measurements were attempted. The profile of the MeOH isotherm consists of three parts. There is a gradual increase in the low P/P_0 region reacting a plateau at an induction pressure of $P/P_0 \sim 0.3$, $N_a = 2.56$ mmol/g. The adsorption isotherm then increases steeply up to a second plateau at $P/P_0 \sim 0.5$, $N_a = 4.57$ mmol/g. Finally, a third plateau is reached at 6.57 mmol/g. We assume that the structural transformation from the triclinic form (**2**) to the monoclinic form (**1**) takes place from the plateau 1 to plateau 2. The heat of immersion was measured at each step and the total value ($-\Delta H_i$ =113.82 J/g) corresponds well to the value observed ($-\Delta H_i$ =107.9 J/g) by direct immersion studies (Supplementary information: Figure S7a). The nanoporous volume was calculated by fitting the adsorption data to the Dubinin–Radushkevich (DR) equation[46]. The logarithmic plot of the DR equation is shown in Figure S7b (Supplementary information). In the case of EtOH adsorption, the profile showed a gradual increase in the low P/P_0 region, reacting a plateau at an induction pressure of P/P_0

= 0.11 and adsorption of ca. 2.5 mmol of EtOH at P/P_0 = 0.8. This behavior demonstrates that **2a** undergoes the same structural change as for the methanol adsorption: conversion from the triclinic (**2a**) to the monoclinic (**1a**) system. There is no second step on the isotherm as the adsorbent is probably too large to penetrate into the cavities.

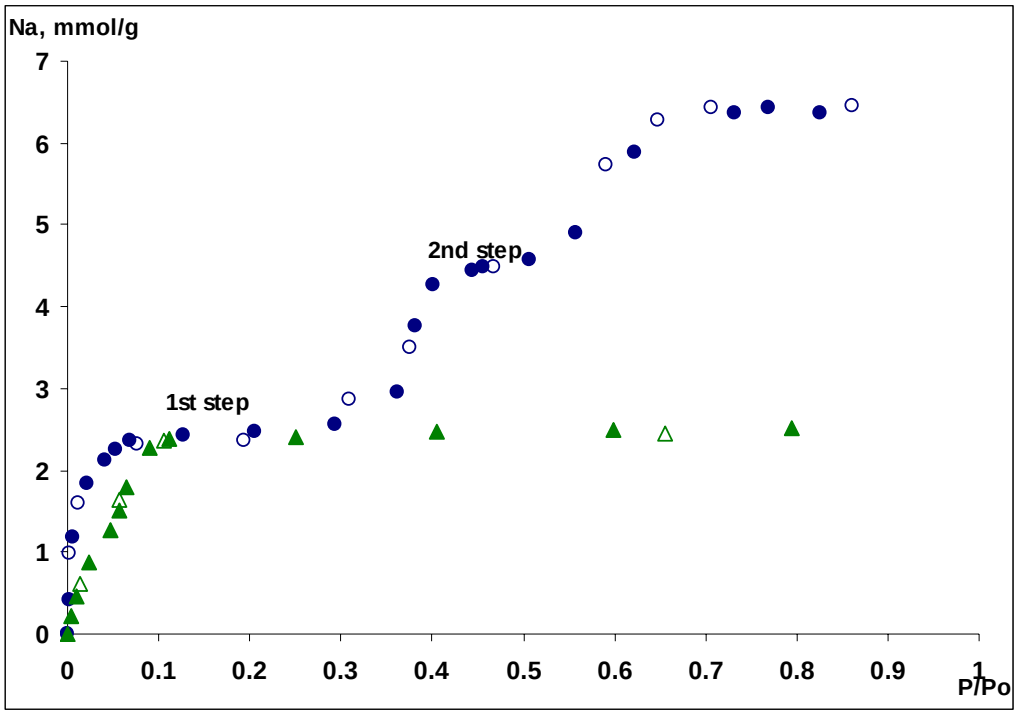

Figure 10. Adsorption/desorption isotherms for vapor adsorption in **2a**, methanol (blue) and ethanol (green) at 293K in the relative pressure range from 10-3 to 1.0 (● adsorption and ○ desorption process).

Conclusions

In summary, we have successfully constructed two new three dimensional chiral bimetallic cyano-bridged frameworks (CBF's) and demonstrated remarkable structural changes associated with the reversible transformations triggered by dehydration/rehydration. The removal of the included solvent molecules from these CBF's, leads to chiral solids which have permanent porosity and framework integrity.

These results show that the synthetic strategy based on cyanide-bridged bimetallic assemblies is advantageous for the formation of flexible nanoporous materials. They show guest-induced structural conversion, that fall within the category of "recoverable collapsing" and "guest-induced reformation" framework materials.

Acknowledgments

This work was supported by the Swiss National Science Foundation (Grant № FN 20-111738).

[1] S. Batten, R. Robson, *Angew. Chem., Int. Ed.* **1998**, *37*, 1460.
[2] Y. Rodriguer-Martin, M. Hernandez-Molina, F. S. Delgado, J. Pasan, C. Ruiz-Perez, J. Sanchiz, F. Lloret, M. Julve, *Cryst. Eng. Commun.* **2002**, 522.
[3] J. M. Rawson, G. D. McManus, *Coord. Chem. Rev.* **1999**, *189*, 135.
[4] W. R. Entley, G. S. Girolami, *Science* **1995**, 397.
[5] C. Janiak, *Dalton Trans.* **2003**, 2781.
[6] S. L. James, *Chem. Soc. Rev.,* **2003**, *32*, 276.
[7] K. Biradha, Y. Hongo, M. Fujita, *Angew. Chem., Int. Ed.,* **2002**, *41*, 3392.
[8] K. Uemura, S. Kitagawa, M. Kondo, K. Fukui, R. Kitaura, H.-C. Chang, T. Mizutani, *Chem. Eur. J.,* **2002**, *8*, 3587.
[9] K. Uemura, S. Kitagawa, K. Fukui, K. Saito, *J. Am. Chem. Soc.* **2004**, *126*, 3817.
[10] D. V. Soldatov, J. A. Ripmeester, S. I. Shergina, I. E. Sokolov, A. S. Zanina, S. A. Gromilov, Y. A. Dyadin, *J. Am. Chem. Soc.* **1999**, *121*, 4179.
[11] A. P. Côté, G. K. H. Shimizu, *Chem. Eur. J.* **2003**, *9*, 5361.
[12] S. Uchida, M. Hashimoto, N. Mizuno, *Angew. Chem., Int. Ed.,* **2002**, *41*, 2814.
[13] O. Saied, T. Maris, J. D. Wuest, *J. Am. Chem. Soc.* **2003**, 14956.
[14] J. Y. Lu, A. M. Babb, *Chem. Commun.* **2002**, 1340.
[15] L. C. Tabares, J. A. R. Navarro, J. M. Salas, *J. Am. Chem. Soc.* **2001**, *123*, 383.
[16] G. Alberti, S. Murcia-Mascarus, R. Vivani, *J. Am. Chem. Soc.* **1998**, *20*, 9291.
[17] M.-H. Zeng, X.-L. Feng, X.-M. Chen, *Dalton Trans.* **2004**, 2217.
[18] K. S. Min, M. P. Suh, *Chem. Eur. J.* **2001**, *7*, 303.
[19] L. Pan, E. B. Woodlock, X. Wang, *Inorg. Chem.* **2000**, *39*, 4174.
[20] H. Li, C. E. Davis, T. L. Groy, D. G. Kelley, O. M. Yaghi, *J. Am. Chem.Soc.* **1998**, *120*, 2186.
[21] K. S. Min, M. P. Suh, *J. Am. Chem. Soc.* **2000**, *122*, 6834.
[22] O.-S. Jung, Y. J. Kim, Y.-A. Lee, J. K. Park, H. K. Chae, *J. Am. Chem.Soc.* **2000**, *122*, 9921.
[23] S.-I. Noro, R. Kitaura, M. Kondo, S. Kitagawa, T. Ishii, H. Matsuzaka, M. Yamashita, *J. Am. Chem. Soc.* **2002**, *124*, 2568.
[24] L. G. Beauvais, M. P. Shores, J. R. Long, *J. Am. Chem. Soc.* **2000**, *122*, 2763.

[25] V. Kiritsis, A. Michaelides, S. Skoulika, S. Golhen, L. Ouahab, *Inorg. Chem.* **1998**, *37*, 3407.
[26] J. Larionova, S. A. Chavan, J. V. Yakhmi, A. G. Froystein, J. Sletten, C. Sourisseau, O. Kahn, *Inorg. Chem.* **1997**, *36*, 6374.
[27] A. V. Nossov, D. V. Soldatov, J. A. Ripmeester, *J. Am. Chem. Soc.* **2001**, *123*, 3563.
[28] M. Verdaguer, A. Bleuzen, V. Marvaud, J. Vaissermann, M. Seuleiman, C. Desplanches, A. Scuiller, C. Train, R. Garde, G. Gelly, C. Lomenech, I. Rosenman, P. Veillet, C. Cartier, F. Villain, *Coord. Chem. Rev.* **1999**, *190-192*, 1023.
[29] M. Ohba, H. Okawa, *Coord. Chem. Rev.* **2000**, *198*, 331.
[30] S. Triki, J. Sala-Pala, F. Thétiot, C. J. Gomes-Garcia, J.-C. Daran, *Eur. J. Inorg. Chem* **2006**, 185.
[31] N. Yanai, W. Kaneko, K. Yoneda, M. Ohba, S. Kitagawa, *J. Am. Chem. Soc.* **2007**, *129*, 3496.
[32] S. Eller, P. Schwarz, A. K. Brimah, R. D. Fischer, *Organometallics* **1993**, *12*, 3232.
[33] R. Eckhardt, H. Hanika-Heidl, R. D. Fischer, *Chem. Eur. J.* **2003**, *9*, 1795.
[34] M. Rüegg, A. Ludi, K. Rieder, *Inorg. Chem.* **1971**, *10*, 1773.
[35] I. P.-Y. Shek, W.-F. Yeung, T.-C. Lau, J. Zhang, S. Gao, L. Szeto, W.-T. Wong, *Eur. J. Inorg. Chem* **2005**, 364.
[36] H. Imai, K. Inoue, K. Kikuchi, Y. Yoshida, M. Ito, T. Sunahara, S. Onaka, *Angew. Chem. Int. Ed.* **2004**, *43*, 5618.
[37] T. Kimura, T. Goto, H. Shintani, K. Ishizaka, T. Arima, Y. Tokura, *Nature* **2003**, *426*, 55.
[38] G. L. J. A. Rikken, E. Raupach, *Nature* **1997**, *390*, 493.
[39] Y. Yamasaki, S. Miyasaka, Y. Kaneko, J.-P. He, T. Arima, Y. Tokura, *Phys. Rev. Lett.* **2006**, *96*, 207204.
[40] W. Kaneko, S. Kitagawa, M. Ohba, *J. Am. Chem. Soc.* **2006**, *129(2)*, 248.
[41] E. Coronado, C. Gimenez-Saiz, J. M. Martinez-Agudo, A. Nuez, F. M. Romero, H. Stoeckli-Evans, *Polyhedron* **2003**, *22*, 2435.
[42] H. Imai, K. Inoue, M. Ohba, H. Okawa, K. Kikuchi, **2003**, *137*, 919.
[43] C. Pariya, F.-L. Liao, S.-L. Wang, C.-S. Chung, *Polyhedron* **1998**, *17*, 547.
[44] R. C. Bansal, J. B. Donnet, F. Stoeckli, *Active Carbon*, Marcel Dekker, New York, **1988**.
[45] F. Stoeckli, D. Hugi-Cleary, T. A. Centeno, *J. Eur. Ceram. Soc.* **1998**, *18*, 1177.
[46] F. Stoeckli, *Russ. Chem. Bull. Int. Ed.* **2001**, *50*, 2265.
[47] M. M. Dubinin, *Progress in Surface and Membrane Science, Vol. 19*, (Ed.: D. A. Cadenhead) ed., Academic Press, London, **1975**.
[48] Stoe., *X-Area, Vol. V1.26 & X-RED32 V1.26*, Software. Stoe & Cie GmbH, Darmstadt, Germany., **2005**.
[49] G. M. Sheldrick, *Acta Cryst.* **2008**, *A64*, 112.
[50] C. Pariya, F.-L. Liao, S.-L. Wang, C.-S. Chung, *Polyhedron* **1998**, *17*, 547.
[51] D. F. Mullica, P. K. Hayward, E. L. Sappenfield, *Inorg. Chim. Acta* **1996**, *253*, 97.
[52] A. L. Spek, *J.Appl.Cryst.* **2003**, *36*, 7.
[53] I. B. Bersuker, *Chem. Rev.* **2001**, *101*, 1067.

[54] B. J. Hathaway, D. E. Billing, *Coord. Chem. Rev.* **1970**, *5*, 143.
[55] L. Shen, H.-T. Wang, Y.-J. Zhang, Z.-M. Jin, *Acta Crystallogr., Sect.C: Cryst.Struct.Commun.* **2004**, *C60*, m180.
[56] J. Cernak, J. Lipkowski, I. Potocnak, A. Hudak, *Monastsh. Chem* **2001**, *132*, 193.
[57] X.-R. Sun, J.-L. Liang, C.-M. Che, N. Zhu, X. X. Zhangb, S. Gao, *Chem.Commun.* **2002**, 2090.
[58] T. Akitsu, Y. Einaga, *Inorg. Chem.* **2006**, *45*, 9826.
[59] J. Rodrıguez-Hernandez, A. Gomez, E. Reguera, *J. Phys. D: Appl. Phys.* **2007**, *40*, 6076.
[60] M. Y. Darensbourg, H. L. C. Barros, *Inorg. Chem.* **1979**, *18*, 3286.
[61] G. O. Morpurgo, V. Mosini, P. Porta, G. Dessy, V. J. Fares, *Chem. Soc., Dalton Trans.* **1981**, 111.
[62] K. R. Dumbar, R. A. Heintz, *Progress in Inorganic Chemistry*, John Wiley & Sons, New York, **1997**.
[63] E. Coronado, C. J. Gomez-Garcia, A. Nuez, F. M. Romero, J. C. Waerenborgh, *Chem. Mater.* **2006**, *18*, 2670.
[64] T. A. Centeno, F. Stoeckli, *Recent Advances in Supercapacitors* **2006**, 57.

Supporting Information

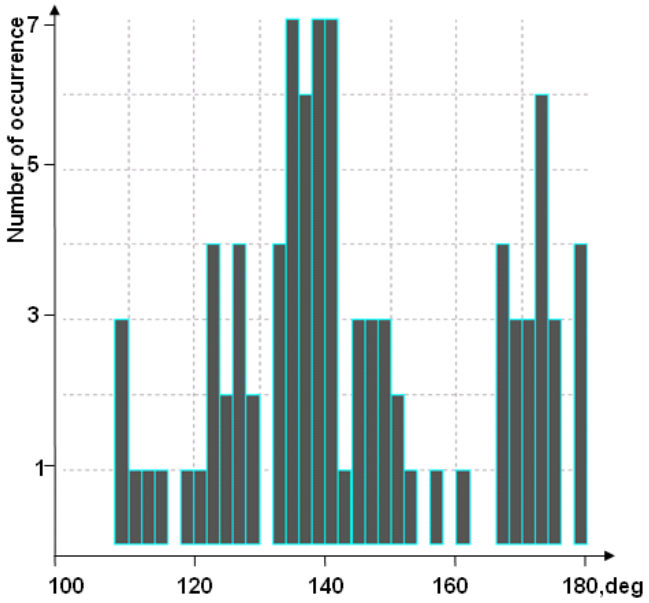

Figure S1. Histogram for Cu─N≡C angle based on Cambridge Structure DataBase search.

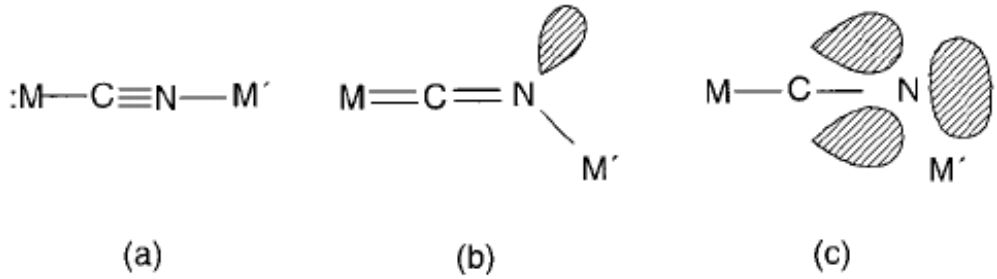

Figure S2. Models for bonding in the M─C≡N─M′ system: (a, b) valence bond models; (c) molecular orbital theory model.

Figure S2a shows the situation for a linear bond, and Figure S2b corresponds to a ─C≡N─M' angle of ca. 120°. Figure S2c (which represents the molecular orbital description of the electron density in the nitrogen region of the C≡N group) points again to the expected relationship between bent Cu─N≡C─ angles and longer C≡N distances.

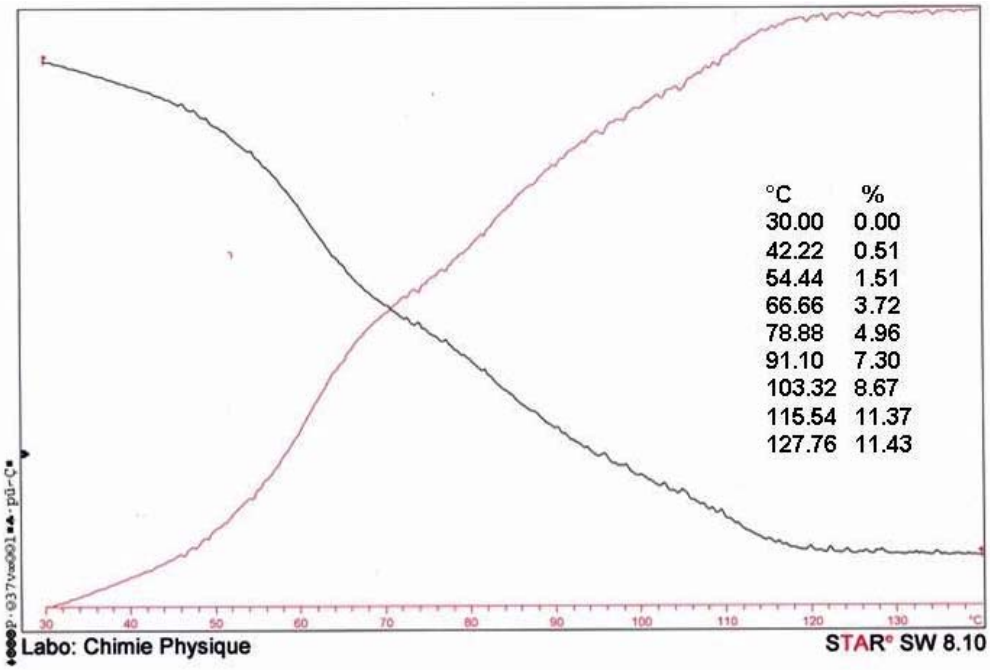

a)

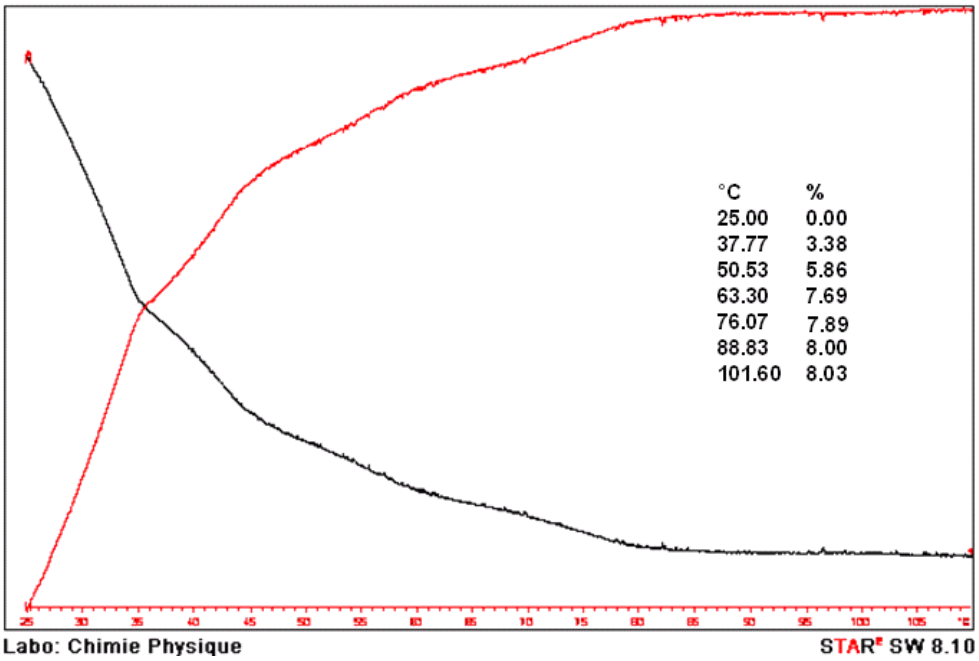

b)

Figure S3. Thermogravimetric curves of: a) complex **1;** b) complex **2.**

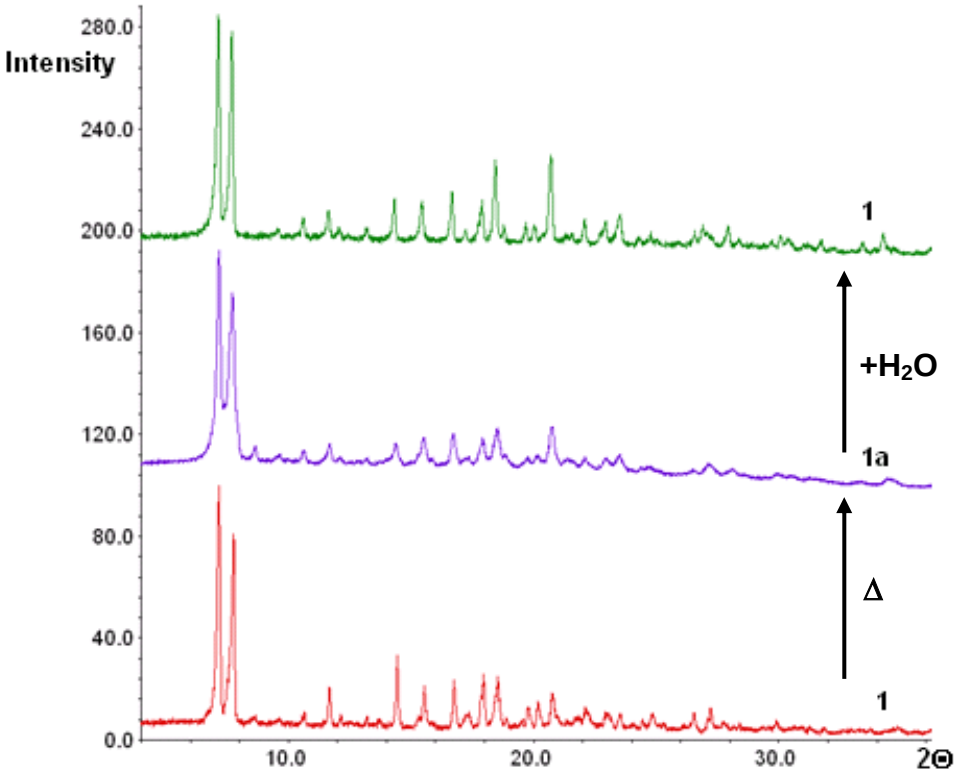

a)

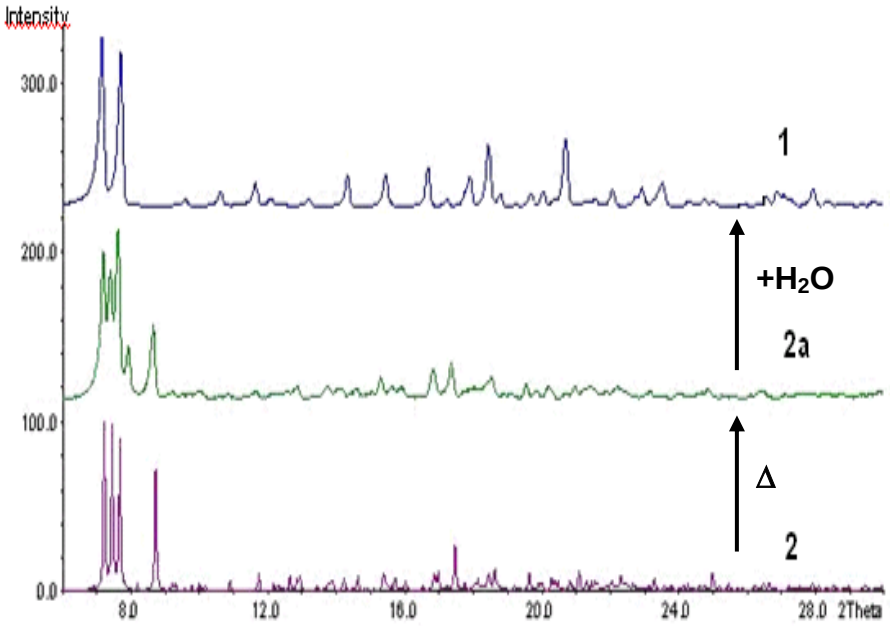

b)

Figure S4. a) Powder diffractograms showing the transformation of **1a** to **1**;
b) Powder diffractograms showing the transformation of **2** into **1,** via **2a**.

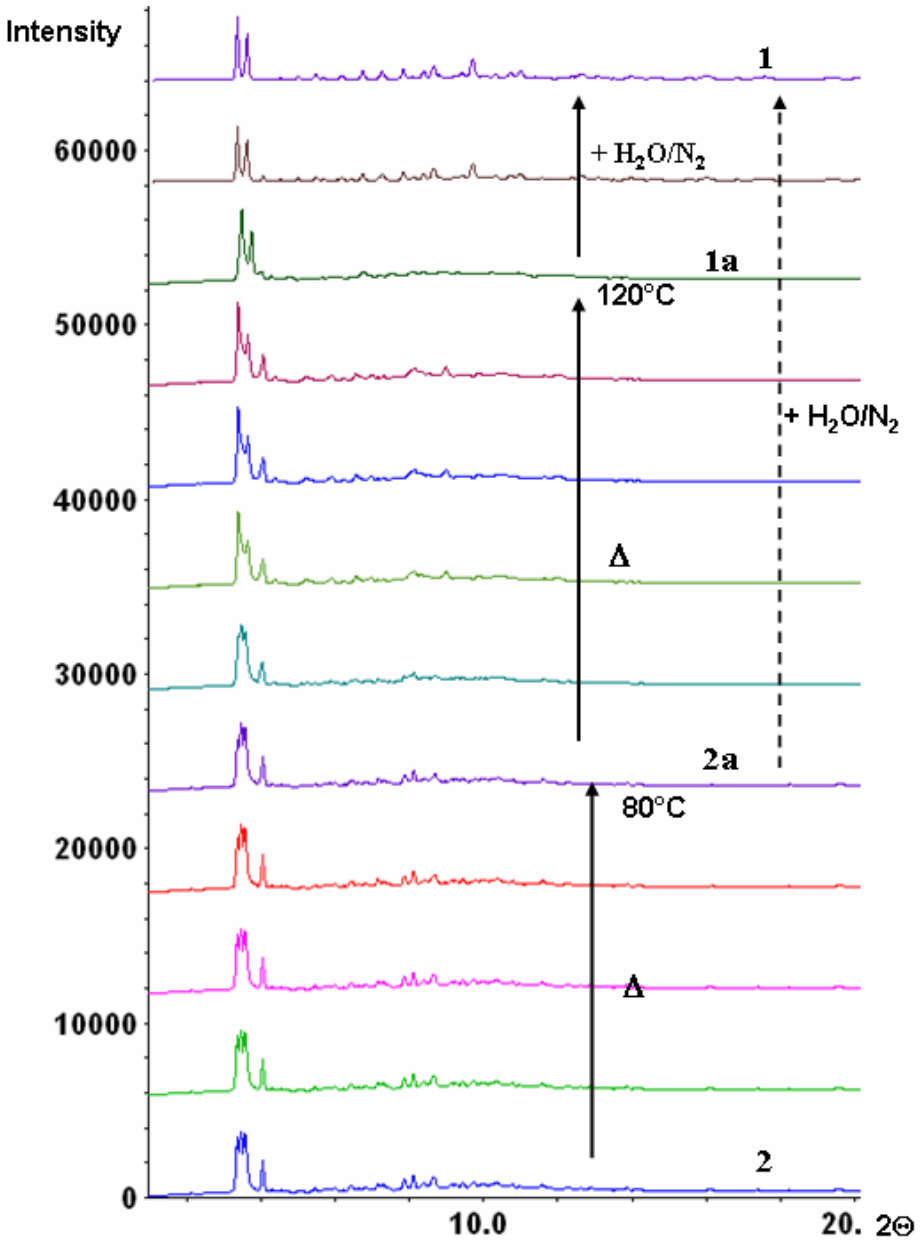

Figure S5. Variable temperature XRPD of complexes **2**, showing the transformations during the loss/addition of water molecules.

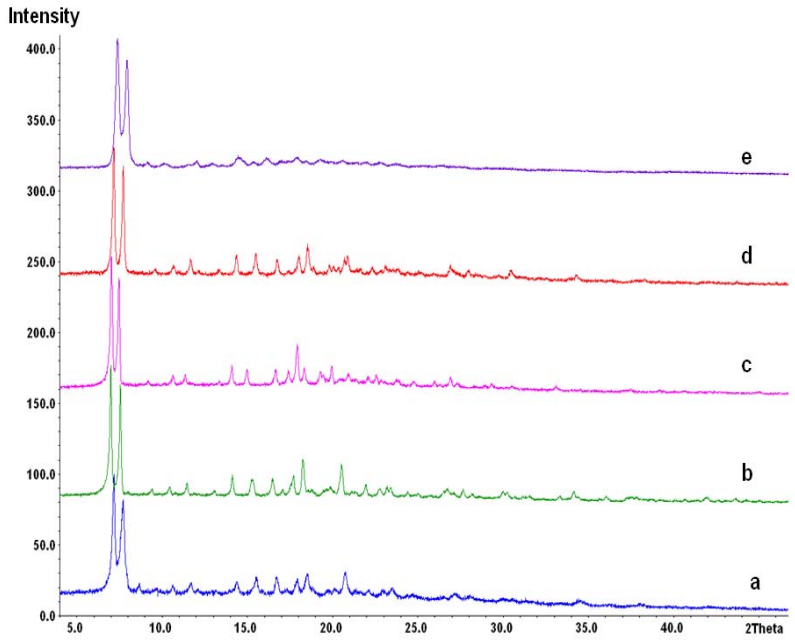

Figure S6a. PXRD of **1a**: a – after TG; immersed into: b – MeOH; c – EtOH; d – MeCN; e – Benzene.

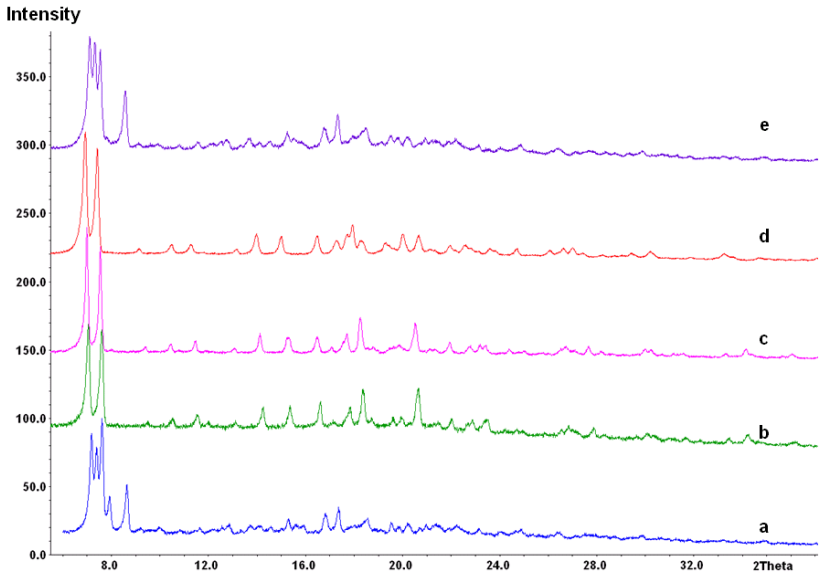

Figure S6b. PXRD of **2a**: a – after TG; immersed into: b – MeOH; c – EtOH; d – MeCN; e – Benzene.

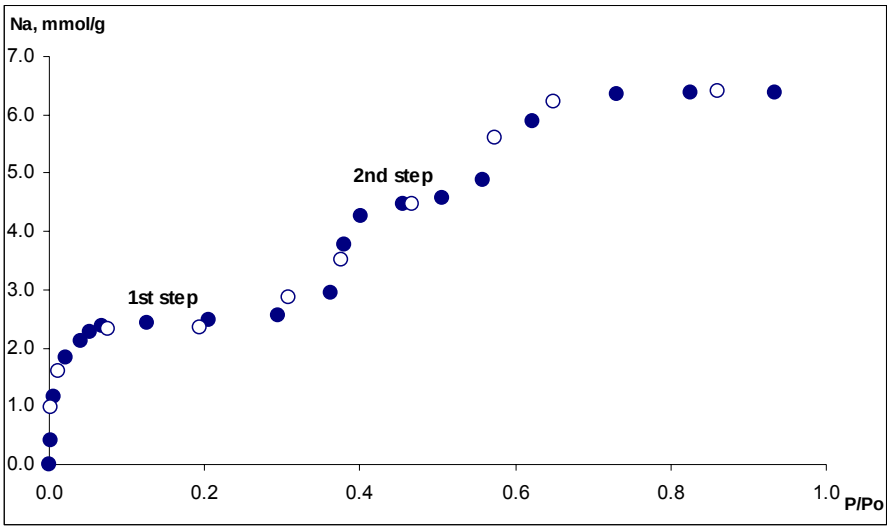

Figure S7a. Isotherm of MeOH vapor on complex **2a** and heat of immersion at three steps of isotherm.

$-\Delta_i H$ [J/g] (preadsorption to the 1step + ($-\Delta_i H$ 2) +($-\Delta_i H$ 3)) = 60. 8 J/g ⟶ calc ($-\Delta_i H$ [J/g]) = 58.47

$-\Delta_i H$ [J/g] (preadsorption to the 2step + ($-\Delta_i H$ 3)) = 31.6 J/g ⟶ calc ($-\Delta_i H$ [J/g]) = 30.12

$-\Delta_i H$ [J/g] (preadsorption to the 3step) = 2.6 J/g ⟶ calc ($-\Delta_i H$ [J/g]) = 21.95

$-\Delta_i H$ [J/g] (directly to the MeOH) experimental = 107.9 ⟶ calc ($-\Delta_i H$ [J/g]) = 113.82

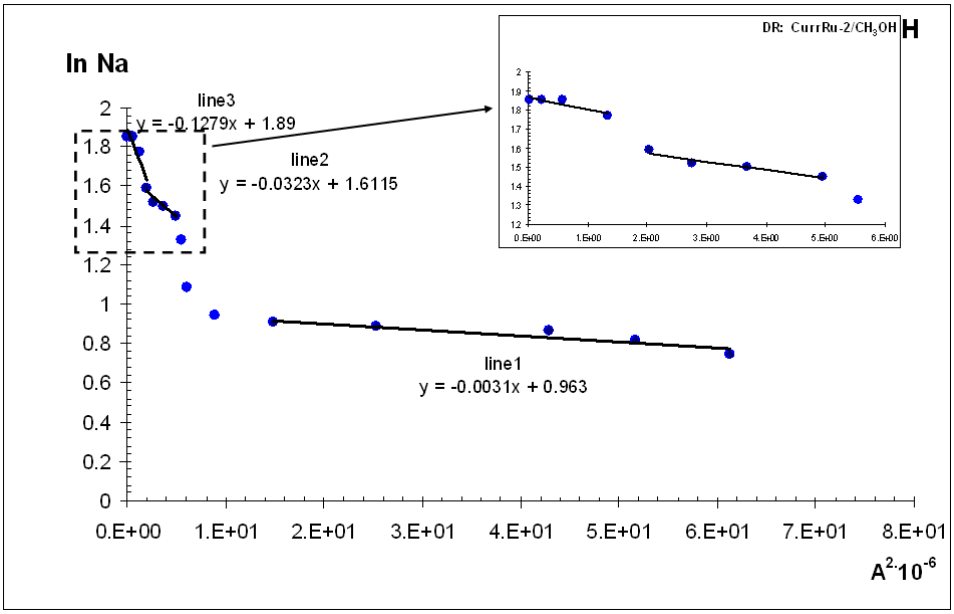

Figure S7b. The logarithmic plot of the DR equation for adsorption on complex **2a** at all three steps.

line 1		line 2		line 3	
E [kJ/mol]=	17.96	E [kJ/mol]=	5.56	E [kJ/mol]=	2.80
W_0 [cm^3/g]=	1.10E-01	W_0 [cm^3/g]=	2.03E-01	W_0 [cm^3/g]=	2.65E-01
N_{a0} [mmol/g] =	2.17	N_{a0} [mmol/g] =	5.01	N_{a0} [mmol/g] =	6.55
$-\Delta H_i$ [J/g] =	58.47	$-\Delta H_i$ [J/g] =	33.40	$-\Delta H_i$ [J/g] =	21.95
Σ ($-\Delta H_i$) [J/g] = 113.82					

Table S1. Selected bond angles (°) in complex **2**.

Cu─N≡C	Cu─N≡C angle,°	Cu─N≡C	Cu─N≡C angle,°
Cu1─N6─C6	107.9(9)	Cu6─ N40─ C80	107.92(8)
Cu2─ N4─ C4	132.5(8)	Cu7─N47─C95	117.59(7)
Cu2─ N5─ C5	114.03(7)	Cu7─ N77─C165	119.79(6)
Cu3─N22─C50	113.42(7)	Cu8─ N52─C108	109.58(9)
Cu3─ N5─C5	114.03(7)	Cu8─ N14─C22	123.80(8)
Cu4─N1─C1	107.40(8)	Cu9─N45─C93	95.11(7)
Cu4─N27─C51	109.78(9)	Cu10─ N19─ C35	107.94(8)
Cu5─N21─C37	131.7(8)	Cu11─N2─C2	96.61(8)
Cu5─N22─C50	96.24(8)	Cu11─N3─C3	109.60(7)
Cu6─N70─C150	100.53(8)	Cu12─N78─C166	114.48(7)

In the structures of compounds **1** and **2** the cyanide group can act as a severely bent bridge, forming Cu─N≡C angles distorted by as much as a 60° from linearity, while maintaining the C≡N triple bond.

Chapter 4. Construction of Metal-Organic Cyano-Bridged (MOCB) Polymers

1D, 2D & 3D

Preface

Whereas single-crystal X-ray crystallography has represented an active area of research since shortly after the discovery of X-rays, the subjects of crystal design and crystal engineering have developed rapidly only in recent years. The synthesis and characterization of multidimensional coordination networks has been an area of rapid growth in recent years. A rational synthetic strategy is the most significant point for the creation of porous coordination polymers.

In this part, results based on the synthesis of the coordination polymers and their crystal characterizations are presented. In Section 4.1 two novel one- and two-dimensional chiral cyano-bridged polymers are described. In Section 4.2 is dedicated to the synthesis of the two dimensional metal-organic cyano-bridged polymer. The strategy by which is obtained a three dimensional system is described in Section 4.3. A unique MOCBF is formed by mutually perpendicular --Cu---L---Cu---L---Cu- chains (where L = 4,4'-bipyridine), which are bridged *via* two symmetry equivalent C ≡ N bonds of the $[Ni(CN)_4]^{2-}$ anions. A search of the Cambridge Crystallographic Data Base revealed only 13 crystal structures of metallocyanide complexes involving 4,4'-bpy, and only five of these concerned first row transition metals. A few three-dimensional coordination polymers based on 4,4'-bpy and cyanide compounds have been reported, but none of them involved tetracyanonickelate (II).

4. 1

1D-$Cu^{II}Fe^{II}$ and 2D-$Cu^{II}Cr^{III}$ Bimetallic Chiral Cyano-Bridged Assemblies

Olha Sereda and Helen Stoeckli-Evans

To be submitted

Abstract

The title compounds, $\{[Cu^{II}L_2][Fe(CN)_5(NO)]\cdot H_2O\}_n$ (**I**) and $\{[Cu^{II}(Lpn)_2]_3[Cr(CN)_6]_2\cdot 5H2O\}_n$ (**II**), (where Lpn = R-1,2-diaminopropane) are new chiral cyano-bridged bimetallic polymers. The asymmetric unit of **I** is composed of two independent molecules of $[Cu(Lpn)_2][Fe(CN)_5NO]\cdot H_2O$. The zigzag cyano-bridged chains, which are parallel to the c axis, consist of alternating chiral $[Cu(Lpn)_2]^{2+}$ cations and $[Fe(CN)_5(NO)]^{2-}$anions. The $[Fe(CN)_5NO]^{2-}$ anion exhibits a distorted octahedral geometry. The average Fe─N distance (1.657(3) Å) is much shorter than the Fe─C distances, which are between 1.928(5) and 1.951(4) Å. Both copper atoms (Cu1 and Cu2) have a distorted octahedral geometry. One of the axial bond distances Cu1─N1≡C1 is 2.334(4) Å with a Cu─N1≡C1 angle of 152.2(3)°, while on the other Cu2─N11≡C12 bond is 2.291(4) with an angle of 150.6(3)°. On the opposite side the axial bond distances are much longer; Cu1─N13≡C13 of 2.980(9) Å, with a rather bent Cu─N13≡C13 angle of 117.43°, and Cu2─N3≡C2 of 3.112(8) Å, with an angle of 116.98°. These axial bonding features of extremely long semi-coordination Cu─N bonds are attributed to the coexistence of pseudo-Jahn-Teller elongation and electrostatic interactions in the infinite one dimensional chain. Compound **II** is a two dimensional cyano-bridged coordination polymer. The asymmetric unit of **II** is composed of three $[Cu(Lpn)_2]^{2+}$cations linked via two $[Cr(CN)_6]^{3-}$ anions, and five water molecules of crystallization. Two independent chromium atoms (Cr1 and Cr2) are present. They are coordinated to three $[Cu(Lpn)_2]^{2+}$cations (Cu1, Cu2 and Cu3) through three cyano nitrogens in a plane to provide 2-D dodecametallocycles constructed by Cr─CN─Cu linkages. All five non-coordinated water molecules, the cyano N atoms and NH_2 groups of the Lpn ligands are involved in O—H···O, O—H···N, N—H···O and N—H···N hydrogen bonds.

Keywords: chiral · cyano-bridged · X-ray · bimetallic polymers

Introduction

The design of high-dimensional molecular systems is closely linked to the in their unique physicochemical phenomena occurring in the bulk [1]. Successful examples of these systems include cyano-bridged complexes, in which a cyanometallate anion serves as the bridging moiety in a multidimensional structure with a second

coordination center [2-5]. In this context, heterometallic and chiral frameworks are of particular interest [6-7]. A chiral network would allow selective binding of chiral guests, and the presence of different types of metal ions may enable specific tuning of the electronic properties. However, only a few examples of chiral cyano-bridged bimetallic complexes have been published so far [8-10]. We have designed and synthesized two new chiral cyano-bridged coordination polymers, $\{[Cu(Lpn)_2][Fe(CN)_5(NO)]\cdot H2O\}_n$ (**I**) and $\{[Cu(Lpn)_2]_3[Cr(CN)_6]_2\cdot 5H2O\}_n$ (**II**), (where Lpn = R-1,2-diaminopropane), and their structures are reported here. Compound **I** is isostructural with $[Cu(1,2\text{-}pn)_2][Fe(CN)_5NO]\cdot H_2O$, synthesized using the racemic form of the ligand, which was found to be highly disordered in the crystal structure [11] (Smékal *et al.*, 2000).

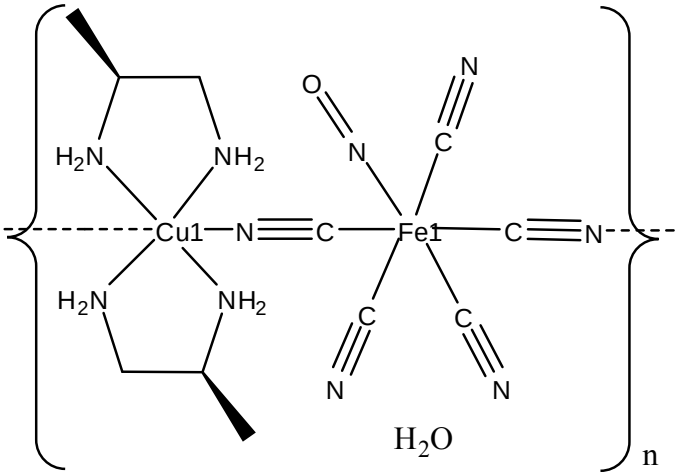

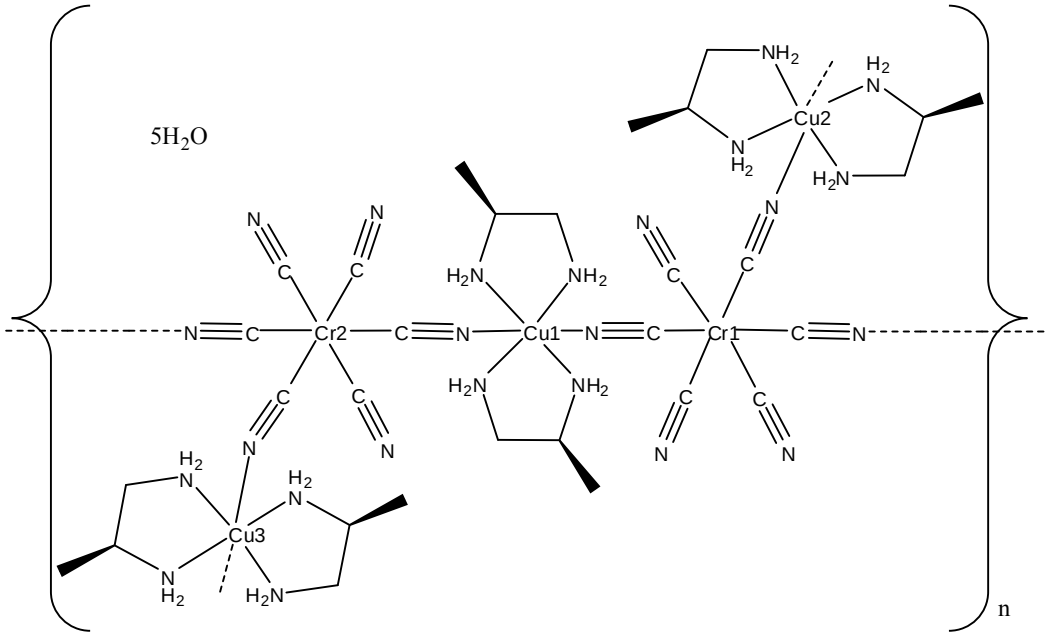

Experimental

A solution of Lpn·HCl (0.1 mmol) in water (1 mL) was adjusted to pH 7-8 by the addition of a solution of KOH (0.12 mmol) in water (0.3 mL). A solution of $CuSO_4 \cdot 5H_2O$ (0.1 mmol) in water (0.8 mL) was added to the Lpn solution under an argon atmosphere. A glass tube (ca. 8 mm diameter, ca. 20 cm long) was charged with this Lpn and copper solution, and a mixture of methanol and H_2O(1/2, 1.5 mL) was gently added as an upper layer. A solution of $Na_2[Fe(CN)_5NO]$ (0.07 mmol) in methanol/H_2O (1/1, 1 mL) was added carefully as a third layer under an argon atmosphere, and then the tube was sealed. Crystals of the complex **I** grew as violets blocks after several weeks. Elemental analysis for $C_{11}H_{22}N_{10}Cu_1Fe_1O_2$, found: C, 29.86; H, 5.07; N, 31.93. calc: C, 29.64; H, 4.97 N, 31.42%. IR spectroscopy (cm^{-1}, KBr disc): ν (OH) 3440 (m), 3320 (m), ν (NH) 3265 (m), 3157 (m), ν (CH) 2971 (m), 2883 (s), ν (CN) 2135 (vs), ν (NO) 1925 (vs), δ (NH2) 1622 (s), δ (CH2) 1398 (s), ν (Fe—C) 659 (s), δ (Fe—CN) 548 (s).

Dark-blue block-like crystals of the compound **II** were prepared in a similar manner to those of **I**, but this time using $K_3[Cr(CN)_6]$ instead of $Na_2[Fe(CN)_5NO]$. Elemental analysis for $C_{30}H_{70}N_{24}Cu_3Cr_2O_5$, found: C, 30.87; H, 5.80; N, 28.41. calc: C, 31.56; H, 6.18 N, 29.44%. IR spectroscopy (cm-1, KBr disc): ν (OH) 3536 (s), ν (NH) 3324 (s), 3269 (s), ν (CH) 2972 (s), 2942 (m), 2882 (m), ν (CN) 2121 (s), δ (NH2) 1593 (s), δ (CH2) 1462 (s), ν (Cr—C) 617, 547 (s), δ (Cr—CN) 455 (s).

Crystal Structure Determination

The intensity data for crystals of compounds **I** and **II** were collected at 173K (-100°C) on Stoe Image Plate Diffraction Systems, equipped either with a one-circle or a two-circle goniometer, using MoKα graphite monochromated radiation (λ = 0.71083 Å). The structures were solved by Direct methods using the program SHELXS-97 [12]. The refinement and all further calculations were carried out using SHELXL-97 [12]. The water and NH_2 H-atoms were located from Fourier difference maps and freely refined for complex **I**; the H-atoms of water for compound **II** were fixed. The remainder of the H-atoms were included in calculated positions and treated as riding

atoms using SHELXL default parameters. The non-H atoms were refined anisotropically, using weighted full-matrix least-squares on F^2. An empirical absorption correction was applied using the multi-scan routine in PLATON [13]; transmission factors: T_{min}/T_{max} = 0.3941/0.5108 for **I,** and T_{min}/T_{max} = 0.5302/0.6169 for **II.** Further crystallographic and refinement details for compounds **I** and **II** are given in Table 1.

Table 1 Crystal data and structure refinement for **I** and **II**

Compound	**I**	**II**
Empirical formula	$C_{11}H_{22}CuFeN_{10}O_2$	$C_{30}H_{70}Cr_2Cu_3N_{24}O_5$
Formula weight	445.79	1141.67
Temperature	173(2) K	173(2) K
Wavelength	0.71083 Å	0.71083 Å
Crystal system	Monoclinic	Monoclinic
Space group	$P2_1$	$P2_1$
Unit cell dimensions	*a* = 6.7987 (3) Å *b* = 17.8910 (10) Å *c* = 15.7161 (8) Å β = 100.482 (4)°	*a* = 10.1474 (10) Å *b* = 17.6136 (10) Å *c* = 15.5376 (14) Å β = 103.973 (11)°
Volume	1879.73 (16) $Å^3$	2694.9 (4) $Å^3$
Z	4	4
Crystal size	0.45 x 0.38 x 0.35	0.40 x 0.30 x 0.30
Crystal color and habit	violet plate	blue block
Density (calculated)	1.575	1.405
Absorption coefficient	1.930	1.612
F(000)	916	1182
Θ range for data collection	1.75 – 29.25	0.14 – 24.90
Absorption correction	Multi-scan	Multi-scan

Data/restraints/parameters	9961/1/455	10308/13/592
Final R indices [I>2sigma (I)]	0.0312	0.0522
R indices (all data)	0.0735	0.1120
Largest diff. peak and hole	0.551 and -0.438 e. Å^3	0.627 and -1.141 e. Å^3
Flack factor	0.018(13)	0.00(3)

Results and Discussion

The molecular structure of complex **I** is illustrated in Fig. 1, and selected geometrical parameters are given in Table 2. The asymmetric unit of **I** is composed of two independent molecules of $[Cu(Lpn)_2][Fe(CN)_5NO]\cdot H_2O$.

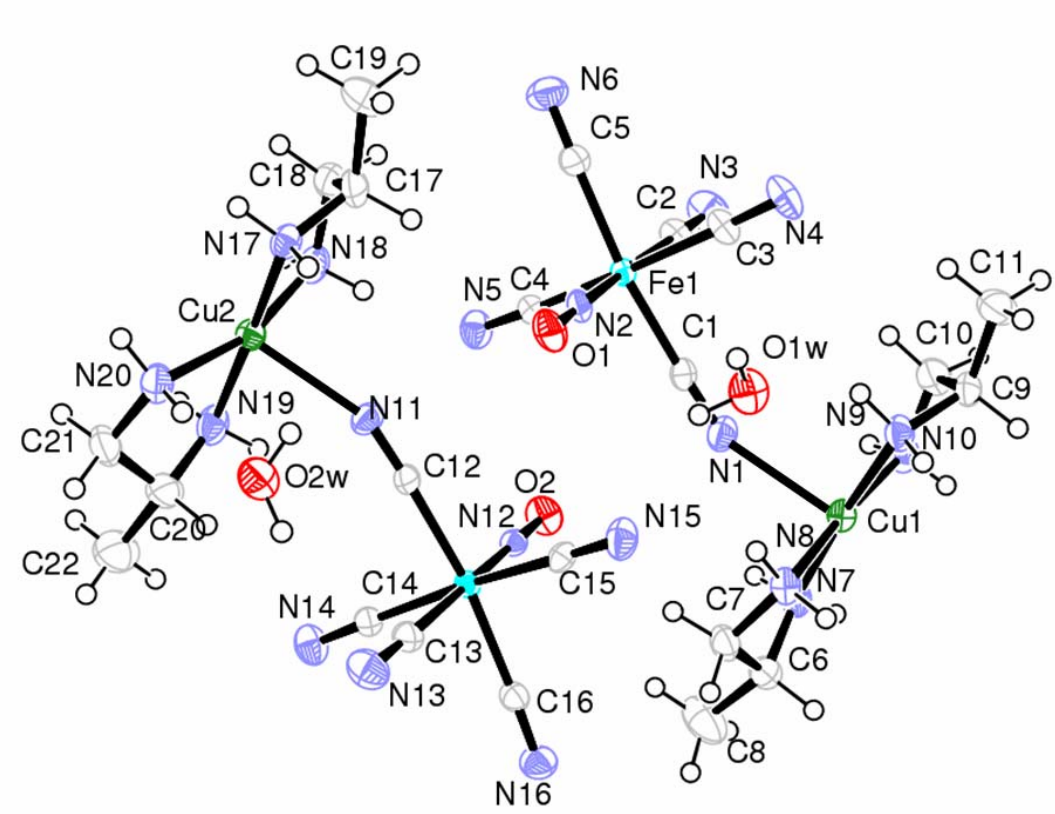

Fig. 1 A view of the asymmetric unit of compound **I**, showing the atom numbering scheme and the displacement ellipsoids drawn at the 50% probability level.

The atoms Fe1 and Fe2 are six coordinated by five carbon atoms from the cyanide ligands (two cyano groups are bridged and two terminal) and by one nitrogen from the nitrosyl group. As usual, the $[Fe(CN)_5NO]^{2-}$ anions exhibit a distorted octahedral geometry. The average Fe─N distance (1.657(3) Å) is much shorter than the Fe-C distances, which are between 1.928(5) and 1.951(4) Å. These values are in good agreement with other polymeric structures reported for nitroprusside [14-15]. The bond distances for the C≡N (average 1.144(6) A°) are similar to those observed in other nitroprussides [16-17].

Table 2 Selected bond lengths (Å) and bond angles (°) for **I**

Bond lengths (Å)			
Cu1—N1	2.334(4)	Fe1—C3	1.929(4)
Cu1—N7	2.001(4)	Fe1—C4	1.945(4)
Cu1—N8	2.002(4)	Fe1—C2	1.951(4)
Cu1—N9	2.029(4)	Fe1—C5	1.940(5)
Cu1—N10	1.999(4)	Fe2—N12	1.647(3)
Cu2—N17	2.011(3)	Fe2—C12	1.935(5)
Cu2—N18	2.016(4)	Fe2—C13	1.936(5)
Cu2—N11	2.291 (4)	Fe2—C14	1.932(4)
Cu2—N20	2.012(4)	Fe2—C15	1.941(4)
Cu2—N19	2.005(4)	Fe2—C16	1.932(5)
Fe1—C1	1.928(5)	O1—N2	1.124(5)
Fe1—N2	1.667(4)	O2—N12	1.137(4)
Bond angles (°)			
Cu1—N1—C1	152.2(3)	Cu2—N11—C12	150.6(3)
Fe1—N2—O1	178.9(3)	Fe2—N12—O2	179.5(3)
Cu1—N7—C6	109.6(3)	Cu2—N17—C17	109.0(2)
Cu1—N8—C7	108.0(2)	Cu2—N18—C18	107.5(3)
Cu1—N9—C9	109.1(3)	Cu2—N19—C20	106.8(3)
Cu1—N10—C10	109.1(3)	Cu2—N20—C21	108.5(3)

Both copper atoms (Cu1 and Cu2) have distorted octahedral geometries. On one side the axial bond distance for Cu1─N1≡C1 is 2.334(4) Å with Cu─N1≡C1 angle of 152.2(3)° and for Cu2─N11≡C12 is 2.291(4) Å with an angle of 150.6(3)°. On the opposite side the axial bond distances are much longer, that is, for Cu1─N13≡C13 it is 2.980(9) Å, with a rather bent Cu─N13≡C13 bond angle of 117.43°, and for Cu2─N3≡C2 it is 3.112(8) Å, with a bond angle of 116.98°. These axial bonding features of extremely long semi-coordination Cu─N bonds are attributed to the coexistence of pseudo-Jahn-Teller elongation and electrostatic interactions in the

infinite one dimensional chain. A similar geometry was found in $[Cu^{II}L_2][M^{II}(CN)_4]\cdot 2H_2O$ (M^{II}= Ni^{II}, Pt^{II} and L = trans-cyclohexane-(1R,2R)-diamine) [18]. The zig-zag cyano-bridged chains along the crystallographic a axis consist of alternating chiral $[Cu(Lpn)_2]^{2+}$cations and $[Fe(CN)_5(NO)]^{2-}$anions (Fig. 2).

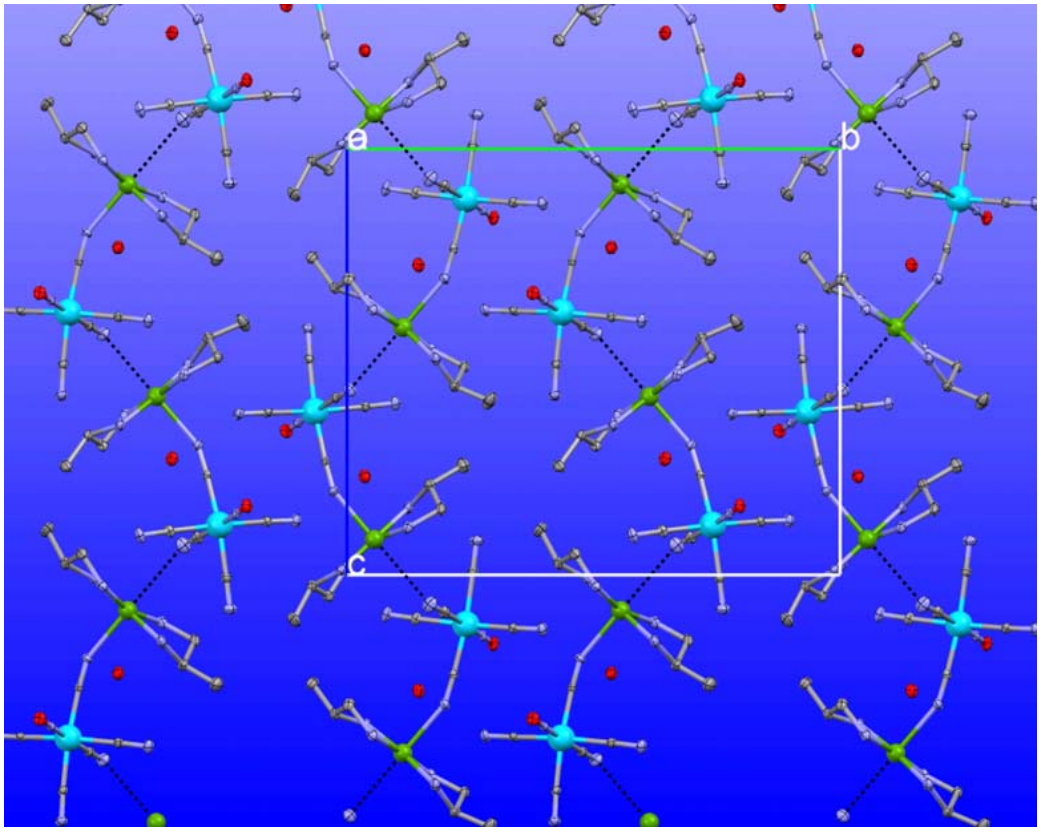

Fig. 2 Crystal packing of compound **I**, viewed along the a axis, showing the one dimensional polymer. (Cu green, Fe blue. The Lpn and water H-atoms have been omitted for clarity).

Two crystallographically independent water molecules are interconnected via hydrogen bonds. It is worth noticing that the water molecules link neighboring chains *via* O—H···Ncyano hydrogen bonds so forming a two dimensional network. Details of hydrogen bonding are given in Table 3.

Table 3 Selected bond lengths (Å) and bond angles (°) for **I**

D—H···A	D—H (Å)	H···A (Å)	D···A (Å)	D—H···A (°)
O1W—H1WA···N15	0.83	2.20	2.932(5)	147
O2W—H2WB···N5^{i}	0.81	2.18	2.969(5)	165
N7—H7A···N15^{ii}	0.92	2.36	3.259(6)	165
N7—H7B···N14^{iii}	0.92	2.09	3.006(6)	173
N8—H8A···N14^{iv}	0.92	2.24	3.118(6)	160
N8—H8B···N15	0.92	2.42	3.209(6)	143
N9—H9A···O1W	0.92	2.49	3.203(5)	134
N9—H9B···N16^{iv}	0.92	2.36	3.154(5)	144
N10—H10A···N16^{iii}	0.92	2.50	3.190(6)	132
N10—H10B···O1W^{ii}	0.92	2.08	2.959(5)	160
N17—H17A···N4^{v}	0.92	2.19	3.052(5)	155
N17—H17B···N5^{i}	0.92	2.29	3.193(5)	169
N18—H18A···N5	0.92	2.34	3.222(6)	161
N18—H18B···N4^{vi}	0.92	2.25	3.083(6)	151
N19—H19A···N6^{vi}	0.92	2.41	3.295(6)	160
N19—H19B···O2W^{ii}	0.92	2.27	3.140(6)	158
N20—H20A···O2W	0.92	2.07	2.986(5)	171

Symmetry codes: (i) *x*+1, *y*, *z*; (ii) *x*−1, *y*, *z*; (iii) −*x*, *y*−1/2, −*z*+1; (iv) −*x*+1, *y*−1/2, −*z*+1; (v) −*x*+1, *y*+1/2, −*z*; (vi) −*x*, *y*+1/2, −*z*.

The molecular structure of complex **II** is illustrated in Fig. 3, and selected geometrical parameters are given in Table 4. The asymmetric unit of **II** consists of three $[Cu(Lpn)_2]^{2+}$ cations (Cu, Cu2 and Cu3) and two $[Cr(CN)_6]^{3-}$ anions, involving atoms Cr1 and Cr2. There are also five water molecules of crystallization present. All the metal atoms are situated on general positions.

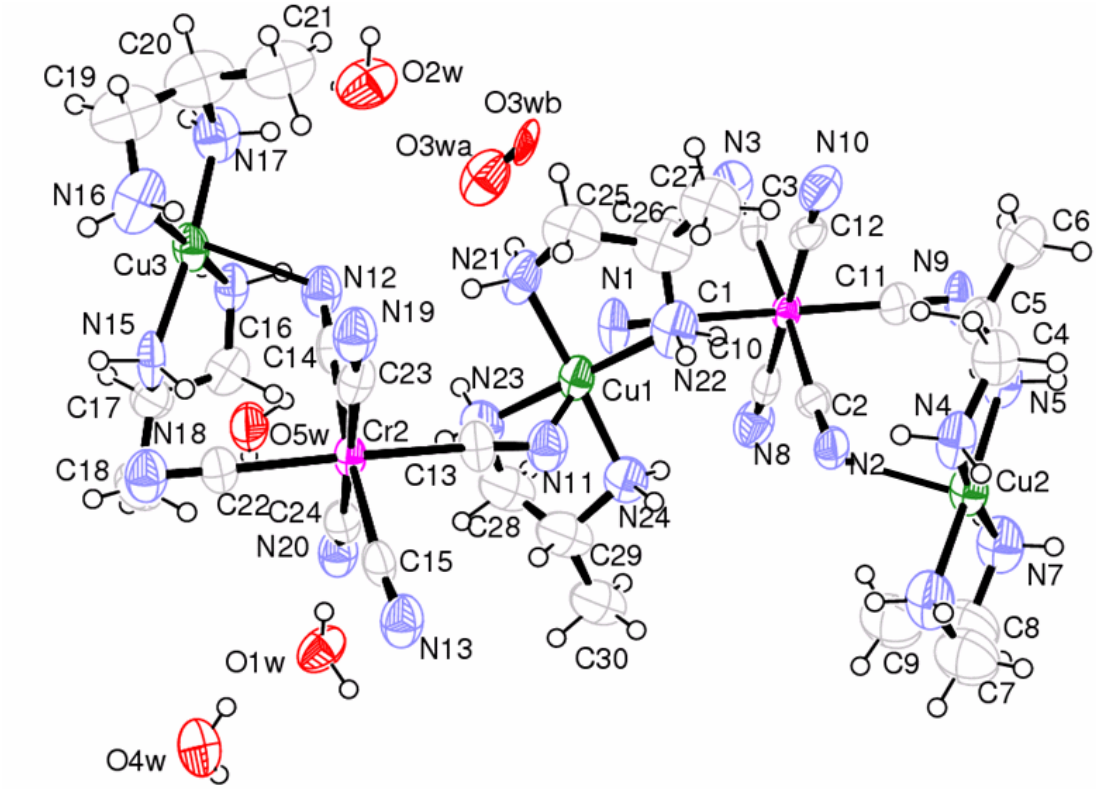

Fig. 3 A view of the asymmetric unit of compound II, showing the atom numbering scheme and the displacement ellipsoids drawn at the 50% probability level.

The coordination polyhedron of the Cu atoms can be described as CuN_4N_2 elongated octahedron, generated by four nitrogen atoms of the Lpn ligands and two nitrogen atoms of the cyanide groups. The Cu–N bond lengths vary between 1.953(8) - 2.022(7) Å for (Cu–N(Lpn)), which is similar to the bond lengths observed in $\{[Cu(ipa)_2]_2Mn(NCS)_6{\cdot}2H_2O\}_n$ [19]. The Cu–N(cyano) bond lengths are in the range of 2.460(7) – 2.859(11) Å. Thus, as for the complex **I**, the Cu atoms in complex **II** show hexacoordinated geometry with a pseudo-Jahn-Teller elongation

Table 4 Selected bond lengths (Å) and bond angles (°) for **II**

Bond lengths (Å)			
Cu1—N1	2.460(7)	Cu3—N16	2.019(9)
Cu1—N11	2.641(9)	Cu3—N17	1.953(8)
Cu1—N21	1.978(9)	Cu3—N13^{ii}	2.859(11)
Cu1—N22	2.002(9)	Cr1—C1	2.061(9)
Cu1—N23	1.996(9)	Cr1—C2	2.084(10)
Cu1—N24	1.984(8)	Cr1—C3	2.067(11)
Cu2—N2	2.542(9)	Cr1—C10	2.054(11)
Cu2—N4	2.004(8)	Cr1—C11	2.076(10)
Cu2—N5	1.994(8)	Cr1—C12	2.053(10)

Cu2—N6	2.005(8)	Cr2—C13	2.061(9)
Cu2—N7	2.013(8)	Cr2—C14	2.074(10)
Cu2—N3^{i}	2.708(9)	Cr2—C15	2.060(10)
Cu3—N12	2.487(9)	Cr2—C22	2.079(9)
Cu3—N14	2.022(7)	Cr2—C23	2.047(9)
Cu3—N15	1.992(8)	Cr2—C24	2.045(10)
Bond angles (°)			
Cu1—N1—C1	125.4(7)	Cu1—N22—C26	110.5(8)
Cu2—N2—C2	131.1(7)	Cu1—N23—C28	108.7(8)
Cu2^{iii}—N3—C3	119.3(8)	Cu1—N24—C29	109.6(7)
Cu2—N4—C4	109.2(6)	Cr1—C1—N1	175.9(8)
Cu2—N5—C5	110.6(6)	Cr1—C2—N2	176.1(8)
Cu2—N6—C7	108.6(7)	Cr1—C3—N3	176.3(9)
Cu2—N7—C8	110.7(7)	Cr1—C10—N8	178.0(9)
Cu1—N11—C13	113.1(7)	Cr1—C11—N9	178.9(9)
Cu3—N12—C14	125.9(8)	Cr1—C12—N10	178.9(8)
Cu3^{iv}—N13—C15	120.8(8)	Cr2—C13—N11	175.7(8)
Cu3—N14—C16	108.6(6)	Cr2—C14—N12	179.1(8)
Cu3—N15—C17	109.4(6)	Cr2—C15—N13	174.3(9)
Cu3—N16—C19	109.7(8)	Cr2—C22—N18	178.0(8)
Cu3—N17—C20	112.0(7)	Cr2—C23—N19	175.8(8)
Cu1—N21—C25	108.9(7)	Cr2—C24—N20	175.5(8)

Symmetry codes: (i) −*x*+1, *y*−1/2, −*z*; (ii) −*x*+2, *y*+1/2, −*z*+1; (iii) −*x*+1, *y*+1/2, −*z*; (iv) −*x*+2, *y*−1/2, −*z*+1.

Each chromium anion, bound to six carbon atoms arising from three terminal and three bridging CN ligands, has an almost regular octahedral coordination geometry (Cr–C bond lengths are in the range 2.045(10) to 2.084(10) Å). Whereas, as expected, the Cr–C–N bond angles vary only over a small range, between 174.3(9) - 179.1(8)°. The corresponding Cu–N–C bond angles deviate significantly from linearity and vary from 113.1(7) to 131.1(7)°. A projection of the crystal packing of **II** (Fig.4) onto the *bc* plane shows a planar rhomboidal grid of chromium atoms (Cr1 and Cr2) belonging to the $[Cr(CN)_6]^{3-}$ anions that bind to three adjacent $[Cu(Lpn)_2]^{2+}$ moieties.

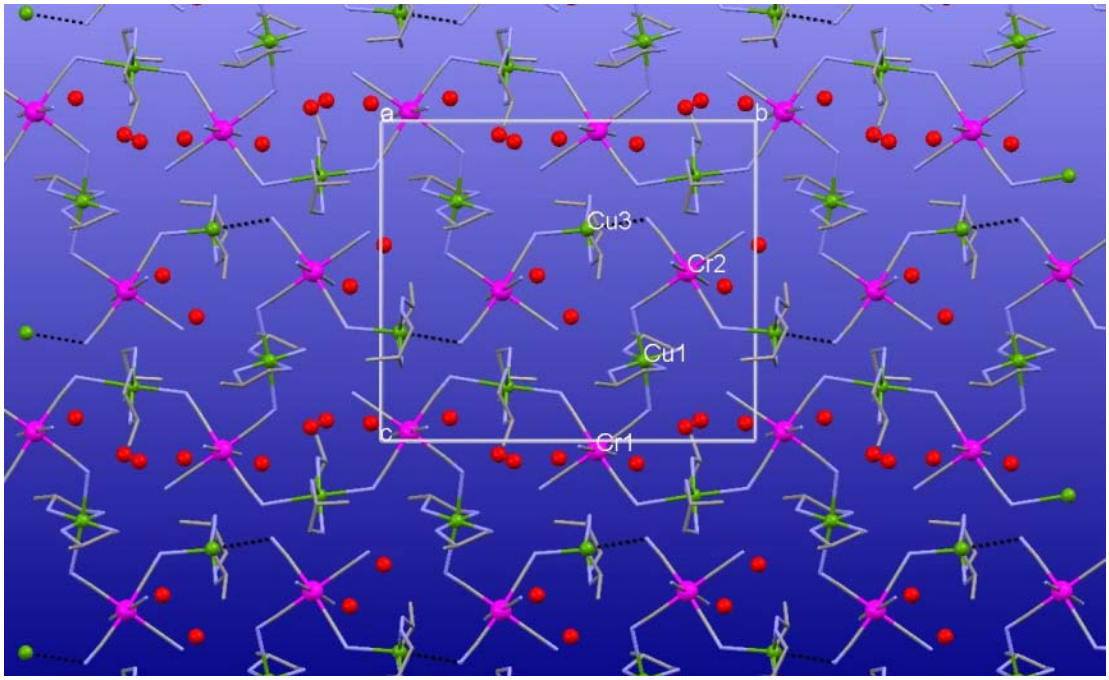

Fig. 4 Crystal packing of compound **II**, viewed along the a-axis, showing the dodeca-metallo cycles. (Cu - green, Cr - pink. The H-atoms of the Lpn and water molecules have been omitted for clarity).

One of the copper ions (Cu1) is located roughly at the center of the short sides of the grid. One of the long sides of the grid is occupied by a ─Cu3─N≡C─Cr2─C≡N─Cu3- trimer, with a central chromium atom sitting exactly along the grid and corresponding to a μ^2-$[Cr(CN)_6]^{3-}$ unit. The other longer side of the grid is occupied by a ─Cu2─N≡C─Cr1─C≡N─Cu2─ trimer. Thus, the structure can be described as layers of dodecanuclear cyclic units in which alternating $[Cu(Lpn)_2]^{2+}$ cations and $[Cr(CN)_6]^{3-}$ anions are linked by CN^- bridges. Closely related 2D bimetallic systems have been found in iron (III) analogs, where $[Fe(CN)_6]^{3-}$ anions binds to three adjacent nickel centers [20-21].

In the crystal structure of **II** all five non-coordinated water molecules, the cyano N atoms and NH_2 groups of the Lpn ligands are involved in O—H···O, O—H···N, N—H···O and N—H···N hydrogen bonds (Table 5).

Table 5 Hydrogen-bond geometry for **II** (Å, °)

D—H···A	D—H (Å)	H···A (Å)	D···A (Å)	D—H···A (°)
O1W—H1WA···N20	0.86	2.01	2.835(11)	161
O1W—H1WB···N19^{iv}	0.86	2.13	2.976(11)	170
O2W—H2WA···N10^{v}	0.86	2.06	2.806(12)	144
O2W—H2WB···N8^{iii}	0.86	2.15	2.971(12)	158
N4—H4A···N18^{ix}	0.92	2.54	3.372(12)	151
O4W—H4WA···N18^{iv}	0.86	2.21	2.992(13)	150
N5—H5A···N1^{i}	0.92	2.47	3.220(11)	139
O4W—H4WB···O1W	0.86	1.91	2.705(12)	152
N6—H6A···N19^{ix}	0.92	2.24	3.153(13)	171
O5W—H5WA···N8^{viii}	0.86	2.22	2.891(13)	135
N7—H7A···O3WA^{i}	0.92	2.19	3.005(13)	148
N7—H7B···O5W^{x}	0.92	2.46	3.154(12)	133
O5W—H5WB···N10^{iii}	0.86	2.40	3.098(12)	139
N14—H14B···N9^{iii}	0.92	2.59	3.360(12)	141
N15—H15B···N11^{ii}	0.92	2.23	3.154(12)	177
N16—H16B···O1W^{xiii}	0.92	2.29	3.159(12)	157
N17—H17A···O5W^{xiii}	0.92	2.59	3.374(12)	144
N17—H17B···O2W	0.92	2.31	3.147(11)	150
N21—H21A···O3WA	0.92	2.05	2.964(14)	172
N21—H21B···N12	0.92	2.49	3.380(13)	163
N22—H22A···N18^{ix}	0.92	2.40	3.258(13)	155
N23—H23B···N9^{iii}	0.92	2.18	3.097(12)	173
N24—H24B···O4W^{xiv}	0.92	2.06	2.968(12)	167

Symmetry codes: (iv) $x-1, y, z$; (v) $-x+2, y+1/2, -z$; (iii) $-x+1, y+1/2, -z$; (ix) $-x+2, y-1/2, -z+1$; (i) $-x+1, y-1/2, -z$; (viii) $-x, y+1/2, -z$; (x) $x, y-1, z$; (ii) $-x+2, y+1/2, -z+1$; (xiii) $x+1, y, z$; (xiv) $-x+1, y-1/2, -z+1$.

Acknowledgement This work was financed by the Swiss National Science Foundation (Grant No. 111732).

References

1. Kahn O. (1993) Molecular Magnetism, VCH: Weinheim, Germany. pp 1-380

2. Fujita N, Ohba M, Okawa H, Matsuda K, Iwamura N (1998) Inorg. Chem. 37**:**842–848

3. Ohba M, Usuki N, Fukita N, Okawa H (1999) Angew. Chem. Int. Ed. 38: 1795–1798

4. Zhang Y-Q, Luo C-L (2006) J. Mater. Chem. 16:4657–4664

5. Tanase S, Reedijk J (2006) Coord. Chem.Rev. 250:2501–2510

6. Cui Y, Evans OR, Ngo HL, White PS, Lin W (2002) Angew. Chem. Int. Ed. 41:1159–1162

7. Mironov YV, Naumov NG, Brylev KA, Efremova OA, Fedorov VE, Hegetschweiler K (2004) Angew. Chem. Int. Ed. 43:1297–1300

8. Imai H, Inoue K, Kikuchi K, Yoshida Y, Ito M, Sunahara T, Onaka S (2004) Angew. Chem. Int. Ed. 43:5618-5621

9. Coronado E, Gimenez-Saiz C, Martinez-Agudo JM, Nuez A, Romero FM, Stoeckli-Evans H (2003) Polyhedron 22:2435–2440

10. Kaneko W, Kitagawa S, Ohba M (2006) J. Am. Chem. Soc. 129:248–249

11. Smékal Z, Trávnicek Z, Marek J, Nadvornik N (2000) Aust.J.Chem.53:225–228

12. Sheldrick GM (2008) Acta Cryst. A64:112–122

13. Spek AL (2003) J. Appl. Cryst. 36:7–13

14. Shyu HL, Wei HH, Wang Y (1997) Inorg. Chim.Acta 258:81–86

15. Chen ZN, Wang JL, Qiu J, Miao FG, Tang WX (1995) Inorg. Chem. 34: 2255–2257

16. Mullica DF, Tippin DB, Sappenfield EL (1992) J. Coord. Chem. 25:175–182

17. Zhang K-L, Xu Y, Wang Z, Jin C-M, You X-Z (2002) Transition Met. Chem. 27: 95–98

18. Akitsu T, Einaga Y (2006) Inorg. Chem. 45:9826–9833

19. Shi J-M, Xu W, Zhao B, Cheng P, Liao D-Z, Chen X-Y (2005) Eur. J. Inorg. Chem. pp. 55–58

20. Kou H-Z, Gao S, Bu W-M, Liao D-Z, Ma B-Q, Jiang Z-H, Yan S-P, Fan Y-G, Wang G-L (1999) J. Chem. Soc., Dalton. Trans. pp. 2477–2480

21. Kou H-Z, Bu W-M, Gao S, Liao D-Z, Jiang Z-H, Yan S-P, Fan Y-G, Wang G-L (2000) J. Chem. Soc., Dalton. Trans. pp. 2996–3000

4. 2

A two dimensional network based on hexacyanocobaltate (III)

Olha Sereda and Helen Stoeckli-Evans

To be submitted

Abstract

The title complex, $\{[(en)Cd(\mu\text{-}en)Cd(\mu\text{-}en)Cd(en)][Co(CN)_6]_2\}_n$, has a two dimensional structure (where en = ethylenediamine). It contains two crystallographically independent Cd^{II} atoms, one of which sits on a twofold axis. There are two en ligands one of which bis-chelates to the Cd atom sitting in a general position, while the other bridges this Cd atom to that sitting on the 2-fold axis. The Cd atom with the bis-chelate en ligand is connected to three equivalent Cobalt atoms *via* cyano bridges, while the other Cd atom is linked to four equivalent Cobalt atoms *via* cyano bridges. In this way zigzag -(en)Cd(μ-en)Cd(μ-en)Cd(en)- chains are linked to form a two dimensional sheet-like structure lying parallel to the *bc* plane.

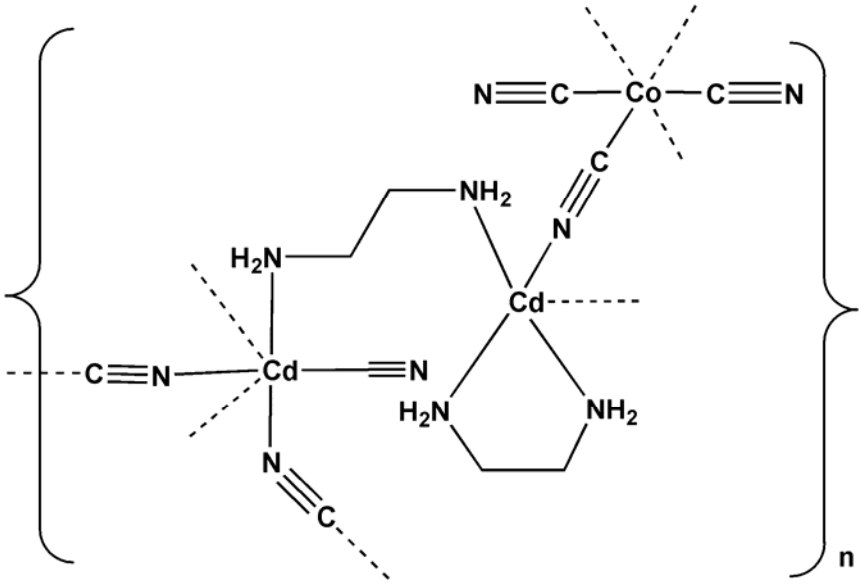

Introduction

Interest in the construction of multinuclear or polymeric metal cyanides has been driven by application-oriented subjects, such as design and synthesis of molecular magnets, light-emitting devices and zeolite-like materials, and also by the advantages of using cyanometallates as building blocks (Cernak *et al.*, 2002; Ohba & Okawa, 2000; Stasicka *et al.*, 1997; Verdaguer *et al.*, 1999; Yanai *et al.*, 2007). The dimensionality of the structures formed can be tuned to some extent by using blocking

ligands, mainly of the amine-type, coordinating several coordination sites on the central atom of the complex cation. Using this approach a large number of inorganic organic hybrid materials based on cyano complexes have be synthesized and structurally and magnetically characterized (Chen *et al.*, 2005; Liu *et al.*, 2006; Ostrovsky *et al.*, 2007).

Ethylenediamine (en) has been used extensively in the synthesis of M^{III} complexes with hexacyano-metallates. In the large majority ionic complexes were obtained. For example, $[Co^{III}(en)_3][Co^{III}(CN)_6].5H_2O$ or $[Co^{III}(en)_3][Cr^{III}(CN)_6].2H_2O$ (Sereda & Stoeckli, 2008), which are isostructural with the $[Fe^{III}(en)_3]^{3+}$ analogues (Bok etal., 1972). Changing the oxidation state of the metal (from 3+ to 2+) coordinating to the en ligand normally produces complexes with the en ligand chelating. Only with Cd^{2+} has en been found in a bridging mode, but only with tetracyanometallates, such as $[Ni(CN)_4]^{2-}$ (Yuge, 1995) or $[Cd(CN)_4]^{2-}$ (Yuge, 1992).

Following this approach, we investigated the system Cd^{2+} / ethylenediamine(en) / $[Co^{III}(CN)_6]^{3-}$. To our surprise an ionic complex was not produced, and we present here the crystal structure of the title compound, $\{[Cd(en)]_3[Co(CN)_6]_2\}_n$ (**I**), a two-dimensional coordination polymer with the en ligand both chelating and bridging.

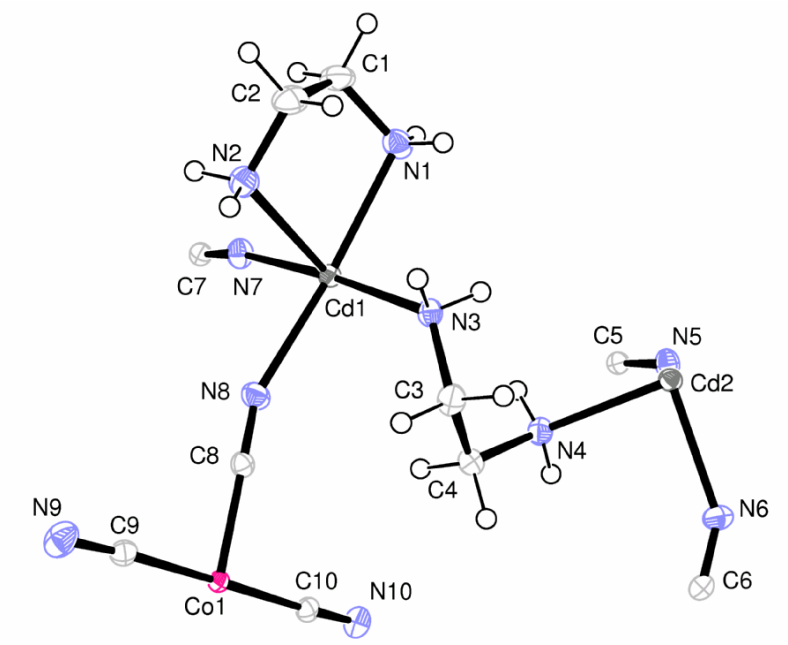

Fig. 1. The asymmetric unit of compound **I**, showing the atom-numbering scheme. displacement ellipsoids are drawn at the 50% probability level.

The molecular structure of complex **I** is illustrated in Fig. 1, and selected geometrical parameters are given in Table 1. The structure consists of zigzag chains, formed by an alternating array of $[Co(CN)_6]^{3-}$ anions and $[Cd(en)_2]^{2+}$cations, so forming a two-dimensional network. The en ligands are bridging and chelating. There are two crystallographically independent Cd^{II} atoms in the structure. Atom Cd1 also exhibits distorted octahedral coordination geometry, involving one chelate-like en ligand, three N-bonded bridging cyano groups, and one N-atom from a bridigng en ligand that links it to atom Cd2. Hence the bridging en ligand bonds *via* atom N3 to Cd1 and atom N4 to Cd2, so forming the zigzag chain (Fig. 2). –Cd1–(μ-en)–Cd2–N≡C–Co1–C≡N–Cd1– metallo-triangles are formed, as shown in Fig. 2. The Cd1-N bond distances vary between 2.3363(14) – 2.4069(15) Å, and the N-Cd1-N bond angles between 73.78(5) – 174.57(5)º. The smallest angle being found for angle N1—Cd1—N2 within the chelate en ring. A similar value of 75.9(1)° was found in $Cd(en)_2Ni(CN)_4$ (Yuge *et al.*,1995).

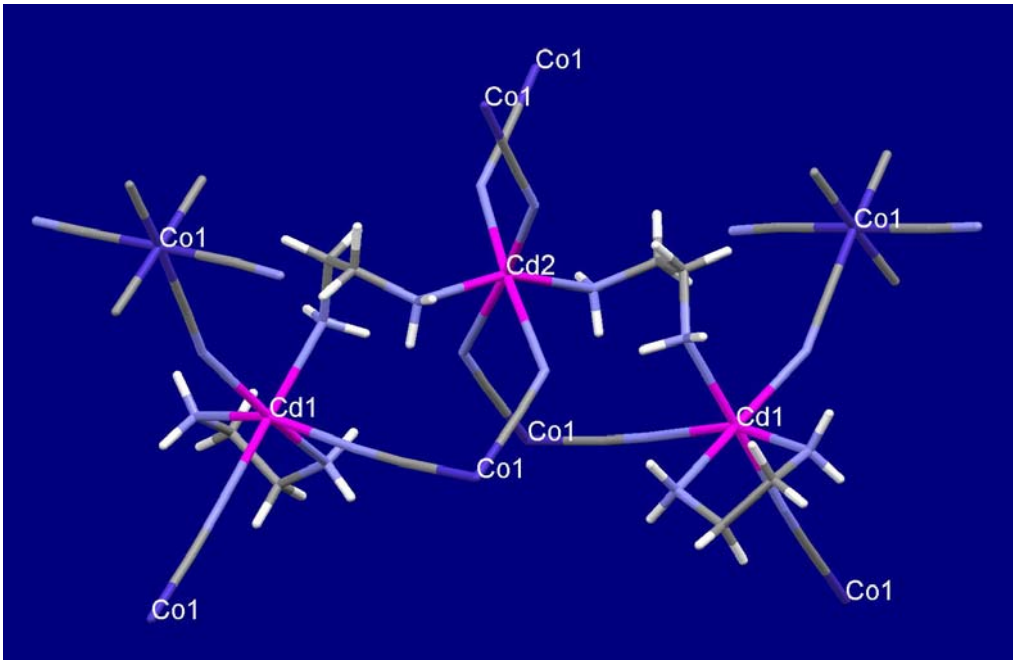

Figure 2. A view of the –Cd1–(μ-en)–Cd2–N≡C–Co1–C≡N–Cd1– metallo-triangles in the crystal structure of compound **I**.

Atom Cd2 sits on a twofold rotation axis and exhibits a distorted octahedral $[CdN_6]^{2+}$ coordination sphere, involving four N-bonded cyano groups and two N-atoms of the bridging en ligand. The Cd2—N(en) bond distance is 2.3013(14), while the Cd2-N(cyano) bond distances are 2.2997(15) and 2.4728(15) Å. These distances are both shorter and longer, respectively, than those involving atom Cd1. The longest distance can be compared with the same distances observed in $(Et_4N)\{[Cd(en)]_4[Fe(CN)_6]_3\}$, that is, 2.439(3) Å (Mal'arová *et al.*, 2003). The N—Cd2—N angles vary from 78.29 (5)° to 172.66(5)°, a geometry similar to that involving atom Cd1.

In the coordination polyhedron of atom Co1, three cyano groups exhibit bridging character while the other three are terminal. The Co1—C bond lengths vary between 1.8875(15) and 1.9063(16) Å. Similar distances, 1.889(8) to 1.902(5) Å, were found in *trans*-$[L_{14}CoNCFe(CN)_5]\cdot 5H_2O$ (where L14 = 6-methyl-1,4,8,11-tetraazacyclo-tetradecan-6-amine; Macpherson *et al.*, 2005). The Co1—C≡N angles deviate only slightly from linearity [175.92(14) – 177.77(14)º]. Some of the Cd—N≡C bonds are bent, with the smallest angle Cd2—*N*5≡C5 being 133.94 (13)°. Such deviations from linearity are not unusual in this type of structure (Mal'arová *et al.*, 2003).

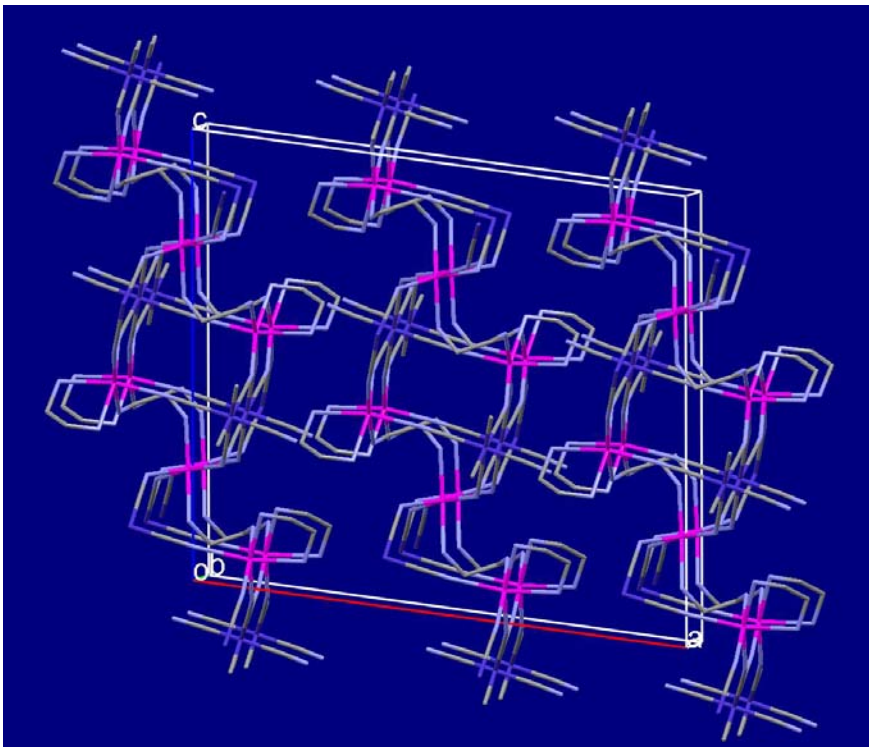

Figure 3. A view down the *b* axis of the crystal packing of compound **I** (H-atoms have been omitted for clarity).

In Fig. 3 it can be seen that the 2-D networks lies parallel to the bc plane and that they stack up the a-axis. It is worth noting that in the IR spectrum of **I**, three absorption bands are present in the 2000–2200 cm^{-1} region. They can be assigned to the presence of terminal (2120 cm^{-1}, weak) and bridging (2137 and 2158 cm^{-1}, strong) cyano groups (Nakamoto, 1977).

Synthesis

Complex **I** was obtained by adding an aqueous (30 ml) solution of $CdCl_2.2H_2O$ (1 mmol, 0.219 g) to 1,2-ethylendiamine (en) (1 mmol, 0.07 ml) with stirring. $K_3[Co(CN)_6]_3.H_2O$ (0.5 mmol, 0.165 g) was then added dropwise and the mixture was stirred for 30 min. To aid crystallization $NaClO_4$ (1 mmol, 0.12 g) was added with stirring and heating for a few minutes. The resulting solution was filtered and the filtrate placed undisturbed in the dark. After several days yellow single crystals were obtained. Elemental analysis for $C_{18}H_{24}N_{18}Cd_3Co_2$, found: C, 23.64; H, 3.29;N, 27.63. calc: C, 22.82; H, 2.55 N, 26.61%.

Crystal data

$C_{20}H_{32}Cd_3Co_2N_{20}$	V = 3288.7 (3) Å^3
M_r = 1007.75	Z = 4
Monoclinic, $C2/c$	Mo $K\alpha$
a = 21.7002 (11) Å	μ = 2.94 mm^{-1}
b = 7.7859 (5) Å	T = 173 (2) K
c = 19.6450 (9) Å	0.42 × 0.33 × 0.30 mm
β = 97.770 (4)°	

Data collection

STOE IPDS-2 diffractometer	4410 independent reflections
Absorption correction: multi-scan MULABS in PLATON (Spek, 2003)	4101 reflections with $I > 2\sigma(I)$
T_{min} = 0.338, T_{max} = 0.416	R_{int} = 0.023
19479 measured reflections	

Refinement

$R[F^2 > 2\sigma(F^2)]$ = 0.018	205 parameters
$wR(F^2)$ = 0.044	H-atom parameters constrained
S = 1.11	$\Delta\rho_{max}$ = 0.56 e Å^{-3}
4410 reflections	$\Delta\rho_{min}$ = −0.60 e Å^{-3}

Selected geometric parameters (Å, °)

Cd1—N1	2.3928 (16)	Cd2—N6	2.2997 (15)
Cd1—N2	2.4069 (15)	Co1—C5^{i}	1.8875 (15)
Cd1—N3	2.3522 (13)	Co1—C6^{ii}	1.8887 (15)
Cd1—N7	2.3423 (15)	Co1—C7^{iii}	1.9032 (15)
Cd1—N8	2.3363 (14)	Co1—C8	1.9021 (16)
Cd1—N10^{i}	2.3636 (15)	Co1—C9	1.8875 (16)
Cd2—N4	2.3013 (14)	Co1—C10	1.9063 (16)
Cd2—N5	2.4728 (15)		
N1—Cd1—N2	73.78 (5)	N6—Cd2—N6^{iv}	88.55 (5)
N1—Cd1—N3	85.30 (5)	C8—Co1—C9	90.97 (7)
N1—Cd1—N7	98.44 (5)	C8—Co1—C10	89.50 (7)
N1—Cd1—N8	164.24 (5)	C7^{iii}—Co1—C8	93.00 (7)
N1—Cd1—N10^{i}	87.32 (5)	C5^{i}—Co1—C8	88.02 (7)

N2—Cd1—N3	96.61 (5)	C6^{ii}—Co1—C8	177.34 (7)
N2—Cd1—N7	88.25 (5)	C9—Co1—C10	178.90 (7)
N2—Cd1—N8	93.64 (5)	C7^{iii}—Co1—C9	89.97 (7)
N2—Cd1—N10^{i}	159.01 (5)	C5^{i}—Co1—C9	89.18 (7)
N3—Cd1—N7	174.57 (5)	C6^{ii}—Co1—C9	87.70 (7)
N3—Cd1—N8	86.82 (5)	C7^{iii}—Co1—C10	91.00 (7)
N3—Cd1—N10^{i}	90.72 (5)	C5^{i}—Co1—C10	89.84 (7)
N7—Cd1—N8	90.45 (5)	C6^{ii}—Co1—C10	91.80 (7)
N7—Cd1—N10^{i}	85.55 (5)	C5^{i}—Co1—C7^{iii}	178.69 (7)
N8—Cd1—N10^{i}	106.43 (5)	C6^{ii}—Co1—C7^{iii}	89.30 (7)
N4—Cd2—N5	78.29 (5)	C5^{i}—Co1—C6^{ii}	89.67 (7)
N4—Cd2—N6	87.00 (5)	Co1^{i}—C5—N5	177.11 (14)
N4—Cd2—N4^{iv}	158.32 (5)	Co1^{ii}—C6—N6	177.77 (14)
N4—Cd2—N5^{iv}	85.66 (5)	Co1^{v}—C7—N7	177.35 (14)
N4—Cd2—N6^{iv}	108.77 (5)	Co1—C8—N8	175.92 (14)
N5—Cd2—N6	93.96 (5)	Co1—C9—N9	176.24 (15)
N5—Cd2—N5^{iv}	84.41 (5)	Co1—C10—N10	176.13 (14)
N5—Cd2—N6^{iv}	172.66 (5)		
Cd1—N7—C7	170.36(14)	Cd2—N5—C5	133.94(13)
Cd1—N8—C8	159.518139	Cd2—N6—C6	143.00813)
Cd1—N10—c10	175.27814)		

Symmetry codes: (i) −*x*, −*y*+1, −*z*; (ii) −*x*, −*y*+2, −*z*; (iii) *x*, *y*+1, *z*; (iv) −*x*, *y*, −*z*+1/2; (v) *x*, *y*−1, *z*.

Hydrogen-bond geometry (Å, °)

D—H···*A*	*D*—H	H···*A*	*D*···*A*	*D*—H···*A*
N2—H2NB···N9^{vi}	0.92	2.62	3.291 (2)	130
N3—H3NA···N5^{iv}	0.92	2.15	3.066 (2)	172
N3—H3NB···N9^{vi}	0.92	2.14	2.960 (2)	147
N4—H4NA···N10^{i}	0.92	2.46	3.338 (2)	161
C1—H1A···N9^{vii}	0.99	2.61	3.407 (2)	138

Symmetry codes: (vi) −*x*+1/2, −*y*+3/2, −*z*; (iv) −*x*, *y*, −*z*+1/2; (i) −*x*, −*y*+1, −*z*; (vii) −*x*+1/2, −*y*+1/2, −*z*.

Refinement

The H-atoms were included in calculated positions and treated as riding atoms: N-H = 0.92 Å, C-H = 0.99 Å, with U_{iso}(H) = 1.2U_{eq}(parent C-atom).))

Computing details

Data collection: *X-AREA* V1.26 (Stoe & Cie, 2005); cell refinement: *X-AREA* V1.26; data reduction: *X-RED32* V1.26 (Stoe & Cie, 2005); program(s) used to solve structure: *SHELXS97* (Sheldrick, 2008); program(s) used to refine structure: *SHELXL97* (Sheldrick, 2008); molecular graphics: *PLATON* (Spek, 2003); software used to prepare material for publication: *SHELXL97*.

Bok, L. D., Leipoldt, J. G. & Basson, S. S. (1972). *Z. Anorg.Allg. Chem.* ***389***, 307-314.

Cernák, J., Orendác, M., Potocnák, I., Chomic, J., Orendacová, A., Skorsepa, J. & Feher, A. (2002). *Coord. Chem. Rev.* **224**, 51–66.

Chen, X. Y., Shi, W., Xia, J., Cheng, P., Zhao, B., Song, H. B., Wang, H. G., Yan, S. P., Liao, D. Z. & Jiang, Z. H. (2005). *Inorg. Chem.* **44**, 4263–4269.

Jagner, S., Ljungstrom, E. & Vannerberg, N.-G. (1974). *Acta Chem.Scand., Ser.A,* ***28***, 623-630.

Liu, C.-M., Gao, S., Kou, H.-Z., Zhang, D.-Q., Sun, H.-L. & Zhu, D.-B. (2006). *Cryst. Growth Des.* **6**, 94–98.

Nakamoto, K. (1997). *Infrared and Raman Spectra of Inorganic and Coordination Compounds*, Part B. New York: Wiley and Sons.

Mal'arová, M., Kuchár, J., Cernák, J. & Massab, W. (2003). *Acta Cryst.* C**59**, m280–m282.

Mal'arová, M., Trávnícek, Z., Zboril, R. & Cernák, J. (2006). *Polyhedron* ***25***, 2935-2943.

Ohba, M. & Okawa, H. (2000). *Coord. Chem. Rev.* **198**, 313–328.

Ostrovsky, S. M., Klokishner, S. I., Palii, A. V. & Dunbar, K. R. (2007). *J. Mol. Struct.* **838**, 138–143.

Sereda, O. & Stoeckli-Evans, H. (2008). CCDC deposited.
Sheldrick, G. M. (2008). *Acta Cryst.* A64, 112-122.
Spek, A. L. (2003). J.Appl.Cryst. 36, 7-13.

Stasicka, Z. & Wasielewska, E. (1997). *Coord. Chem. Rev.* **159**, 271–294.

Stoe & Cie (2005). *X-Area V1.26 & X-RED32 V1.26 Software*. Stoe & Cie GmbH, Darmstadt, Germany.

Verdaguer, M., Bleuzen, A., Marvaud, V., Vaissermann, J., Seuleiman, M., Desplanches, C., Scuiller, A., Train, C., Garde, R., Gelly, G., Lomenech, C., Rosenman, I., Veillet, P., Cartier, C. & Villain, F. (1999). *Coord. Chem. Rev.* **190–192**, 1023–1047..

Yanai, N., Kaneko, W., Yoneda, K., Ohba, M. & Kitagawa, S. (2007). *J. Am. Chem. Soc.* **129**, 3496–3497.

Yuge, H. & Iwamoto, T. (1992). J. Inclusion Phenom. Mol. Recog. Chem. 14, 217-235.

Yuge, H., Mamada, A., Asai, M., Nishikioro, S. & Iwamoto, T. (1995). *J. Chem. Soc. Dalton Trans.* pp. 3195–3205.

4. 3

Poly-[(*trans*-bis-(μ-4,4'-bipyridine-*N*,*N*'))-diaquacopper(II)-tetracyanonickelate(II)]: a Metal-Organic Cyano-Bridged Framework (MOCBF)

Olha Sereda and Helen Stoeckli-Evans

Acta Crystallographica, Section C (2008), C64(6), m221-m223.

Abstract

The structure of the title compound, $\{[Cu^{II}(4,4'\text{-bpy})H_2O)_2][Ni^{II}(CN)_4]\}_n$ (where 4,4'-bpy = 4,4'-bipyridine) was shown to be a metal-organic cyano-bridged framework (CBMOF), compossed essentially of –Cu–bpy–Cu–bpy–Cu– chains linked by $[Ni(CN)4]^{2-}$ anions. Both the metal atoms sit on special positions; the copper atom occupies an inversion center while the Ni atom of the cyanometallate sits on a 2-fold axis. The 4,4'- bpy ligand is also situated about a center of symmetry located at the center of the bridging C—C bond. The scientific impact of this structure lies in the unique manner in which the framework is built up. The arrangement of the –Cu–4,4'–bpy–Cu–4,4'–bpy–Cu– chains, which are mutually perpendicular and non intersecting, create large channels running parallel to the *c* axis. Within these channels the $[Ni(CN)4]^{2-}$ anions coordinate to successive copper atoms so forming zigzag –Cu—N≡C—Ni—C≡N—Cu- chains. In this manner a three-dimensional framework structure is constructed. To our knowledge this arrangement has never been observed previously in any of the many copper (II) 4,4'-bipyridine framework complexes synthesized so far. The coordination sphere of the copper atom is completed by two water molecules. The framework is further strengthened by O—H···N hydrogen bonds involving the water molecules and the symmetry equivalent non-bridging cyano N-atoms.

Comment

The synthesis and characterization of multidimensional coordination networks has been an area of rapid growth in recent years. The aim of this intense activity is the deliberate design of materials with specific properties, for example electronic, magnetic, optical, catalytic, ion exchange, absorption, *etc* (Chae *et al.*, 2004; Janiak, C. 2003; Fujita *et al.*, 1994; Noro *et al.*, 2000; Tabares *et al.*, 2001; Coronado *et al.*, 2000). Among these materials, multidimensional cyano-bridged complexes, prepared by the self-assembly of specifically designed precursors (typically a cyanometallate complex that acts as a ligand and a transition metal complex with available coordination sites), are playing an important role in areas such as molecule-based magnets, magneto-optic materials, ion exchange, materials for storing gases, host–guest chemistry, *etc*. (Dunbar & Heintz, 1997; Ferlay *et al.,* 1995; Cernák *et al.*, 2002). Most approaches to design nanoporous coordination polymers have involved the employment of rigid bidentate heteroaromatic N-donor ligands, such as pyrazine

(pyz) or 4,4'-bipyridine (4,4'-bpy), to connect metal ions so giving cationic networks (Hagrman *et al.*, 1999). Surprisingly the ligand 4,4'-bpy has not been used extensively as a bridging ligand with metallocyanides to form multidimensional complexes. A search of the Cambridge Crystallographic Data Base (version 5.18, last update Nov. 2007; Allen *et al.*, 2002) revealed only 13 crystal structures of metallocyanide complexes involving 4,4'-bpy, and only five of these concerned first row transition metals. A few three-dimensional coordination polymers based on 4,4'-bpy and cyanide compounds have been reported (Soma *et al.*, 1994; Teichert & Sheldrick, 2000), but none of them involved tetracyanonickelate (II). Here we describe the synthesis and structure of a new metal-organic cyano-bridged framework (MOCBF) formed from 4,4'-bipyridine, copper sulfate and tetracyanonickellate, (**I**). The molecular structure of the asymmetric unit of I is shown in Fig 1, and selected geometrical parameters are given in Table 1.

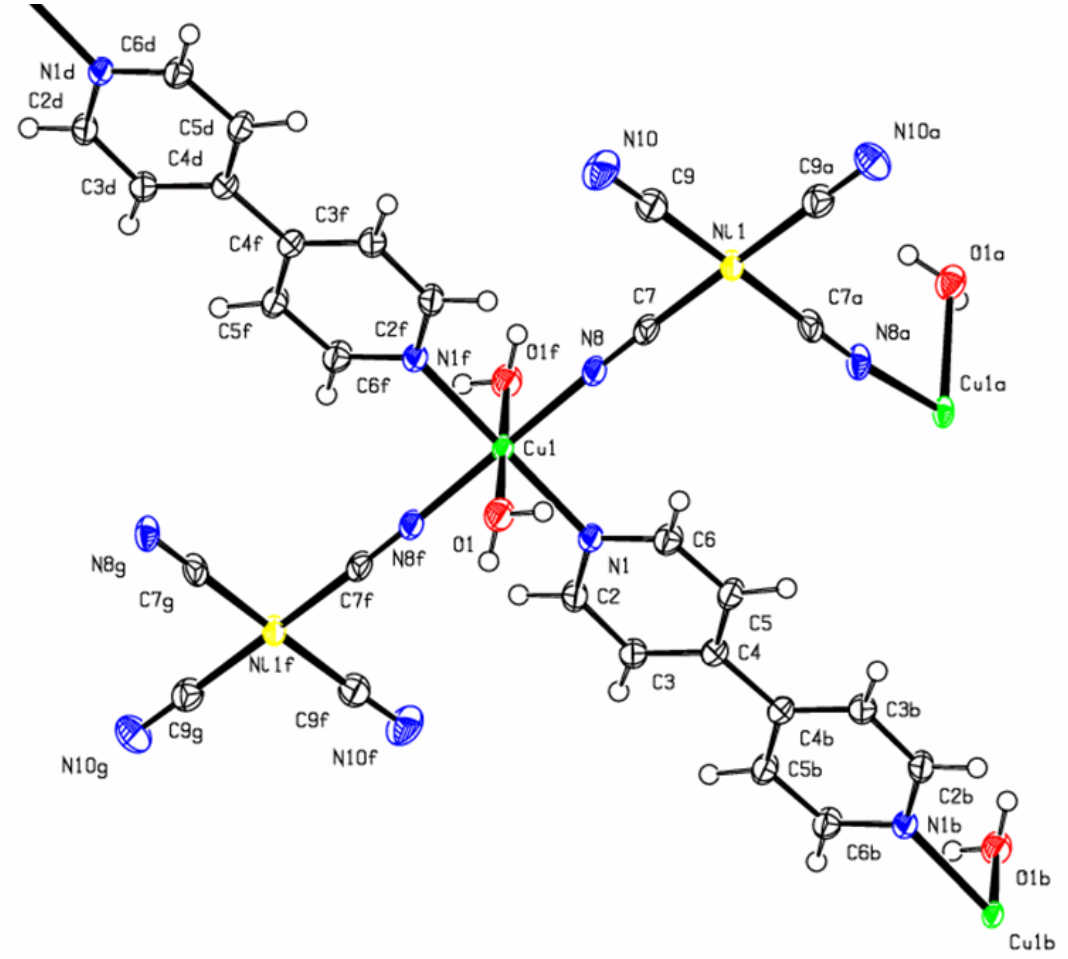

Figure 1. A view of the asymmetric unit of compound **I**, showing the atom numbering scheme and the displacement ellipsoids drawn at the 50% probability level. Symmetry codes: a = 1-x,y,1/2-z; b = 1-x,-y,1-z; d = -1/2+x,1/2+y,-1+z 1; f = 1/2-x,1/2-y,-z.

The crystal structure analysis of **I** revealed that it has a neutral three-dimensional framework, built up of $[Cu(4,4'\text{-bpy})_2(H_2O)_2]^{2+}$ cations and $[Ni(CN)_4]^{2-}$ anions. The copper (II) atom is located on an inversion center, while the nickel (II) atom sits on a 2-fold rotation axis.

Table 1. Selected bond lengths (Å) and bond angles (°) for **I**

Bond lengths (Å)			
Cu1─O1w	2.4199(15)	Ni1─C7	1.858(2)
Cu1─N1	2.0605(16)	Ni1─C9	1.865(2)
Cu1─N8	1.9754(17)	Ni1···Ni1^{i}	3.7514(6)
Bond angles (°)			
$O1_W$—Cu1—N1	87.19(6)	N8—Cu1—N8^{ii}	180
$O1_W$—Cu1—N8	91.46(6)	C7—Ni1—C9	89.98(9)
$O1_W$—Cu1—$O1_W^{ii}$	180	C7—Ni1—C7^{iii}	89.30(9)
$O1_W$—Cu1—N1^{ii}	92.81(6)	C7—Ni1—C9^{iii}	179.23(10)
$O1_W$—Cu1—N8^{ii}	88.54(6)	C9—Ni1—C9^{iii}	90.74(10)
N1—Cu1—N8	90.09(7)	Ni1—C7—N8	178.18(19)
N1—Cu1—N1^{ii}	180	Ni1—C9—N10	178.6(2)
N1—Cu1—N8^{ii}	89.91(7)		

Symmetry codes: (i) $-x+1, -y+1, -z$; (ii) $-x+1/2, -y+1/2, -z$; (iii) $-x+1, y, -z+1/2$.

The 4,4'-bpy ligand is also situated about a center of symmetry located at the center of the bridging C—C bond. The Cu atom has a distorted octahedral geometry, being coordinated to four N atoms in the equatorial plane, two from cyanide ligands and two from the 4,4'-bpy ligands. The axial positions are occupied by two water molecules. The coordination polyhedron of the Cu atoms can be described as $Cu(N)_2(H_2O)_2(NC)_2$ or CuN_4O_2. Two of the four C≡N groups of the $[Ni(CN)_4]^{2-}$ anion are non-bridging, while the other two bond to the Cu1 atoms, giving rise to Ni—C≡N—Cu bridges and forming zigzag 2a). The nickel atom has a square-planer arrangement and the mean Ni—C and C—N bond lengths are similar to the values reported for other tetracyanonickelate salts (Miyoshi *et al.*, 1973; Cernák & Lipkowski,1999; Akitsu & Einaga, 2006; Broring *et al.*, 2007). The Ni—C≡N bond angles are almost linear and there is no difference between that involving the bridging N-atom (N8) and the non-

bridging N-atom (N10). The Cu1—N≡C bond angles are slightly bent. The centrosymmetric 4,4'-bpy ligands bonded to the Cu atoms in *trans* positions gives rise to the formation of –Cu-4,4'-bpy –Cu-4,4'-bpy - chains which run at right-angles to one another (Fig. 2 b).

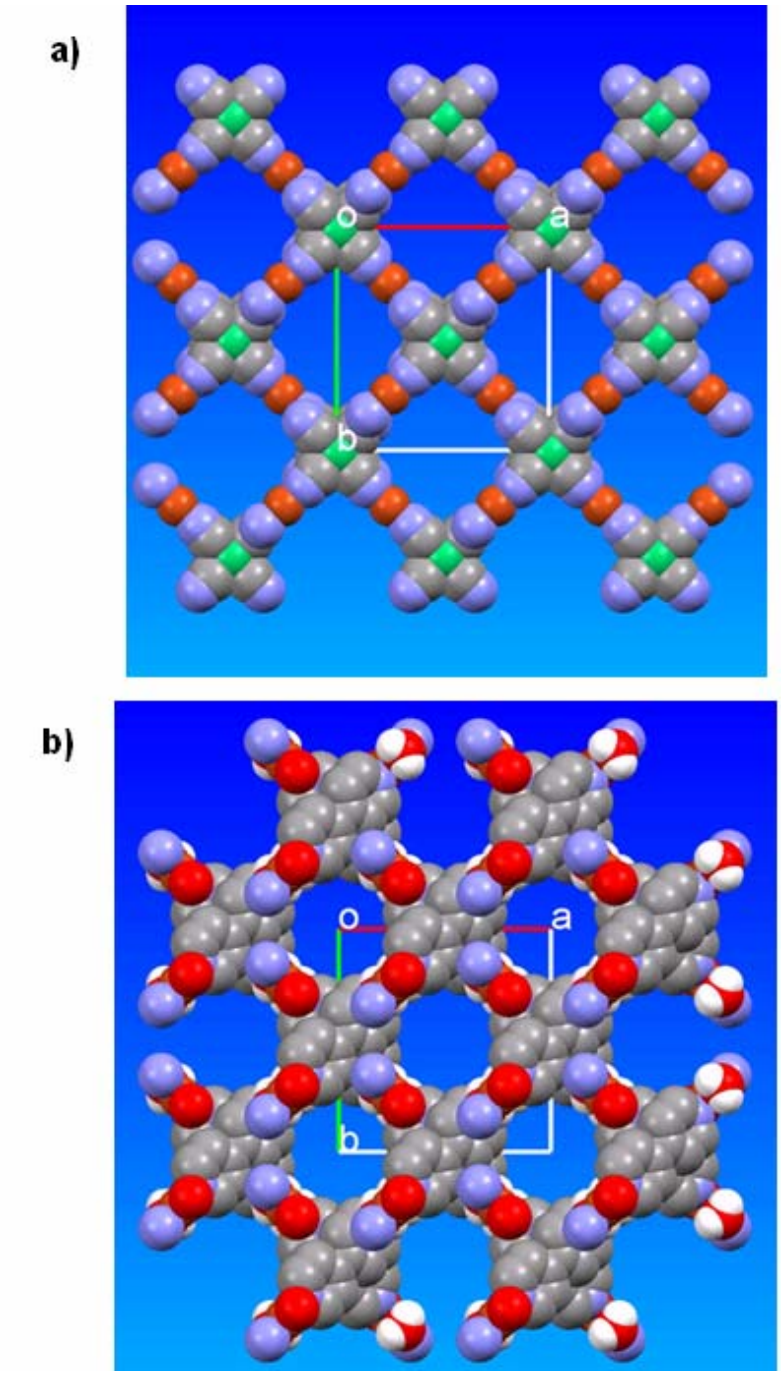

Figure 2. Crystal packing of compound **I** showing:
a) a view down the *a* axis of the zigzag –Cu—N≡C–Ni—C≡N—Cu- chains, extending in the c direction. Cu orange ball, Ni green ball;
b) a view down the *c* axis of the mutually perpendicular arrangement of the –Cu-4,4'-bpy-Cu-4,4'-bpy- chains (the 4,4'-bpy H-atoms have been omitted for clarity).

They are separated by a distance of *ca* 3.27 Å. These chains are connected to one another *via* two of the four C≡N groups of the $[Ni(CN)_4]^{2-}$ anions, so giving rise to the three-dimensional nature of the compound (Fig. 3). The shortest Ni···Nii distance is 3.7514 (6) Å.

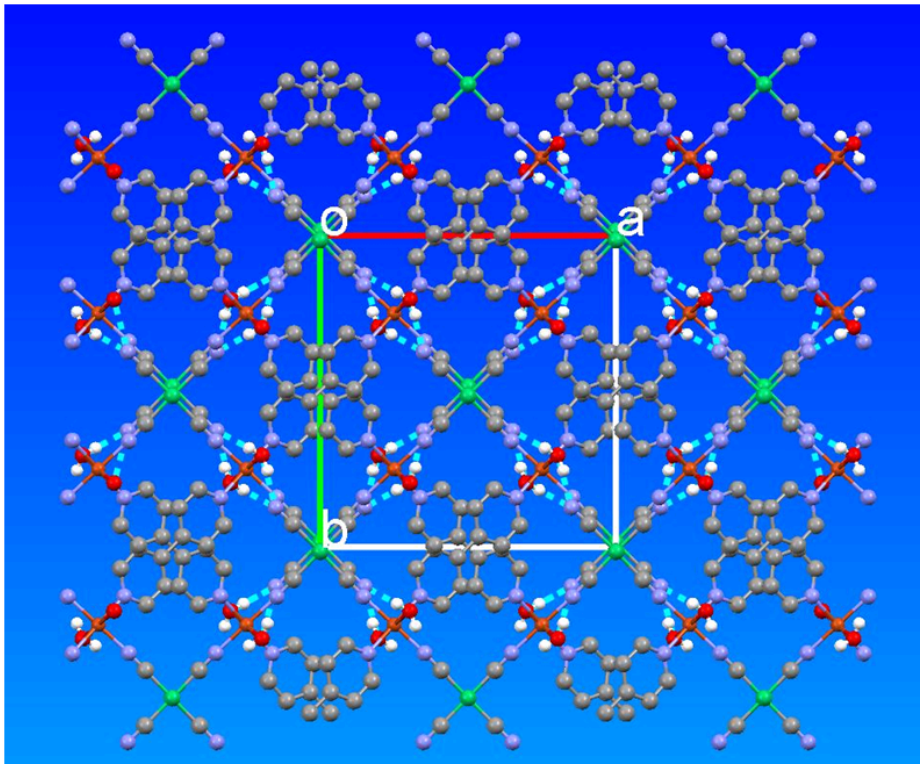

Figure 3. Crystal packing of compound **I**, viewed along the *c* axis. The O—H···N hydrogen bonds are shown as blue dashed lines, see Table 2 for details. (Cu orange, Ni green. The 4,4'-bpy H-atoms have been omitted for clarity).

The structure is further stabilized by O—H···N hydrogen bonds involving the coordatinated water molecules and the nitrogen atoms of the non-bridging cyano groups (Table 2). There are also two C—H···O interactions involving the water molecules and two hydrogen atoms of symmetry related 4,4'-bpy ligands.

Table 2. Hydrogen-bond geometry (Å, °)

D—H···*A*	*D*—H	H···*A*	*D*···*A*	*D*—H···*A*
O1W—H1W···N10^{iv}	0.85(2)	2.04(2)	2.886(3)	177(2)
O1W—H2W···N10^{v}	0.84(2)	2.15(2)	2.976(3)	169(3)
C2—H2···N8^{ii}	0.95	2.43	2.964(3)	115
C6—H6···N8	0.95	2.46	2.957(3)	112

Symmetry codes: (iv) *x*, −*y*+1, *z*+1/2; (v) −*x*+1/2, *y*−1/2, −*z*+1/2; (vi) *x*+1/2, −*y*+1/2, *z*+1/2.

Experimental

To an aqueous solution of $CuSO_4 \cdot 5H_2O$ (2 mmol, 0.499 g, 20 ml) was added with stirring $K_2[Ni(CN)_4]$ (2 mmol, 0.489 g) in 20 ml of H_2O. A blue precipitate formed at once and was dissolved by adding appropriate amounts of citric acid (1.8 g), and 2-aminoethanol (1.6 ml) to adjust the pH to 9, giving a final volume of *ca*. 100 ml. About 30 ml of this solution was very carefully layered onto 20 ml of an ethylene glycol solution of 4,4'-bpy (1 mmol, 0.156 g). Green crystals of (I) appeared at the interface of the two solutions after several weeks. Analysis calculated for $C_{14}H_{12}CuN_6NiO_2$: C 40.18, H 2.89, N 20.08%; found: C 40.64, H 3.09, N 20.72%. IR spectrum (KBr disk): ν(O—H) 3513 s, 3456 s, 3379 s h; ν(ArC-H) 3144w, 3109w, 3088w; ν(C—H) 3061 s, 3045 s; ν(C≡N) 2142 s,2121 s; ν(ArC-C),1641vs, 1615vs, 1537*m*, 1493*m*, 1435s; γ (O—H, C—C, ArC-Hin-plane) 1388 s, 1369 s, 1238*m*, 1212*m*, 1153w, 1099*m*, 1012w; γ (ArC-Hout-of-plane) 866w, 728*m*, 688*m*, 660 sh; ν(Ni—C, Cu—N) 553w, 483*m*,454*m*.

Refinement

The water H-atoms were located from difference Fourier maps and freely refined: O—H = 0.77 (3) and 0.80 (3) Å. The remainder of the H-atoms were included in calculated positions and treated as riding atoms: C—H = 0.95 Å, with *U*iso(H) = 1.2Ueq (C).

Computing details

Data collection: *X-AREA* V1.35 (Stoe & Cie, 2006); cell refinement: *X-AREA* V1.35; data reduction: *X-RED32* V1.31 (Stoe & Cie, 2006); program(s) used to solve structure: *SHELXS97* (Sheldrick, 2008); program(s) used to refine structure: *SHELXL97* (Sheldrick, 2008); molecular graphics: *ORTEP-3* (Farrugia, 1997) and Mercury (Macrae *et al.*, 2006); software used to prepare material for publication: *SHELXL97*.

Crystal data

$C_{14}H_{12}CuN_6NiO_2$	$V = 1552.2\ (4)\ Å^3$
$Mr = 418.55$	$Z = 4$
Monoclinic, $C2/c$	Mo $K\alpha$
$a = 15.158\ (2)$ Å	$\mu = 2.60\ mm^{-1}$
$b = 14.8108\ (15)$ Å	$T = 173\ (2)$ K
$c = 7.4512\ (11)$ Å	$0.50 \times 0.45 \times 0.40$ mm
$\beta = 111.892\ (11)^o$	
Data collection	
STOE IPDS-2 diffractometer	1389 independent reflections
Absorption correction: multi-scan MULscanABS (Spek, 2003)	1248 reflections with $I > 2\sigma(I)$
$T_{min} = 0.246$, $T_{max} = 0.352$ 8011 measured reflections	$R_{int} = 0.037$
Refinement	
$R[F^2 > 2\sigma(F^2)] = 0.021$	120 parameters
$wR(F^2) = 0.054$	H atoms treated by a mixture of independent and constrained refinement
$S = 1.04$	$\Delta\rho_{max} = 0.22\ e\ Å^{-3}$
1389 reflections	$\Delta\rho_{min} = -0.26\ e\ Å^{-3}$

Acknowledgements

This work was supported by the Swiss National Science Foundation (Grant No. FN 20–111738).

References

Akitsu, T. and Einaga, Y. (2006). Inorg. Chem. **45**, 9826-9833.

Allen, F. H. (2002). *Acta Crystallogr.* **B58**, 380–388.

Broring, M., Prikhodovski, S., Brandt, C. D. & Tejero, E. C. (2007). *Chem. Eur. J.* **13**, 396– 406.

Cernák, J. & Lipkowski, J. (1999). *Monatsh. Chem.* **130**, 1195–1206.

Cernák, J., Orendác, M., Potocnák, I., Chomic, J., Orendacová, A., Skorsepa, J. & Feher, A. (2002). *Coord. Chem. Rev.* **224**, 51–66.

Chae, H. K., Siberio-Perez, D. Y., Kim, J., Go, Y.-B., Eddaoudi, M., Matzger, A. J., O'Keeffe, M. & Yaghi, O. M. (2004).*Nature*, **427**, 523–527.

Coronado, E., Galan-Mascaros, J. R., Gomez-Garcıa, C. J. & Laukhin, V. (2000). *Nature*, **408**, 447–449.

Dunbar, K. R. & Heintz, R. A. (1997). *Prog. Inorg. Chem.* **45**, 283–391.

Ferlay, S., Mallah, T., Ouahes, R., Veillet, P. & Verdaguer, M. (1995). *Nature*, 3**78**, 701–703.

Fujita, M., Kwon, Y. J., Washizu, S. & Ogura, K. (1994). *J. Am. Chem. Soc.* **116**, 1151–1152.

Hagrman, P. J., Hagrman, D. & Zubieta, J. (1999). *Angew. Chem. Int. Ed.* **38**, 2638–2684.

Janiak, C. (2003). *J. Chem. Soc. Dalton Trans.* pp. 2781–2804.

Macrae, C. F., Edgington, P. R., McCabe, P., Pidcock, E., Shields, G. P., Taylor, R., Towler, M. & van de Streek, J. (2006). *J. Appl. Cryst.* **39**, 453–457.

Miyoshi, T., Iwamoto, T. & Sasaki, Y. (1973). *Inorg. Chim. Acta*, **7**, 97–101.

Noro, S., Kitagawa, S., Kondo, M. & Seki, K. (2000). *Angew. Chem. Int. Ed.* **39**, 2082–2084.

Sheldrick, G. M. (2008). *Acta Cryst.* **A64**, 112-122.

Soma, T., Yuge, H. & Iwamoto, T. (1994). *Angew. Chem. Int. Ed.* **33**, 1665–1666.

Spek, A. L. (2003). *J. Appl. Cryst.* **36**, 7–13.

Stoe & Cie. (2006). *X-AREA* V1.35 & *X-RED32* V1.31 Software. Stoe & Cie GmbH, Darmstadt, Germany.

Tabares, L. C., Navarro, J. A. R. & Salas, J. M. (2001). *J. Am. Chem. Soc.* **123**, 383–387.

Teichert, O. & Sheldrick, W. S. (2000). *Z. Anorg. Allg. Chem.* **626**, 1509–1513.

Chapter 5. Another example of Adsorption and Immersion Calorimetry Studies on a Nanoporous Solid

5. 1

Adsorption of Morphine from Aqueous Solutions by Carbons

Olha Sereda & Fritz Stoeckli

1. Introduction

The adsorption and calorimetry techniques used in the present PhD were also applied to investigate the condition for a swift removal of morphine from aqueous solutions by nanoporous carbons. This specific research was carried out within the framework of the CTI project No8871.1 involving the Institute of Microtechnology (Professor JP. Farine, Head of the academic team), several industries and two hospitals.

The task consisted in finding the experimental conditions under which morphine (Fig. 1) could be rapidly eliminated from a standard aqueous solution used in clinical conditions. In this context, immersion calorimetry[1] and adsorption of sparingly soluble organics from aqueous solutions[2, 3], two topics investigated in our laboratory and used in this PhD, played an important role. By analogy with aqueous solutions of phenol, the sorptive capacity of different carbons for morphine was characterized by their enthalpies of immersion and the determination of the adsorption isotherm from aqueous solutions under equilibrium conditions. Both techniques give self-consistent results and by using the extension of the Dubinin-Radushkevich-Kaganer equation to liquid solutions[4] it was possible to determine the so-called *affinity coefficient* of morphine. This parameter is of fundamental importance, since it allows the prediction of the adsorption equilibrium of this molecule by a given carbon, at different relative concentrations c_{eq}/c_{sat} and over a range of temperature. The relevance to pharmacology is obvious.

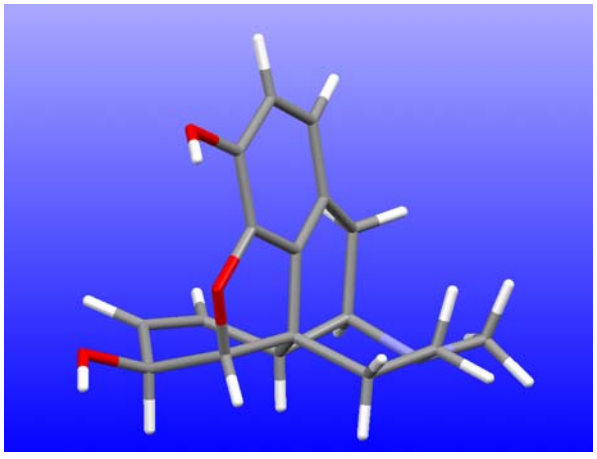

Figure 1. A three dimensional view of the morphine molecule.[5]

As far as the adsorption kinetic was concerned, we used the technique based on the determination of concentrations in the aqueous solutions by UV spectroscopy with the help of a suitable calibration curve. It appeared that a removal of more than 99% of morphine from the liquid phase could be achieved in less than 10 minutes by a good quality carbon, by using particles of less than 400 μm and an amount in excess by a factor of three with respect to the actual saturation capacity.

2. Experimental

The adsorption kinetics of morphine at room temperature (20°C) were determined by adding either 0.300 g or 0.400 g of active carbon PC94-11 to 5 ml of the standard solution (1g morphine/100 ml), with an initial shaking creating the slurry. Then, at regular intervals (5, 10, 20, .. minutes and up to several days) samples of 0.1 ml of the liquid were removed with the help of a micro-pipette. These probes were diluted in 50 to 100 ml of pure water and the concentrations of morphine left in solution, c_{sol}, were determined by UV spectroscopy. The reference is the maximum found at 210 nm. As shown in Figure 1, the calibration curve established in our laboratory covers the range of concentrations between $0.30 \cdot 10^{-5}$ mmol/ml and $3.50 \cdot 10^{-5}$ mmol/ml. This domain is required by the spectrometer and explains the need for a strong dilution of the solutions under investigation, where the concentrations c_{sol} are much higher.

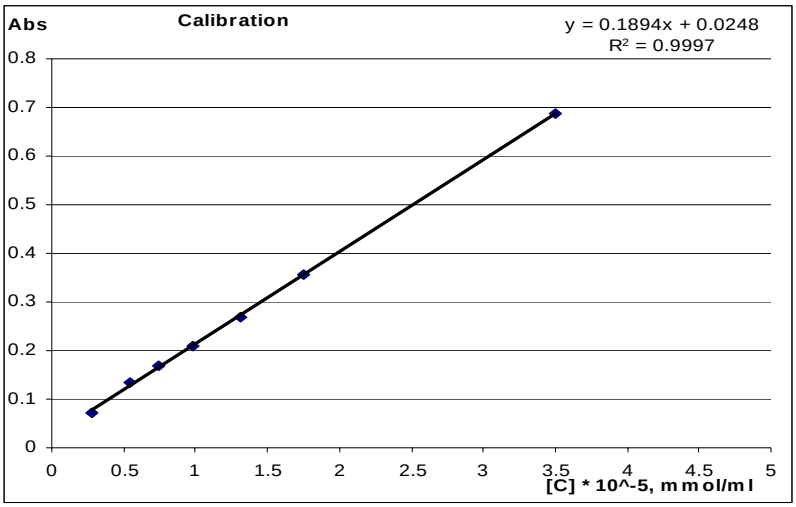

Figure 2. UV calibration curve for diluted aqueous morphine solutions at room temperature (The UV spectrum was determined with a *Cary 300* spectrometer, using a quartz cell of 1 cm path length).

3. Results and discussion

Figure 3 shows typical spectra of the diluted probes after several minutes for the experiment with 0.300 mg of carbon PC94-11. With the help of the calibration curve based on the maximum of the peak near 210 nm one obtains the concentration in the diluted solution. This, in turn, leads to the concentration in the original 5 ml solution, c_{sol}, and finally to the amount adsorbed by the carbon at the given time t.

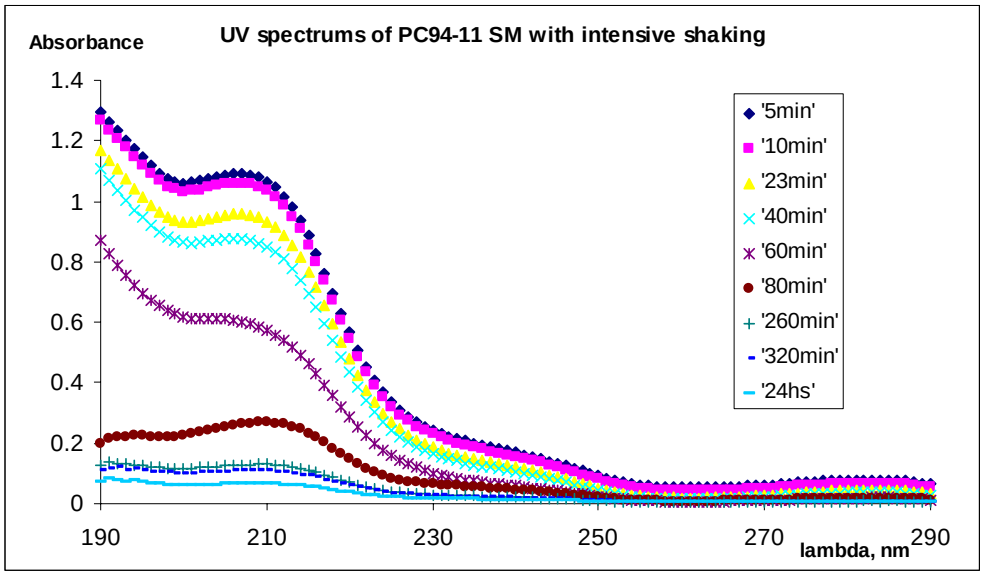

Figure 3. UV spectra of diluted solution of PC94-11(Ø ~ 50-100 μm), contact times between 5 minutes and 24 hours and initial shaking.

Table 1 shows the percentage of morphine removed by 0.400 g and 0.300 g of carbon PC94-11 with different particle sizes Ø, as a function of time and under different conditions of shaking.

Table 1. Kinetics for the removal of morphine from the standard solution (10 g of morphine / litre) in a reduced version, using 5 ml (0.175 mmol morphine) and 0.300g of carbon PC94-11. The quantity c_{sol}/c_{sat} is the relative concentration of morphine in the solution (c_{sat} = 0.221 mmol/ml at room temperature).
At time t = 0, c_{sol}/c_{sat} = 0.035/0.221 = 0.158

Carbon, mg Ø (μm)	Time, minutes	Morphine in sol mmol in 5 ml	c_{sol}/c_{sat}	Morphine adsorbed, mmol/g carbon	Removed %	Conditions
	0	0.175	0.158	0	0	
	5	0.132	0.120	0.0883	24.35	
	10	0.128	0.116	0.0856	26.62	
	23	0.116	0.105	0.0772	33.85	moderate
300	40	0.106	0.096	0.0704	39.67	shaking
(~100	80	0.072	0.080	0.053	54.23	
μm)	260	0.016	0.014	0.0107	90.84	
	320	0.013	0.012	0.0089	92.40	
	410	0.008	0.007	0.0054	95.38	
	5	0.102	0.093	0.0683	41.45	
	10	0.099	0.090	0.066	43.44	
	20	0.095	0.086	0.0633	45.71	
	40	0.090	0.081	0.0600	48.55	
300	60	0.081	0.074	0.0543	53.45	intensive
(~100	80	0.070	0.063	0.0468	59.90	shaking
μm)	160	0.048	0.043	0.0320	72.54	
	380	0.010	0.009	0.0065	94.39	
	1440	0.001	0.001	0.0007	99.36	

(The Table continues on the following page)

Carbon, mg Ø (μm)	Time, minutes	Morphine in sol mmol in 5 ml	c_{sol}/c_{sat}	Morphine adsorbed, mmol/g carbon	Removed %	Conditions
	0	0.175	0.158	0	0	
	5	0.013	0.012	0.0067	92.34	
400	10	0.006	0.005	0.0028	96.81	intensive
(~100 μm)	33	0.005	0.004	0.0025	97.16	shaking
	55	0.004	0.004	0.0022	97.52	
	360	0.004	0.004	0.0021	97.59	
	540	0.004	0.004	0.0020	97.66	
	5	0.048	0.043	0.0238	72.75	
	10	0.040	0.036	0.0198	77.36	
	20	0.032	0.029	0.0160	81.76	moderate
400	30	0.024	0.022	0.0120	86.23	shaking
(~100 μm)	40	0.020	0.018	0.0101	88.50	
	85	0.014	0.013	0.0071	91.84	
	340	0.0084	0.0076	0.0042	95.17	
	1080	0.0063	0.0057	0.0032	96.38	
	5	0.166	0.150	0.0831	5.05	
400	20	0.113	0.102	0.056	35.42	no shaking
(~100 μm)	40	0.089	0.081	0.0447	48.90	
	75	0.071	0.064	0.0353	59.69	
	1440	0.020	0.18	0.0102	88.36	
	5	0.0064	0.00058	0.0003	99.63	
	10	0.00043	0.00039	0.0002	99.76	
400	20	0.00013	0.00012	0.0001	99.92	Good initial
(≤ 40 μm)	30	0.00003	0.00003	0.00001	99.98	mixing
	35	0.000010	0.000009	0.000005	99.99	
	5	0.0312	0.0282	0.0155	82.20	
	15	0.0216	0.0216	0.0119	86.35	
400	25	0.0197	0.0179	0.0098	88.73	no initial
(≤ 40 μm)	35	0.0158	0.0143	0.0078	91.00	mixing
	45	0.0116	0.0105	0.0057	93.38	
	55	0.0087	0.0079	0.0043	95.04	
	65	0.0065	0.0059	0.0032	96.29	

Table 1 clearly shows that the most efficient elimination of morphine within 5 minutes of contact time is achieved by 0.400 g / 5ml (or 80 g/ litre) with a particle size Ø < 40 μm. This requires a good initial mixing of the slurry and leads to an elimination of more than 99 per cent within 5 minutes (Fig. 4).

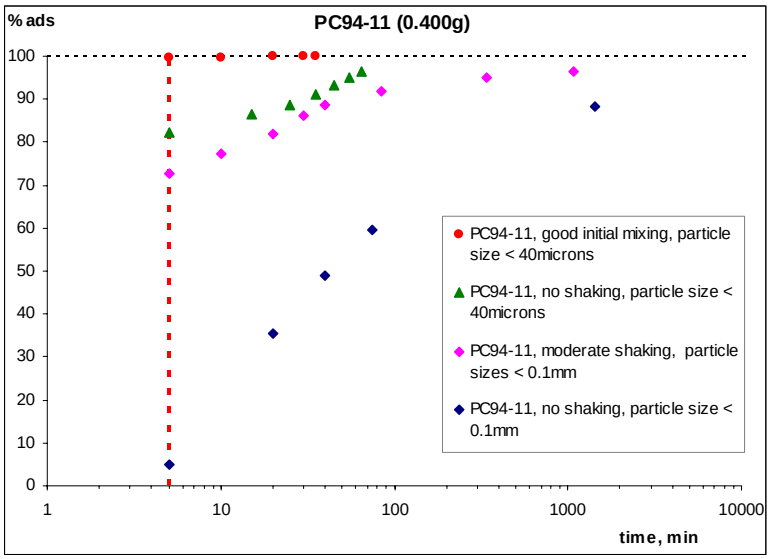

Figure 4. Removal of morphine from the standard solution (5 ml), as a function of time for 0.400 g of carbon PC94-11 with particle sizes Ø< 40 μm and Ø ~ 50-100 μm. The vertical dotted line corresponds to 5 minutes.

Another activated carbon, of similar quality, has also been tested. However, its performance was not as good for the removal of morphine (Fig. 5).

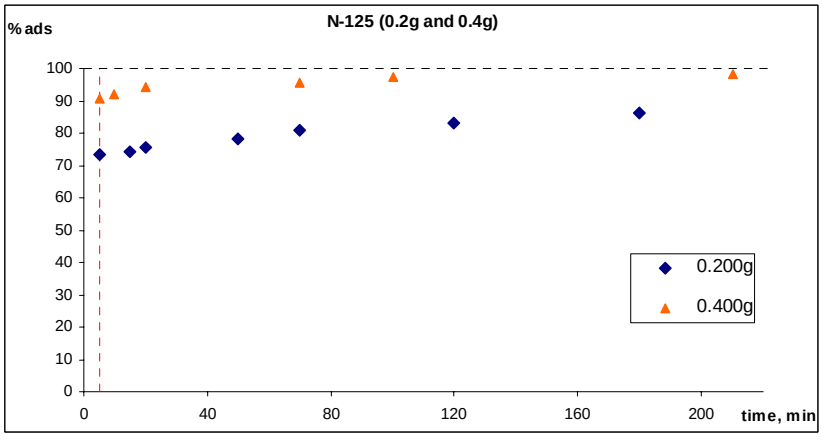

Figure 5. Removal of morphine under strong and moderate shaking from the standard solution (5 ml), as a function of time for carbon N-125 with particle sizes Ø ~ 50-100 μm.

The complete saturation of the carbon takes place only at high relative concentrations of morphine in the solution (c_{sol}/c_{sat} > 0.1). However, the concentration $c_{sol}(t)$

decreases in the liquid phase and a final equilibrium is established only at $t \rightarrow \infty$. From a practical point of view, it is reached after 48 hours and corresponds to the equilibrium concentration c_{eq} and the corresponding amount adsorbed $N_a(c_{eq}/c_{sat})$. These quantities, shown in Figure 6 (below), are very useful in another context, as they appear in the modified Dubinin-Radushkevich-Kaganer equation (DRK) examined by Stoeckli et al.[6-8]

$$Na = N_{am}\exp[-(RT\ln(c_s/c_{eq})/E_s)^4] \quad (1)$$

This expression is a modification of the classical Dubinin-Radushkevich equation for vapour-solid adsorption used in the context of the present thesis (Chapter 3)

$$N_a = N_{ao}\exp[-(RT\ln(p_s/p_{eq})/\beta E_o)^2] \quad (2)$$

In the case of Eqn (1), relative pressures have been replaced by relative concentrations and the exponent is equal to 4. The major difference is the fact than in the case of sparingly soluble organics removed from aqueous solutions, adsorption is limited to the coating of the micropore walls by a monolayer, as opposed to the volume filling process characterizing adsorption from the vapour phase (this has been illustrated in the case of phenol adsorbed from aqueous solutions and from the vapour phase).[4]

Both equations have the advantage that they can represent adsorption over a large range of temperatures and relative pressures or concentrations. It is one of the fundamental properties of Dubinin-Polanyi theory, which are not met by many other approaches. The only required parameters for the vapour (or the solute) are the saturation pressure (p_s) or concentration (c_s) at the different working temperatures.

E_s, the so-called characteristic energy of adsorption, is a temperature invariant function of the solute and of the solid. It has been shown that, by analogy with adsorption from the vapour phase, one can introduce an *affinity coefficient* (scaling factor) specific for a given solute (i),

$$\beta_s(i) = E_s(i)/E_o \quad (3)$$

This parameter is independent of the carbon and typical values are shown in Table 2.

Figure 6 shows the logarithmic plot of Eqn (1) for the adsorption data obtained at 293 K and 313 K after an equilibrium time of no less than three days. It appears that the principle of temperature invariance postulated by Dubinin's theory fully applies, as the data for the two temperatures lead to a single line. From the graph one obtains the characteristic energy E_s(morphine) = 28.9 ± 0.2 kJ mol^{-1} and a monolayer capacity N_{am} = 1.25 ± 0.03 mmol g^{-1} . Since the accessible surface area of the carbon is 820 m^2 g^{-1}, it follows that the molecular surface area of morphine (Fig. 1) is approximately $109 \cdot 10^{-20}$ m^2.

Since E_o of carbon PC94-11 is 21 kJ mol^{-1}, Eqn (3) leads to the affinity coefficient β_s(morphine) = 1.37 ± 0.02.

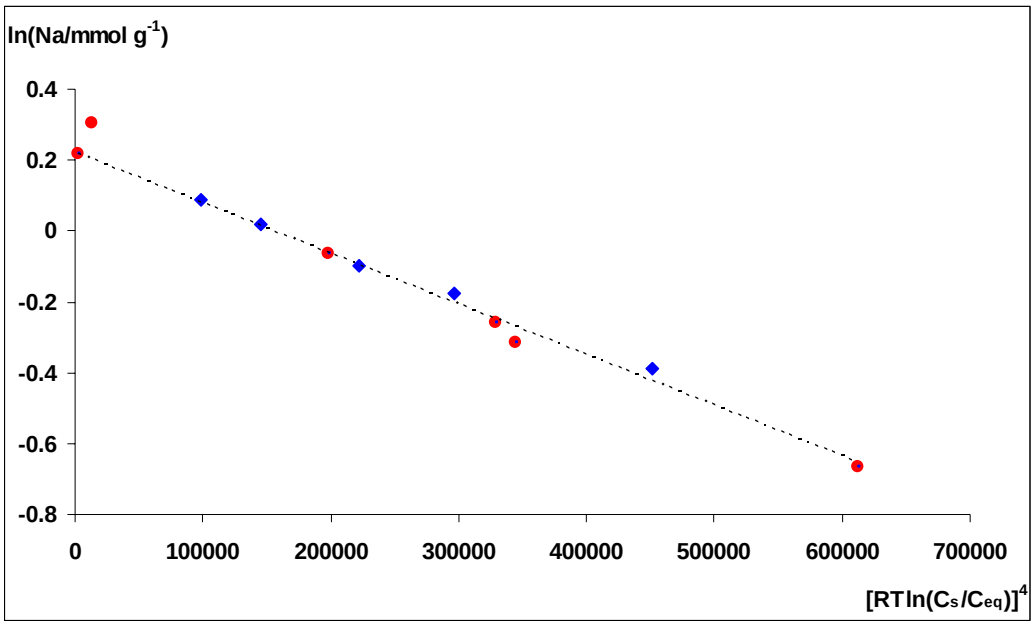

Figure 6. Logarithmic plot of Eqn (1) for the adsorption of morphine onto carbon PC94-11 after no less than 72 hours, which corresponds effectively to the final equilibrium. Data for 293 K (♦) and 313 K (●).

The new parameter β_s(morphine) = 1.37 ± 0.02 can be used to predict, with the help of Eqn (1), the adsorption equilibrium of this molecule from an aqueous solution by any porous carbon, provided that its characteristic energy E_o is known. As shown elsewhere,[2,8] Eqn (1) is valid over a relatively wide range of temperature around room temperature and therefore it may be relevant to pharmacology (adsorption at body temperature). Table 2 shows typical values of β_s.

Table 2. Typical solution affinity coefficients β_s for adsorption from aqueous solutions

Solulte	phenol	chloroform	benzene	benzoic acid	caffeine	morphine
$\beta_s(i) = E_s(i)/E_o$	1.03	0.52	0.54	0.8	1.28	1.37 ± 0.02

4. Information on immersion calorimetry[9]

In the case of immersion calorimetry, which takes place in a confined volume (~1 cm^3), the concentrated aqueous solution (c/c_{sat} ~0.6 to 0.8), leads to a relatively fast adsorption kinetic. This is confirmed by the shape of the curve showing the evolution of the heat transfer monitored by the 180 thermocouples of the calorimeter (initial slope and maximum). The calorimeter[9] is shown in Figure 7.

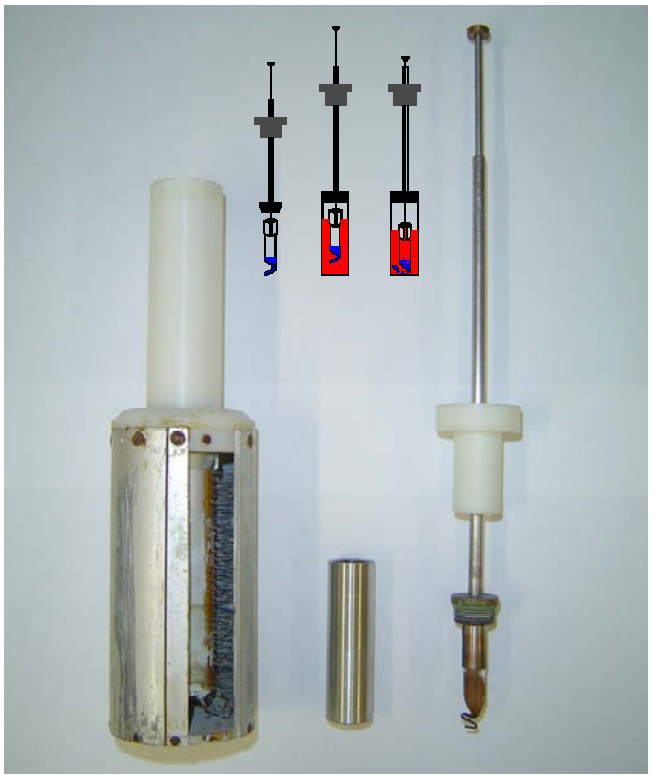

Figure 7. Immersion calorimeter: main part with the 180 termocouples (left), the tube containing the liquid (centre) and the sample holder with the outgassed sample (right). The inset shows the filling of the sample holder following the breaking of the capillary at the bottom. The enthalpy of immersion is monitored by the voltage difference in the thermocouples V(t).

As shown in Fig. 8, the curves normed to the transfer of 1 Joule absolute are the same for the microporous carbon PC94-11 and the non-porous carbon black N234-G. The energy (enthalpy) released in the process corresponds to the coating of the carbon surface by the solute and the filling of the remaining micropore volume by water. The energy associated with the latter is much smaller and therefore a good correlation is found between the adsorption energy of the solute and the surface area of the carbon (For phenol, caffeine and morphine adsorbed onto a non porous reference carbon black one obtains respectively -0.105 ± 0.004 J m^{-2}, -0.112 ± 0.010 J m^{-2} and -0.093 J m^{-2}). The value of -76.2 ± 0.1 J g^{-1} obtained for the enthalpy of immersion of carbon PC94-11 into a concentrated solution of morphine corresponds therefore to 76.2/ 0.093 = 820 m^2 g^{-1}.

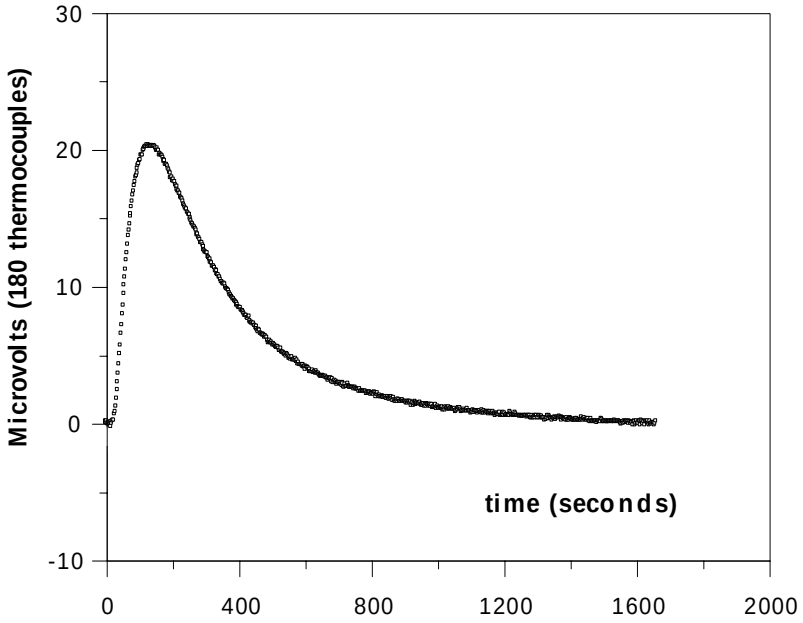

Figure 8. Thermal response for the immersion of nanoporous carbon PC94-11 (□) and graphitized carbon black N234-G (▲, non porous) into a concentrated aqueous solution of morphine at 293 K. The curves, normalized to integrals of 1 Joule absolute, are practically identical. The effective enthalpies of immersion, given by the integrals of the original curves, are respectively - 76.2 and - 7.4 J/g of solid.

In the case of more dilute solutions corresponding to the clinical system under investigation, diffusion in the relatively large liquid phase reduces considerably the rate of adsorption. In order to speed up the removal of the solute, it is therefore necessary to disperse small carbon particles (Ø < 400 μm) and ensure good shaking of the solution. The adsorption kinetic is strongly influenced by the dispersion of the carbon (reduced path from the liquid to the solid), which means small particles and,

again, a large amount of carbon. Moreover, active mixing (shaking/stirring) also increases the speed of removal. The slurry resulting from small particles has an adverse effect on attempts to recover the liquid phase before most of the morphine is removed (the 5 minute target). For example, filtering off the liquid phase will increase the contact with the carbon and speed up the adsorption process.

4. Conclusions

In this project it was shown than 99% of morphine can be adsorbed in 5 minutes from an aqueous solution by activated carbon PC94-11, with particles of less than 400 μm and an amount in excess by a factor three with respect to the actual saturation capacity. Clearly, the main parameters for a speedy elimination are: an excess of carbon, small particles and good initial mixing of the solid with the solution.

This specific study has also provided subsidiary information on the affinity coefficient for the adsorption of morphine from aqueous solutions, β_s(morphine) = 1.37 ± 0.02. This new parameter, of relevance to pharmacology, allows the prediction of the adsorption equilibrium of this molecule by activated carbons, by using the modified Dubinin-Radushkevich-Kaganer Eqn (1).

[1] F. Stoeckli, *Russ. Chem. Bull. Int. Ed.* **2001**, *50*, 2265.

[2] F. Stoeckli, in *X International Conference, Vol. 1*, Moscow, Russia, **2006**, pp. 21.

[3] E. Fernandez, S. Gotovac, D. Hugi-Cleary, M. V. Lopez-Ramon, F. Stoeckli, *Chimia* **2003**, *57*, 616.

[4] E. Fernandez, D. Hugi-Cleary, M. V. Lopez-Ramon, F. Stoeckli, *Langmuir* **2003**, *19*, 9719.

[5] S. Scheins, M. Messerschmidt, P. Luger, *Acta Crystallogr., Sect.B: Struct.Sci.* **2005**, *61*, 443.

[6] F. Stoeckli, V. López-Ramon, C. Moreno-Castilla, *Langmuir* **2001**, *17*, 3301.

[7] E. Fernandez, D. Hugi-Cleary, V. López-Ramon, F. Stoeckli, *Langmuir* **2003**, *19*, 9719.

[8] D. Hugi-Cleary, A. Slasli, F. Stoeckli, *Helv. Chim. Acta* **2005**, *88*, 470.

[9] R. C. Bansal, J.-B. Donnet, F. Stoeckli, *Active Carbon*, Marcel Dekker, New York,**1988**.

Chapter 6. Conclusions

This project deals with one of the most intriguing and important topics of the contemporary chemical research in the field of coordination polymers. The aim of the present work was to synthesize new metal-organic chains (1D), networks (2D) and frameworks (3D), based mainly on metallo-hexacyanides. Our interests were especially centered on the synthesis of cyano bridged frameworks that can be sufficiently robust to display permanent porosity, allowing the reversible adsorption of small molecules.

In the first part of the thesis, new bimetallic cyano-bridged polymers, which show remarkable reversible structural transformations induced by dehydration and subsequent rehydration, were synthesized. These molecular transformations are often accompanied by a colour change and have been shown by *in-situ* X-ray powder diffraction and immersion calorimetry to be completely reversible. Two new $Cu^{II}Cr^{III}$ 3D and 1D coordination polymers exhibiting ferromagnetism were synthesized and fully characterized. The 3D compound shows three-dimensional ferromagnetic ordering at ca. 4K. The 1D chiral polymer shows a weak intra-chain ferromagnetic exchange, as a result of magnetic orbital orthogonality between Cr(III) and Cu(II) in the chain, with very long Cu-N(cyano) distances due to the long Jahn-Teller axis of the copper(II) ions.

All the metal-organic cyano-bridged frameworks synthesized have been studied and characterized by gravimetric adsorption of vapours and immersion calorimetry. The immersion calorimetry technique, applied mainly to carbons, provides an insight into the filling of nanopores. The enthalpy of immersion, $\Delta_i H$, into different solvents suggests either their exclusion from the structure or their uptake. It was shown for some cases that the measured heat is not the heat of the immersion but

the heat of transformation of the structure. Within the framework of Dubinin's theory it was possible to show the coherence between the immersion calorimetry and the gravimetric adsorption results. The size of the adsorbent molecule has a significant influence on the adsorption processes, as was shown by these experiments.

A specific study of adsorption of morphine solutions by the different carbons has also provided subsidiary information on the affinity coefficient for the adsorption of morphine from aqueous solutions, β_s(morphine) = 1.37 ± 0.02. This new parameter, of relevance to pharmacology, will allow the prediction of the adsorption equilibrium of this molecule by activated carbons, by using the modified Dubinin-Radushkevich-Kaganer equation. It was found that the main parameters for a speedy elimination of morphine from the aqua solution, are: an excess of carbon, small particles and good initial mixing of the solid with the solution.

The results presented in this thesis support the optimistic forecast that MOF's are a diverse and rapidly growing class of functional materials. The use of cyanide bridging ligands has allowed the rational design and fuctionalization of their structures, allowing their properties to be rationally tuned. It has been shown that the chiral frameworks have unusual sorption properties quiet distinct from those seen in aluminosilicate zeolites. In addition, the synthetic strategy we have used here is extremely advantageous for the formation of flexible nanoporous materials. They show guest-induced structural transformations and some of them fall within the category of "recoverable collapsing" and "guest-induced reformation" framework materials. The work described here demonstrates the rational construction of flexible porous frameworks and the characterization of cooperative adsorption using Powder X-ray diffraction.

The research presented here is particularly relevant in the context of solid state chemistry since the rational design of solids has important ramifications for the development of new materials with unusual properties. We anticipate that our approach will be viable for the future construction of cavity-containing frameworks using other bridging organic ligands, and we also anticipate this approach will be applicable for the design of flexible porous materials.

Appendix

Appendix 1

Chiral cyanide-bridged bimetallic networks based on cyclohexane-1,2-diamine

Olha Sereda[a], Antonia Neels[a], Helen Stoeckli-Evans[a] & Joan Ribas[b].

[a]Institut de Chimie, Université de Neuchâtel, Av. de Bellevaux 51,CH-2007 Neuchâtel, Switzerland

[b]Departament de Química, Universitat de Barcelona, Av. Diagonal, 647, 08028 Barcelona, Spain

E-mail:olha.sereda@unine.ch

Hexa- and tetra-cyanometallates are very interesting synthons for material design as they have the potential to produce fascinating metal-organic frameworks. Chiral structures are a new target for the lattice architecture in the field of metal-organic frameworks (MOF's) and magnetic materials. With this optic in mind we have constructed new chiral MOF's, some of which exhibit ferromagnetism. Cyclohexane-1,2-diamine (chxn) has been incorporated into cyanide containing complexes previously [1], [2], [3]. We report here on some new examples of one-, two- and three-dimensional chiral networks derived from both forms of the chxn (1S,2S and 1R,2R) and hexa- and tetra-cyanometallates : $[M_x(chxn)_y]^{n+}$ + $[M(CN)_z]^{m-}$, where M_x = Cu, Ni; M = Ni, Co, Cr, Ru; n = 4, 6, m = 2, 3, 4.

Hexacyano networks:

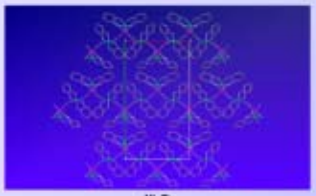

Ni_Ru
2-Dimensional zig-zag polymer

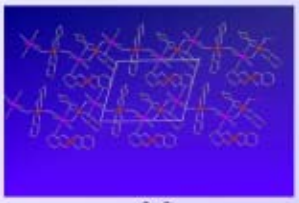

Cu_Cr
1-Dimensional zig-zag chain

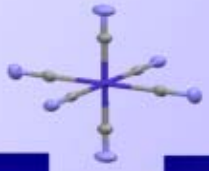

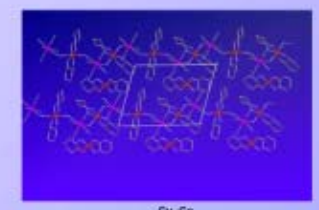

Cu_Co
1-Dimensional zig-zag chain

Ni_Co
2-Dimensional structure

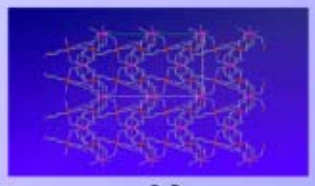

Cu_Ru
3-Dimensional network

Magnetic properties:

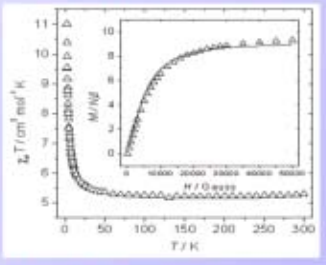

For example, the Cu_Cr system.

The magnetic behavior of this 1-dimensional zig-zag chain is characteristic of a weak ferromagnetic interaction. The experimental magnetic data were fitted using the following isotropic Heisenberg Hamiltonian:

$$H = -2J(S_{Cu(i)}S_{Cr(i+1)})$$

The best least-square fit, shown in the Figure above, gives J = + 1.64 cm^{-1}, g = 2.03 and R = 2.80 x 10^{-4}, where $R = \Sigma[(\chi_{obs}T)_i - (\chi_{calc}T)_i]^2 / \Sigma[(\chi_{obs}T)_i]^2$.

Tetracyano network:

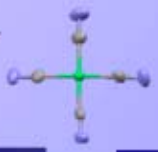

Cu_Ni
Binuclear complex
Single crystal, monoclinic P 2$_1$

+ 2H$_2$O

110 °C
- 2 H$_2$O

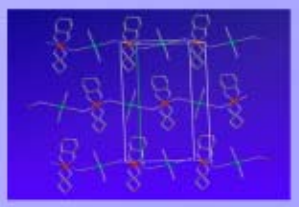

Cu_Ni after TG,
gives a 1-dimensional zig-zag chain.
Powder diffraction analysis, orthorhombic P 2$_1$2$_1$2$_1$

This structural transformation is reversible!

[1] E. Coronado, C.J. Gómez-García, A. Nuez, F.M. Romero, E. Rusanov, H. Stoeckli-Evans, *Inorg. Chem.* **2002**, 41, 4615.
[2] E. Coronado, C. Giménez-Saiz, J.M. Martínez-Agudo, A. Nuez, F.M. Romero, H. Stoeckli-Evans, *Polyhedron* **2003**, 22, 2435.
[3] E. Coronado, C. Giménez-Saiz, A. Nuez, V. Sanchez, F.M. Romero, *Eur. J. Inorg Chem* **2003**, 4288.

Appendix 2

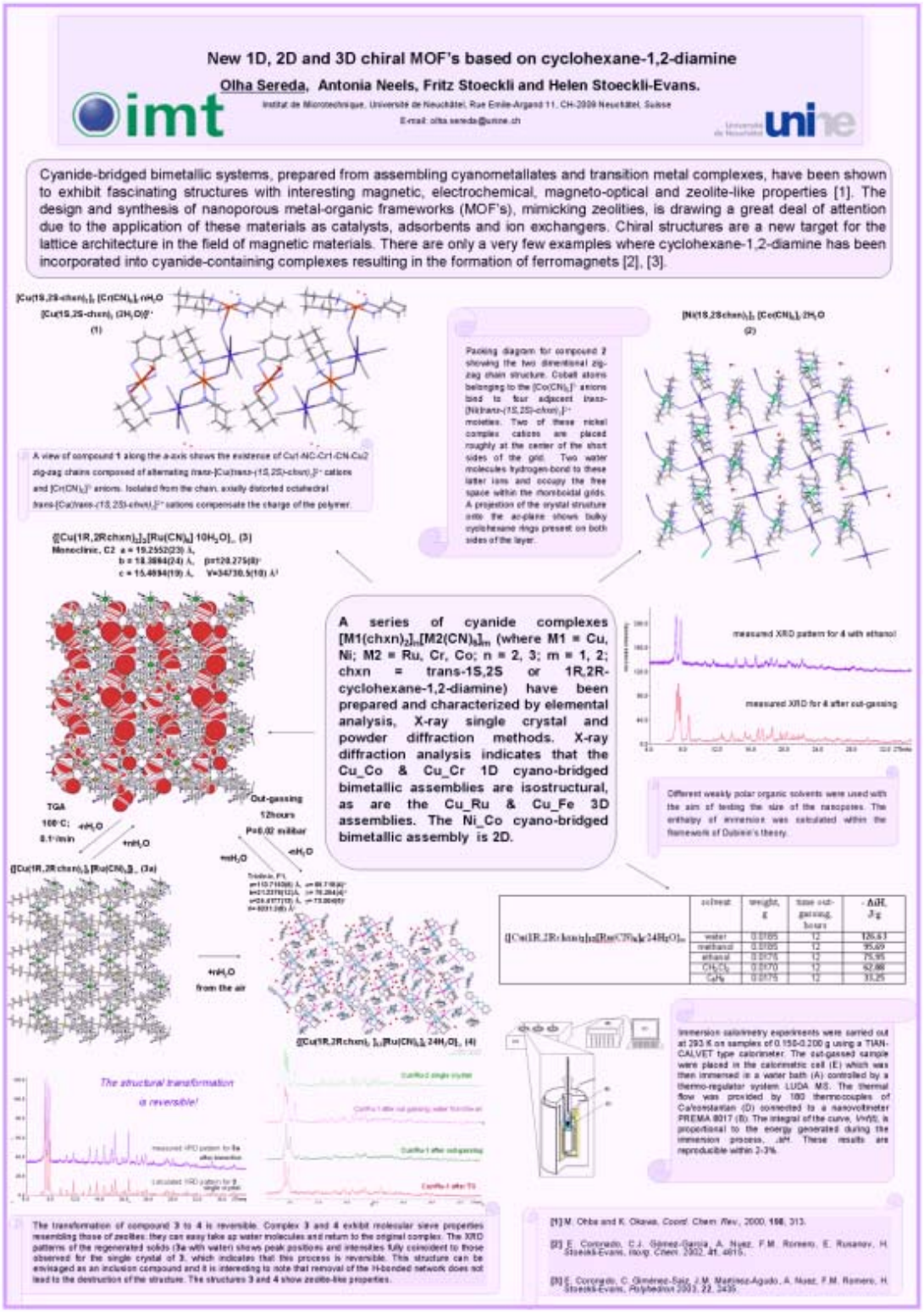
New 1D, 2D and 3D chiral MOF's based on cyclohexane-1,2-diamine
Olha Sereda, Antonia Neels, Fritz Stoeckli and Helen Stoeckli-Evans.
imt
unine
Cyanide-bridged bimetallic systems, prepared from assembling cyanometallates and transition metal complexes, have been shown to exhibit fascinating structures with interesting magnetic, electrochemical, magneto-optical and zeolite-like properties [1]. The design and synthesis of nanoporous metal-organic frameworks (MOF's), mimicking zeolities, is drawing a great deal of attention due to the application of these materials as catalysts, adsorbents and ion exchangers. Chiral structures are a new target for the lattice architecture in the field of magnetic materials. There are only a very few examples where cyclohexane-1,2-diamine has been incorporated into cyanide-containing complexes resulting in the formation of ferromagnets [2], [3].
A series of cyanide complexes [M1(chxn)2]n[M2(CN)6]m (where M1 = Cu, Ni; M2 = Ru, Cr, Co; n = 2, 3; m = 1, 2; chxn = trans-1S,2S or 1R,2R-cyclohexane-1,2-diamine) have been prepared and characterized by elemental analysis, X-ray single crystal and powder diffraction methods. X-ray diffraction analysis indicates that the Cu_Co & Cu_Cr 1D cyano-bridged bimetallic assemblies are isostructural, as are the Cu_Ru & Cu_Fe 3D assemblies. The Ni_Co cyano-bridged bimetallic assembly is 2D.
TGA
100°C; 0.1°/min
Out-gassing 12hours
P=0.02 mBar
The structural transformation is reversible!
measured XRD pattern for 4 with ethanol
measured XRD for 4 after out-gassing
Different weakly polar organic solvents were used with the aim of testing the size of the nanopores. The enthalpy of immersion was calculated within the framework of Dubinin's theory.
Immersion calorimetry experiments were carried out at 293 K on samples of 0.150-0.200 g using a TIAN-CALVET type calorimeter. The out-gassed sample were placed in the calorimetric cell (E) which was then immersed in a water bath (A) controlled by a thermo-regulator system LUDA MS. The thermal flow was provided by 100 thermo-couples of Calorestatan (D) connected to a nanovoltmeter PREMA 8017 (B). The integral of the curve, Int(t), is proportional to the energy generated during the immersion process, -ΔH. These results are reproducible within 2-3%.
The transformation of compound 3 to 4 is reversible. Complex 3 and 4 exhibit molecular sieve properties resembling those of zeolites; they can easy take up water molecules and return to the original complex. The XRD patterns of the regenerated solids (3a with water) shows peak positions and intensities fully coincident to those observed for the single crystal of 3, which indicates that this process is reversible. This structure can be envisaged as an inclusion compound and it is interesting to note that removal of the H-bonded network does not lead to the destruction of the structure. The structures 3 and 4 show zeolite-like properties.
[1] M. Ohba and K. Okawa, Coord. Chem. Rev., 2000, 198, 313.
[2] E. Coronado, C.J. Gómez-García, A. Nuez, F.M. Romero, E. Rusanov, H. Stoeckli-Evans, Inorg. Chem. 2002, 41, 4615.
[3] E. Coronado, C. Giménez-Saiz, J.M. Martínez-Agudo, A. Nuez, F.M. Romero, H. Stoeckli-Evans, Polyhedron 2003, 22, 2435.

Appendix 3

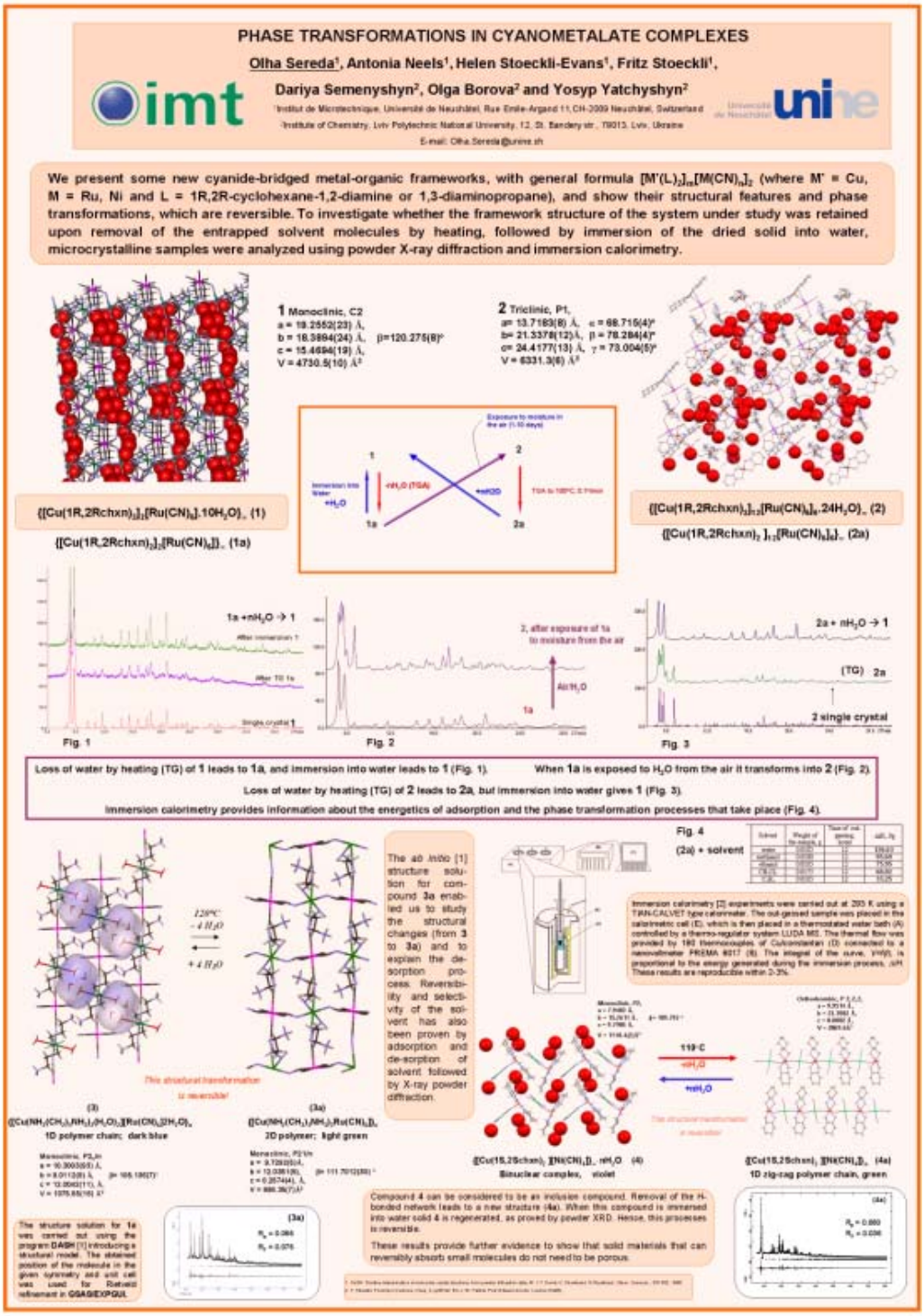
PHASE TRANSFORMATIONS IN CYANOMETALATE COMPLEXES
Olha Sereda[1], Antonia Neels[1], Helen Stoeckli-Evans[1], Fritz Stoeckli[1],
Dariya Semenyshyn[2], Olga Borova[2] and Yosyp Yatchyshyn[2]
[1]Institut de Microtechnique, Université de Neuchâtel, Rue Emile-Argand 11,CH-2009 Neuchâtel, Switzerland
[2]Institute of Chemistry, Lviv Polytechnic National University, 12, St. Bandery str., 79013, Lviv, Ukraine
E-mail: Olha.Sereda@unine.ch
We present some new cyanide-bridged metal-organic frameworks, with general formula [M'(L)2]n[M(CN)6]2 (where M' = Cu, M = Ru, Ni and L = 1R,2R-cyclohexane-1,2-diamine or 1,3-diaminopropane), and show their structural features and phase transformations, which are reversible. To investigate whether the framework structure of the system under study was retained upon removal of the entrapped solvent molecules by heating, followed by immersion of the dried solid into water, microcrystalline samples were analyzed using powder X-ray diffraction and immersion calorimetry.
1 Monoclinic, C2
a = 19.2552(23) Å,
b = 18.3894(24) Å, β=120.275(8)°
c = 15.4694(19) Å,
V = 4730.5(10) Å3
2 Triclinic, P1,
a= 13.7183(8) Å, α = 68.715(4)°
b= 21.3378(12)Å, β = 78.284(4)°
c= 24.4177(13) Å, γ = 73.004(5)°
V = 6331.3(6) Å3
{[Cu(1R,2Rchxn)2]3[Ru(CN)6].16H2O}n (1)
{[Cu(1R,2Rchxn)2]3[Ru(CN)6]}n (1a)
{[Cu(1R,2Rchxn)2]3[Ru(CN)6].24H2O}n (2)
{[Cu(1R,2Rchxn)2]12[Ru(CN)6]8}n (2a)
Exposure to moisture in the air (1-10 days)
+nH2O (TGA)
+nH2O
TGA to 100°C, 0.7 h/min
Immersion into Water
+nH2O
1a +nH2O → 1
After immersion 1
After TG 1a
Single crystal 1
Fig. 1
2, after exposure of 1a to moisture from the air
Air/H2O
1a
Fig. 2
2a + nH2O → 1
(TG) 2a
2 single crystal
Fig. 3
Loss of water by heating (TG) of 1 leads to 1a, and immersion into water leads to 1 (Fig. 1). When 1a is exposed to H2O from the air it transforms into 2 (Fig. 2).
Loss of water by heating (TG) of 2 leads to 2a, but immersion into water gives 1 (Fig. 3).
Immersion calorimetry provides information about the energetics of adsorption and the phase transformation processes that take place (Fig. 4).
120°C
- 4 H2O
+ 4 H2O
This structural transformation is reversible!
The ab initio [1] structure solution for compound 3a enabled us to study the structural changes (from 3 to 3a) and to explain the desorption process. Reversibility and selectivity of the solvent has also been proven by adsorption and de-sorption of solvent followed by X-ray powder diffraction.
Fig. 4
(2a) + solvent
Immersion calorimetry [2] experiments were carried out at 293 K using a TIAN-CALVET type calorimeter. The out-gassed sample was placed in the calorimetric cell (E), which is then placed in a thermostated water bath (A) controlled by a thermo-regulator system LUDA MS. The thermal flow was provided by 180 thermocouples of Cu/constantan (D) connected to a nanovoltmeter PREMA 6017 (B). The integral of the curve, ∫W(t)dt, is proportional to the energy generated during the immersion process, ΔH. These results are reproducible within 2-3%.
(3)
{[Cu(NH2(CH2)3NH2)2(H2O)2][Ru(CN)6]2H2O}n
1D polymer chain; dark blue
(3a)
{[Cu(NH2(CH2)3NH2)2][Ru(CN)6]}n
2D polymer; light green
119°C
+nH2O
+nH2O
{Cu(1S,2Schxn)2 [Ni(CN)4]}n nH2O (4)
Binuclear complex, violet
{Cu(1S,2Schxn)2 [Ni(CN)4]}n (4a)
1D zig-zag polymer chain, green
The structure solution for 1a was carried out using the program DASH [1] introducing a structural model. The obtained position of the molecule in the given symmetry and unit cell was used for Rietveld refinement in GSAS/EXPGUI.
(3a)
Compound 4 can be considered to be an inclusion compound. Removal of the H-bonded network leads to a new structure (4a). When this compound is immersed into water solid 4 is regenerated, as proved by powder XRD. Hence, this processes is reversible.
These results provide further evidence to show that solid materials that can reversibly absorb small molecules do not need to be porous.
(4a)

Sereda Olha

Chemin des Grands-Pins, 2,
2000, Neuchâtel
Tel.: +41788351632
olha.sereda@unine.ch
28 years old
Married

EDUCATION:

April 2005 - PhD student at the University of Neuchâtel
Thesis subject: "Bimetallic Metal-Organic Chains, Networks and Frameworks (MOC's, MON's & MOF's) Based on Cyanides: Structure and Physical Properties.

2002 – 2005 Scientific collaboration with the group of Prof. D. Semenyshyn, Institute of Chemistry and Chemical Technologies, Lviv Polytechnic National University, Lviv, Ukraine. Worked in the field of coordination chemistry, synthesis of hexacyanoruthenate (II) complexes and their characterizations.

M.Sc (2000 - 2002)
Institute: **Lviv Polytechnic National University, Lviv, Ukraine**
M.Sc Thesis: "Environmental consequences of hexacyanoruthenate complexes"
Domain: Chemistry and Chemical Technologies. Ecology (*Mention – Excellent*)

B.Sc (1997-2000)
Institute: **Lviv Polytechnic National University**
Lviv, Ukraine
Domain: Chemistry and Chemical Technologies. Ecology (*Mention – Excellent*)

PROFESSIONAL SKILLS:

Experience of handling the following instruments & techniques, which are used in the development and characterization of samples. X-ray diffraction and Powder X-ray diffraction. Adsorption and desorption techniques. Spectroscopy: (UV-Visible, FT-IR, AAS)

COMPUTER SKILLS:

Experience of working in computer application software packages like MS Office, Excel, Origin, ChemDraw, Chemwind.

LANGUAGES: English, Russian, Polish and Ukraine, French

RESEARCH INTEREST: Crystallography, Design of MOFs, Host-Guest Chemistry, Coordination chemistry, Analytical chemistry

PUBLICATIONS:

1. Borova, O.Ya.; Voznyak, Z.R.; Sereda-Chervatyuk, O. A.; Semenyshyn, D.I. Physical-chemical investigation for 1,3- and 1,4-phenilendiamin hexacianoferrates (II). *Visnyk of the Lviv Polytechnic National University.* 414, (2000), 32-34.

2. Borova, O.Ya.; Sereda-Chervatyuk, O. A.; Kochubeyj V.V. Physical-chemical investigation for hexamethylendiamine hexacyanoruthenate (II). *Visnyk of the Lviv Polytechnic National University.* 488, (2003), 42- 45.

3. Sereda, O. A.; Borova, O. Ya.; Semenishin, D. I.

Synthesis and physical-chemical investigation of methylamine hexacuanoruthenate(II). *Ukrainskii Khimicheskii Zhurnal (Russian Edition)* 71(7-8), (2005), 99-102.

4. Stoeckli-Evans, H.; Typilo, I.; Semenyshyn, D.; Sereda, O.; Gladyshevskii, R. Crystal structure of terbium potassium octacyanotungstate(IV) heptahydrate. Polish Journal of Chemistry (2007), 81(12), 2031-2038.

5. Sereda O., Neels A., Stoeckli F., Stoeckli-Evans H. and Filinchuk Ya. "Sponge-Like" Reversible Transformation of a Bimetallic Cyanometallate Polymer *Crystal Growth and Design* (2008), *8* (7), 2307–2311.
PhD thesis: Chapter 2, Section 2.1.

6. Sereda O., Ribas J. and Stoeckli-Evans H.
New 3D and Chiral 1D $Cu^{II}Cr^{III}$ Coordination Polymers Exhibiting Ferromagnetism. *Inorganic Chemistry* (2008), 47(12), 5107-5113.
PhD thesis: Chapter 2, Section 2.2.

7. Sereda O., Neels A., Stoeckli F. and Stoeckli-Evans H.
Chiral bimetallic assemblies and coordination polymers based on tetracyanonickelate: a striking reversible structural transformation.
Crystal Growth and Design (2008), submitted
PhD thesis: Chapter 2, Section 2.3.

8. Sereda O., Stoeckli F. and Stoeckli-Evans H.
Bimetallic Metal-Organic Cyano-Bridged Frameworks.
Crystal Growth and Design (2008), submitted
PhD thesis: Chapter 3, Section 3.1.

9. Sereda O. and Stoeckli-Evans H.
Poly-[(*trans*-bis-(μ-4,4'-bipyridine-*N*,*N*'))-diaquacopper(II)-tetracyanonickelate(II)]: a Metal-Organic Cyano-Bridged Framework (MOCBF).
Acta Crystallographica, Section C (2008), C64(6), m221-m223.
PhD thesis: Chapter 4, Section 4.3.

10. Sereda O., Stoeckli F., Filinchuk Ya., Pattison P. and Stoeckli-Evans H.
Transformation of a Chiral Nanoporous Cyano-Bridged Framework Triggered by Dehydration/Rehydration
To be submitted
PhD thesis: Chapter 3, Section 3.2.

11. Sereda O. and Stoeckli-Evans H.
$Cu^{II}Fe^{II}$ and $Cu^{II}Cr^{III}$ Bimetallic Chiral Cyano-Bridged Assemblies
Ready to be submitted
PhD thesis: Chapter 4, Section 4.1.

12. Sereda O. and Stoeckli-Evans H.
A 2D network based on hexacyanocobaltate (III)
Ready to be submitted
PhD thesis: Chapter 4, Section 4.2.

CONFERENCES AND WORKSHOPS

Participated in…..

1. "Lviv Chemistry read -2003", Held on 10-14th of May, **2003**. Lviv, Ukraine. Poster presentation: "Thermogravimetrical and IR spectroscopy investigations for hexacyanoruthenate (II) complexes with aliphatic amines "

2. "BRM – 2003", September 22-26, **2003**, Doneck, Ukraine. Poster presentation: "Synthesis, IR spectroscopy investigation of hexacyanoruthenate (II) and octacyanotungstate (IV) complexes with aliphatic amines "

3. XXI International Chugaev Conference on Coordination Chemistry, June 10-13, **2003,** Kujv, Ukrainian Poster presentation: "Physico-chemical investigation of hexamethylendiamine hexacyanoruthenate (II) "

4. Fall Meeting of the Swiss Chemical Society, October 13, **2005**, Lausanne, Switzerland Poster presentation: "Chiral cyanide-bridged bimetallic networks based on cyclohexane-1,2-diamine" (Appendix 1)

5. 3ème Cycle Workshop on "Advanced Materials: Magnetism, Light Emission and Charge Transport"; September 18-22, **2006**, Villars-sur-Ollon, Switzerland.

6. 23rd European Crystallographic Meeting ECM23, August 6-11, **2006**, Leuven, Belgium Poster presentation: "New 1D, 2D and 3D chiral MOF's based on cyclohexane-1,2-diamine" (Appendix 2)

7. 10th European Powder Diffraction Conference (EPDIC)**,** September 1- 4, **2006**, Geneva, Switzerland Poster presentation: "PHASE TRANSFORMATIONS IN CYANOMETALATE COMPLEXES" (Appendix 3)

8. Fall Meeting of the Swiss Chemical Society, October 13, **2006**, Zurich, Switzerland. Poster presentation: "PHASE TRANSFORMATIONS IN CYANOMETALATE COMPLEXES"

9. Meeting of the Swiss Society for Crystallography, October 20, **2006**, Bern, Switzerland. Poster presentation: "PHASE TRANSFORMATIONS IN CYANOMETALATE COMPLEXES"

10. International Workshop "Watching the Action II: Non Ambient X-Ray Powder Diffraction Methods for In-House Instruments". September 26-28, **2007**. Mülheim an der Ruhr, Germany

11. Workshop "In-situ synchrotron measurements" at Swiss-Norwegian Beam Lines (SNBL) at the European Synchrotron Radiation Facility (ESRF). October 10-14, **2007** Grenoble, France